Geoelectric Monitoring

Current Research and Perspectives for the Future

Book of extended abstracts
International Workshop within the frame of the FWF project TEMPEL (TRP 175-N21) and the 7th FP European project SafeLand
November 30th – December 2nd, 2011, Vienna

Berichte der Geologischen Bundesanstalt, Nr. **93**

Geological Survey of Austria

Cover: Geoelectric Monitoring of Permafrost at Mölltaler Glacier with view to the Sonnblick 2010,
Picture by Robert Supper.

ISSN 1017-8880

Medieninhaber und Verleger: Geologische Bundesanstalt, Neulinggasse 38, A 1030 Wien.
www. geologie.ac.at
Redaktion: Robert Supper & Stefanie Kauer
Layout: Stefanie Kauer
Lektorat: Christian Cermak
Verlagsort: Wien
Herstellungsort: Wien
Ziel der „Berichte der Geologischen Bundesanstalt“ ist die Verbreitung wissenschaftlicher Ergebnisse.
Satz: Geologische Bundesanstalt
Druck: Offset-Schnelldruck Riegelnik, Piaristengasse 8, A 1080 Wien

Table of Contents

Introductory Foreword

In the frame of the FWF Translational Brainpower project **TEMPEL** (Geoelectric properties: temporal change as failure indicator - TRP 175-N21) and the 7th Framework Program European Project **SafeLand** (Living with landslide risk in Europe), the Austrian Geological Survey hosted the ***"First International Workshop on Geoelectric Monitoring - GELMON 2011"*** - in Vienna. The workshop was held at the Geological Survey of Austria from the 30th of November to the 2nd of December 2011.

Geoelectrical monitoring has significantly developed over the recent years as an emerging branch in applied geophysics. Several groups have achieved very selective knowledge in this field of geoelectrics.
The intention of the GELMON workshop therefore was to bring the different groups together, to present results and to discuss the way forward. The scope of the workshop was not only focused on the presentation of state-of-the-art results but also on the discussion of special topics of data acquisition, processing, inversion and interpretation.

When the idea of the workshop was born, we were thinking of a small workshop with 20 to 30 participants. Presentations on all related aspects of geoelectrical monitoring were requested, covering the field from technical issues to the presentation of recent case study results. Specialists in the field of geoelectrics and related scientific disciplines were invited to submit their abstracts on diverse topics on geoelectric monitoring. After sending out the invitations we were overwhelmed by the quantity of interested people. Finally, almost 100 scientists from 18 countries registered for participation, whereas more than half of them were willing to contribute to the workshop by oral or poster presentation.
This unexpectedly huge number of participants highlights the importance of geoelectric monitoring all over the world and intensifies the need of cooperation and communication.
All important aspects of geoelectric monitoring, including monitoring of landslides, permafrost, CO_2, geothermal sites and contaminations, applications in hydrology and engineering, but also some contributions on instrumentation, data acquisition and data inversion were discussed during the workshop in Vienna. The discussions after the presentations highlighted the need of innovation and technological progress especially in the area of geoelectrical time-lapse/4D inversion and data quality assessment.

Finally it was decided to repeat this successful event in a two years cycle. The majority of participants voted again for Vienna as meeting venue. Therefore the 2nd Workshop on Geoelectrical Monitoring will take place in November 2013 again in Vienna and organised by the staff of the Geophysical Department of the Geological Survey of Austria.

This book contains the collection of extended abstracts summarizing the content of the talks held during this workshop and is intended to be a reference in geoelectric monitoring.

This is also the place to thank all the people from GSA who were involved in the organization of this workshow (especially Birgit Jochum, David Ottowitz, Stefanie Kauer and Anna Zöchbauer) for their enthusiastic help.

Robert Supper
Chairman of GELMON 2011
Vice President of the Austrian Geophysical Society

This book is dedicated to the memory of Erich Niesner,
31.01.1955 - 22.4.2012,

one of the pioneers of geoelectric monitoring in Austria,

and
to the memory of Knut Seidel,
21.01.1953 - 07.05.2012

geophysicist at GGL Geophysik und Geotechnik Leipzig GmbH.

Instrumentation and Data Acquisition Technology

Internal of our Geoelectric Monitoring System, picture by R. Supper

A Data Acquistion System for Geoelectric Monitoring

TORLEIF DAHLIN[1] and PETER JONSSON[1]

[1] Engineering Geology, Lund University, Box 118, S-221 00 Lund, Sweden.

torleif.dahlin@tg.lth.se

Introduction

A data acquisition system has been developed for automatic monitoring of variations in resistivity and induced polarisation (IP) effects, plus self potentials (SP). The system consists of electrodes, electrode cables, resistivity-IP instrument, relay switches, lightning protection, power supply, internet connection, etc. We have migrated through several generations of the system dating back to our first remote installation with automatic daily measurements in 1996. The system(s) have been used for a number of applications. Automated long-term monitoring has been done at 3 embankment dams in northern Sweden, out of which 2 are active at the moment (DAHLIN et al., 2001; SJÖDAHL et al., 2008, 2009). The purpose is to develop techniques for detecting anomalous leakage and internal erosion in the embankment dam, where the annual temperature variation is viewed as a natural tracer.

Short-term monitoring with the same objective has been done on embankment dams a couple of times, also with the aim to detect internal defects and anomalous leakage paths (SJÖDAHL et al., 2010, 2011). Here the monitoring period has been a few days in connection with planned change in reservoir water level.

Short-term monitoring has also been done at 4 different waste sites in southern Sweden, typically for 1-2 weeks, including 4 separate monitoring campaigns on one of the sites (JOHANSSON et al., 2011; ROSQVIST et al., 2011). The aim has been to detect variation in content and migration of fluids and gas in waste.

The intention of this article is to outline the main features of the system and summarise the experiences gained of geoelectrical monitoring. Glimpses of different steps in the development are given, from the earliest to the most recent version will be described here.

Before monitoring with permanently installed data acquisition systems started we did a time lapse survey on Lövön embankment dam in Sweden, where we installed and left the electrodes in place but connected the electrode cables and the instrument each time of measuring (JOHANSSON and DAHLIN, 1996). In this study it became very clear that the type of electrodes consisting of steel rods that are normally used for geoelectrical imaging surveys were poorly suited for long term measurements as the electrode grounding contact deteriorated seriously from one measurement time to the next. We then switched to buried plate electrode that functioned much better.

Electrodes and Electrode Cables

Stainless steel plates are preferred as electrodes for the resistivity-IP measurements, where we use sizes between 0.125m x 0.125m (short term monitoring) and 0.25m x 0.25m (long term monitoring, see Fig. 1). The plate electrodes are buried at shallow depths, providing much larger contact area than regular cylindrical electrodes. The electrodes are fitted to the electrode cables so that only stainless steel and no other metals are exposed to the environment in order to avoid

galvanic elements and corrosion. The electrode cables are specifically made for monitoring installations with no exposed metal surfaces, and hence no exposed parts carrying dangerous currents and potentials. Lightning protection is connected between each incoming electrode and the relay switches and the instrument, and the power supply is also protected against over-voltage.

Fig. 1: Design of electrodes used for permanent installations for geoelectrical monitoring and photo from field installation in progress on Hällby embankment dam 1996.

At a couple of the embankment dam sites non-polarisable electrodes for SP measurement were included. In those cases every 2nd electrode is a stainless steel plate and every 2nd is non-polarisable. Only the steel places have been used for current transmission, while the non-polarisable one have been used for measuring SP as well as potentials for resistivity and IP.

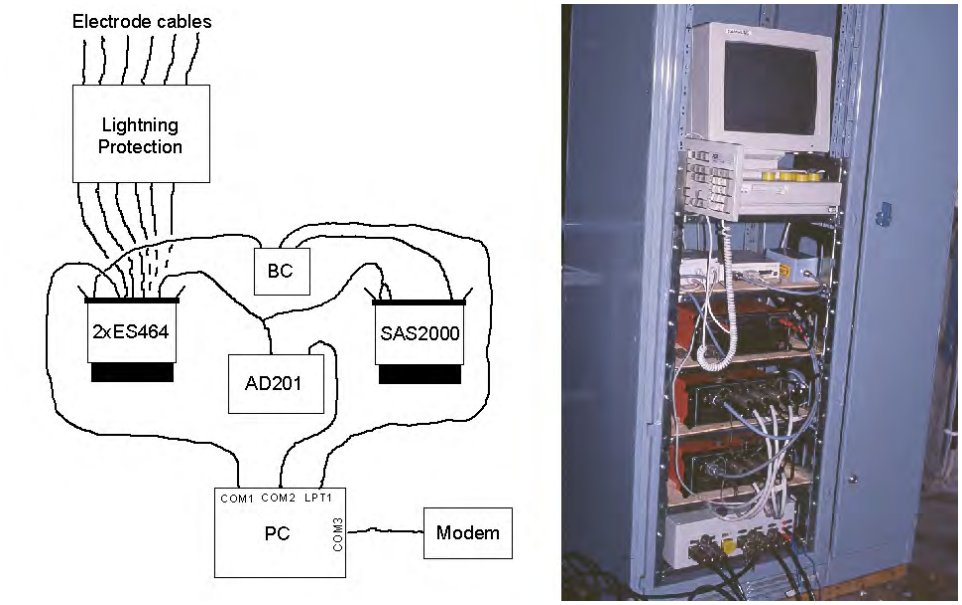

Fig. 2: The first permanently installed data acquisition system on Hällby embankment dam, installed in 1996.

Instrumentation

The first generation of the system installed consisted of a mixture of components, an ABEM Booster SAS2000 was used to transmit current, two units of ABEM Electrode Selector ES464 to

switch electrodes, a Lawson Labs AD201 24 bit A/D-converter for measuring potentials, and lightning protection designed and built at Lund University (Fig. 2). The data acquisition was controlled by a standard desktop PC via serial ports and a parallel port interface for controlling the SAS2000.

The second generation of the system installed also used an ABEM Booster SAS2000 to transmit current and 1-2 units (depending on site) of ABEM Electrode Selector ES464 to switch electrodes. Measurements and control of the transmitter was taken over by a Terraohm RIP224 receiver and control unit equipped with 24 bit A/D-converters, which was designed and built at Lund University as the lightning protection. The data acquisition was controlled by a standard desktop PC via serial ports.

Fig. 3: Temporary installation of the present data acquisition system on a landfill in 2011.

The most recent data acquisition system comprises an ABEM Terrameter LS configured for automatic measuring at pre-selected intervals (Fig. 3). The instrument has a built-in relay switch that handles 64 electrodes, but we have expanded it with a number of Electrode Selector ES10-64C relay switches to allow for more electrodes. The instrument software runs on a Linux platform, and timing of the data acquisition is controlled by cron. Each time it is due cron starts up acquisition software and carries out measurements according to the selected protocol(s). After finishing a measurement round the instrument turns off the software and all data acquisition hardware, which means that the power consumption in stand-by mode is minimised. In this case a PC is not needed to control the data acquisition, but depending on the speed of the Internet it may an advantage with a compact industrial type PC for more stable remote control and data transfer.

Remote Control and Data Transfer

In the early systems remote control and data transfer was done via telephone modem using pcAnywhere. The telephone lines were often poor and communication with the data acquisition system required endless patience and was a source of lots of frustration.

Remote control and data transfer is nowadays done via a mobile broadband internet modem with built-in router, etc. The monitoring systems transfer data automatically via SFTP, using a data transfer system design is outlined in Fig. 4. Data archiving has been identified as a field needing a systematic approach, and a standardised data format is also needed.

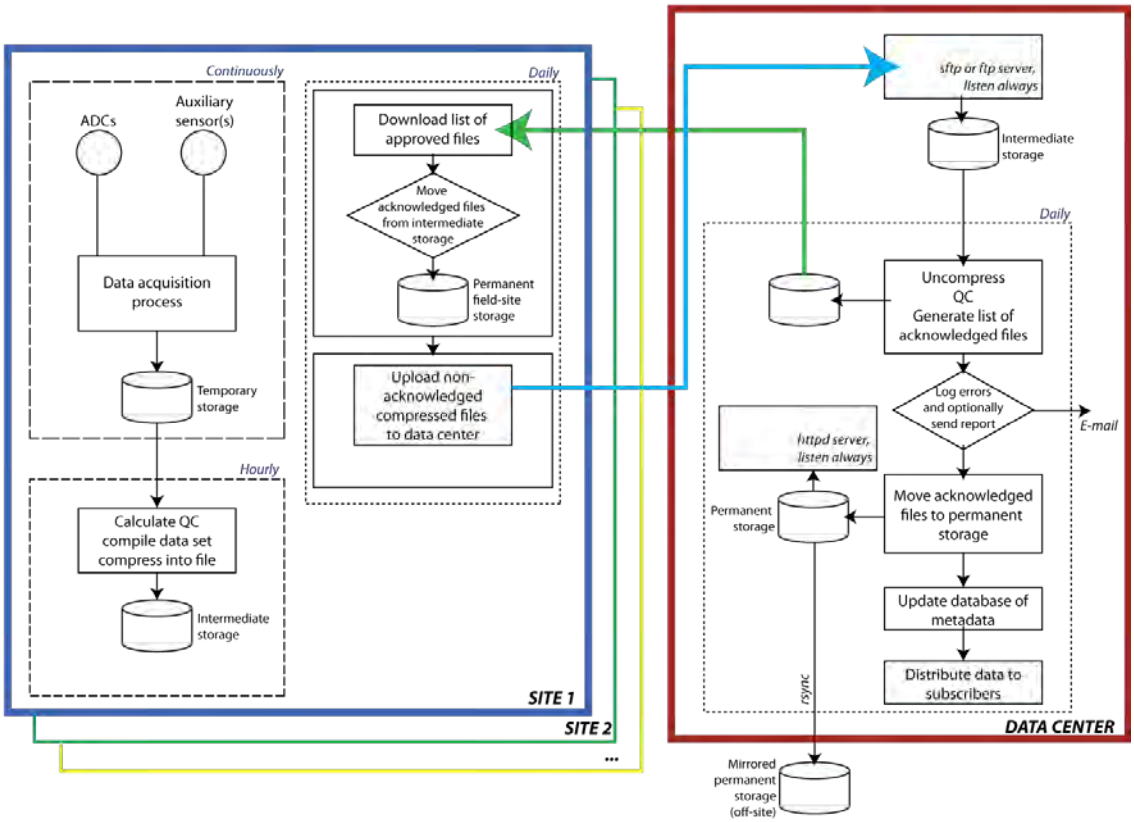

Fig. 4: Overview of data transfer system principles.

Power Supply

Power supply has so far been provided by the power net grid. In cases where power consumption is provided by batteries or solar panels the latest system can be optimised for minimum power consumption via standby mode between measurements. Adjusting output power and optimising the measuring protocol to reduce the number of current transmissions by using the multi-channel capability are other ways to save energy.

Experiences

The data acquisition systems have mostly operated in a stable way, with occasional breakdowns. The reasons for problems during the period 1996 to 2011 have been (listed in order of frequency):

- Modem and Internet connection breakdown and stability at the monitoring site has by far been the largest problem through the years. In recent years more stable solutions have come.
- Transmitter malfunction due to worn out components has occurred a handful times due to worn out polarity switch relay or transistor. It should be noted that the transmitters used have been SAS2000 which were designed for manual resistivity surveying in the 1970-ties and never were intended for automated imaging many hours every day year after year.
- Relay malfunction in the electrode selectors (3 occasions).
- Malfunction of server in Lund due to lightning transient.

- Electrode disconnection by animals (short-term monitoring).
- Remote cable damage (short-term monitoring).
- Electrode connection corrosion (open take-outs in short-term monitoring), see Fig. 5.
- Damaged serial port in a PC due to electric transient (one occasion).
- Damaged input channel of RIP224 due to electric transient (one occasion).

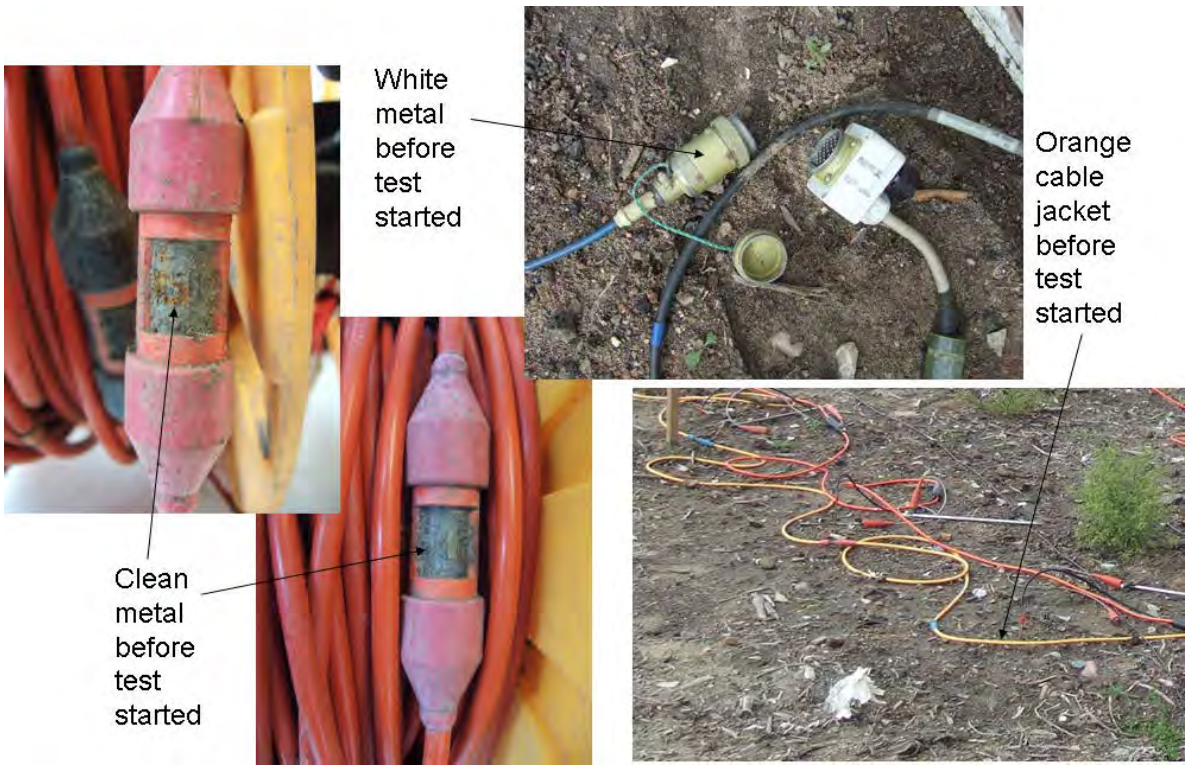

Fig. 5: Photographs showing corrosion, etching and bleaching of electrode cables and connectors resulting from a few weeks exposure to the atmosphere on a landfill.

Summary and Conclusions

The overall experiences of our geoelectrical monitoring activities can be summarised as follows:

- Automatic monitoring has been carried out at a number of sites since 1996.
- Data acquisition and transfer solutions have mostly been stable.
- Most trouble has been caused by communication problems.
- Poor ground to electrode contact was reduced by buried plate electrodes.
- Corrosion problems were eliminated by insulated pig-tail electrode connections.
- Long time series of IP data remain to be analysed.

Acknowledgements

Thord Lundgren has been instrumental in design and construction of instruments used for the monitoring. Sam Johansson and Pontus Sjödahl at HydroResearch have been cooperation partners throughout dam monitoring work. Elforsk, DSIG (Dam Safety Interest Group within CEATI) and the dam owners have funded the work.

The short term monitoring of landfills was carried out within the MaLaGa project (**Ma**pping of **La**ndfill structures and **Ga**s migration based on geophysical measurements) in co-operation between Lund University, NSR AB and Tyréns AB, with funding from Swedish Waste Management

(Avfall Sverige), Swedish Gas Centre (Svenskt Gastekniskt Center AB), Sven Tyréns Stiftelse, NSR AB, SYSAV AB and VETAB AB.

References

DAHLIN, T., SJÖDAHL, P., FRIBORG, J. and JOHANSSON, S., 2001: Resistivity and SP Surveying and Monitoring at the Sädva Embankment Dam, Sweden. – In: MIDTTØMME, G.H., HONNINGSVÅG, B., REPP, K., VASKINN, K.A. and WESTEREN, T. (Eds): Dams in a European Context, 107-113, Balkema/Swets & Zeitlinger, Lisse.

JOHANSSON, S. and DAHLIN, T., 1996: Seepage monitoring in an earth embankment dam by repeated resistivity measurements. – European Journal of Engineering and Environmental Geophysics, **1**(3), 229-247.

JOHANSSON, S., ROSQVIST, H., SVENSSON, M., DAHLIN, T. and LEROUX, V., 2011: An alternative methodology for the analysis of electrical resistivity data from a soil gas study. – Geophysical Journal International, **186**, 632-640.

ROSQVIST, H., LEROUX, V., DAHLIN, T., SVENSSON, M., LINDSJÖ, M., MÅNSSON, C-H., and JOHANSSON, S., 2011: Mapping landfill gas migration using resistivity monitoring. – Waste and Resource Management, **164**(1), 3-15.

SJÖDAHL, P., DAHLIN, T., JOHANSSON, S. and LOKE, M.H., 2008: Resistivity monitoring for leakage and internal erosion detection at Hällby embankment dam. – Journal of Applied Geophysics, **65**, 155–164.

SJÖDAHL, P., DAHLIN, T. and JOHANSSON, S., 2009: Estimating seepage flow from resistivity monitoring data at the Sädva embankment dam. – Near Surface Geophysics, **7**, 463-474.

SJÖDAHL, P., DAHLIN, T. and JOHANSSON, S., 2010: Using the electrical resistivity method for leakage detection in a blind test at the Røssvatn embankment dam test facility in Norway. – Bulletin of Engineering Geology and the Environment, **69**, 643–658.

SJÖDAHL, P., JOHANSSON, S. and DAHLIN, T., 2011: Investigation of shallow leakage zones in a small embankment dam using repeated resistivity measurements. Internal erosion in embankment dams and their foundations. – In: FRY, J.-J., RIHA, J. and JULINEK, T. (Eds.): Proceedings of the Institute of Water Structures FCE BUT Brno, 26.-29. April 2011, Brno, Czech Republic, **13**, 165-172.

Development of multi-transmission high speed survey system and the application of geyser monitoring

MOTOHARU JINGUUJI

National Institute of Advanced Industrial Science and Technology AIST Tsukuba Central #7, Tsukuba, Ibaraki 305-8567, Japan.

m.jinguuji@aist.go.jp

Summary

A new resistivity survey system, which is capable of very fast data acquisition compared with conventional DC resistivity system, has been developed in AIST. The key feature to speed up the measurement is that the system transmits multiple currents of different frequencies from different transmitter electrodes simultaneously. The transmitted signals are separated in frequency domain at a receiver electrode is identified by each respective frequency. The receiver electrodes are also multiple and simultaneously measured by using a multiple receiving function. The newly developed system has been tested by measurements at some experiment yards and the result shows success. The new developed system can obtain many datasets of resistivity in short time. Therefore, this system is suitable for the data acquisition using the statistic methods of time series, and the high speed geological monitoring. This paper introduces the outline of this system and the example of application to the monitoring of a geyser.

Introduction

A new resistivity survey system, which is capable of very fast data acquisition compared with conventional DC resistivity system, has been developed in AIST. The key feature is that the system transmits multiple currents of different frequencies from different transmitter electrodes simultaneously.

Figure 1 shows a conceptual diagram of the multi-transmission resistivity system and a conventional single transmission system. In the conventional system, a single frequency current is transmitted from an electrode pair.

The new developed system has a multi-channel transmission function, and currents that contain multiple frequencies are transmitted from multiple electrodes pairs. The new multi-transmission system sends electric currents from multiple electrodes simultaneously. Frequency of the current sent from one electrode pair is different from those of the other electrode pairs. Superimposed signals of these frequencies observed at a receiver electrode pair is separated into each frequency using a synchronized detection circuits.

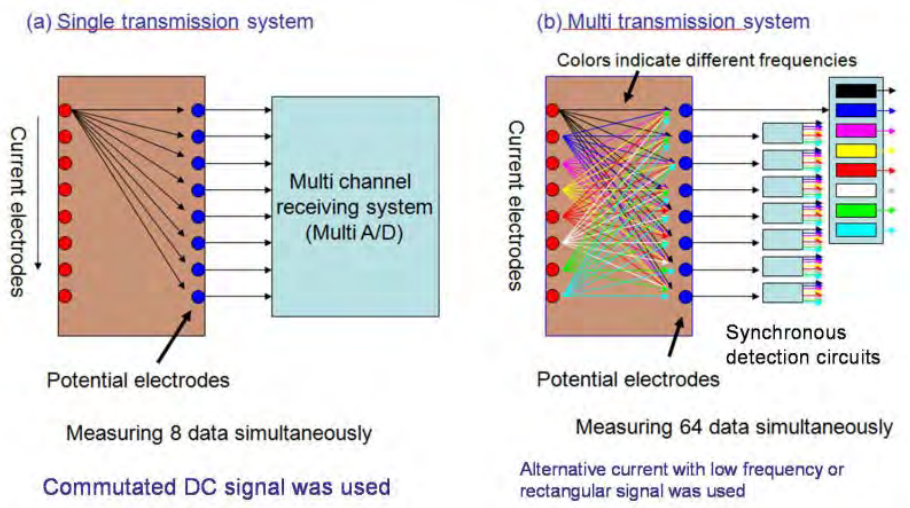

Fig. 1: Comparison of conceptual diagrams of the systems.

As in the case of the conventional system, the receiving function of the multi-electrode can be easily incorporated in the new system. As an example, Figure 1b shows a case of eight multiple current electrodes and eight multiple receiver electrodes. The new system can obtain 64 data at one time using 64 synchronized detection circuits, while the conventional system can measure eight data at once. The synchronized detection circuit that uses in the multi-transmission system has a very sharp band pass filter characteristic, in order to separate the frequencies of the signals. As a result, it can remove unwanted environmental noises efficiently. Therefore, the system can be used in the location of noisy environment.

Figure 2 shows the comparison of 2D inversion images between the multi-transmission system and the ordinary system using Pole-Pole method.

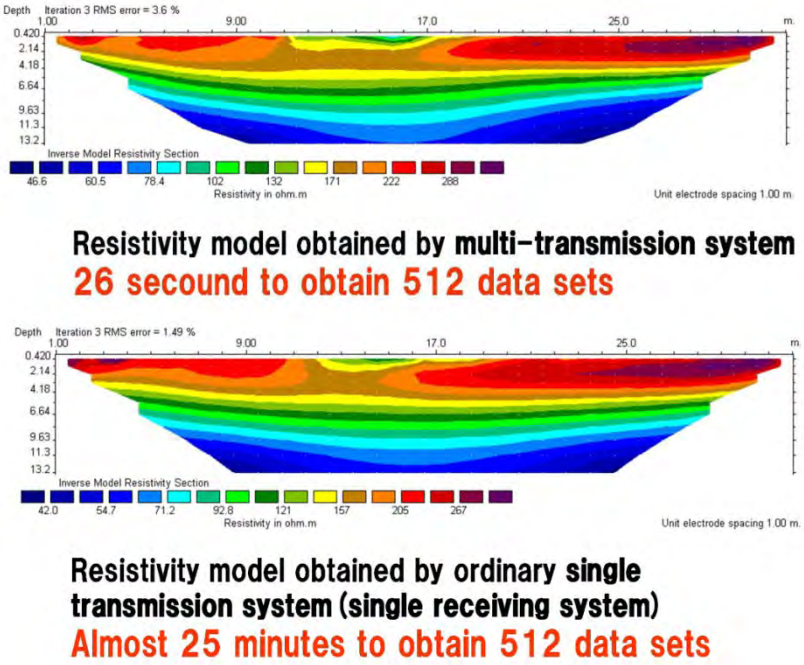

Fig. 2: Comparison of 2D inversion images between the multi-transmission system and the ordinary system.

Almost same images obtain from these instruments. However the multi transmission system is much faster than the ordinary single transmission system. Multi-transmission system can obtain data much faster than that of ordinary system. So, this system is suitable for the high speed monitoring.

Application of geyser monitoring

Multi-transmission system is suitable for high speed monitoring of geological phenomenon, because the system can be enable to the high speed data acquisition. The geyser is the one of the geological phenomenon that changes rapidly. In this section, we show an example of the geyser monitoring that used multi-transmission system.

Fig. 3: A location of Onikobe geyser in Japan (Referenced by Google map).

Fig. 4: A photo of Onikobe geyser.

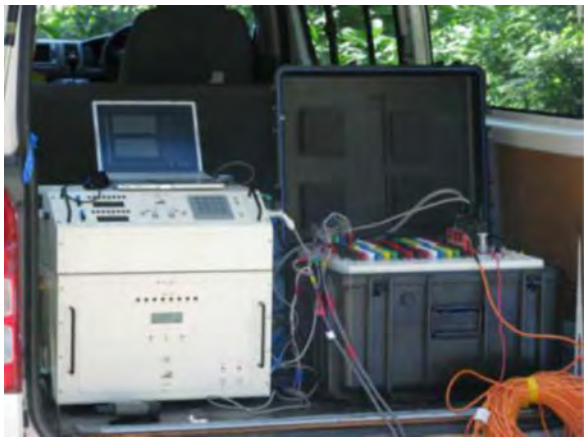

Fig. 5: A photo of multi-transmission resistivity meter.

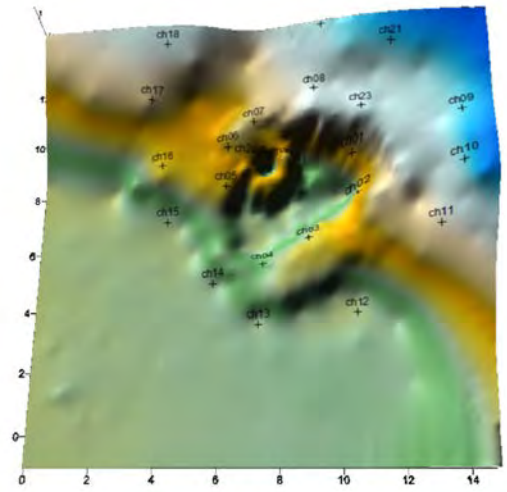

Fig. 6: 3D terrain and superimposed electrodes location.

Onikobe geyser in Yamagata Prefecture, the cycle time of eruption is from 6 minutes to 12 minutes, duration time is from 60 seconds to 90 seconds and erupt up to 15m high degree, is one of the famous tourist destination geyser in Japan (Fig. 3 and Fig. 4). In general, geysers are considered its eruption cycle has a certain period, but the eruption cycle of Onikobe geyser has some other certain variability regularity of duration and cycle of eruption.

Generally speaking, geyser's eruption cycle and duration time are limited in short time, relatively. In order to observe the geyser by using resistivity monitoring, it needs the electrical resistivity meter which is faster than ever. The multi-transmission high-speed resistivity meter developed by AIST can measure much faster than ordinary system (Fig. 5).

This instrument can measure 64 datasets (8x8) at a time. The numbers of electrode of the monitoring of Onikobe geyser are 8 electrodes for the transmission, and 16 electrodes for the receiving. Therefore, the sampling time of the measurement of Onikobe geyser is about 11 seconds including switch of scanner.
Onikobe geyser is located in the dimpled terrain. Figure 6 shows the view of three-dimensional terrain using the non-prism laser survey instrument and superimposed electrodes location.

Fig. 7: Electrodes used for monitoring of geyser.

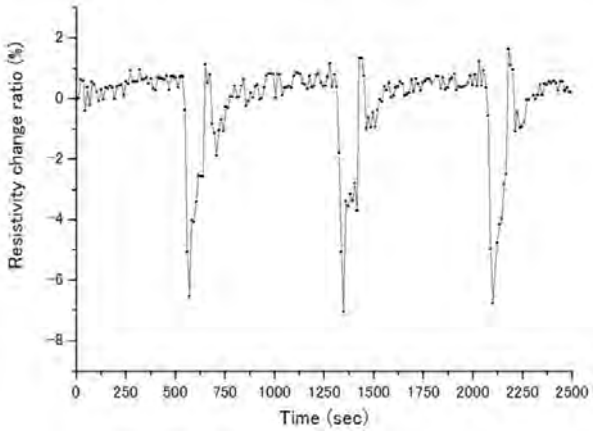

Fig. 8: Resistivity change with time at an electrode which connected casing pipe of geyser.

The Pole-pole method was used for the resistivity measurement. 24 Electrodes were set around geyser (Fig. 7). The electrodes from ch1 to ch8 were used for the current, and the electrodes from ch9 to ch24 were used for the potential. The electrode ch24 was connected to the iron casing pipe of geyser.

Figure 8 shows the resistivity change with time at the electrode which connected casing pipe of geyser (Current ch1, Potential ch24). The resistivity change reflects the geological status around casing pipe. The clear decrease of resistivity was confirmed during eruption status of geyser. The pattern of resistivity change is almost same pattern observed by MISHIMA et al. (2007). In the figure, the resistivity change ratio is the normalized with respect to the initial value. The resistivity decrease is almost 6 % at maximum.

Multi-transmission system can obtain 128 time series data within 11 seconds. So, we tried to the analysis of apparent resistivity using other electrodes data.

Figure 9 shows the plan view of the apparent resistivity during eruption of the geyser. In the figure, the depth information does not use and the only horizontal information uses for the plot. The data position of apparent resistivity is the center of the current electrode and potential electrode.
In the Fig. 9, we can confirm an obvious decrease anomaly of resistivity at the right upper of the location of geyser (ch24). Also, the increase area of resistivity is confirmed obviously around this decrease anomaly. Figure 10 shows resistivity changes at the point of low resistivity anomaly (Current ch5, Potential ch9), increase of resistivity (Current ch2, Potential ch12) and the casing pipe of geyser (Current ch1, Potential ch24), respectively.

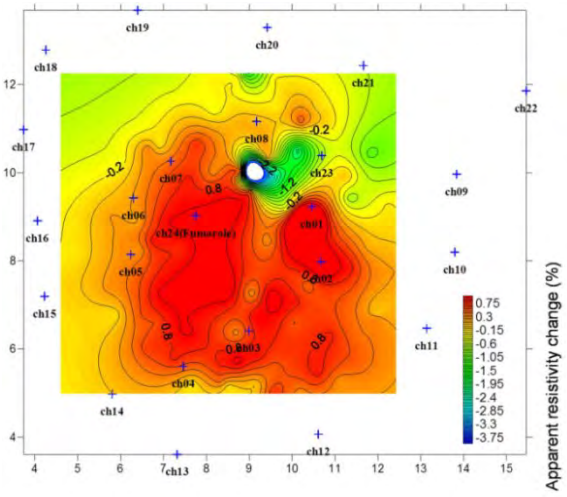

Fig. 9: A plan view of the apparent resistivity change during eruption of geyser.

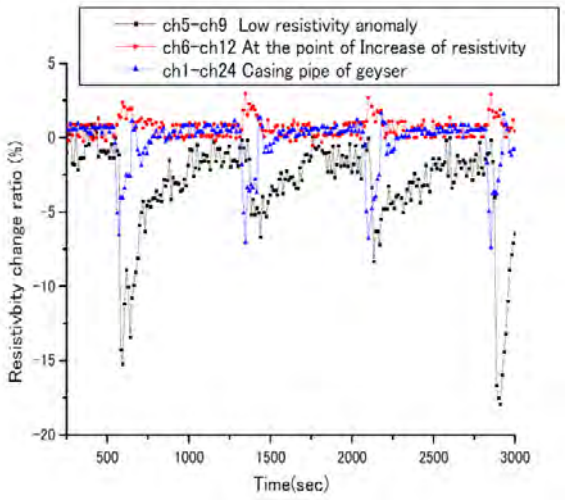

Fig. 10: Resistivity changes at the point of typical changes.

The drops of peek of resistivity at low resistivity anomaly are slightly delayed as compared to the drop of peek at the position of casing pipe. In addition, the resistivity changes at the anomaly late to recover compared with the resistivity change at the position of casing pipe. At the area of resistivity increase, the resistivity increase when the eruption seems to be occurred. But, the change is small. Figure 11 shows plan views of the change of resistivity per 45 seconds.
We can interpret of the eruption mechanism of the geyser from these changes of resistivity. It is estimated that the location of chamber of hot water is the low resistivity anomaly which is 2m away from the geyser. The low resistivity anomaly indicates the existence of flows of hot water to the chamber. This resistivity drop of the low resistivity anomaly has begun to late compare with the resistivity drop at the casing pipe. And then, foaming of hot water occurs due to the reducing of pressure by discharge of the hot water. The eruption of geyser is begun by the foaming. The resistivity increases due to the low water saturation during the foaming. The area of increasing of resistivity is 5m2 surrounding the geyser, but its change is not so large. The change of resistivity (change ratio) is only few percent, too. This shows the foaming of hot water is occurred in the relatively wide area.

The resistivity at the low resistivity anomaly recovers slowly and continuously until the next eruption. This shows that the water level of hot water at the chamber drops slowly after eruption has finished.

Conclusion

We developed a new resistivity survey system, which is capable of very fast data acquisition compared with conventional DC resistivity systems and carried out the resistivity monitoring at Onikobe geyser. As a result, the clearly changes of resistivity were observed during eruption of the geyser. These changes do not inconsistent with the eruption mechanism of Onikobe geyser that has been considered so far.

We show that these resistance changes are explained by the eruption mechanism. On the other hand, the area which the foaming has occurred is relatively wide. The comprehensive validation is required using other monitoring method data in future.

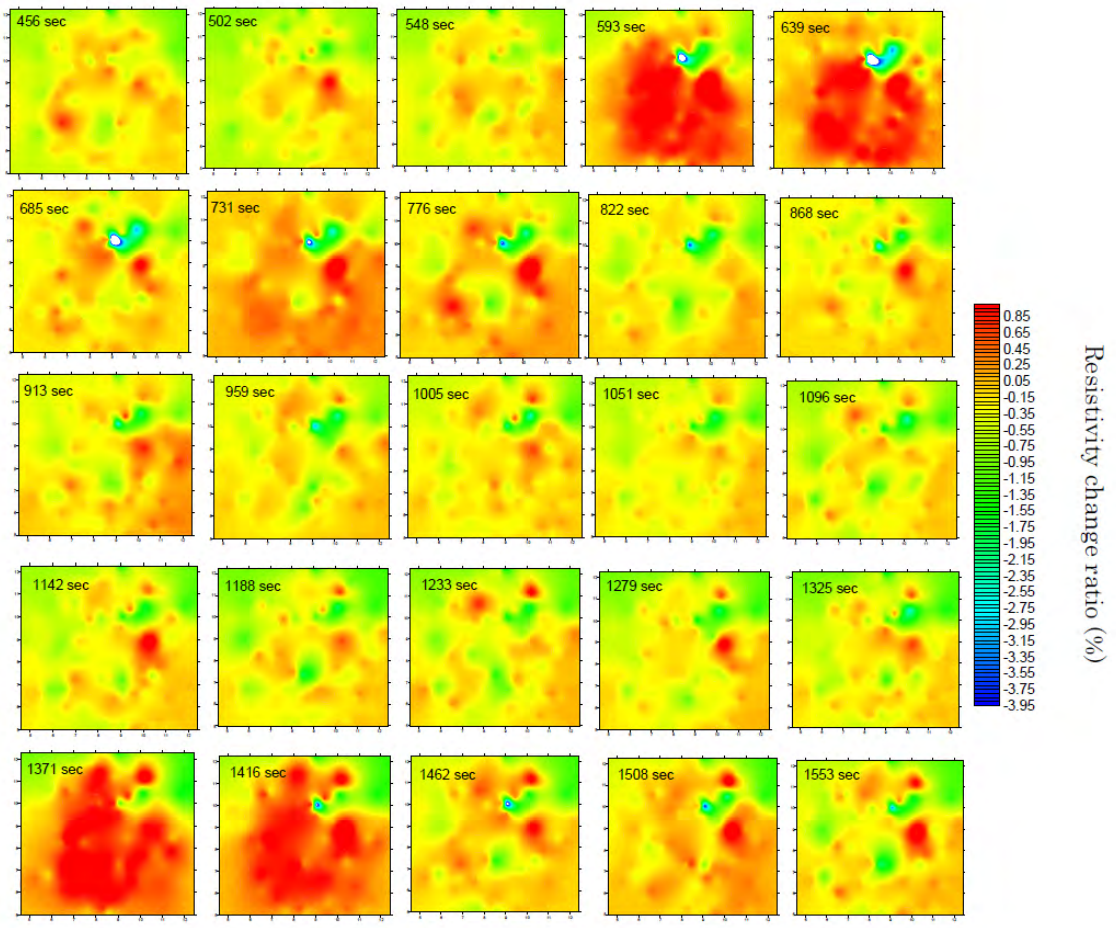

Fig. 11: Plan views of the change of resistivity per 45 seconds.

Reference

MISHIMA, S., OGAWA, Y., SABO, K. and TAKAKURA, S., 2007: Observation of resistivity change of Onikobe geyser. – Conductivity Anomaly 2007, 60-65.

The GEOMON 4D electrical monitoring system: current state and future developments

ROBERT SUPPER[1], ALEXANDER RÖMER[1], GERHARD KREUZER[2], BIRGIT JOCHUM[1], DAVID OTTOWITZ[1], ANNA ITA[1] and STEFANIE KAUER[1]

[1] Geological Survey of Austria, Neulinggasse 38, 1030 Wien, Austria.
[2] LIFTOFF, Kölblgasse 11/1, 1030 Wien, Austria.

Robert.Supper@geologie.ac.at

Introduction

In 2000, after the Geophysical Department of the Geological Survey of Austria had successfully applied the geoelectric method to investigate the structure of the large landslide of Rindberg near Sibratsgfäll (JARITZ et al., 2004; SUPPER et al., 2009), the Torrent and Avalanche Control Vorarlberg contracted the Geological Survey of Austria to develop a permanent geoelectrical monitoring system for landslides. At that time it was found that most of the commercially available systems were optimised to perform conventional investigation surveys and at that time none of the systems could fulfil the requirements of permanent geoelectric monitoring (high resolution, high speed of data acquisition, high reliability, recording of full signal samples for noise detection, remote controlled maintenance and automatic data transfer). Therefore, in late 2000 the design of an innovative system was started (SUPPER and RÖMER, 2003). The first 29-electrode prototype was installed to observe the mudflow of Rindberg near Sibratsgfäll in spring 2002, where it was continuously measuring since that time till the end of 2007 with a few unforeseen interruptions due to lightning strokes. Based on the results gathered during operation of the prototype, the system was redesigned and optimised for monitoring purpose as well as for "conventional" field surveys within the following years and finally reached its maturity state in 2006. At the end of 2007 after 5 years of operation, the maintenance of the system at Sibratsgfäll was abandoned since a significant part of the cables had been cut due to large displacements.

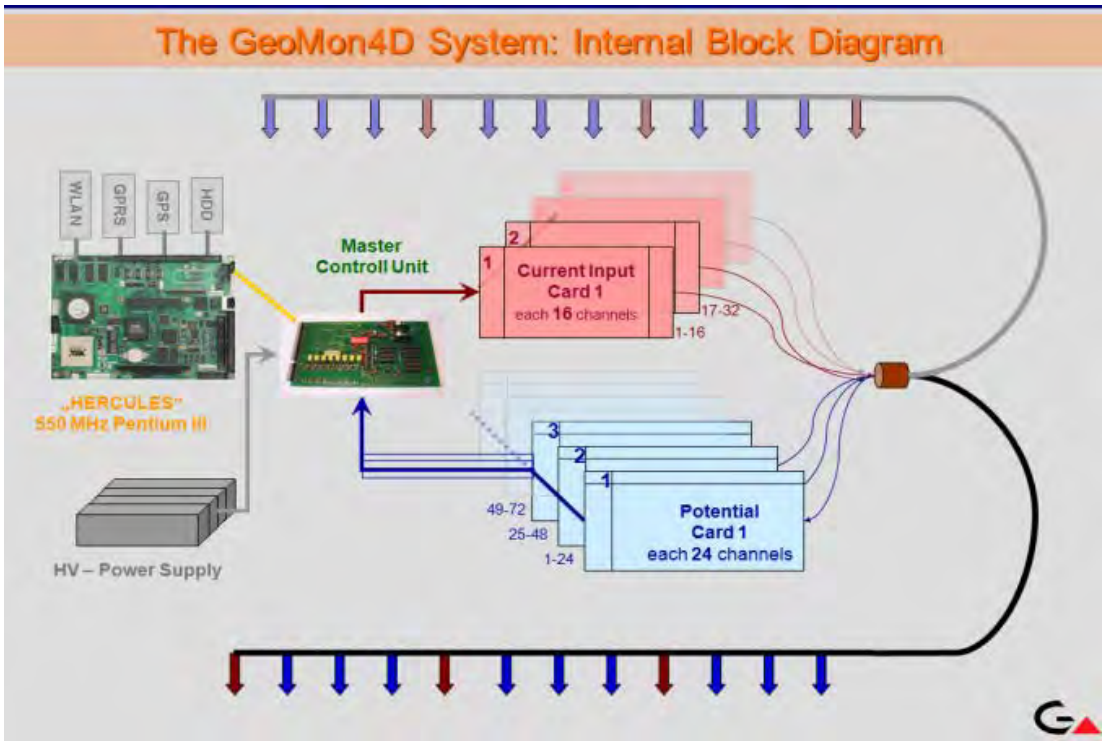

Fig. 1: Architecture of the GEOMON4D system.

The GEOMON 4D System

The GEOMON4D instrument, as it is today, is based on technically mature components and offers a completely open architecture, allowing installation of any number of current or potential electrodes by adding parallel or serial cards (cp. Fig. 1). The principal characteristics are the high speed of data acquisition (approx. 3000 measurements/hour in single channel mode) and recording of the full signal (usually 1000 samples per single configuration) for noise analysis and filtering.

Since the hydrological processes which could lead towards triggering of a landslide could be built up gradually or sudden, our monitoring system for surveillance of these processes is capable of surveying long period changes (within months; e.g. permafrost related phenomena) as well as short sudden impacts (within minutes or hours; e.g. strong rainfalls). It provides a point shot of the current status of the subsurface, which practically means, that data acquisition time has to be much less than the period of expected changes. The instrumentation provides high resolution data, by keeping the error of each single measurement low (e.g. by selecting only measurements with a low noise content for further processing) and by using many different electrode configurations, which visually means to “illuminate” each subsurface block from as many different direction as possible and to sample its ”shadow”. The data set produced shows a high reliability and is used as an additional tool for local authorities to decide about timely warning. The possibility of repeating the measurements at short time intervals allows verifying anomalous trends.

Most areas under observation are usually not easily accessible, but data sets have to be regularly processed. Therefore the possibility of remote maintenance and automatic data delivery by email is essential and consequently GPRS (General Packet Radio Service) data transfer was implemented. Maintenance can be performed fully remote-controlled and data (measurement

results, test sequences and log files, containing information about system and GPRS connection status) are sent automatically via email to the data processing centre. Consequently, immediate availability of information for local stakeholders can be guaranteed, which is very important in the case of sudden hazards like mud flows. The general layout of the remote control network is displayed in Figure 2.

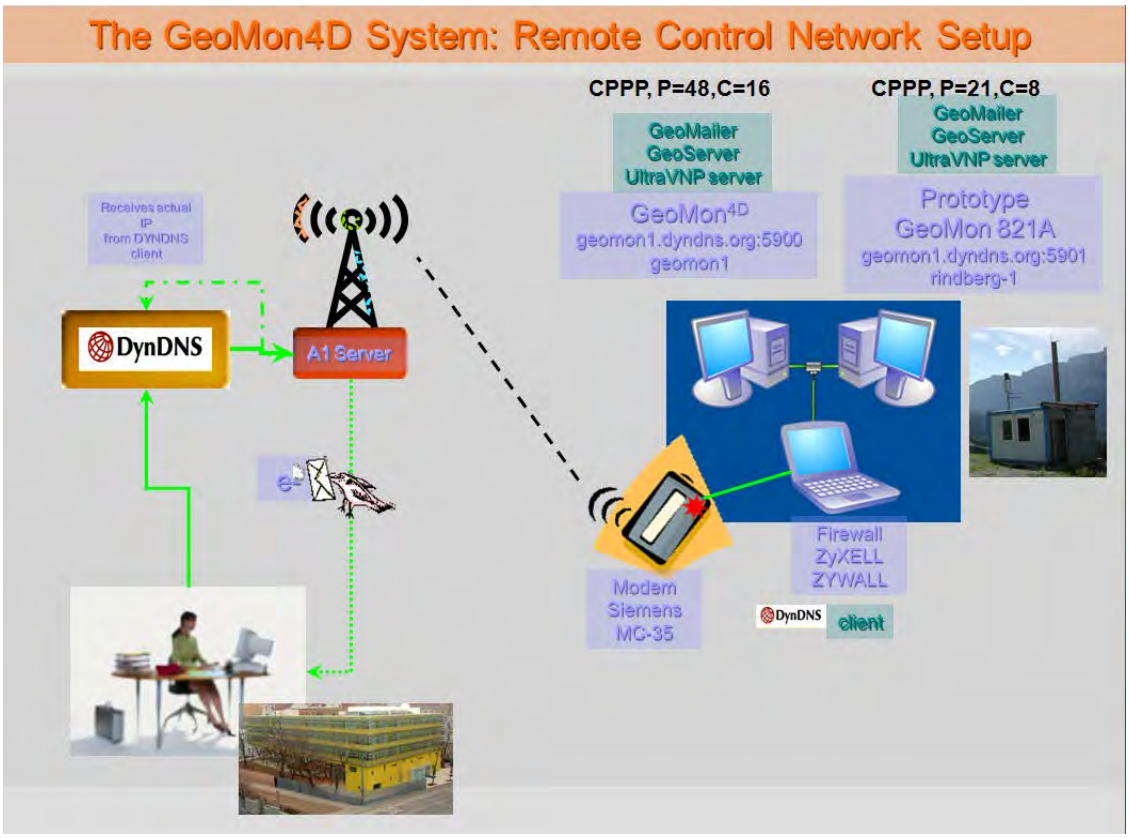

Fig. 2: Diagram explaining the setup of the remote control network.

Further Requirements

A big challenge in geoelectric monitoring is the assurance of power supply. To use the local power grid proved to be unreliable and very expensive (500 m cable cost about 14,000 Euro). Therefore, fuel cells were chosen for power supply, being less expensive, mobile (a fuel cell can be transported from an abandoned monitoring site to a new site), and very reliable. The fuel cell is driven by methanol, whereas the respective methanol tanks have to be changed about every 8 months.

Furthermore, the optimum way of installing the arrays (surface, trenches, different kinds of cables and connectors) was tested over years and a lightning protection device for multi-core cables had to be developed. It proved to be useful, in terms of persistence and maintenance, to dig cables and electrodes if this was possible.

The necessity to monitor landslide stability conditions has induced C.S.G. (Centro Servizi di Geoingegneria, Italy) to develop an innovative multiparametric monitoring system of stability called D.M.S. (patent pending and trade mark C.S.G. S.r.l.). This device measures with high accuracy and precision displacements in 2 or 3 directions (both horizontal and vertical at all the prefixed depths), piezometric water levels and soil temperature, thus allowing the complex

analysis of dynamics of any landslide, e.g. deformation analysis, movements, sliding surface's depths or piezometric variations (FOGLINO et. al., 2006). In late 2009, both innovative technologies (geoelectric monitoring and DMS) were coupled for the first time on the landslide of Gschliefgraben and they are operating since then without any failure.

Future Developments

Currently six Geomon4D instruments are operating simultaneously for monitoring purposes on different landslides in Austria, Italy and France and two instruments are permanently used by the staff of the Geological Survey of Austria for usual tomographic surveys. The results from our monitoring sites have shown that there is a critical lack of inversion routines that could handle permanent monitoring data. Some commercial codes (RES2DINV and AGI EearthImager) were tested but did only partially lead to satisfying results. Therefore future developments will focus on 4D Inversion (in cooperation with Jung-Ho KIM from KIGAM, Korea), data correlation and interpretation. At the end of 2012 a completely redesigned version of the Geomon4D system will be available incorporation all the experience gathered from the operation of the TEMPEL monitoring network between 2009 and 2012.

Acknowledgements

The development of the Geomon4D prototype system was financially supported by the Torrent and Avalanche Control (WLV), Section Vorarlberg, the county of Vorarlberg and internal funds of the Geological Survey of Austria in frame of the Bund-Bundesländer-Kooperation (project VC-07). Further developments were financed by internal funds of the Geological Survey of Austria and by funds coming from the 7th FP project "SafeLand – Living with the landslide risk in Europe" and from the project "TEMPEL - **Temp**oral changes of geo**el**ectrical properties as possible indicator of future failure of high risk landslides", funded by the Austrian Science Fund (FWF)-TRP 175-N21 in frame of the Translational Brainpower Program. Additional financial support was given by the Central Institute for Meteorology and Geodynamics (ZAMG) for developing the lightning protection. We acknowledge the support of A. Reiterer, Torrent and Avalanche Control (WLV), Section Vorarlberg, who had the idea to apply the geoelectrical technique for landslide monitoring and initiated the funding for the prototype system and G. Hübl, who shared our minds in the pioneer times of the Geomon4D.

References

FOGLINO, L., LOVISOLO, M. and DELLA GIUSTA, A., 2006: Contribution of DMS monitoring systems in the analysis of slide micro-movements for early warning management, risk assessment and evaluation of mitigating actions. – Geophysical Research Abstracts, Vol. 8, 06122, Vienna.

JARITZ, W., REITERER, A. and SUPPER, R., 2004: Landslide Rindberg (Vorarlberg): Multidiscipline Research. – Proceedings of the 10th Interpraevent Congress, Riva del Garda.

SUPPER, R. and RÖMER, A., 2003: New Achievements in Developing a High Speed Geoelectrical Monitoring System for Landslide Monitoring. – Proceedings of the Environmental and Engineering Geophysical Society, 9th Meeting Prag, Prag.

SUPPER, R., RÖMER, A. and JOCHUM, B., 2009: Geoelectrical measurements for natural hazard monitoring. – SEGJ 9th International Symposium, Extended Abstracts, Sapporo.

Effects of borehole design on complex electrical resistivity measurements

ANDREA TREICHEL[1], JOHAN A. HUISMAN[1], YULONG ZHAO[3], EGON ZIMMERMANN[3], ODILIA ESSER[1], ANDREAS KEMNA[2] and HARRY VEREECKEN[1]

[1] Agrosphere, IBG-3, Forschungszentrum Jülich, Germany.
[2] Department of Geodynamics and Geophysics, University of Bonn, Germany.
[3] Central Institute for Electronics, ZEL, Forschungszentrum Jülich, Germany.

a.treichel@fz-juelich.de

Abstract

Recent studies have shown that electrical resistivity measurement in boreholes can be influenced by the borehole design and the aquifer properties. It was found that large boreholes and aquifers with a large formation factor are particularly prone to erroneous resistivity measurements. However, effects of the borehole casing have not been considered yet. Within the context of the 4DEIT project, we have developed a broadband borehole Electrical Impedance Tomography (EIT) measurement system that enables complex electrical resistivity measurements of unprecedented accuracy. To support the interpretation of these borehole EIT measurements, the aim of this study is to investigate the effect of PVC borehole casing and the complex nature of the electrical conductivity on the EIT measurements. In order to do so, we used a 2D axisymmetrical finite element model that solves the Poisson equation. The borehole is located at the rotational axis and the 2D coordinates are the radius of the cylinder and the depth along the borehole. The finite element discretization consists of triangular elements which are smaller near the borehole. To get realistic values for the complex resistivity, we analyzed spectral induced polarization measurements made on aquifer material from the Krauthausen test site using Debye decomposition. The resulting complex resistivity values were implemented in our model together with an effective representation of the borehole casing that considers the resistivity of PVC and the slotted fraction. This model was then used to investigate the effect of borehole diameters, effective properties of the borehole casing, and the formation factor on the complex resistivity. To validate the simulations, we performed measurements in a water column. For this, a symmetrical rain barrel filled with tap water was used. It was concluded that the properties of the borehole casing have a large impact on the apparent resistivity when two current electrodes are situated in the same borehole.

Applications in Geothermal Monitoring

Geoelectrical monitoring of the geothermal field of Vulcano Island, 1999

An Example of Electrical Resistivity Tomography Monitoring in Geothermal Sites: Balçova-Izmir Case Study

MAHMUT G. DRAHOR[1, 2], MERIÇ A. BERGE[2], ÖZDE BAKAK[3] and CANER ÖZTÜRK[4]

[1] Dokuz Eylül University, Center for Near Surface Geophysics and Archeological Prospection (CNSGAP), Tinaztepe Campus, 35160 Buca-Izmir/Turkey.
[2] Dokuz Eylül University, Engineering Faculty, Department of Geophysics, Tinaztepe Campus, 35160 Buca-Izmir/Turkey.
[3] Dokuz Eylül University, The Graduate School of Natural and Applied Sciences, Department of Geothermal Energy, Tinaztepe Campus, 35160 Buca-Izmir/Turkey.
[4] GEOIM Engineering, Consulting, Software and Construction Ltd. 35070 Bornova-Izmir/Turkey.

goktug.drahor@deu.edu.tr

Abstract

In this study, the shallow fluid flow changes according to climatic effects on a geothermal site were investigated using electrical resistivity tomography method (ERT). Monitoring studies achieved by time lapse electrical resistivity tomography, which were the key studies to observe the subsurface resistivity distribution of the investigated lines. The studies were performed at Balçova geothermal site, in the city of İzmir-Turkey, which has been operating in house heating since 1990's. The main source of the groundwater in the area is rainfall. Our ERT monitoring studies were performed between March 2010 and February 2011. We aimed to obtain information on the shallow conductive layers that allow the transport of the fluids. Therefore, the investigations which will be succeeded on shallow aquifer system near the boreholes could be important to characterize the subsurface while the geothermal operations. In conclusion, monitoring studies showed that subsurface characteristics were importantly changed according to borehole operation and seasonality rainfall. Results were also supported with the synthetic forward modeling studies.

Introduction

The geophysical surveys have commonly been applied in the investigation of geothermal sites since 1960's. These surveys have an important role on the determination of reservoir characteristic and geological properties of the geothermal system. One of the objectives of geophysical surveys is to determine the location of faults carrying hot waters, reservoir characteristic, various physical changes in the system. On the basis of these results, the appropriate drillsite locations are determined and the time-related physical changes around the drillsites are controlled. In recent years, the combinations of geophysical methods have been utilized in the exploration of geothermal systems in the world.

Important information about a geothermal site is obtained by different geophysical investigation techniques such as electrical resistivity, self-potential, electromagnetic, magnetics, seismic, etc. Electrical and electromagnetic prospection of geophysics is the most powerful research techniques in geothermal investigations. Using these techniques, faults and fissures, reservoir

characteristics, altered and mineralized zones, the properties of geothermal fluids, the magma chamber locations and entire tectonic structures could be determined.

Recently, geophysical monitoring studies are of great importance in near surface geophysical applications. Many investigators gathered information about the temporal subsurface changes by using geophysical monitoring studies. These are very useful to define the permafrost environment, landslide, engineering, geothermal, hydrology, contamination and CO_2 monitoring investigations. In near surface applications of geophysics, the electrical resistivity tomography (ERT) monitoring studies have been progressively used recently. However, the geothermal application of ERT monitoring is rarely seen. This study aims to manifest the importance of ERT monitoring in near surface investigations of geothermal sites. Therefore we investigated a geothermal site that contains the shallow fluid flow by the ERT technique. Time lapse inversion was a key study to monitor the resistivity distribution under the measuring lines. In the modeling stage, inversion facilities were investigated by the simulation of a synthetic injection model. In the time lapse inversion process, the initial model approach was used to constrain the later time data sets.

Geothermal in Turkey

Neotectonic activity in Anatolia, Turkey, is mostly related to the northerly movement of the Arabian Plate towards the Eurasian Plate. The Anatolian Plate comprises many small fragments between seismically active fracture zones with numerous geothermal hot springs in the active areas (Figure 1a). On the basis of this tectonic framework, Turkey can be divided into four main geothermal regions (along the magmatic belts of western, eastern and central Anatolia and along the north Anatolian fault zone). The Büyük Menderes and Gediz grabens of western Anatolia tend to be important features from the geothermal viewpoint, with many hot water springs located along the fault zones of these grabens (DRAHOR and BERGE, 2006).

Turkey has extensive geothermal resources that have been utilized for heating of residences, power plant, greenhouse heating, and for spas. Since 2005 several new plants have been constructed. Four new binary units of about 8 MW each have been installed, three for exploiting medium enthalpy reservoir (two by Dora – MB group, in Aydın-Salavatlı area, and one by Tuzla – Dardanel Energy, at Çanakkale and one using the separated brine (140 ◦C)) from the Kızıldere plant, before its use for district heating, operated by Bereket. A new 47 MW double flash unit was commissioned in 2009 at Germencik with the possibility of a second 47 MW unit. It is one of the largest plants in Europe, just behind the Italian standard 60 MW units. Several additional areas have been allocated to private companies for further surface and deep exploration. Since 2005 an increase of about 70 MW in installed capacity has been achieved. The target for 2015 is about 200 MW. The geothermal potential of the country is estimated to be about 30,000 MW (MERTOĞLU et al., 2003; SERPEN et al., 2009).

Balçova Geothermal Site and Geology

ERT monitoring studies were performed on an important geothermal site found in the southern part of İzmir Bay. This area named Balçova geothermal system is about 20 km west of city of İzmir, and operated in heating by Balçova Termal Ltd since 1990's. Many injection and re-injection holes were drilled in the area during the operational processes. Approximately 50 wells have been drilled by the General Directorate of Mineral Research and Exploration of Turkey (MTA) both for developing and monitoring geothermal energy production (Figure 1b). The depths of the wells

vary from 100 m (shallow) to more than 2 km (deep). The first geophysical surveys in Turkey were carried out in this area in the mid of 1960's. These studies consist of electrical resistivity, self-potential (SP) and drilling. Later on, large scale SP studies (ERCAN et al., 1986) and resistivity and magnetotelluric soundings (MTA, 2001) were also applied.

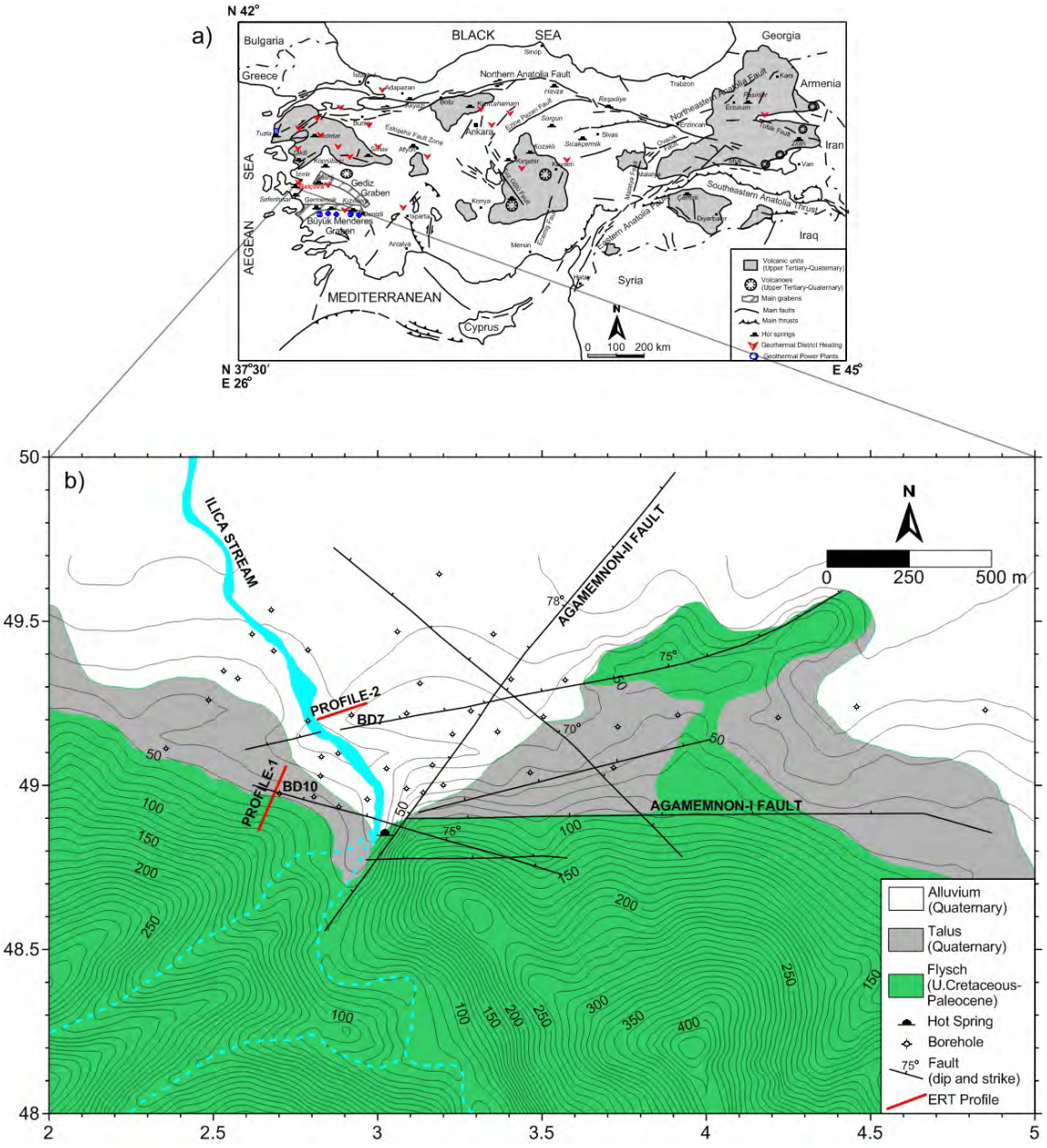

Fig. 1: a) Tectonic and geothermal activity map of Turkey (after ŞIMŞEK, 2001) and b) geological map of Balçova Geothermal Site (modified from YILMAZER, 1989 and AKSOY, 2001).

The area around the Balçova geothermal site consists of Alluvium, talus and Izmir flysch (Fig. 1b). Upper Cretaceous Izmir flysch consists of metasandstones, limestone, granodiorites, serpentinite-diabase, rhyolites and phyllites. Fractured metasandstones and fault zones existing in limestone and granodiorites are permeable. Other zones of the Izmir flysch formation can be thought as impermeable. Flysch formation exceeding 2000 m depth, occupies the most of the volume of the field. This formation has some fissures, fractures and faults and the permeability is appeared in these zones. Limestone and granodiorites have fractures and faults that create secondary

permeability. Serpentinite and rhyolites are thought as impermeable zones (SATMAN et al., 2001). Above the flysch formation alluvium and talus thickness of which change between 0 and 200 m take place. Although alluvium has some permeability, most parts of talus are impermeable. Alluvium existing over the field has good porosity and some permeability. Some shallow wells produce water mainly from this zone. Talus exists in southern part of the field in small amounts compared to area covered by alluvium (POLAT, 2010).

The thermal activity is manifested by hot springs that form mainly along the major fault systems in the area (EŞDER and ŞIMŞEK, 1975). As a result of intense graben tectonics, the aquifer of the geothermal system is controlled by dipping strike-slip and active normal faults (TEZCAN, 1966; YILMAZER, 1989).

There are two different aquifer systems in Balçova geothermal site. One of them is the hot water aquifer system found in the allochtonous limestone with Upper Cretaceous Age in the İzmir flysch formation. This formation is impermeable, and the hot waters in the aquifer are discharged by faults. The primary fault zone in the area is the Agamemnon-1 fault that cuts directly the aquifer system. The second aquifer has cold water found in the alluvium with Quaternary Age, and it is charged by surface waters. In the area, there are many water wells in the alluvium, their depths are changed 25-80 m generally. The water table is mostly changed between 11 and 20 m depths in the northern part of the area. Underwater flow direction is mainly from south to north direction (ERDOĞAN, 1990).

Our ERT monitoring studies were performed between March 2010 and February 2011. The investigations were continued along this period. We aimed to obtain the information on the difference of physical changes of shallow parts of aquifer zone in the geothermal system. These consist of fluid changes, environmental characteristics, temperature changing and re-injection process in the site. To reach this goal ERT monitoring study was preferred. ERT investigation was repeated over two lines during the different investigation periods (Figure 1b).

Synthetic Modelling Studies for Injection Model

To show the effectiveness of the ERT monitoring studies on geothermal applications, we generated a synthetic injection model using Res2Dmod software (Geotomo software). The forward and inversion modeling studies were performed during this study to determine the changes related with time. In the first stage, we carried out a forward modeling studies for various time scales (t = 0, 1, 2 and 3 unit; unit is equal to month for our problem). At first there is no any injection process in this model (t = 0). Five horizontal layers that show the alluvium in the area are extended to 50 m below. The resistivity and depth of horizontal layers are given in the figure as 250 Ωm-10 m, 150 Ωm-3 m, 75 Ωm-7 m, 25 Ωm-5 m and 15 Ωm-25 m respectively. The borehole resistivity is 200 Ωm and its thickness is 2 m, while the depth of borehole is extended to 20 m. The affected area from injection was considered as a conductive zone, and the resistivity of this zone was given as 2 Ωm in the model. Thus, the resistivity value of adjacent area of the borehole was reduced according to time of injection process (Figure 2). During the forward modeling stage we used 61 electrodes with 5 m interval. Data sets were produced for Wenner and Wenner-Schlumberger arrays. Therefore the synthetic apparent resistivity data were produced for various time periods (for before and after pumping periods; t = 0, 1, 2 and 3 unit). In the second stage, the inversion process was achieved to present the effects of temporal changes for various time slices. This stage was investigated in two different approximations; smoothness inversion and time-lapse smoothness inversion using Res2Dinv software. The time-lapse inversion of the data

sets was carried out using a joint inversion technique where the model obtained from the reference data set was used to constrain the inversion of the later time data sets (LOKE, 1999). Thus, reliability and resolution of the ERT method could be investigated by the modeling stage.

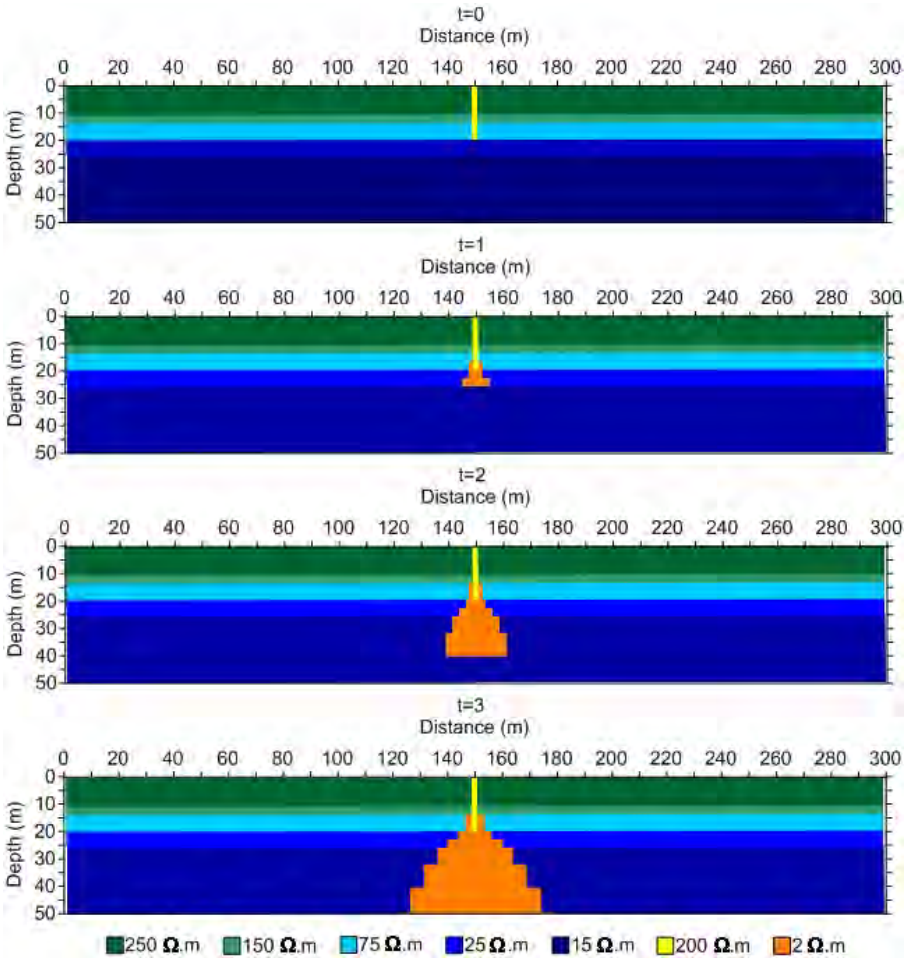

Fig. 2: Synthetic subsurface resistivity models for injection process related with different times (t = 0, 1, 2 and 3 unit; unit is equal to month for our problem).

Inversion results of injection model for different monitoring times are given in Figure 3 for Wenner and Wenner-Schlumberger arrays. These arrays produced close resistivity models to the synthetic injection models after the inversion. We can closely identify the subsurface resistivity values. Besides, after the t = 1 period, reduced resistivity zone clearly appeared on the inverted models. The changes caused by the injection process are appeared at the 20 m depth in both Figures 3a and 3b. Therefore, increasing in conductive zone is clearly seen in the inverted model sections. But, Wenner-Schlumberger array gives more reliable results than Wenner. The resistivity reducing effect is clearer under the borehole. In addition, we did not confirm the important changes between the standard and time lapse inversion models. Finally, we can clearly conclude that ERT is the useful technique to monitor the temporal changes in the subsurface according to the injection scenario. Also Wenner-Schlumberger configuration was given more reliable result than the Wenner array in the synthetic modeling stage.

Data Acquisition and Processing

To monitor the shallow changes near the boreholes, we selected two different investigation lines in Balçova site. The lines are represented in Figure 1b as profile 1 and 2. Profile 1 has almost north-south direction, while the profile 2 has almost east-west orientation. The lengths of profiles are 220 and 140 m for line 1 and 2 respectively. Profile 1 is located near the borehole-BD10, which is a re-injection hole. This borehole was used between beginning of October 2010 and the end of April 2011 as a re-injection well. Profile 2 is also located near the borehole BD-7, is a production well. This borehole did not work between April and September 2011. Overall 2D ERT data was collected by Wenner and Wenner-Schlumberger configurations along these two lines. During the measurements electrode intervals were selected as 5 m and data was collected for 8-10 levels. Before the interpretation, measured apparent resistivity data was processed by using 2D inversion technique (LOKE and BARKER, 1996; TRIPP et al., 1984; DEGROOT-HEDLIN and CONSTABLE, 1990; SASAKI, 1992). Res2Dinv software, which tries to optimize a starting subsurface model by minimizing the differences between the measured and calculated data, was used in this study. Finite-element method was used in the forward modeling to produce the calculated data. In the time lapse inversion scheme, one data set was selected as a base and inversion process was implemented on this data set. Then, obtained resistivity model was used as a starting model in the inversions of the consecutive data sets. The inversion models were obtained after 6 iterations.

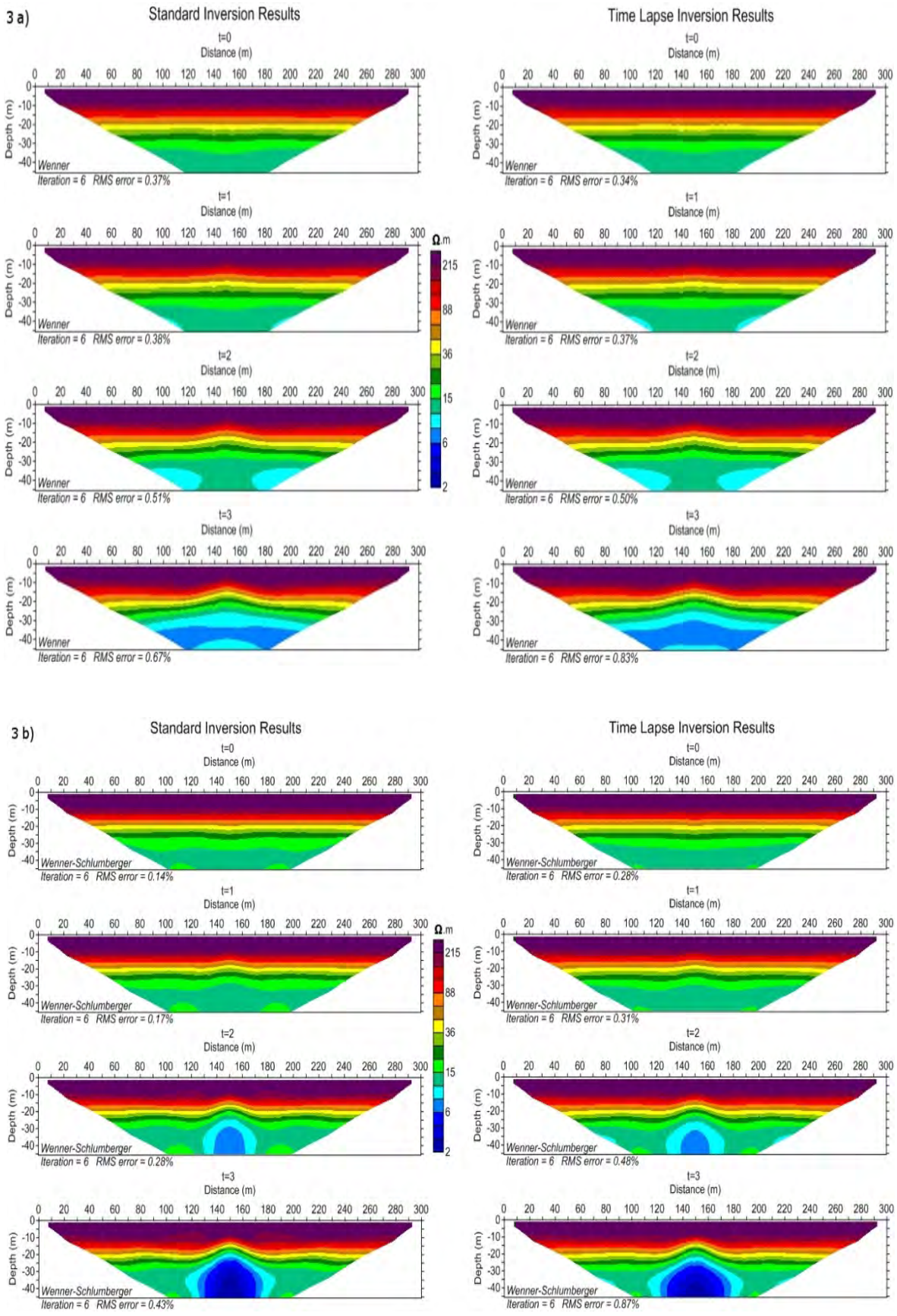

Fig. 3: 2D model sections obtained from the synthetic injection models; a) Wenner and b) Wenner-Schlumberger arrays.

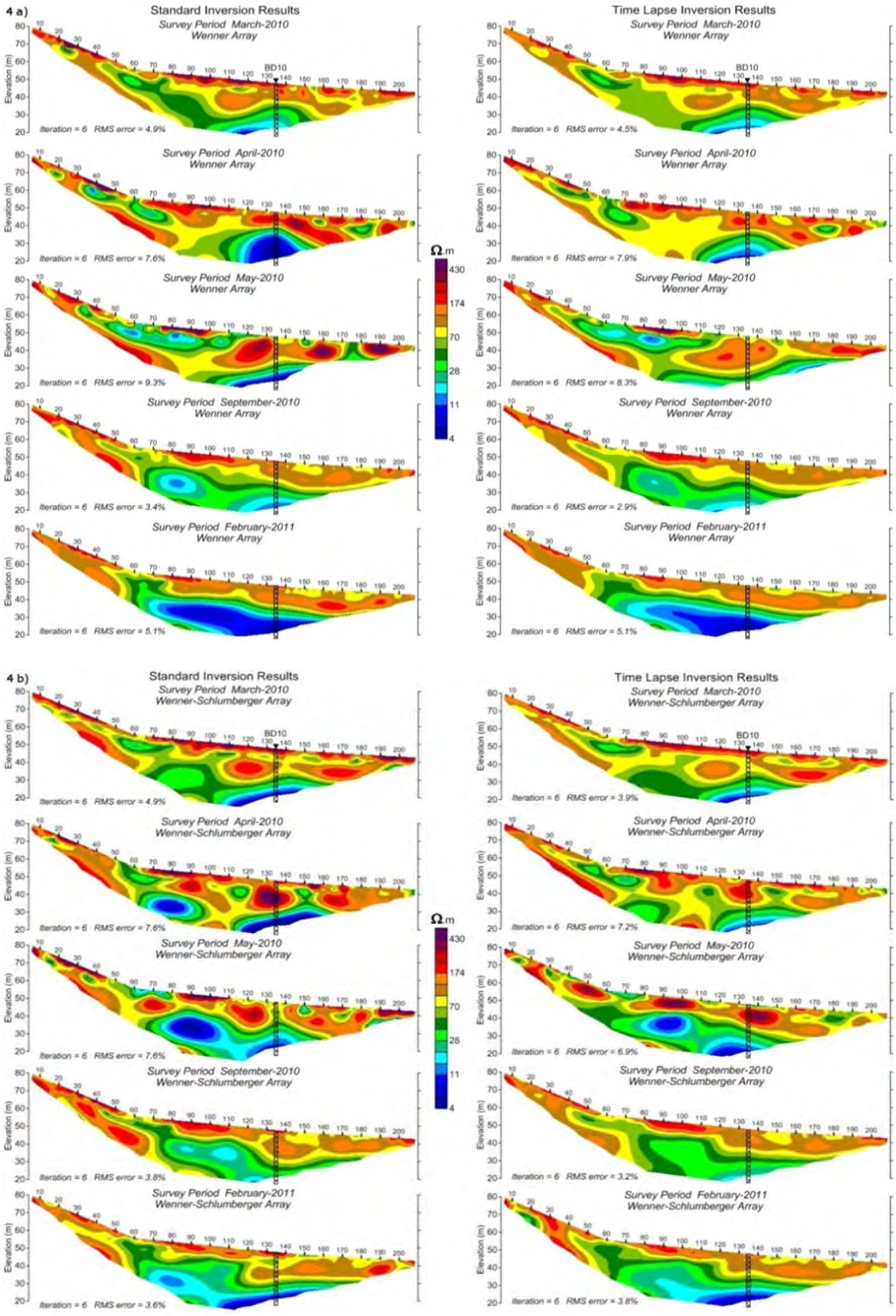

Fig. 4: 2D standard and time-lapse ERT model sections of Profile-1; a) Wenner and b) Wenner-Schlumberger arrays.

Interpretation

Standard and time-lapse inversion results of profile 1 are given in Figure 4. As can be seen from the figure, Wenner and Wenner-Schlumberger arrays are generally produced similar inversion models after six iterations for standard inversion approach. In all inverted resistivity sections, we can firstly observe resistive layers, which is almost 5m thickness. This layer has an interruption between 60-70 m of the line. This interruption could also be followed to the deeper part of the inversion models for all measuring periods. Therefore, we think that it could be a fault zones (possibly Agamemnon-1 fault given in Figure 1b). According to geologists, this fault has almost vertical angle. We know that this kind of fault zones that have extremely fracture and fissure properties might be recharge passages in the porous and permeable environments. Therefore, the groundwater streaming from the surface or the reservoir can be transported inside these zones. The section obtained from March 2010 data shows that the conductive zone is almost displayed in proximity of borehole-BD10. Overall model sections have closely similarity for standard and time-lapse inversion results. The conductive zones are importantly changed during the monitoring periods. The conductive zone is enlarged in the results of April 2010 data for standard inversion sections. But there is no any important change in time-lapse models of April 2010. This situation depends on the selected initial inversion model in time-lapse approximation. The conductive zone is increased in the results of Wenner-Schlumberger of May 2010 data, while it decreases in the results of Wenner configuration of May 2010 data. In September 2010 result, all sections are very similar to each other (for standard and time-lapse results). After the yearly period, the results obtained February 2011 data are partially resembled again the first model (March 2010). However, the conductive zone in the deeper part of the sections is still enlarged in whole sections both standard and time-lapse inversion. Therefore, we can determine that the important changes are formed by the climatic effects (rainfall, etc.), fault recharges and production process, which is valid the re-injection operation for this line due to the BD-10 re-injection well.

Profile-2 has almost a flat topography and lie near the borehole-BD7, which is a production well. The production was not made between April and September 2010 due to the moderate and hot weather conditions. All inversion sections show the horizontal layering model, which is used during the synthetic modeling stage (Figure 5). Resistive strata (>150 Ωm) are almost horizontal and extended 10 and 15 m below from the surface. Conductive strata are located under this zone, and their average resistivity is about 15 Ωm. High conductivity in the deeper part of the sections is commonly observed in the results of March and April 2010. The harmony between used configurations is very good in all sections. In addition, the results of standard and time-lapse inversion are very compatible. As a result, we can say that the climatic conditions in this profile could be affected the resistivity changes in the subsurface more than the production process.

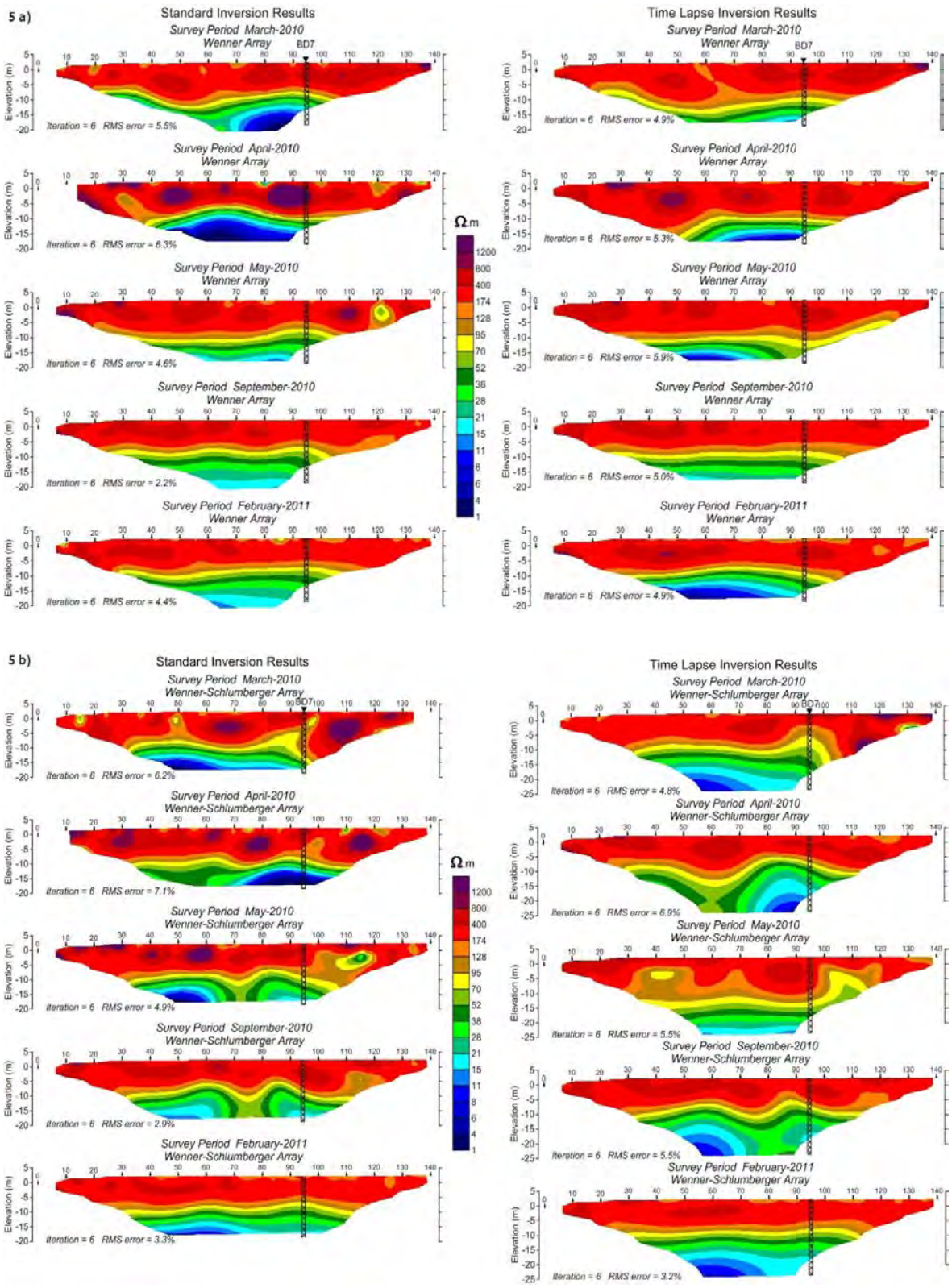

Fig. 5: 2D standard and time-lapse ERT model sections of Profile-2; a) Wenner and b) Wenner-Schlumberger arrays.

Conclusion

The results of shallow ERT monitoring studies in Balçova geothermal site indicated that the used method was very useful to investigate the changing of different physical characteristics of shallow

parts in a geothermal system. Particularly, the determination of these changes can be very important to determine the liquid runaways during the production stage. Therefore we can say that operational processes make an impact on physical alterations resulting together with the changes on the shallow subsurface characteristics. But, it should not be forgotten that the climatic effects such as rainfall and rapid daily temperature changes could be very important in the changes of resistivity in near surface investigations. Therefore, the rainfall and temperature records should be compared with the inversion results to achieve more interpretive results.

Time-lapse inversion results give us more interpretive results than the standard inversion approximation for both synthetic and field studies. But we can determine that the identification of initial model is also important to constrain the later time data sets. In addition, this study showed that the selection of configuration type is essential to obtain more interpretive results. Thus, various configurations should be tested to confirm the suitable configuration for this problem.

Overall results presented that ERT monitoring gives us very informative results on the determination of changes of subsurface characteristics during the operations. Therefore, we can observe the noticeable near surface changes depending on the operation processes in an operated site.

As a result, operating system of geothermal companies could be run more efficiently by the help of geophysical monitoring studies.

References

AKSOY, N., 2001: Balçova-Narlıdere jeotermal sisteminin izleyiciler ile incelenmesi. – PhD Thesis, Dokuz Eylül University, Izmir, Turkey.

DE GROOT-HEDLIN, C. and CONSTABLE, S., 1990: Occam's inversion to generate smooth, two-dimensional models from magnetotelluric data. – Geophysics, **55**, 1613-1624.

DRAHOR, M.G. and BERGE, M.A., 2006: Geophysical investigations of the Seferihisar geothermal area, Western Anatolia, Turkey. – Geothermics, **35**, 302-320.

ERCAN, A.Ö., DRAHOR, M.G. and ATASOY, E., 1986: Natural polarization studies at Balçova geothermal field. – Geophysical Prospecting, **34**, 475-491.

ERDOĞAN, B., 1990: İzmir-Ankara Zonu'nun, İzmir ile Seferihisar arasındaki bölgede stratigrafik özellikleri ve tektonik evrimi. – TJK Bülteni, **2**, 1-20.

EŞDER, T. and ŞIMŞEK, Ş., 1975: Izmir Seferihisar alanı Çubukludağ grabeni ile dolayının jeolojisi ve jeotermal olanakları. – MTA report, Ankara.

LOKE, M.H., 1999: Time-lapse resistivity imaging inversion. – Proceedings of the 5th Meeting of the Environmental and Engineering Geophysical Society European Section, Em1.

LOKE, M.H. and BARKER, R.D., 1996: Rapid least-squares inversion of apparent resistivity pseudosections by a quasi-Newton method. – Geophysical Prospecting, **44**, 131-152.

MERTOĞLU, O., BAKIR, N. and KAYA, T., 2003: Geothermal Application Experiences in Turkey. – Proceedings of the European Geothermal Conference, Szeged, Hungary.

MTA, 2001: Balçova jeotermal alanı (İzmir Çeşme otobanı kuzeyi) jeoermal enerji arama projesi jeofizik etüdü raporu. Ankara, Turkey.

POLAT, C., 2010: Numerical modeling of Balçova Geothermal Field. – Msc thesis, Middle East Technical University, Ankara, Turkey.

SASAKI, Y., 1992: Resolution of resistivity tomography inferred from numerical simulation. – Geophysical Prospecting, **40**, 453-463.

SATMAN, A., SERPEN, U. and ONUR, M., 2001: Reservoir and production performance of Izmir Balcova-Narlidere geothermal field. – Report for Izmir City Council, Istanbul.

ŞIMŞEK, Ş. 2001: An overview of geothermal developments in Turkey. – Proc. ITIT Symposium on Geothermal in Asia, Tokyo, Japan, 17-23.

SERPEN, U., AKSOY, N., ONGUR, T., YUCEL, M. and KAYAN, I., 2009: Geoscientific investigations on north of Balçova geothermal system in Turkey. – International Journal of Geology, **3**, 87-96.

TEZCAN, K., 1966: İzmir Agamemnon jeofizik etüdlerinin jeotermik enerji bakımından değerlendirilmesi. – MTA report, İzmir

TRIPP, A.C., HOHMANN, G.W. and SWIFT, C.M. Jr., 1984: Two-dimensional resistivity inversion. – Geophysics, **49**, 1708-1717.

YILMAZER, S., 1989: Geochemical features of Balçova Hot Springs and geothermal energy possibilities for the area. – PhD Thesis, Akdeniz University, Isparta, Turkey.

Comparison of temperature estimates from heat transport model and electric resistivity tomography during a shallow heat injection and storage experiment

THOMAS HERMANS[1, 2], MOUBARAK DAOUDI[1], ALEXANDER VANDENBOHEDE[3], TANGUY ROBERT[1], DAVID CATERINA[1, 2] and FRÉDÉRIC NGUYEN[1]

[1] University of Liège, Belgium, ArGEnCo, GEO³, Applied Geophysics.
[2] F.R.S.-FNRS, Belgium.
[3] Ghent University, Belgium, Department of Geology and Soil Science, Research Unit Groundwater Modeling.

thomas.hermans@ulg.ac.be

Abstract

Groundwater resources are increasingly used around the world as geothermal systems. Understanding physical processes and quantification of parameters determining heat transport in porous media is therefore important. Geophysical methods may be useful in order to yield additional information with greater coverage than conventional wells. We report a heat transport study during a shallow heat injection and storage field test. Heated water (about 50°C) was injected for 6 days at the rate of 80 l/h in a 10.5°C aquifer. Since bulk electric resistivity variations can bring important information on temperature changes in aquifers (water electric conductivity increases about 2%/°C around 25°C), we monitored the test with surface electric resistivity tomography and demonstrate its ability to monitor spatially temperature variations. Time-lapse electric images clearly show the decrease and then the increase in bulk electric resistivity of the plume of heated water, during respectively the injection and the storage phase. This information enabled to calibrate the conceptual flow and heat model used to simulate the test. Inverted resistivity values are validated with borehole electromagnetic measurements (EM39) and are in agreement with the temperature logs used to calibrate the parameters of the thermo-hydrogeological model for the injection phase. The short term evolution of the ERT-derived temperature and the temperature logs is coherent for both a qualitative and quantitative use of ERT-derived temperature. However, the mid- and long-term evolution need to account for other phenomena such as variations of TDS content as a function of temperature to quantitatively use ERT estimates as temperature proxy. This field work demonstrates that surface electric resistivity tomography can monitor heat injection and storage experiments in shallow aquifers. These results could potentially lead to a number of practical applications, such as the monitoring or the design of shallow geothermal systems or the use of heated water to replace salt water in tracer tests.

Introduction

The production of geothermal energy is increasingly growing worldwide. Groundwater, through the use of geothermal heat pumps, accounts for a major part in the thermal energy use and installed capacity (LUND, 2010).

Geothermal energy does not rely only on high temperature and deep systems. Indeed, very low temperature systems (<30°C) are much more easily accessible, relatively abundant in alluvial or coastal plains for example, involve lower implementation costs and may be used for cooling or heating (ALLEN and MILENIC, 2003).

To design and exploit geothermal energy systems through pumping or storage of water, engineers must estimate the parameters governing heat transport processes. These are mainly heat capacity and thermal conductivity of fluid and solid. Engineers generally rely on standard calculation charts, which may not be representative of *in situ* conditions, such as the influence of the soil/rock, the well and the fluid, or on thermal response tests in wells, which deliver only well-centered information (similar to pumping tests). In this context, electric resistivity tomography (ERT) can bring relevant spatial and temporal information through the correlation between temperature and bulk electric resistivity changes with a greater coverage than single wells for *in situ* studies. In analogy to salt tracer tests regularly performed in the field of hydrogeophysics, one can monitor temperature variations of aquifers and exploit their effect on electric conductivity (PTAK et al., 2004; HERMANS et al., 2012).

In this paper, we extended the work of VANDENBOHEDE et al. (2011) and HERMANS et al. (2012) who monitored a heated water injection test with ERT and showed that ERT-derived temperatures could reproduce qualitatively and quantitatively temperatures obtained with a calibrated thermo-hydrogeological model. However, in this first test, only the injection phase was monitored. Here, we look at the possibility of monitoring the storage phase with ERT. Heated water (about 50°C) was injected for 6 days at the rate of 80 l/h in a 10.5°C aquifer and the storage phase was monitored for ten days.

First, we will review the site-specific petrophysical relationships and briefly present the study site. Then, the results of the injection test will be presented. After that, we will present the results of the storage phase and highlight the challenges associated with it. Finally, we will draw conclusions.

Petrophysics

In the range of temperature considered in this test (10 to 50°C), a linear dependence between water electric conductivity and temperature can be assumed (HAYLEY et al., 2007; HERMANS et al., 2012)

$$\frac{\sigma_T}{\sigma_{25}} = m(T - 25) + 1 \tag{1}$$

where σ_T is the water electric conductivity at temperature *T* (in °C) and m is the fractional change in electric conductivity per degree Celsius. The value of m can be experimentally determined and is equal to 0.02125 in this specific case (HERMANS et al., 2012).

A similar relationship can be used to model surface conductivity. However, in our case, the experiment took place in a sandy aquifer free of clays. Even if silica grains have a surface conductivity, it is in our case three orders of magnitude below water electric conductivity and was thus neglected (REVIL and LINDE, 2006 ; HERMANS et al., 2012).

Using Archie's law, the link between bulk electric conductivity and temperature is therefore straightforward. Indeed, if surface conductivity is neglected, the ratio of Archie's law between two time-steps enables to deduce the water electric conductivity ratio

$$\frac{\sigma_{b2}}{\sigma_{b1}} = \frac{\sigma_{w2}}{\sigma_{w1}} \quad (2)$$

where σ_b is the bulk electric conductivity and σ_w is the water electric conductivity. In equation 2, σ_{b1}, σ_{b2} and σ_{w1} are known from ERT measurements for the first two parameters and from well water samples for the latest. Finally, using equation 1, the temperature of water can be easily deduced.

Study site

The field experiments took place on the campus De Sterre of Ghent University, Belgium. The subsurface is composed of two layers. The upper layer lies from 0 to -4.4 m and corresponds to homogeneous Quaternary fine sands. From -2 m down to -4.4 m, these sands are found at saturation. Below -4.4 m, a clay layer of Tertiary age is found, forming a low permeability layer. The injecting well was drilled down to -4.4 m; it is made of a PVC casing with a screen of 90 cm at the bottom of the Quaternary layer. The temperature in the aquifer was 10.5°C.

Injection phase (HERMANS et al., 2012)

A first test was done in February 2010 to monitor the injection during 3 days of heated water (48°C) into the 10.5°C aquifer. During this test, tap water was used for injection. However, tap water and formation water do not have the same electric conductivity, which are 374 and 676 µS/cm at 10.5°C respectively. Consequently, the increase in conductivity with temperature was partly counterbalanced by the lower conductivity of injection water.

An additional step was thus necessary to derive temperatures from ERT measurements. We had to calculate with a flow and transport model the water electric conductivity distribution resulting from the injection of less conductive water and to use the corresponding σ_{25} value in equation 1 instead of using the reference value from formation water (HERMANS et al., 2012).

This process led to Fig. 1 where temperatures from calibrated modeling and ERT after 3 days of injection are compared. Temperatures monitored with ERT are quite consistent with the thermo-hydrogeological model after 72h. The maximum temperature deduced from ERT is 45°C which is only 3°C below the mean temperature of injection. The width and thickness of the plume are also satisfactory. The enlargement of the plume can be easily explained by the smoothness constraint used to regularize the model differences in the inversion process. Nevertheless, it is in part counterbalanced by the spatial distribution of the proportion of tap and formation water obtained from hydrogeological simulations. More details can be found in HERMANS et al. (2012).

Storage phase

During the first test, the aim was to see if ERT measurements were able to predict temperatures in the aquifer. In a second attempt, we tried to extend the process to the storage phase of the experiment and to avoid the step of flow modeling to predict temperatures. Due to logistic constraints, it was not possible to inject formation water directly. So, we decided to inject cold tap water in the well during two weeks to have a bell of injected water around the well before the beginning of injection of heated water. This also enables a larger contrast in terms of electric conductivity. In addition, we extended the injection of heated water to 6 days. We used a dipole-

dipole configuration with an electrode spacing of 60cm to reach the targeted depth of investigation (3 to 4.5m). Reciprocal measurements were taken for each time-step to assess the level noise and data were weighted accordingly during the inversion. Specific considerations about the noise level were presented in NGUYEN et al. (2011).

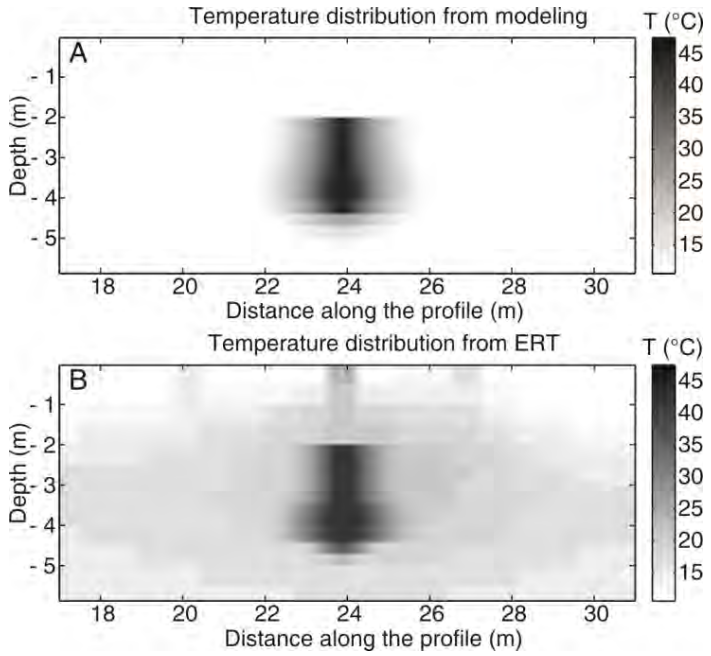

Fig. 1: Petrophysical laws enabled to transform resistivity values into temperatures. The plume detected after 3 days of injection with ERT (B) is in accordance with the plume calculated with a calibrated thermo-hydrogeological model (A), (HERMANS et al., 2012).

During the storage phase, ERT is able to highlight the decrease in temperature of injected water, which corresponds to a decrease in the resistivity anomaly. The decrease in resistivity is maximum at the end of injection; then, it tends progressively to zero. Fig. 2 shows this anomaly after 4 days (A) and 9 days (B) of cooling. At this time, a decrease in resistivity of -20% compared to the background is still visible. The plume is enlarged due to the smoothing effect of the regularization. In this case, the effect would be also visible in an ERT-derived temperature section (in contrast with Fig. 1), because the effect is not counterbalanced by the contrast of conductivity between formation and injection water. Note also the increase of resistivity in the upper part of the image, due to the desaturation of the unsaturated area which was almost saturated for the background due to a rainfall event.

We validated the obtained resistivity values with borehole measurements. We performed electromagnetic measurements in the well with an EM39 device to obtain a conductivity log (Fig. 3A). The results are very similar four days after the end of injection, which proves that ERT is a reliable tool to predict electric conductivity.

However, when we look at the correspondence with temperature logs (Figs. 3B and 3C), we see that the results are much worse than in Fig. 1. Since electric conductivity seems to be correctly resolved, we assume that the discrepancy results from the transformation of electric conductivity to temperatures. Fig. 2A is taken 10 days after the beginning of injection, compared to 3 days for Fig. 1. Some other phenomena may be responsible for a change in electric conductivity other than

the temperature effect for mid- and long-term sections. These could be related to modifications of the TDS content related with absorption/desorption or dissolution/precipitation phenomena that are both affected by temperatures since most chemical constants are temperature dependent. An effect of diffusion between formation and injection water is also possible since a concentration gradient exists.

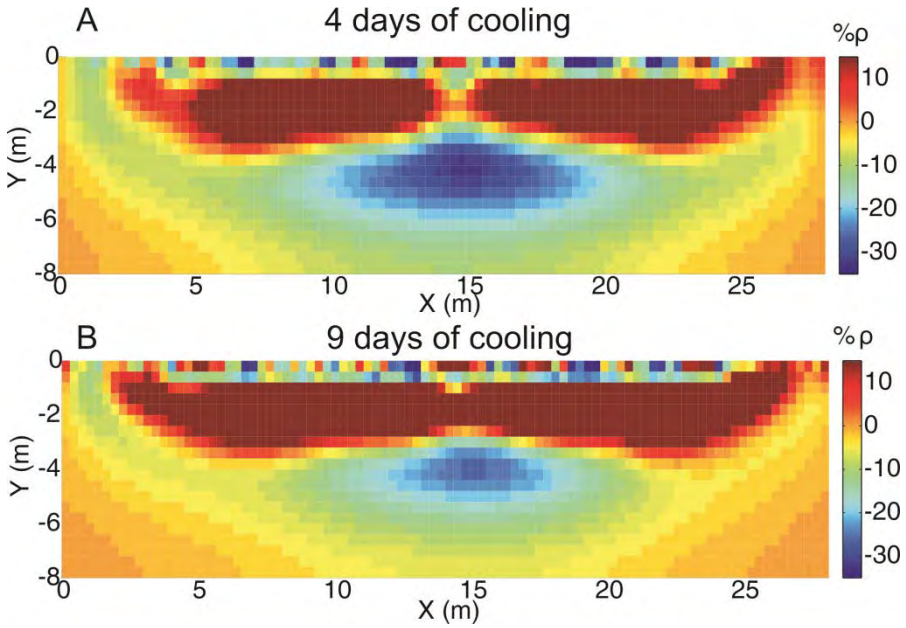

Fig. 2: ERT time-lapse images show, as expected, a decrease of the resistivity anomaly during the cooling phase between 4 (A) and 9 (B) days of cooling. In the upper part of the model, an increase in resistivity due to a change of saturation in the unsaturated zone related to changing weather conditions (for the background, the soil was almost saturated due to strong precipitations) is also visible.

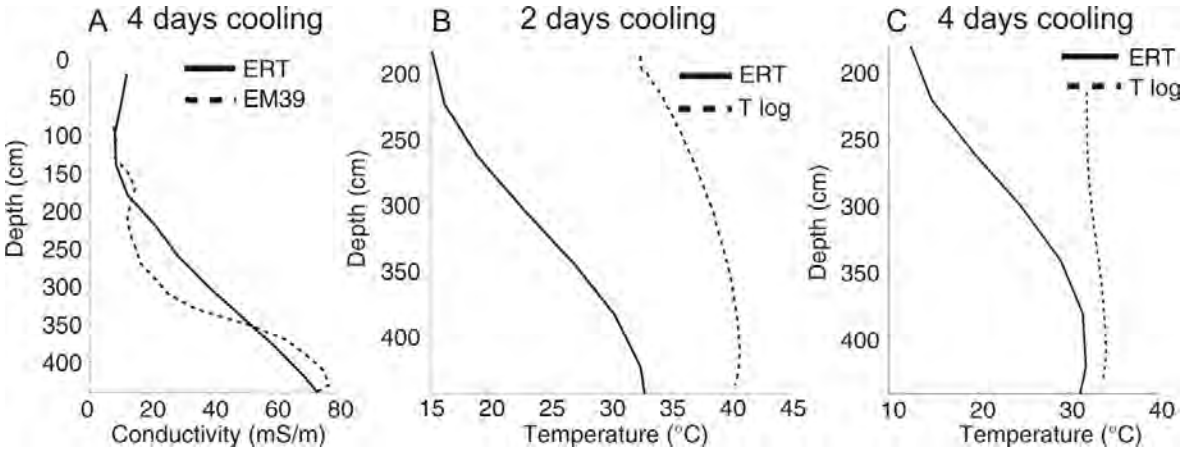

Fig. 3: ERT measurements were validated using EM39 measurements (A). In the zone of injection, ERT is really closed to EM39 data. Once transformed in temperatures, we observe a gap between ERT and temperatures logs after both 2 days (B) and 4 days of cooling (C). Since, this gap was not observed for the injection phase (Fig. 1), a more complex petrophysical relationship may be necessary to understand the phenomenon.

Conclusion

This work demonstrates the ability of ERT to monitor qualitatively and quantitatively shallow geothermal tests. If the injection of tap water can be a drawback since it can reduce the measured contrast, combined with a flow and transport model, it enables to improve the estimation of temperatures in the aquifer. This injection scheme could be use in combination with traditional pumping and tracer tests to derive in a first step hydraulic conductivity and dispersivity, and in a second step, thermal properties. Coupled inversions could also be developed to avoid the regularization step of ERT inversions.

If we consider an electrode spacing *a* of 60cm, we can deduce guidelines for further studies, since we imaged successfully a plume of heated water at a depth of 5*a*, a thickness of 4*a* and a width of 5*a* with a dipole-dipole configuration (a = 3 and n ≤ 13).

Laboratory measurements must be performed to further study the complex effect of temperature on the electric conductivity of water for mid- and long-term experiments, including potential changes related to dissolution and absorption phenomena.

Our approach should in time contribute to the development of *in situ* techniques to characterize groundwater and porous matrix properties governing heat transfer in the subsurface and to monitor shallow geothermal resources exploitation. It could also contribute to the development of techniques of thermal tracers, when salt tracers are not allowed.

References

ALLEN, A. and MILENIC, D., 2003: Low-enthalpy geothermal energy resources from groundwater in fluvioglacial gravels of buried valleys. – Applied Energy, **74**, 9-19.

HAYLEY, K., BENTLEY, L.R., GHARIBI, M. and NIGHTINGALE, M., 2007: Low temperature dependence of electrical resistivity: Implications for near surface geophysical monitoring. – Geophysical research letters, **34**, L18402.

HERMANS, T., VANDENBOHEDE, A., LEBBE, L. and NGUYEN, F., 2012: A shallow geothermal experiment in a sandy aquifer monitored using electric resistivity tomography. – Geophysics, **77**(1), B11-B21.

LUND, J.W., 2010: Direct utilization of geothermal energy. – Energies, **3**, 1443-1471.

NGUYEN, F., KEMNA, A., ROBERT, T., HERMANS, T., CATERINA, D. and FLORES-OROZCO, A., 2011: Inversion of multi-temporal geoelectrical data sets: insights from several case studies. – GELMON, 1st International Workshop on Geoelectrical Monitoring, Vienna, Austria, December 1st.

PTAK, T., PIEPENBRINK, M. and MARTAC, E., 2004: Tracer tests for the investigation of heterogeneous porous media and stochastic modeling of flow and transport-a review of some recent developments. – Journal of Hydrology, **294**, 122-163.

REVIL, A. and LINDE, N., 2006: Chemico-electrochemical coupling in microporous media. – Journal of colloid and interface science, **302**, 682-694.

VANDENBOHEDE, A., HERMANS, T., NGUYEN, F. and LEBBE, L., 2011: Shallow heat injection and storage experiment: heat transport simulation and sensitivity analysis. – Journal of hydrology, **409**, 262-272.

Applications in Permafrost Monitoring

Installation of Geoelectrical Monitoring System at Kitzsteinhorn 2011, picture by D. Ottowitz

Electrical resistivity monitoring for the detection of changes in mountain permafrost at different time scales

CHRISTOF KNEISEL[1], TOBIAS RÖDDER[1], NILS ROTH[1] and DANIEL SCHWINDT[1]

[1] Institute of Geography and Geology, University of Würzburg, Am Hubland, D-97074 Würzburg, Germany.

kneisel@uni-wuerzburg.de

Introduction

Permafrost is thermally defined as subsurface material that remains below the freezing point for at least two consecutive years. The presence of moisture in the subsurface of alpine environments thereby leads to permafrost consisting of a variable content of ice, liquid water, air and subsurface material. Geophysical methods have been widely used to characterise areas of perennially frozen ground and locate massive ice. Permafrost problems resolvable by geophysical techniques include the assessment of spatio-temporal changes in subsurface geophysical properties due to permafrost cooling, warming, aggradation or degradation through geophysical monitoring (KNEISEL et al., 2008). Due to the great sensitivity of electrical resistivity to the transition from unfrozen to frozen materials, electrical resistivity measurements constitute one of the standard geophysical methods in permafrost investigation (KNEISEL and HAUCK, 2008). With a repetition of electrical resistivity measurements along the same profile temporal changes within the subsurface can be investigated. Degradation or aggradation of ground ice in areas with permafrost takes place at different time scales and includes short-term (daily to weekly), medium-term (seasonal) and long-term (annual to decadal) changes. In recent years, electrical resistivity monitoring approaches have been able to detect temporal variations in frozen ground (KNEISEL, 2006, 2010; HILBICH et al., 2008, 2011; ROTH, 2011) and frozen rock walls (KRAUTBLATTER, 2010), respectively. In this contribution we present data and results from three alpine sites with different permafrost characteristics. Changes in frozen ground conditions are derived from electrical resistivity monitoring data with different temporal resolution and thus enable the investigation of time-dependent processes.

Study areas

All three investigation sites are located in the Upper Engadin, an inner-alpine dry valley in the south-eastern Swiss Alps. Comparatively low precipitation and high incoming radiation do not allow for a pronounced glaciation, but enable permafrost to exist at higher altitudes (>2500 m a.s.l.) and sporadically even below the timberline. Within the north-west exposed glacier forefield at Val Muragl (2700 m a.s.l.) electrical resistivity measurements have been conducted annually during snow free months to assess the year-to-year variability in active layer thickness and permafrost conditions. A fixed electrode array was installed at a supercooled scree slope at Val Susauna (1665 m a.s.l.) to detect changes in resistivity pattern with higher temporal resolution. Between 2008 and 2011 measurements have been conducted in a 6-8 week interval.

In March 2011 an automated monitoring system with daily resolution was installed at a small rock glacier (2680 m a.s.l.) in the Murtèl/Corvatsch area to increase the process understanding within the active layer during snowmelt.

Technical details and data acquisition

Basic information on array type, instrumentation, period of data acquisition and the total length of the data record is summarized in Table 1. Three different array types are used depending on the intended horizontal/vertical resolution and the surface conditions.

Some data sets had to be omitted due to erroneous values, which were in most cases caused by difficult contact resistance during winter. Problems with the communication between the automated monitoring system and the computer at Murtèl hindered the data transfer for several days.

	Val Muragl	**Val Susauna**	**Murtèl/Corvatsch**
Altitude [m a.s.l.]	2700	1665	2680
Morphology/Substrate	glacier forefield, medium to fine grained till	talus slope, wooded, thick moss/humus cover	small rock glacier, coarse debris
Instrumentation	Syscal Junior Switch, Iris Instruments	Syscal Junior Switch, Iris Instruments	Geotom-Res-IP, Geolog
Array length [m]	35, 70	105	70
No. of electrodes	36	36	36
Electrode spacing [m]	1, 2	3	2
Array types measured	Wenner/Wenner-Schlumberger	Wenner/Dipole-Dipole	Wenner/Wenner-Schlumberger
No. of measurements	25	26	59/46
Period of data acquisition	snow-free months	year-around, 6-8 week interval	March-June 2011, almost daily
Data record	2005-2010	2008-2011	2011

Tab. 1: Key information on electrical resistivity monitoring setups and measurements.

Results

The multiannual development of frozen ground with electrical resistivity tomograms of a 35 m profile in the Val Muragl is shown in Figure 1. There is a clear trend towards absolute resistivity changes in the center of the high-resistivity anomaly (Fig. 1a). The 4-years period shows a decrease of resistivity in the order of 15-20 % within the permafrost body (Fig. 1b). Much more variation, however, can be observed in the resistivity distribution within the uppermost 5 m (active layer). In this zone, the impact of the existent moisture conditions during the time of data acquisition is evident. Time-lapse inversion shows variations in ground resistivity, reaching relative changes as high as +/- 45 %. However, the yellowish colors of the active layer (<5 kΩm) indicate non-frozen conditions and the absolute changes in resistivity values are rather small (1-2 kΩm). So far, no deepening of the active layer has been observed, while absolute values within the permafrost body dropped from 24 kΩm to 19 kΩm.

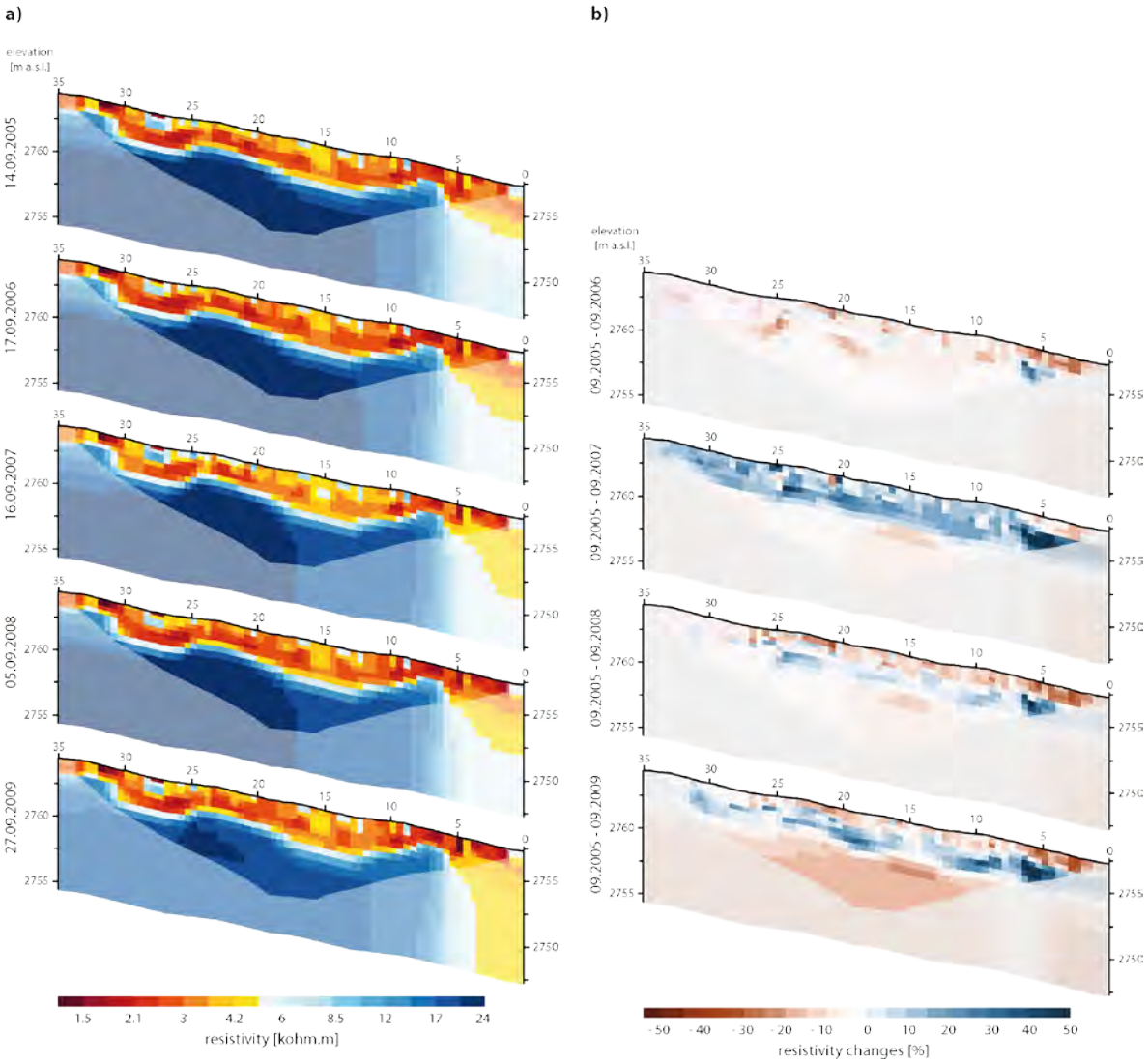

Fig. 1: a) Multiannual resistivity distribution (2005-2009) within the glacier forefield Muragl measured at the end of the thawing period. b) Time-lapse tomograms showing changes in resistivity related to the initial conditions in 2005. Parts of the geological model that are not constrained by data are faded, as done for the following figures.

Figure 2a shows the development of resistivity values within a talus slope with permafrost (Val Susauna) throughout the seasons. In summer and autumn 2009, an anomaly is visible in the bottom half of the slope with highest resistivity values of 100 kΩm in August, which are decreasing towards 80 kΩm in October. Resistivity values in the surrounding material increase between the two measurements. A marked increase – as seen in the central time-lapse tomogram (Fig. 2b) – occurred during winter leading to resistivity values as high as 900 kΩm in March 2010, which is attributed to a drastic reduction in liquid water content. In July 2010 the resistivity distribution resembles the initial situation the year before. The uppermost 2-3 m, representing the active layer, are well below 15 kΩm. However, values within the active layer as well as inside the anomaly at the foot of the slope are still higher compared to the autumn measurement.

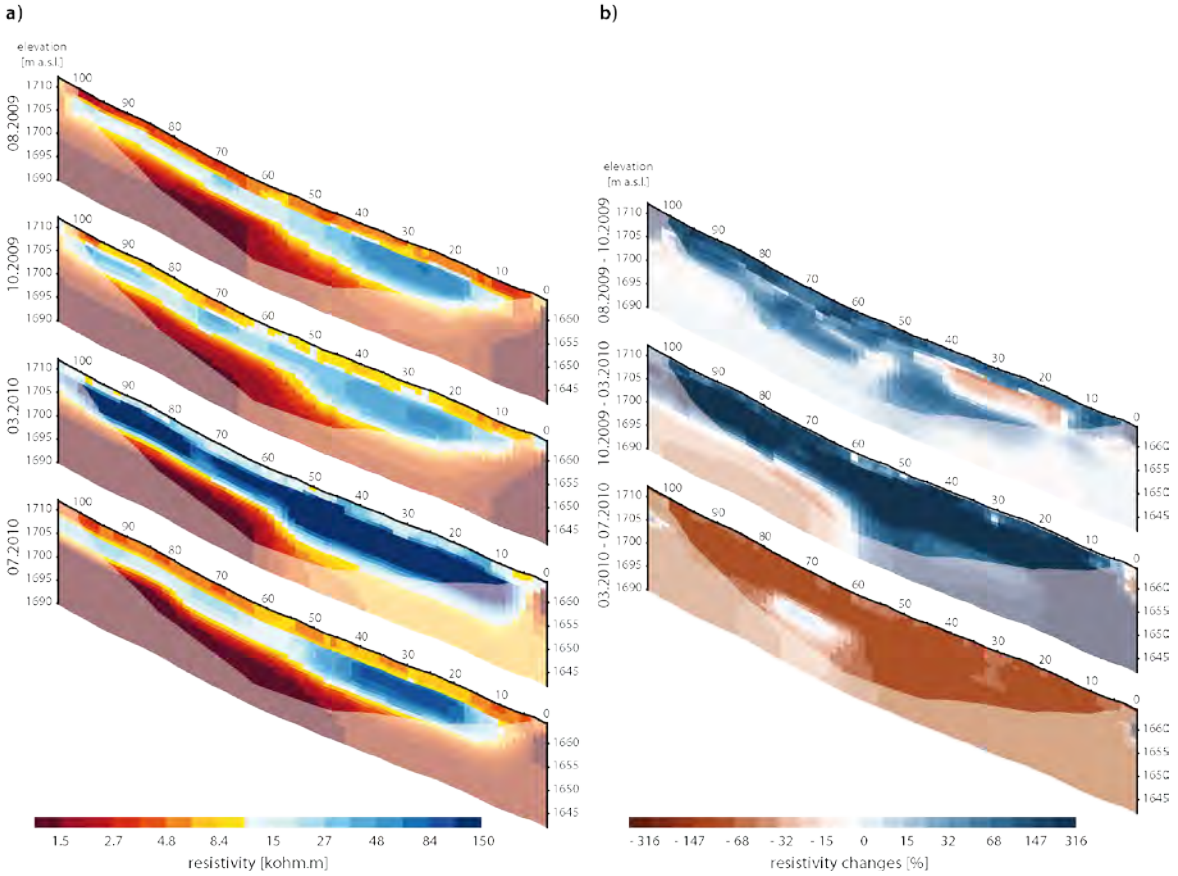

Fig. 2: a) Subsurface resistivity distribution within the talus slope in Val Susauna between August 2009 and July 2010. Color transition from yellow to blue refers to the presence of frozen ground with increasing resistivity values. b) Resistivity changes (time-lapse) between two succeeding measurements.

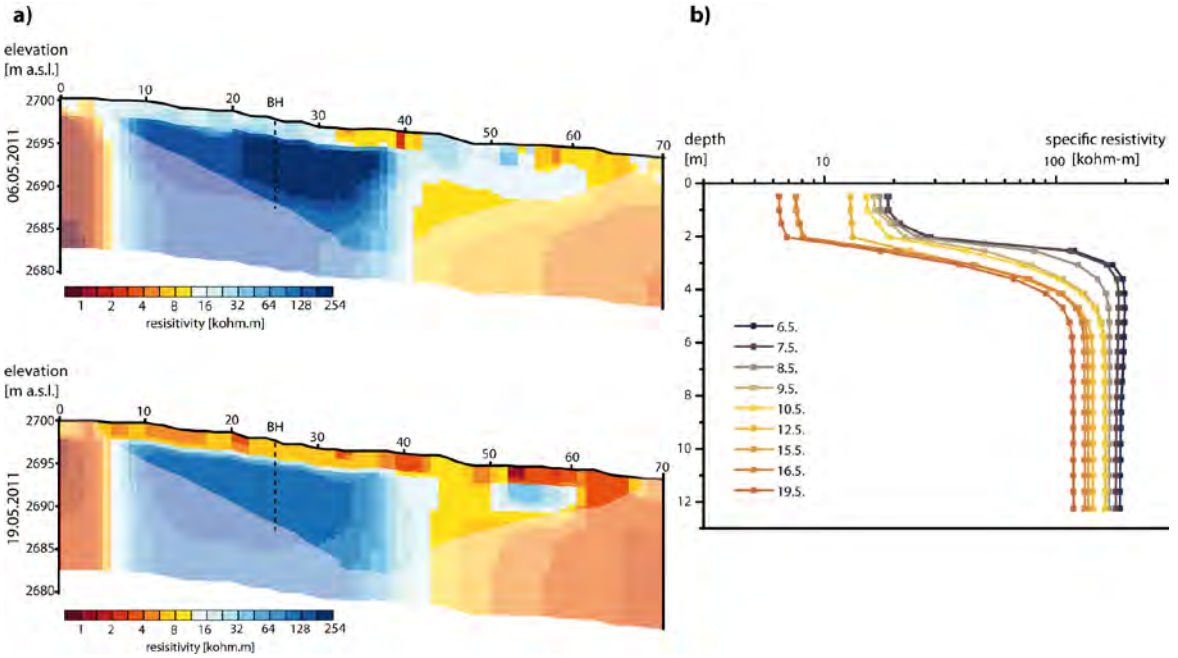

Fig. 3: a) Resistivity values on 06.05. and 19.05.2011 at monitoring Murtèl. b) Virtual borehole at horizontal distance 25 m indicating resistivity distribution with depth for nine consecutive measurements.

Resistivity changes on shorter time scales are resolved with the automated monitoring at the Murtèl site. The two tomograms in figure 3 highlight the resistivity distribution at the beginning and the end of a two week period, respectively. On the right hand side (Fig. 3b), resistivity values of each single data set obtained within this period is plotted as virtual borehole at horizontal position 25 m, i.e. in the centre of the high-resistivity anomaly. The largest absolute reduction of ground resistivity with up to 100 kΩm is observed below a depth of 3 m. However, values around 100 kΩm are still indicative for permafrost conditions. In contrast, the uppermost layer shows the largest relative decrease in resistivity. The lowering near the surface down to 2 m depth – from about 20 kΩm to 3 kΩm – coincides with the onset of the snowmelt and percolating melt water at that site.

Discussion and Conclusion

The use of geoelectrical monitoring systems allows for the investigation of changes and processes that occur within mountain permafrost environments over different time scales. Varying the frequency of measurements, enhances the interpretability of permafrost-related problems such as seasonal and long-term permafrost evolution but also the effect of percolating water. The operation of automated monitoring systems marks a further step towards a very efficient observation of short-time processes within the active layer and the frozen ground below. Nevertheless, repeated measurements with a larger interval are necessary and useful for the investigation of seasonal and annual changes of permafrost conditions in terms of degradation and aggradation processes and resultant consequences for sediment storage/supply as well as environmental changes. It has to be noted, that the resistivity distribution, especially near the surface and within the active layer, depends on a large extent on the meteorological conditions prior to the measurement and prevailing moisture conditions (e.g. HILBICH et al., 2011). Using a fixed monitoring setup simplifies a regular implementation of the measurement, even though it has to be done manually. However, the installation allows for a perennial accessibility of the investigated site.

The example from Val Susauna with maximum resistivity values, ranging between 80 kΩm in autumn and >900 kΩm in March, shows the high temporal variability in subsurface conditions during a year of measurements. Extremely increasing subsurface resistivities during winter mark an immense cooling with a decrease in the liquid water content. In spring, percolating melt water refreezes on the supercooled talus material, leading to an increase in ice volume accompanied by rising temperatures due to the release of latent heat during the freezing process. As a consequence, the liquid water content is increased leading to a distinct decrease in resistivity values of the permafrost body between March and July. The large range in resistivity values is caused by a thermal-driven circulation within the talus slope (Chimney-effect, e.g. HARRIS and PEDERSEN, 1998) which is responsible for the seasonal cycle of massive ice growth and degradation throughout the year.

A more detailed understanding of the processes that occur at short time scales within permafrost-affected landforms was gained with an automated monitoring system. It is shown from the Murtèl data that the onset of snowmelt and subsequent infiltration of water coincides with a reduction of active layer resistivity of about 700% within two weeks. Inside the permafrost body, absolute values also decrease (around 100 kΩm). However, they are still indicative for frozen ground conditions.

The application of ERT monitoring systems on different time scales has significantly enhanced the understanding of permafrost related problems. Especially the introduction of automatic monitoring systems, allowing for data acquisition with a high temporal resolution, marks a further step in permafrost research. Problems that arise with the use of the fixed and automated monitoring system are related to damage of the electrode array (broken contacts to the electrodes over time), moisture within the plug and interrupted power supply (data gaps due to power failure at the remote laptop).

Acknowledgements

The authors gratefully acknowledge the German Research Foundation (DFG) for financial support of the project 'Spatial assessment of permafrost characteristics and dynamics in alpine periglacial environments' (KN542/8-1) within the project cluster 'Sensitivity of Permafrost to Climate Change'. The study about permafrost below the timberline was supported by a personal grant (D. Schwindt) from the "Bayerische Graduiertenförderung nach dem Bayerischen Eliteförderungsgesetz" (BayEFG).

References

HARRIS, S.A. and PEDERSEN, D.E., 1998: Thermal regimes beneath coarse blocky materials. – Permafrost and Periglacial Processes, **9**, 107-120.

HILBICH, C., HAUCK, C., HOELZLE, M., SCHERLER, M., SCHUDEL, L., VÖLKSCH, I., VONDER MÜHLL, D. and MÄUSBACHER, R., 2008: Monitoring mountain permafrost evolution using electrical resistivity tomography: A 7-year study of seasonal, annual, and long-term variations at Schilthorn, Swiss Alps. – Journal of Geophysical Research, **113**, F01S90, doi: 10.1029/2007JF000799.

HILBICH, C., FUSS, C. and HAUCK, C., 2011: Automated time-lapse ERT for improved process analysis and monitoring of frozen ground. – Permafrost and Periglacial Processes, **22***,* 306-319.

KNEISEL, C., 2006: Assessment of subsurface lithology in mountain environments using 2D resistivity imaging. – Geomorphology, **80***,* 32-44.

KNEISEL, C., 2010: The nature and dynamics of frozen ground in alpine and subarctic periglacial environments. – The Holocene, **20***,* 423-445.

KNEISEL, C. and HAUCK, C., 2008: Electrical methods. – In: HAUCK, C. and KNEISEL, C. (Eds.): Applied geophysics in periglacial environments. – Cambridge University Press, Cambridge, 1-27.

KNEISEL, C., HAUCK, C., FORTIER, R. and MOORMAN, B. 2008: Advances in geophysical methods for permafrost investigations. – Permafrost and Periglacial Processes, **19**(2)*,* 157-178.

KRAUTBLATTER, M., 2010: Patterns of multiannual aggradation of permafrost in rock walls with and without hydraulic interconnectivity (Steintälli, Valley of Zermatt, Swiss Alps). – In: OTTO, J.C. and DIKAU, R. (Eds.): Landform – Structure, Evolution, Process Control. – 199-219, Berlin – Heidelberg, Springer.

ROTH, N., 2011: Widerstands-Temperatur-Monitoring und thermal-offset Studien im alpinen Permafrost. Val Muragl/Oberengadin, Schweiz. – Unveröffentlichte Examensarbeit, Universität Würzburg.

Permafrost monitoring at Mölltaler Glacier and Magnetköpfl

DAVID OTTOWITZ[1], BIRGIT JOCHUM[1], ROBERT SUPPER[1], ALEXANDER RÖMER[1], STEFAN PFEILER[1] and MARKUS KEUSCHNIG[2, 3]

[1] Department of Geophysics, Geological Survey of Austria, Neulinggasse 38, 1030 Wien.
[2] University of Salzburg / Department of Geography and Geology / Research Group Geomorphology and Environmental Systems.
[3] AlpS - Centre for Climate Change Adaptation Technologies, Innsbruck, Austria.

david.ottowitz@geologie.ac.at

Introduction

Changes of climate parameters due to global warming generate increased permafrost warming and deglaciation in alpine regions. These processes are mainly responsible for an increasing rock fall activity and decreasing slope stability in these areas. Consequently permafrost thawing will produce serious environmental and engineering problems, which can also affect regions below the permafrost (e.g. large rock falls). As details about the underlying processes are still not fully understood it seems to be an interesting field of research. Especially geoelectric monitoring could be a promising method to analyse melting and freezing processes of the shallow subsurface and the status of the permafrost at deeper areas, because of the large resistivity contrast between frozen and melted soil or rock.

The application of the geoelectric method for permafrost investigations is reported by many authors, e.g. HAUCK, 2002; HAUCK and VONDER MÜHLL, 2003; KNEISEL, 2004; MARESCOT et al., 2003.

The activities in permafrost regions of the Department of Geophysics of the Geological Survey of Austria started in the year 2006 with the installation of a first geoelectric test profile equipped with the GEOMON^{4D} (SUPPER and RÖMER, 2003) on the summit of the Sonnblick Mountain (3106 m a.m.s.l.). The very special conditions at this location lead to several problems in data acquisition which result in a discontinuous data set. Additionally the quality of the collected data was unsatisfying due to the impact of various steel installations in the summit area of the mountain. Nevertheless the gain in experience for the operation of a monitoring system at these high alpine conditions was invaluable. All further improvements of the monitoring system for permafrost measurements are based on this knowledge.

Technological developments

The resistivity of frozen soil can reach values of several hundred kOhmm. Commercial geoelectric systems and also our GEOMON^{4D} system are not constructed to deal with these high resistivities. The main problem is the unrestricted current injection which leads to potential differences that are out of the system range (+/- 10 V for the GEOMON^{4D} system). Theoretical calculations of the potential difference for a specific injection current in a high resistivity environment (homogeneous halfspace) using a simple Wenner configuration show the importance of the input current reduction. Fig. 1 shows calculated potential differences related to subsurface resistivity for a constant input current of 10 mA.

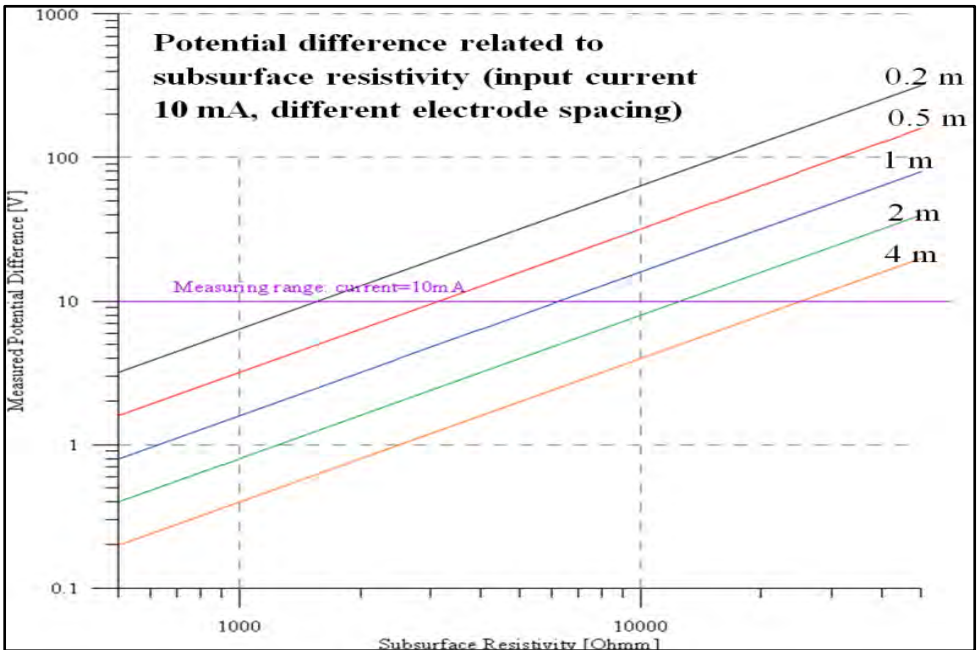

Fig. 1: Theoretical calculation of potential differences for a constant input current using a Wenner configuration with different electrode spacing.

The purple line represents the maximum input voltage of our monitoring system so that the intersection with the calculated potential differences defines the highest subsurface resistivity at which a reliable measurement can be achieved. Fig. 1 shows clearly that with the given input current, which is already quite low, it could be even for the largest considered electrode spacing difficult to perform measurements at permafrost conditions, where we expect resistivities higher than 50 kΩm. Based on these theoretical considerations we adapted the power supply of the GEOMON^{4D} to this special demand, changing it from a constant output voltage (48 – 391 V for common applications) to a constant output current (2 – 20 mA) balanced at a level which takes into account the maximum input voltage of +/- 10 V. This adaption ensures reliable measurements at subsurface resistivities up to several hundred kOhmm. Although it is a feasible solution to force the potential differences within the measuring range of the system, it should be considered to enlarge this range in future to improve the data quality, which is in most cases directly dependent on the amount of injected current.

Our experience from the test measurements on the Sonnblick showed that it is essential to use a lightning protection to fuse the device from overvoltage occurring along the monitoring profile. The sources for the appearance of this overvoltage are still not completely clear but the fact that damages to the system occurred especially during summertime indicates a clear correlation to thunderstorms. The used lightning protection cannot resist voltages which would occur in the very unlikely case of direct lightning strike to the monitoring profile, but it is very effective for the more likely case of a lightning event in the surrounding area with corresponding high potential differences in the subsurface. However, the implementation of the lightning protection results in clear reduction of maintenance work involving damages of electronic components of the device.

The areas of interest for permafrost monitoring are placed in high alpine areas, so in most cases there is no connection to the power grid. Even though we had this opportunity at the test site on

the Sonnblick (connection to the power grid of the meteorological observatory) it turned out as a disadvantage, because the measurements were disturbed by various installations in the surrounding of the building. Consequently it is necessary to use an independent power supply. We solved this problem with a fuel cell system (Fig. 2), consisting of the fuel cell SFC Efoy Pro© 600 with a charging capacity of 600 Wh/day and a current of 1 A, which is connected to 72 Ah batteries. The system includes two methanol canisters with a total capacity of 56 l and a GSM modem for remote control.

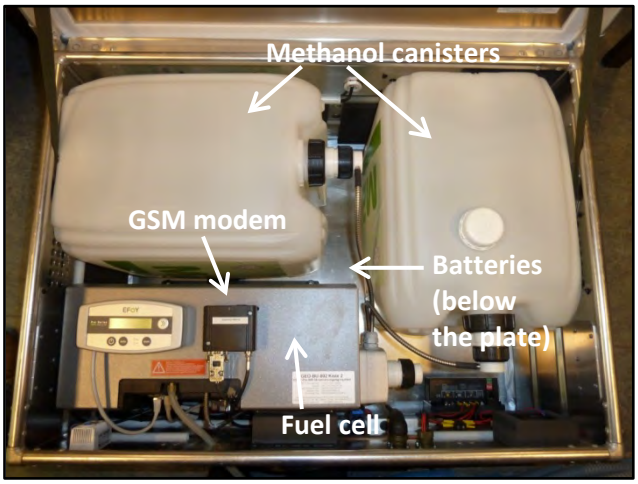

Fig. 2: The used fuel cell system.

Our experience at the monitoring site Mölltaler Glacier (2750 m a.m.s.l.) showed that it is very reliable even at extreme conditions during wintertime. The low fuel consumption (depending on the measurement activity and temperature conditions) allowed a maintenance free operation for about 8 months.

Monitoring site Mölltaler Glacier

This monitoring site is placed within the Mölltaller Glacier skiing area (Carinthia) on a plateau at an altitude of about 2750 m a.m.s.l. close to the mountain station of the “Eissee” cable car (see Fig. 3). There were several reasons why we chose this area for our investigations. First of all it is very easy accessible due to the well-developed infrastructure of the skiing area and secondly it is near to the Sonnblick mountain (about 5 km linear distance), where we have access to soil temperature data.

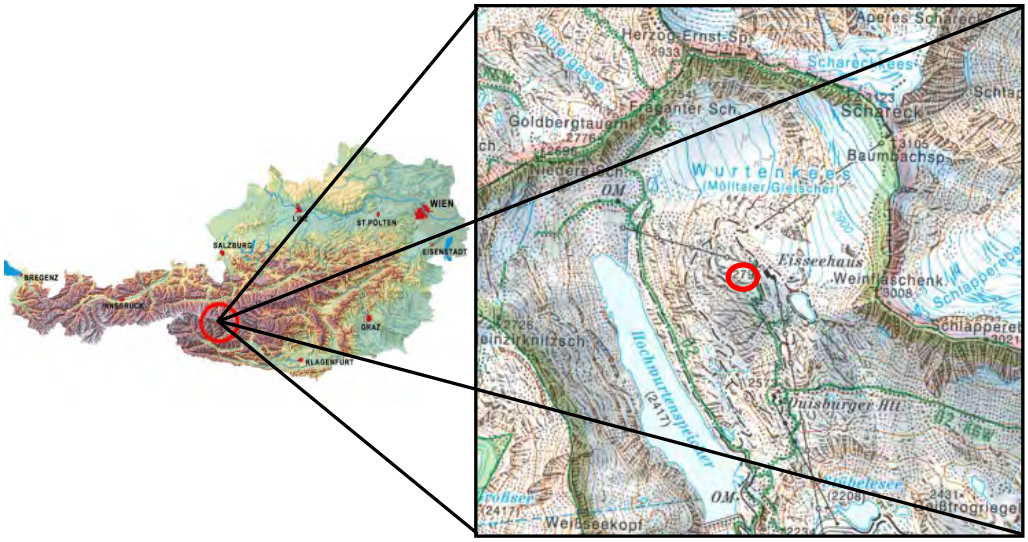

Fig. 3: Location of the monitoring site (indicated by a red circle).

The geoelectric profile was installed in NW – SE direction and it was equipped with the adapted GEOMON^{4D} powered by a fuel cell system (see previous section). The profile consists of 81 electrodes with a spacing of 1 m. The maximum depth of investigation for this configuration is about 15 m. The system started its operation on the 28th of September 2010. The measurement, a gradient array containing 2590 data points, is executed automatically once a day and the data is sent the following day by e-mail to the office in Vienna. The data processing which is partly performed automatically is split in two different parts. The output of the first part is a large number of apparent resistivity time series of different electrode combinations. This data is plotted and compared to the soil temperature data from the Sonnblick observatory. The second part of the data processing consists of the data inversion and produces 2D resistivity models of the subsurface.

Fig. 4 shows two examples for the comparison between time series of soil temperature and relative apparent resistivity for electrode combinations which are related to different depths of penetration.

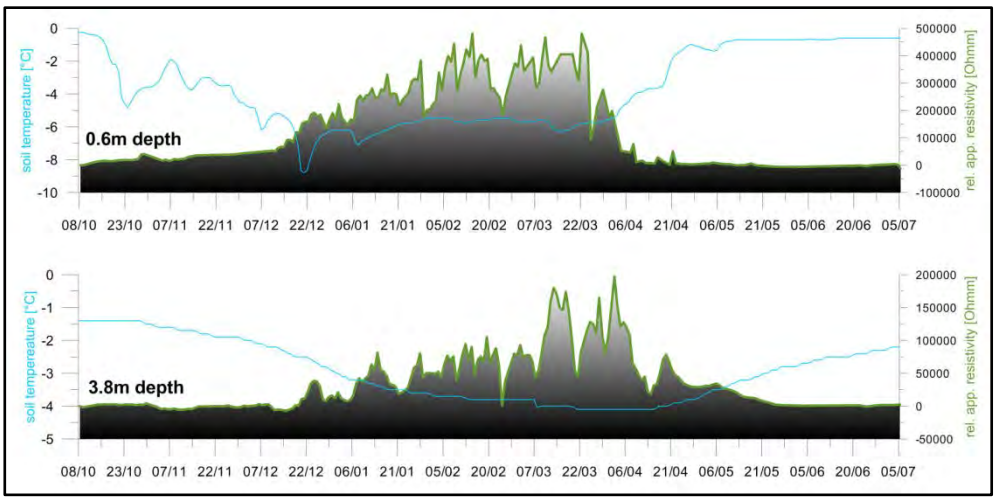

Fig. 4: Comparison between relative apparent resistivity and soil temperature for two different depths.

In both examples there is a clear correlation between low soil temperatures and very high apparent resistivities. Apart from the fact that we have different ranges of soil temperature at these two depths there is a clear time shift in areas with lowest temperatures and highest resistivities as well. This is caused by the behaviour of the temperature wave travelling through the subsurface. Although this example shows a nice correlation between soil temperature and apparent resistivity the interpretation has to stay on a quantitative level, because of the strong dependence of soil temperature on local conditions (e.g. lithology, slope position and angle, elevation). This shows the importance that additional measurements (especially soil temperature) should be performed on site, to enable a detailed and verified interpretation of geoelectric data.
Fig. 5 shows inversion results calculated with the AGI Earthimager 2D software of the whole monitoring period. It starts with the 9th of October 2010 and ends with the inversion result of the 24th of June 2011 with an interval of about 15 days.
The shallow part of the subsurface (the first 3 m) shows strong temporal changes of the resistivity. This behaviour is correlated with the freezing and melting process of the topmost layer. A continuous increase of resistivity in this part is seen for the results 1-12. Result 12 which corresponds to the end of March shows the largest extension of the high resistivity (frozen) zone. In result 13 (9th of April) there is already a decrease of resistivity (especially on the surface) visible. The following resistivity models illustrate the melting process till the end of June. At this time we reach more or less the initial resistivity distribution in the shallow part of the subsurface (9th of October 2010).
At deeper parts of the depth section hardly any resistivity changes took place and due to the relatively low values of 1000 to 15000 Ωm we conclude that there is no indication for permafrost at this location. This could be explained by the fact that our profile is placed on a southwest facing slope, where permafrost is very unlikely at this altitude.

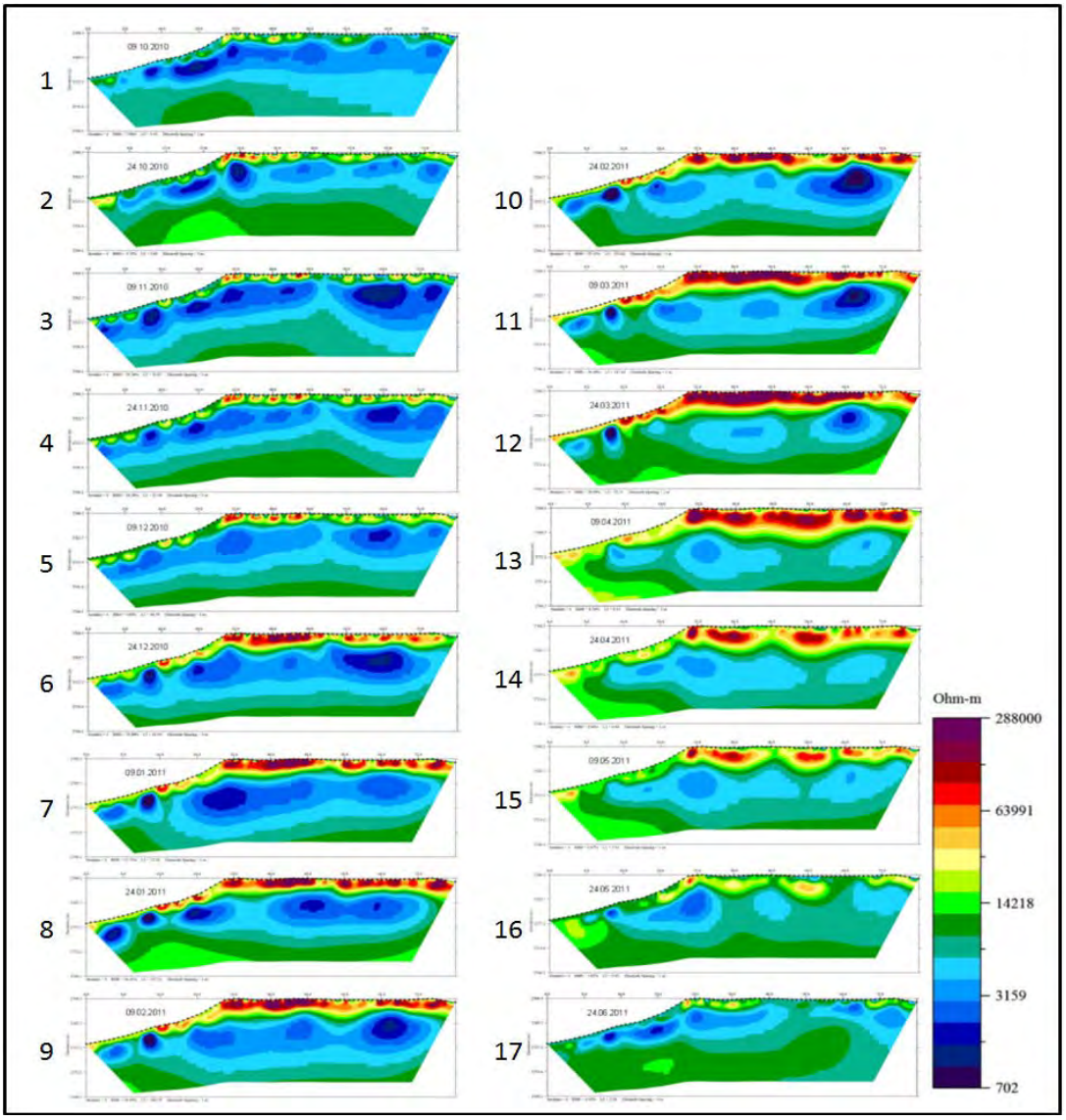

Fig. 5: Selected inversion results covering the whole monitoring period.

Altogether the operation of the monitoring system was very successful and we produced a high quality geoelectric dataset for almost a whole seasonal period. As there was no expectation for new information if we continue our measurements at this location, we decided to search for a new monitoring site where additional measurements (e.g. soil temperature) should be available on site.

Monitoring site Magnetköpfl

This monitoring site where our measurements started in October 2011 is placed on the Magnetköpfl (2957 m a.m.s.l.) which is a peak below the Kitzsteinhorn (Salzburg). A major advantage of this location is the availability of additional data (e.g. soil temperature, ERT), which is collected in the framework of the MOREXPERT project (alpS – Centre for Climate Change Adaptation Technologies, Innsbruck, Austria). In addition to several measuring points of near surface rock temperature in the surrounding area we have also two measuring points (near

surface rock temperature) directly on the geoelectric profile. Soil temperature data from two boreholes (30 m depth) is also available. We used the same monitoring system as on the Mölltaler Glacier working with same settings. As the investigations are still going on we can present at this time only preliminary results. Unfortunately soil temperature data of our monitoring period is not available yet.

Fig. 6 shows inversion results of the freezing process in late autumn 2011. Especially in the shallow part there is a significant increase of resistivity visible. In deeper areas in comparison the changes are much smaller and considering the displayed colour bar we see that the resistivities are in the range of 100 to 150 kΩm. These high values and the negligible change during the freezing process indicate the presence of permafrost at depth. In the left part of the depth section we have the strongest influence of the freezing process to the measured resistivities. This could be explained by the fact that we have solid rock at this part, where low temperatures penetrate much faster than at weathered conditions with rock waste what we observed along the rest of the profile. We are confident that with additional information of soil temperature data we will be able to verify these assumptions.

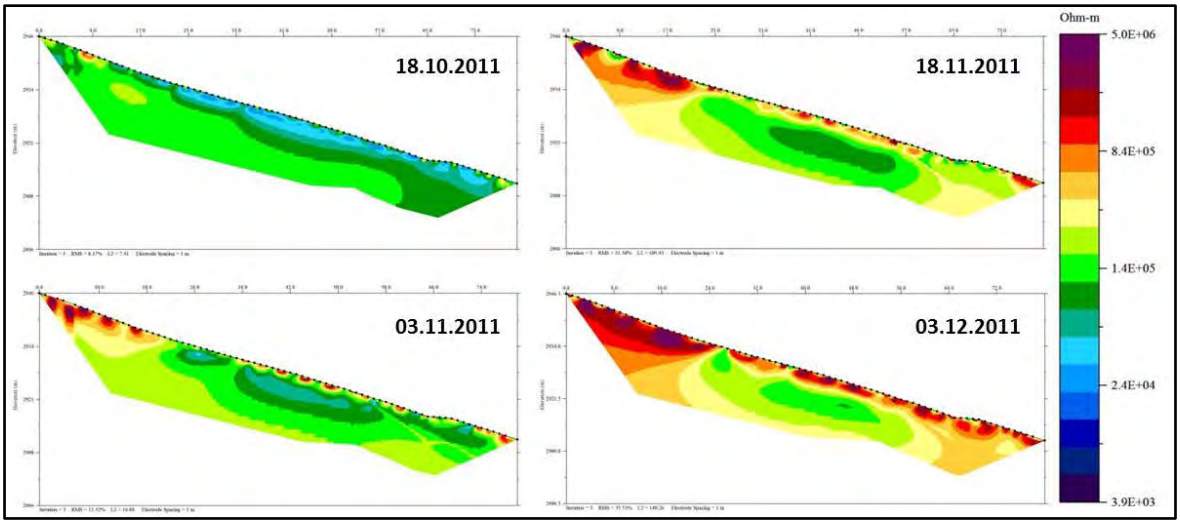

Fig. 6: Inversion results covering the freezing process.

We plan to continue our geoelectric monitoring at the Magnetköpfl at least to summer 2012 to cover an entire seasonal period.

Conclusions

With our monitoring measurements we showed that resistivity is a very useful parameter for the detection of permafrost as well as for the investigation of freezing and melting processes in the topmost layer. Nevertheless there is still the need of some improvements to ensure a detailed and verified interpretation of geoelectric data.

Acknowledgements

The soil temperature data from the Sonnblick was kindly provided by the Central Institute of Meteorology and Geodynamics, Vienna (ZAMG). The geoelectric monitoring is funded by the Austrian Science Fund (FWF) – project TEMPEL (TRP 175).

References

HAUCK, C., 2002: Frozen ground monitoring using DC resistivity tomography. – Geophysical research letters, **29**(21): 2016, doi:10.1029/2002GL014995.

HAUCK, C. and VONDER MÜHLL, D., 2003: Permafrost monitoring using time lapse resistivity tomography. – Proceedings of the 8th International Conference on Permafrost, Zürich, Switzerland, 361-366.

KNEISEL, C., 2004: New insights into mountain permafrost occurrence and characteristics in glacier forefields at high altitude through the application of 2D resistivity imaging. – Permafrost and Periglacial Processes, **15**, 221-227.

MARESCOT, L., LOKE, M.H., CHAPELLIER, D., DELALOYE, R., LAMBIEL, C. and REYNARD, E., 2003: Assessing reliability of 2D resistivity imaging in mountain permafrost studies using the depth of investigation index method. – Near Surface Geophysics, **1**, 57-67.

SUPPER, R. and RÖMER, A., 2003: New Achievements in Developing a High Speed Geoelectrical Monitoring System for Landslide Monitoring. – Proceedings of the Environmental and Engineering Geophysical Society, 9th Meeting Prag.

Applications in CO_2 monitoring

Assessment of borehole resistivity tomography for subsurface CO_2 leakage: Lab-scale preliminary study

EUN-SEOK BANG[1], JEONG-SUL SON[1], MYEONG-JONG YI[1], JUNG-HO KIM[1] and J. CARLOS SANTAMARINA[2]

[1] Korea Institute of Geoscience and Mineral Resources, Daejeon, Korea.
[2] Georgia Institute of Technology, Atlanta, Georgia, USA.

esbang@kigam.re.kr

Instructions

Global warming and extreme weather events are a hot issue in the world today. Carbon dioxide (CO_2), one of the greenhouse gases, has been nominated as the main culprit of this international concern (UNITED STATES ENVIRONMENTAL PROTECTION AGENCY, 1997). The carbon capture and storage (CCS) technique is grabbing attention because the current energy paradigm that focuses on fossil fuel cannot be changed abruptly. However, CO_2 geological sequestration faces difficulties related to non-homogeneous underground conditions, poorly characterized interconnected geo-systems, and complex hydro-chemo-mechanical effects that involve reservoir rock and cap-rock mineralogy, saturating fluid, and injected fluid. Thus, it is considered as risky and uncertain, and there is the possibility of CO_2 leakage. For monitoring CO_2 storage sites, use of geophysical tomography methods has been studied (ARTS et al., 2000). CO_2 gas migration due to storage or leakage changes the resistivity of the medium, and it can be monitored through resistivity tomography (NAKATSUKA et al., 2010). If a resistivity survey can catch the complex phenomena caused by subsurface CO_2 leakage, it should be considered as a concrete option for monitoring CO_2 storage sites. In this study, we developed a unique laboratory facility for observing the evolution of subsurface CO_2 leakage. And we attached a resistivity measurement system based on borehole resistivity tomography. We attempted to get resistivity images when the phenomena related to CO_2 leakage were taking place in the tank. These images were compared with the time-lapsed photos and we analyze and discuss the applicability of the resistivity survey.

Experiments

The schematic diagram of the testing systems in this study is shown in Fig. 1. A very thin transparent tank (W x H x D=300 mm x 600 mm x 2 mm) was used for specimen preparation. Thickness was only 2 mm and it could be considered as a two dimensional model. The tank was filled with different sizes of glass-beads to form controlled layered stratigraphies; then the medium was saturated with water mixed with a universal pH indicator. The color changes to the yellow and red color families with decreasing pH values. To capture the evolution of gas invasion and diffusion, photos were taken at regular intervals. Flow paths, displacements, invading volume, pH and density contours of carbonated water were extracted by subsequent image analyses.

The measurement system for resistivity tomography was attached to the CO_2 gas migration monitoring system. Eleven electrodes were installed at the left and right boundaries of the tank. Two or more electrodes were installed at the top plate. The testing equipment for the resistivity survey was Syscal Pro from IRIS instruments. The survey method was a mixture of in-line and cross

surveys. The connected CO_2 gas bubbles traversing the medium of the tank can be a barrier to measure reasonable potential between the left and right parts of the electrodes. The in-line survey will help this kind of problem. The array types were modified pole-dipole and dipole-dipole, which were specially designed for this lab test.

Various inversion schemes for resistivity tomography have been developed. A 3D inversion algorithm considering topography of a site and locations of electrodes has already been in general (YI et al., 2001). Now a 4D inversion algorithm for the dynamic earth has been developed (KIM et al., 2009). Conventional inversion algorithms are not applicable for this study because the tank is perfectly isolated. A modified inversion scheme based on general 3D forward modeling was developed. It considered the shape of the container and the bottom line was put to earth to find solutions in forward modeling. Active constraint balancing was used to enhance the resolving power of least squares inversion (YI et al., 2003). The main soil model for our resistivity survey monitoring is anticline structure, which is a typical type of structural/stratigraphical trapping for CO_2 geological sequestration (Fig. 1b-1). It is a three-layered model. Coarse glass-beads were used for the reservoir and upper layers. Fine glass-beads were used for the cap-rock. Red circles indicate trapped CO_2 gas inside pores.

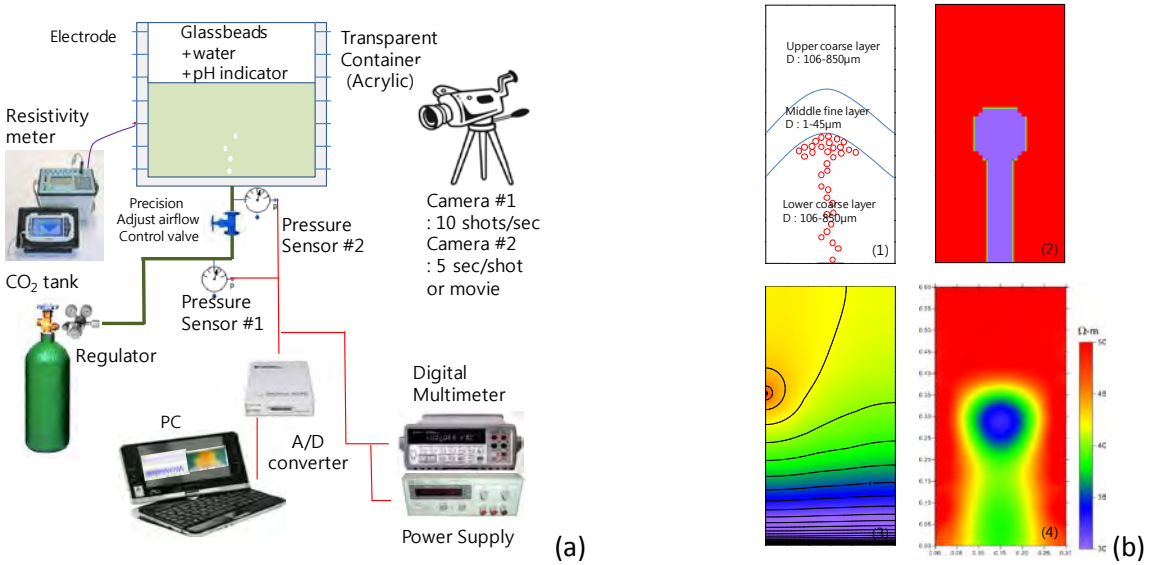

Fig. 1: Schematic diagram of the testing systems for monitoring CO2 gas migration (a) and verification of the inversion procedure for resistivity tomography through numerical modeling (b): Depressurized CO2 gas was injected into a transparent thin gap container though a needle. Bubble pressure was monitored with a pressure sensor attached near the injection point. Pictures were taken for recording and image processing. (1) soil model for the feasibility test of resistivity tomography and expected form of trapped CO2 gas bubble inside the medium, (2) simple model for numerical verification, (3) a typical potential contour during mono-pole current, (4) inversion result using numerical data.

The proposed inversion scheme was verified using numerical data. Fig. 1b-2 is a simplified resistivity model for the main soil model shown in Fig 1b-1. The resistivity of the anomaly caused by CO_2 dissolved water was 30 Ωm while the resistivity of the background medium was 50 Ohm-m. The size of model was 300 mm x 600 mm x 2 mm and the interval of the imaginary electrode was 50 mm. This is same dimensions as the experimental setup. The size of the elements was 1 mm x 1 mm x 0.5 mm and the number of nodes were 904,505 (301x601x5). Fig. 1b-3 shows an example of the potential contour when a current was injected through an imaginary monopole electrode at 0.35 m of the left boundary. The bottom line was put to earth while the other

boundaries were considered as having the Neumann condition. Thus, the potential was zero at the bottom line. Using all twenty-two electrodes, in-line, cross, reverse-cross surveys were performed though dipole-dipole electrode arrays. Inversion was done using a total of 216 measurement data items. The constructed image of resistivity is shown in Fig. 1b-4. The block size for the inversion was 5 mm x 5 mm and total number of blocks was 450. Due to the smoothness constraint, it appears that the boundary of the anomaly has expanded, but it shows well the low resistivity anomaly at the center of the model. Furthermore, the resistivity value is similar to the original value of the model. Thus, it appears that the proposed inversion scheme for resistivity survey works well for this kind of lab-scale study.

Results and discussion

Fig. 2 shows the representative time-lapse images taken by a digital camera for the simulation of CO_2 injection. Fig. 2a is for the sea bottom mountain model. The path of CO_2 gas migration is easily observed. The color of the pore water near the conduit is changed due to acidification because CO_2 is dissolved and makes carbonated water. Pore-water is pH sensitive because the universal pH indicator is mixed. It changes color with different pH values. In this way, the path of the CO_2 gas is clearly detected. The direction of gas migration is upward due to buoyancy. When medium is not homogenous, injected CO_2 tries to find an easier way to migrate, so the direction of gas migration can be horizontal and sometimes downward. This model was non-homogeneous due to segregation of the glass-beads when the specimen was prepared. Therefore, the path of the CO_2 gas was not simple and it changed with time. The bottom graph of Fig. 2a shows the time history of the bubble pressure inside. When the gas migrated, the pressure of the gas bubbles changed. There is a drop point [2] in the graph which means the gas bubble broke through the medium of glass-beads. After that, there were repeated fluctuations of pressure due to continuous gas migration.

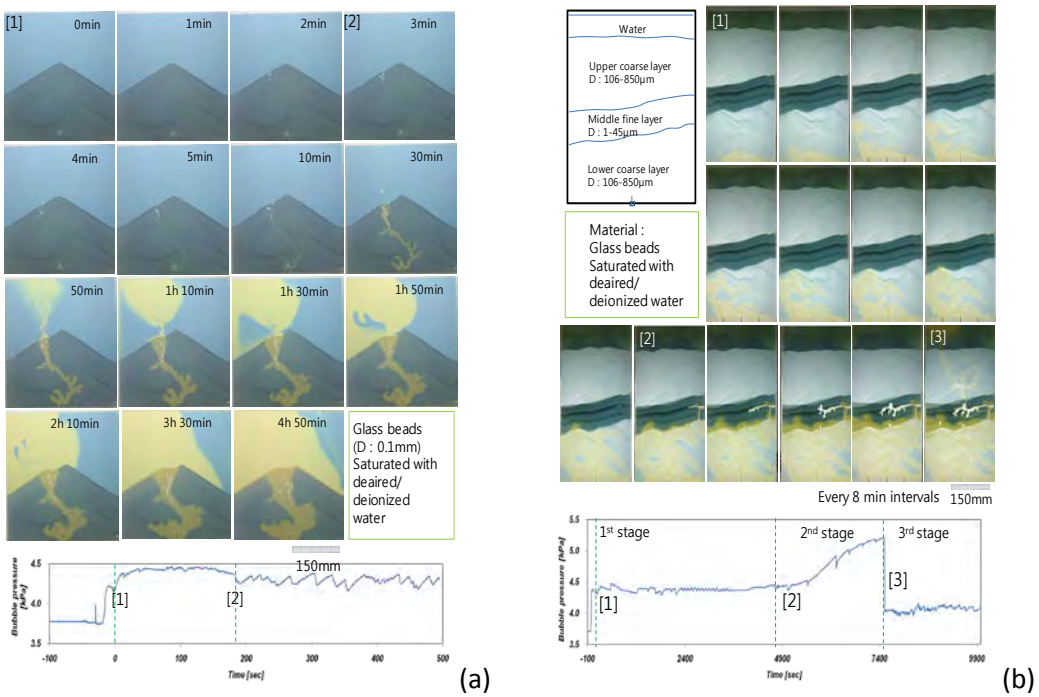

Fig. 2: The results of CO_2 gas injection test (time-lapse digital images and time history of gas bubble pressure): (a) a sea bottom mountain model, (b) a layered glassbead-water mixture system having a find middle layer.

In the three-layered model containing a fine layer, other interesting phenomena related to gas migration were observed as shown in Fig. 2b. There were three stages. In the first stage, CO_2 gas migrated into interconnected pores displacing pore-water in the bottom layer. There was no big pressure build-up. There are just small pressure fluctuations during the gas migration. Otherwise, in the second stage, high pressurized gas made cracks in the fine middle layer to advance. The bubbles pressure increased continuously and dropped a little repeatedly when the gas advanced into the fine layer making cracks. When the gas broke through into the second fine layer, the bubble pressure dropped abruptly at point [3] in the bottom graph of Fig. 2b. After that, the CO_2 gas migrated freely through the percolated path that was the third stage. When the bubble pressure is larger than the air entry value of the medium and smaller than confining pressure, it migrates into the interconnected pores. On other hand, when the bubble pressure is smaller than the air entry value of the medium and larger than the confining pressure, it migrated by open mode discontinuity.

Fig. 3 shows representative photos of the test in which CO_2 gas was injected into the tank containing only water. The initial color was in the blue family. The color changed into the yellow and red color families around the path of the bubble rising. Furthermore, the area of carbonated water expanded or enlarged from diffusion and convection. During the CO_2 gas injection, a resistivity tomography survey was performed periodically. However, those resistivity images do not well agree with the photos. It may be that there are artifacts due to erroneous measurement procedure and inversion scheme. An additional experiment is being done to modify the results of the resistivity survey. Another application test using the main soil model of Fig. 1b-1 is also being done. The feasibility of the resistivity tomography survey for complex phenomena related to CO_2 leakage will be discussed later.

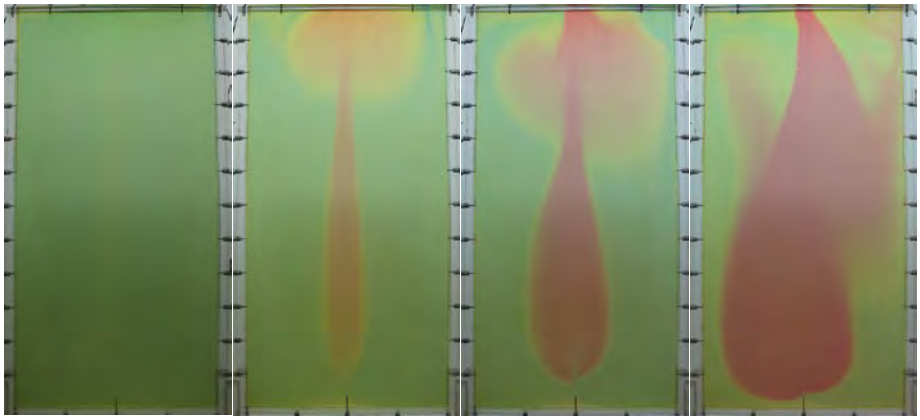

Fig. 3: Representative photos for CO_2 gas injection and application of resistivity tomography survey.

Conclusion

A unique laboratory facility for observing the evolution of subsurface CO_2 leakage was developed. A resistivity measurement system based on borehole resistivity tomography was included. A universal pH indicator especially helped the movement of carbonated water to be monitored effectively. The nature of CO_2 gas migration, the effect of fine-grained layers such as the cap-rock, water acidification near conduits and subsequent diffusion and the convection of carbonated water were observed. This study was a first step to understanding the salient characteristics of subsurface CO_2 leakage and an assessment of the applicability of borehole-based resistivity tomography. The path of CO_2 gas migration in the medium of a tank is easily observed. The color

of water near the path of the CO_2 changes from acidification because CO_2 is dissolved and makes carbonated water. Carbonated water tends to move downward because carbonated water is denser than the surrounding water. Carbonated water with a lower pH has a relatively larger density. An inversion scheme was developed based on 3-D forward modeling that considers the shape of the container. Through numerical modeling, the proposed inversion scheme was verified. Nevertheless, to use the scheme with real experimental data, a refined testing procedure and modification of the proposed inversion scheme are necessary and will be pursed.

Acknowledgements

Support for this research was provided by the USA Department of Energy, the Goizueta Foundation and the basic research project of KIGAM.

References

ARTS, R., BREVIK, I., EIKEN, O., SOLLIE, R., CAUSSE, E. and VAN DER MEER, B., 2000: Geophysical methods for monitoring marine aquifer CO_2 storage – Sleipner experiences. – In: WILLIAMS, D., DURIE, B., MCMULLAN, P., PAULSON, C. and SMITH, A. (Eds.): Proc. of the 5th Int. Conf. on Greenhouse Control Technologies, Cairns, 366-371.

KIM, J.H., YI, M.J., PARK, S.K. and KIM, J.G., 2009: 4-D inversion of DC resistivity monitoring data acquired over a dynamically changing earth model. – Journal of Applied Geophysics, **68**(4), 522–532.

NAKATSUKA, Y., XUE, Z., GARCIA, H. and MATSUOKA, T., 2010: Experimental study on CO_2 monitoring and quantification of stored CO_2 in saline formations using resistivity measurements. – International Journal of Greenhouse Gas Control, **4**, 209–216.

UNITED STATES ENVIRONMENTAL PROTECTION AGENCY, 1997: Climate Change and New York. – Available from http://yosemite.epa.gov/oar/globalwarming.nsf.

YI, M.J., KIM, J.H., SONG, Y., CHO, S.J., CHUNG S.H. and SUH, J.H., 2001: Three-dimensional imaging of subsurface structures using resistivity data, Geophysical Prospecting, **49**, 483–497.

YI, M.J., KIM, J.H. and CHUNG, S.H., 2003: Enhancing the resolving power of least-squares inversion with active constraint balancing. – Geophysics, **68**, 931–941.

CO_2 injection test in a shallow aquifer- feasibility of geoelectrical monitoring

HENDRIK LAMERT[1], ULRIKE WERBAN[1], CLAUDIA SCHÜTZE[1], ANITA PETER[2], ANDREAS DAHMKE[2], MATTHIAS BEYER[3] and PETER DIETRICH[1, 4]

[1] UFZ - Helmholtz Centre for Environmental Research, Permoserstr. 15, 04318 Leipzig, Germany.
[2] University of Kiel, Institute for Geosciences, Ludewig-Meyn-Str. 10, 24118 Kiel, Germany.
[3] GICON GmbH, Tiergartenstr. 48, 01219 Dresden, Germany.
[4] University of Tübingen, Center for Applied Geoscience, Hölderlinstr. 12, 72074 Tübingen, Germany.

hendrik.lamert@ufz.de

Understanding the impact of CO_2 on near surface groundwater systems plays a key role for the assessment of effects caused by potential CO_2 intrusions into shallow aquifers. Potential CO_2 intrusion into groundwater can be caused by: (1) naturally occurring geogenic processes and (2) anthropogenic processes, e.g., at air-sparging sites, by potentially leaking geothermal probes that use CO_2 as a heat transfer medium, as well as at CCS sites (Carbon Capture and Storage).
CCS technology is an approach that has the aim of reducing net CO_2 emissions into the atmosphere. However, the availability of efficient methods for detecting and monitoring potential CO_2 degassing in both deep geological formations and the shallow subsurface is a prerequisite for the deployment of CCS, as well as for public acceptance of this technology, which has been the topic of much controversial debate in recent times. Before implementing geological sequestration of CO_2, a sound risk assessment and monitoring strategy is absolutely necessary.
The aim of the presented project is to emulate a CO_2 intrusion scenario by injecting controlled and temporally limited gaseous CO_2 into a shallow aquifer. This field study was performed at a former military air field in north-eastern Germany over a period of 10 days in March and April 2011. One of the main objectives is to develop and test different methods for monitoring CO_2 and/or geochemically altered groundwater (PETER et al., 2012).
Three CO_2 injection wells and 34 monitoring wells in total were installed at the test site up to a depth of approximately 20 m below ground surface level. Monitoring wells were installed along as well as perpendicular to the main groundwater flow direction (Figure 1) and allow for groundwater sampling before, during and after the CO_2 injection period. Additionally, CO_2 injection wells and 33 monitoring wells are equipped with a total of 300 ring-shaped copper electrodes for implementing geoelectrical measurements. The electrodes are installed at pre-defined depths at the outer surface of the well material and allow for high resolution electrical conductivity (inverse of resistivity) monitoring, covering the whole thickness of the sandy CO_2 injection horizon (LAMERT et al., 2012).

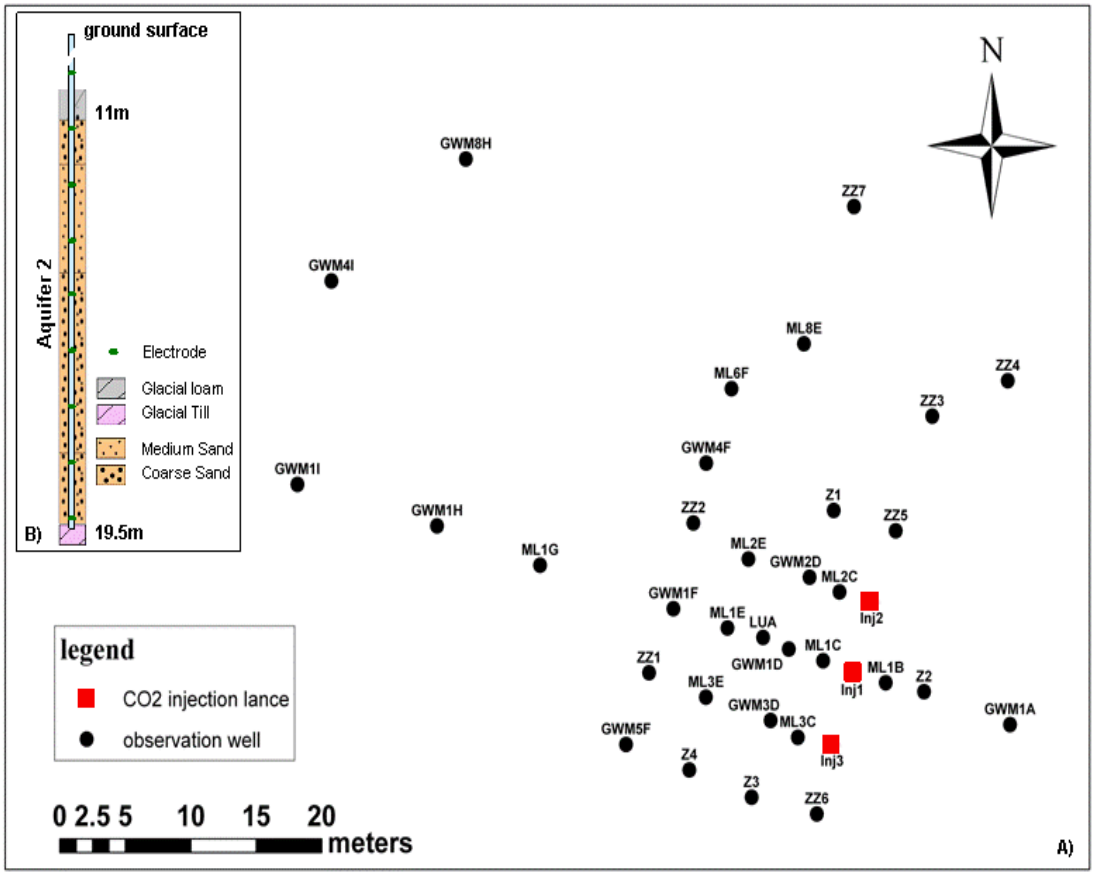

Fig. 1: A) Test site Wittstock. Regional groundwater flow is directed from GWM1A to GWM1 (LAMERT et al., 2012).
B) Schematic geological profile of injection horizon and illustration of a well equipped with electrodes (LAMERT et al., 2012).

Gaseous CO_2 injection into shallow groundwater systems generally causes increased gasphase content in the soil pore space, which accordingly leads to decreased bulk electrical conductivity of the subsurface. However, subsequent dissolution of CO_2 generally leads to decreased pH values and increased electrical fluid conductivity depending on site-specific geological conditions (e.g. presence or absence of buffering materials) and dynamic geochemical processes (e.g. cation-exchange processes).

Breakthrough curves of apparent electrical conductivity (σ_a) show significant variations of σ_a in the order 15 % to 30 % which are affected by the injected CO_2. Groundwater samples are used to validate geoelectrical data. Values for pH and fluid conductivity (σ_f) of groundwater samples (taken from 15 m depth) are exemplarily presented for well ML1E (Figure 2). At well ML1E, pH values decreased from about 6.4 to 5.2 and σ_f of groundwater samples increased from about 500 µS/cm to 800 µS/cm (LAMERT et al., 2012).

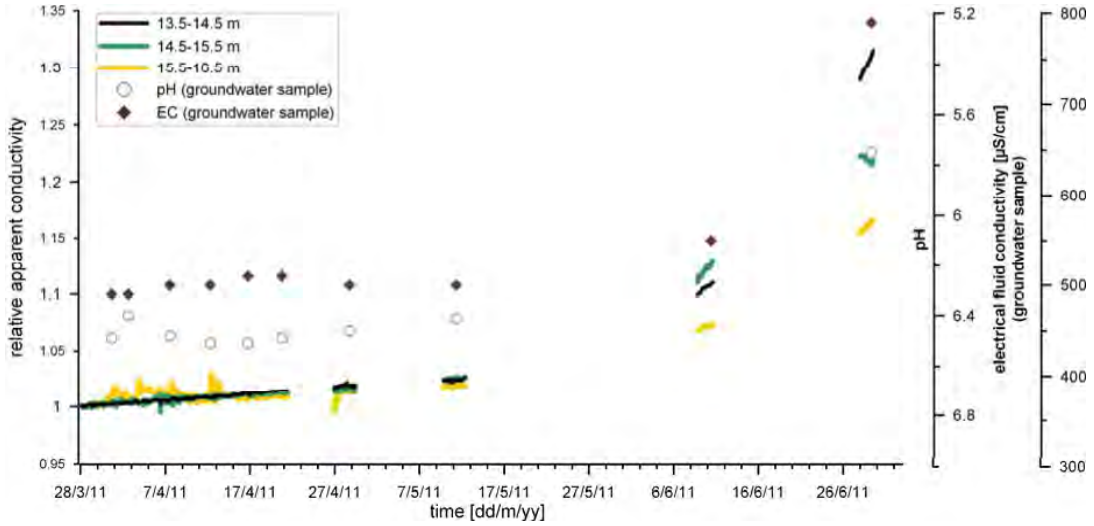

Fig. 2: Field parameters pH and σ_f of groundwater samples (symbols) and temporal variation of apparent electrical conductivity σ_a relative to baseline measurements (solid lines) at well ML1E (1.1" diameter well) for 5 monitoring campaigns performed at the Wittstock site; electrode configuration: Wenner (AMNB). Depths [meter below ground level] of potential electrodes M - N are given in the legend (LAMERT et al., 2012).

In addition to geoelectrical monitoring results, field parameters of groundwater samples also indicate significant alteration in groundwater chemistry caused by the injected CO_2 (PETER et al., 2012). Geoelectrical monitoring results and field parameters are clearly related (Figure 2). This field study has shown the feasibility of geoelectrical measurements for monitoring CO_2 intrusions into shallow aquifers. However, the scope and application of geoelectrical monitoring of CO_2 intrusions strongly depends upon site-specific conditions with respect to dynamic (geochemical) processes, as well as the measuring setup used. The monitoring setup which was used during the presented field experiment permits the detection of small-scale variations in both σ_a (apparent electrical conductivity by geoelectrical breakthrough curves) and σ_f (fluid conductivity of groundwater by groundwater sampling). In order to apply this monitoring strategy at real CCS sites, this approach must therefore be adapted for significantly larger areas, i.e. several km^2.
The presented field study clearly demonstrates that interpretation of geoelectrical breakthrough curves can be used for rapid initial process understanding. However, only using geoelectrical breakthrough curves for comprehensive understanding of gas phase migration processes and the spreading of CO_2 plume in the groundwater is insufficient. Therefore, complementary multiphase simulations should be used. Geoelectrical inversion might be an additional option.

References

LAMERT, H., GEISTLINGER, H., WERBAN, U., SCHÜTZE, C., PETER, A., HORNBRUCH, G., SCHULZ, A., POHLERT, M., KALIA, S., BEYER, M., GROSSMANN, J., DAHMKE, A. and DIETRICH, P., 2012: Feasibility of geoelectrical monitoring and multiphase modeling for process understanding of gaseous CO_2 injection into a shallow aquifer. – Environmental Earth Sciences, **67**(2), 447-462.

PETER, A., LAMERT, H., BEYER, M., HORNBRUCH, G., HEINRICH, B., SCHULZ, A., GEISTLINGER, H., SCHREIBER, P., DIETRICH, P., WERBAN, U., VOGT, C., RICHNOW, H.H., GROSSMANN, J. and DAHMKE, A., 2012: Investigation of the geochemical impact of CO_2 on shallow groundwater: Design and implementation of a CO_2 injection test in Northeast Germany. – Environmental Earth Sciences, **67**(2), 335-349.

Monitoring of geological CO_2 storage with electrical resistivity tomography (ERT): Results from a field experiment near Ketzin/Germany

CORNELIA SCHMIDT-HATTENBERGER[1], PETER BERGMANN[1], TIM LABITZKE[1], STEPHAN SCHRÖDER[1], KAY KRÜGER[1], CARSTEN RÜCKER[2] and HARTMUT SCHÜTT[3]

[1] Helmholtz Centre Potsdam, GFZ German Research Centre for Geosciences, Centre for CO_2 Storage, Telegrafenberg, 14473 Potsdam, Germany.
[2] Technical University Berlin, Department of Applied Geophysics, Ernst-Reuter-Platz 1, 10587 Berlin, Germany.
[3] Statoil ASA, Grenseveien 21, 4035 Stavanger, Norway.

conny@gfz-potsdam.de

Introduction

Geoelectrics has proven to be a valuable monitoring method as part of the required surveillance concept in geological carbon dioxide capture and storage (CCS) projects, since the electrical resistivity of a porous reservoir rock is highly dependent on the presence or absence of CO_2. Experimental (RAMIREZ and Friedmann, 2008) and numerical studies (CHRISTENSEN et al., 2006) demonstrated the promising application of electrical resistivity tomography (ERT) for CO_2 plume detection.

For the Ketzin storage pilot site (Fig. 1), where CO_2 is injected into a deep saline aquifer at roughly 650 m depth (WÜRDEMANN et al., 2010), numerical models predicted a CO_2 saturation of approximately 50% for large parts of the plume. Archie's equation predicts an increase of the resistivity by a factor of approximately 3 for the reservoir sandstone, and laboratory tests on Ketzin reservoir samples support this prediction (KUMMEROW and SPANGENBERG, 2011). Feasibility studies show that tracking the CO_2 plume may be doable with crosshole resistivity surveys under these conditions. The installed permanent vertical electrical resistivity array (VERA) was the first permanent ERT array in a CCS operation world-wide. It was followed by the deepest ERT array (3000 m) at the Cranfield test site in Mississippi, USA (CARRIGAN et al., 2009), and very recently by a planned installation at the typical industrial storage depth of about 1500 m at the Spanish Hontomin site (LEDO et al., 2011). The Ketzin VERA system showed promising results during its run-time since the start of injection in June 2008 until today, and it has mapped the predicted resistivity contrast due to the CO_2 in the rock pores (KIESSLING et al., 2010). Furthermore, the permanent electrodes establish a valuable interface for additional CSEM/MT measurements on a larger spatial scale (GIRARD et al., 2001).

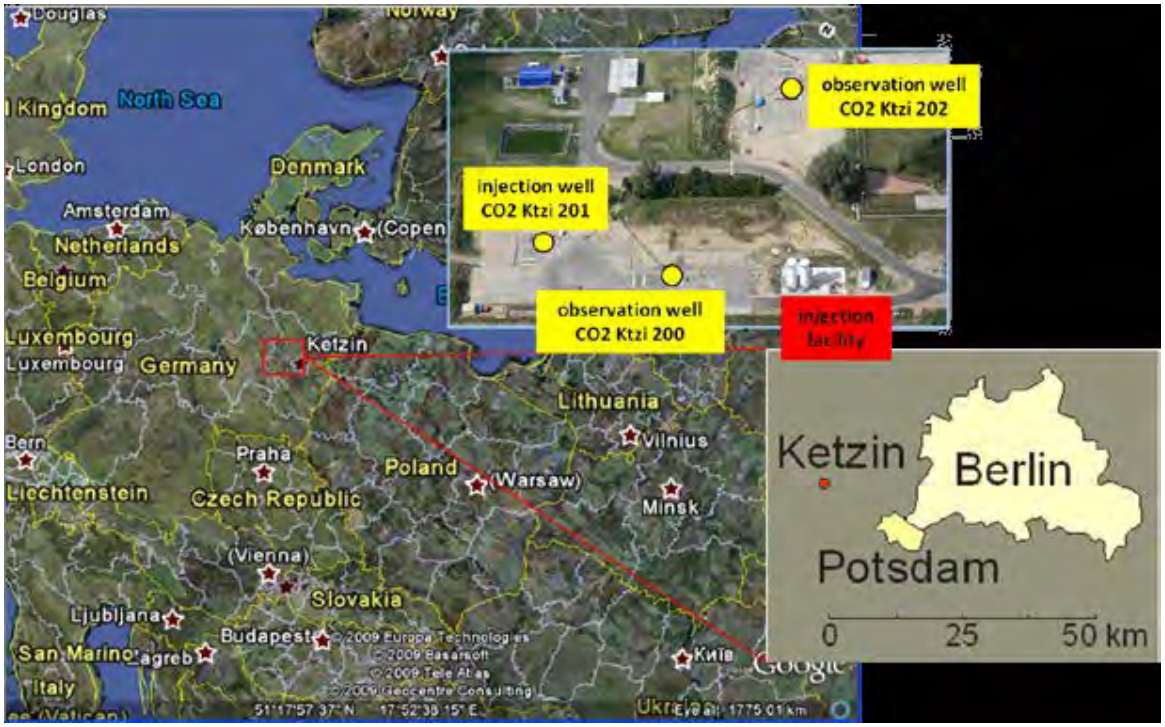

Fig. 1: Location of the Ketzin site in Europe. Inset maps show details of the test site, and its close vicinity to the cities of Berlin and Potsdam.

The Ketzin ERT concept

Ketzin is located in the North East German Basin (NEGB) at about 25 km west of Berlin, and the immediate environment of the CO_2 pilot test site is farmland. The three wells (one injection and two observation wells) arranged in triangular manner were drilled through the Stuttgart Formation, which is situated at about 630-710 m depth. The target storage sandstone reservoir is located at a depth ranging from 630-650 m. The Stuttgart Formation is lithologically heterogeneous, consisting of sandy channel-(string)-facies rocks with good reservoir properties alternating with muddy floodplain-facies rocks of poor reservoir quality (FÖRSTER et al., 2006; NORDEN et al., 2010).

Based on the existing site-specific knowledge we deployed 45 permanent electrodes on the electrically insulated casings of the three Ketzin wells in a depth interval from roughly 590 m to 740 m with spacing of about 10 m (Fig. 2). The electrodes are connected to the current supply and data registration units at the surface through custom-made cables. This deep electrode array allows for the acquisition of electrical resistivity tomography (ERT) data sets at high repetition frequencies and at moderate cost, without interfering with the injection operations.

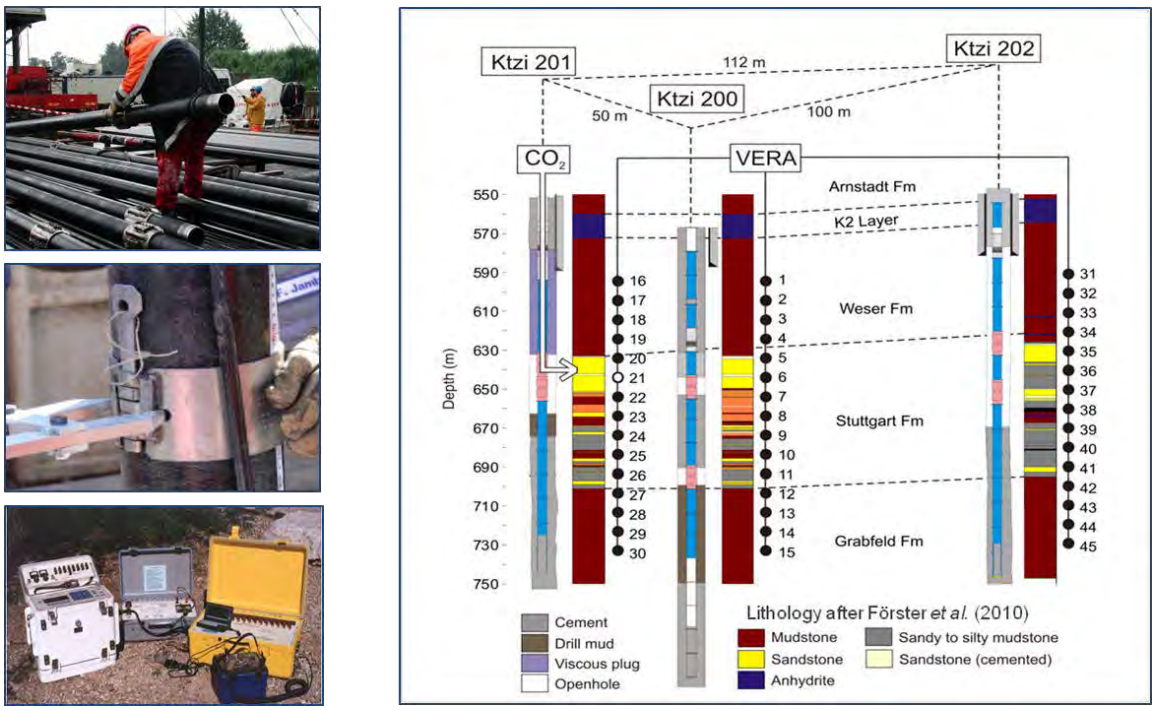

Fig. 2: Relevant components of the Ketzin VERA system: Insulated casing, stainless-steel electrodes, and data acquisition unit from ZONGE Engineering Inc. (left side, from top to bottom).

Well completion scheme, lithology (after FÖRSTER et al., 2010) and electrode positions of the VERA system (black dots) for the three wells at the Ketzin site (right side).

For the Ketzin monitoring concept, the permanent crosshole measurements which are covering the near-wellbore area were combined with surface-downhole surveys at selected time windows during the phase of regular CO_2 injection. These large-scale surveys deploy 16 dipoles (dipole length of 150 m) on two concentric circles at the surface with the radii of 800 and 1500 m, and potential dipoles at the VERA system in all three wells (KIESSLING et al., 2010). Baseline data sets have been measured prior to the CO_2 injection, and monitoring data sets are recorded while CO_2 is being injected. The recorded current and potential raw data are converted to apparent resistivity, and inverted to obtain 3D images of the resistivity distribution in the reservoir. Hence, one can provide information about the saturation state of the reservoir independently from seismic methods. From the technical point of view, the VERA system has to operate under challenging conditions, e.g. the very complex heterogeneity of the reservoir zone, and the potential high possibility of corrosion by high saline formation water and CO_2 in the subsurface environment. The system must have long-term stability, so that it can effectively contribute to the multi-disciplinary monitoring program.

In the frame of a feasibility study the forward modeling based on laboratory and logging results provided a first rough estimate about the distribution of the injected CO_2. The schematic tomography "cube" of the volume imaged by VERA (Fig. 3) shows the CO_2 plume that can be assumed to follow mainly gravity along the structural trend of the anticline, i. e. migrating toward N, N-W. The high-sensitivity zones of the VERA system image this behavior with a radius of about 30 m around each well. A simple 3-layer model has been derived from resistivity log analysis. The thin reservoir target zone was assumed to be saturated with 50% CO_2. Forward modeling based on this simple Archie-model is shown at the bottom of the left side. Here, we find a confirmation of the above sketched performance of the VERA array.

But we should be aware: The preferred flow path depends also on a more complex porosity and permeability distribution, and the CO_2 plume will most likely have a modified shape reflecting the local variations of geology.

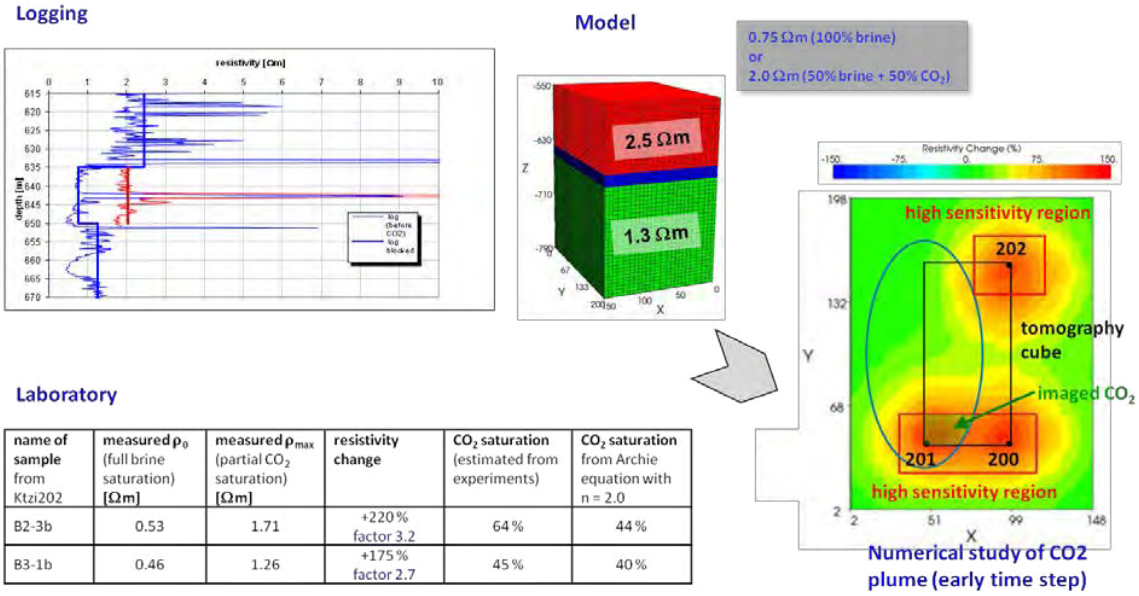

name of sample from Ktzi202	measured ρ_0 (full brine saturation) [Ωm]	measured ρ_{max} (partial CO_2 saturation) [Ωm]	resistivity change	CO_2 saturation (estimated from experiments)	CO_2 saturation from Archie equation with n = 2.0
B2-3b	0.53	1.71	+220 % factor 3.2	64 %	44 %
B3-1b	0.46	1.26	+175 % factor 2.7	45 %	40 %

Fig. 3: Numerical study of the CO_2 plume migration imaged by the VERA system (right side), based on a simple 3-layer resistivity model underlined by laboratory data from petrophysical flow-through experiments and by logging results (modified after KIESSLING et al., 2010). The thin target reservoir zone and the relative low resistivity contrast before and after CO_2 injection pose a major challenge to the detectability of the monitoring system.

Data analysis and CO_2 plume detection

Assigned to the four major topics which are: Array design – acquisition – processing – evaluation, we can structure the Ketzin geoelectric concept as modular monitoring system (MMS) with key-modules for realizing an efficient work flow to achieve reliable results from the field data, regarding the CO_2 plume propagation (SCHMIDT-HATTENBERGER et al., 2011).

We have studied the ERT raw data in joint interpretation with the process data from the CO_2 injection operation. Significant temporal variations have been detected between the field data sets of the individual crosshole repeat measurements. This behavior is still being analyzed along the storage process time history, regarding an eventual origin or influence by the injection process.

Due to time constraints arising from the large number of measurements for a manifold of electrode configurations (ABMN schedules), only short signal cycles of 16 s have been recorded. In Fig. 4, we see data examples varying from very good signal quality to spiky and very noisy behavior, or to nearly distorted records. For the preprocessing of the shortened signal time series we had to develop an adapted workflow. This approach provides an adequate powerful tool in comparison to the commonly used selective stacking procedure (STORZ et al., 2000) which is not applicable here.

The preprocessing scheme runs after the following steps: (1) identification of all ABMN combinations from one measurement day, (2) filtering according to data quality control, i.e. upper and lower signal level check of voltage and current as well as their standard deviation, mean

values, and error estimation, (3) decision making: useful field data YES or NO, (4) merging by an appropriate average process for identical ABMN combinations, either by simple mean or median filtering, depending on the number of measured values (Fig. 4, left side), (5) curve fit of the data points from merging process, (6) interpolation to achieve continuous data series.

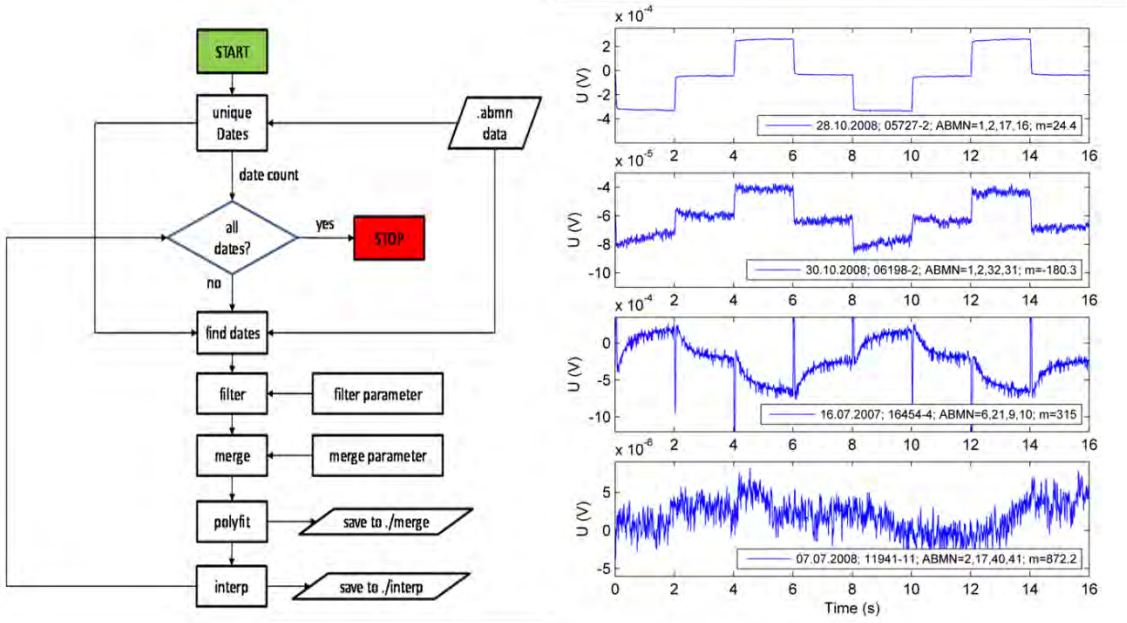

Fig. 4: Prepocessing workflow (left side), applied to all ABMN time series of the measured crosshole electrode configurations, represented by a set of typical signal forms recorded during the field measurements (right side).

To obtain more certainty for the inversion results derived from the processed data, we tried and tested various inversion program codes. Some of them are suitable for quick in-field inversion to get first estimations of results, due to their user-friendly menu-driven workflow. Finally, we remained with the Open Source Code BERT, which stands for "Boundless Electrical Resistivity Tomography" (RÜCKER et al., 2006; GÜNTHER et al., 2006). The script-driven program allows the handling of a large observation space in order to minimize disturbing boundary effects. Furthermore, the program can deal in optimal way with the information-bearing parts of the data sets by a weighted-error procedure inside the inversion operator. The non-regular grid based on tetrahedral elements supports the investigation of areas with several tens of km (surface-downhole measurements) until areas with tens of meters (crosshole measurements), in a smooth transition.

Time-lapse results in 2D and 3D mode were investigated at different phases of injection, in joint evaluation with the current process data of the injection well (Fig. 5). A significant resistivity signature related to the CO_2 migration was detected in the major observation plane between the injection well and the first observation well (Ktzi201-Ktzi200).

Since autumn 2009, an increasing influence of degradation effects at some of the electrode cable take-outs were observed. This process affects a reduction of the 3D effect, and as a result of this some electrodes must be excluded from interpretation, and some of them even from the inversion procedure.

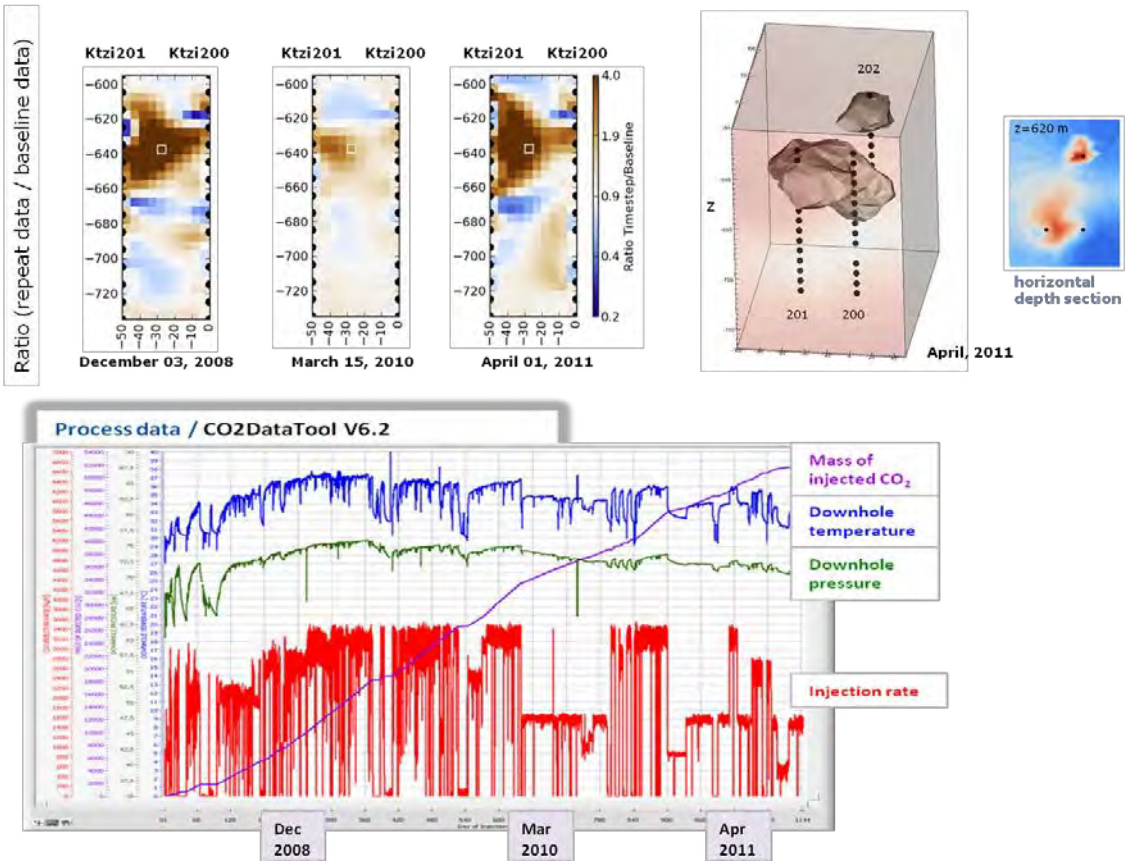

Fig. 5: 2D and 3D time-lapse results (BERT inversion program) assigned to certain phases of CO_2 injection with different flow-rates.

Conclusions

The technology for a permanent ERT downhole installation has been successfully site-proofed. The VERA system has been detected the CO_2 signature in the near-wellbore area, shown in a series of time-lapse inversion results. Due to thoroughly preprocessing work consolidated data sets could be established for the inversion procedure. Due to being a potential method, ERT lacks in imaging of structures at a similar detail as seismic monitoring. Therefore, we address current work on the incorporation of structural seismic information as a priori constraints in the ERT inversion.The general objective of our case study aims to deliver a realistic and reliable specification for the deployed ERT monitoring system, as contribution to the operational reservoir management of the CO_2 storage process.

References

CARRIGAN, C.R., RAMIREZ, A.L., NEWMARK, R.L., AINES, R. and FRIEDMAN, S.J., 2009: Application of ERT for tracking CO_2 plume growth and movement at the SECARB Cranfield site, presented at: 8th Annual Conference on Carbon Capture & Sequestration, Pittsburgh, PA, United States, 4-7 May, 2009 [CD-ROM].

CHRISTENSEN, N.B., SHERLOCK, D. and DODDS, K., 2006: Monitoring CO_2 injection with cross-hole electrical resistivity tomography. – Exploration Geophysics, **37(1)**, 44–49.

FÖRSTER, A., NORDEN, B., ZINCK-JØRGENSEN, K., FRYKMAN, P., KULENKAMPFF, J., SPANGENBERG, E., ERZINGER, J., ZIMMER, M., KOPP, J., BORM, G., JUHLIN, C., COSMA, C. and HURTER, S., 2006: Baseline characterization of the CO2SINK geological storage site at Ketzin, Germany. – Environmental Geosciences, **13**(3), 145-161.

FÖRSTER, A., SCHÖNER, R., FÖRSTER, H.-J., NORDEN, B., BLASCHKE, A.-W., LUCKERT, J., BEUTLER, G., GAUPP, R. and REHDE, D., 2010: Reservoir characterization of a CO_2 storage aquifer: the Upper Triassic Stuttgart Formation in the Northeast German Basin. – Marine and Petroleum Geology, **27**(10), 2156-2172.

GIRARD, J.F., COPPO, N., ROHMER, J., BOURGEOIS, B., NAUDET, V. and SCHMIDT-HATTENBERGER, C., 2001: Time-lapse CSEM monitoring of the Ketzin (Germany) CO_2 injection using 2 x MAM configuration. – Energy Procedia, **4**, 3322-3329.

GÜNTHER, T., RÜCKER, C. and SPITZER, K., 2006: Three-dimensional modeling and inversion of dc resistivity data incorporating topography – II. Inversion. – Geophysical Journal International, **166**, 506-517.

KIESSLING, D., SCHMIDT-HATTENBERGER, C., SCHUETT, H., SCHILLING, F., KRUEGER, K., SCHOEBEL, B., DANCKWARDT, E., KUMMEROW, J. and THE CO_2SINK GROUP, 2010: Geoelectrical methods for monitoring geological CO_2 storage, First results from crosshole and surface-downhole measurements from the CO2SINK test site at Ketzin (Germany). – International Journal of Greenhouse Gas Control, **4**, 816-826.

KUMMEROW, J. and SPANGENBERG, E., 2011: Experimental evaluation of the impact of the interactions of CO_2-SO_2, brine, and reservoir rock on petrophysical properties: A case study from the Ketzin test site, Germany. – *Geochemistry Geophysics Geosystems*, **12**, 5, Q05010.

LEDO, J., QUERALT, P., MARCUELLO, A., OGAYA, X., ESCALAS, M., PIÑA, P., BOSCH, D. and VILAMAJÓ, E., 2011: Review of EM Methods Applied for the Characterization and Monitoring of the Hontomin (Spain) CO_2 Storage Pilot Plant. – 1st Sustainable Earth Sciences Conference & Exhibition –Technologies for Sustainable Use of the Deep Sub-surface, 8.-11. November 2011, Valencia, Spain, EarthDoc-55542.

NORDEN, B., FÖRSTER, A., VU-HOANG, D., MARCELIS, F., SPRINGER, N.I. and LE NIR, I., 2010: Lithological and petrophysical core-log interpretation in CO2SINK, the European onshore research storage and verification project. – SPE Reservoir Evaluation & Engineering, **13**(2), 179-192.

RAMIREZ, A. L. and FRIEDMAN, S. J., 2008: Joint reconstruction of CO_2 plumes using disparate data, presented at: 7th Annual Conference on Carbon Capture & Sequestration, Pittsburgh, PA, United States, 5.-8. May, 2008 [CD-ROM].

RÜCKER, C., GÜNTHER, T. and SPITZER, K., 2006: Three-dimensional modeling and inversion of dc resistivity data incorporating topography – I. Modelling. – Geophysical Journal International, **166**, 495-505.

SCHMIDT-HATTENBERGER, C., BERGMANN, P., KIESSLING, D., KRÜGER, K., RÜCKER, C., SCHÜTT, H. and KETZIN GROUP, 2011: Application of a Vertical Electrical Resistivity Array (VERA) for monitoring CO_2 migration at the Ketzin site: First performance evaluation. – Energy Procedia, **4**, 3363-3370.

STORZ, H., STORZ, W. and JACOBS, F., 2000: Electrical resistivity tomography to investigate geological structures of the earth's upper crust. – Geophysical Prospecting, **48**, 455-471.

WÜRDEMANN, H., MOELLER, F., KUEHN, M., HEIDUG, W., CHRISTENSEN, N.P., BORM, G., SCHILLING, F.R., and THE CO_2SINK GROUP, 2010: CO_2SINK-From site characterisation and risk assessment to monitoring and verification: One year of operational experience with the field laboratory for CO_2 storage at Ketzin, Germany. – International Journal of Greenhouse Gas Control, **4**, 938-951.

Geophysical and soil gas monitoring methods for the characterization of CO_2 degassing sites – What can we learn from natural analogues?

CLAUDIA SCHÜTZE[1], UTA SAUER[1], HENDRIK LAMERT[1] and PETER DIETRICH[1]

[1] UFZ – Helmholtz Center for Environmental Research, Dept. Monitoring and Exploration Technologies.

claudia.schuetze@ufz.de

Several research and development projects on **Carbon Dioxide Capture and Storage** (CCS) have been initiated in the last few years, and demonstration projects are currently being implemented all over the world (FISCHEDIK et al., 2007). Furthermore, governments in different countries are stimulating the commercial deployment of CCS (e.g. USA, UK and Australia). However, uncertainties still exist concerning large-scale implementation of this emergent technology. Until now, both the assessment of environmental & safety risks and the validation of available monitoring technologies to monitor leakage paths are still missing. A main issue when attempting to gain public acceptance of this new method is ensuring provision of appropriate monitoring practices, aimed at delivering health, safety and environmental risk assessment, so that potential risks that may arise from CO_2 storage are minimized.

The goal of the MONACO project (**Mon**itoring **a**pproach for geological **CO_2** storage sites using a hierarchic observation concept; funded by GEOTECHNOLOGIEN Program), which was initiated in September 2011, is the development of reliable tools to work on different usable scales at geological CO_2 storage sites, both during and after operational phases. The project aims to develop monitoring technologies, especially to identify CO_2 migration paths and leakages from the shallow subsurface into the atmosphere.

Successful monitoring depends on the tools selected and requires the identification of appropriate methods to provide necessary information in real time. Within the frame of this project, an integrative hierarchic monitoring concept is proposed, with the aim of reliably detecting and assessing possible leakages from storage formations into the shallow subsurface (including aquifers and unsaturated zones, plus degassing of CO_2 into the atmosphere). As part of this concept, several methods and technologies from different disciplines (such as chemistry, hydrogeology, and geophysics) will be either combined or used complementary to one another. This hierarchical approach – with method developments and applications ranging from remote sensing, to regional measurements, to local insitu measurements (Fig. 1) – will allow large spatial areas to be consistently covered, and for efficient increase in spatial and temporal resolution to occur e.g. as required for the investigation of suspected or critical CO_2 degassing zones.

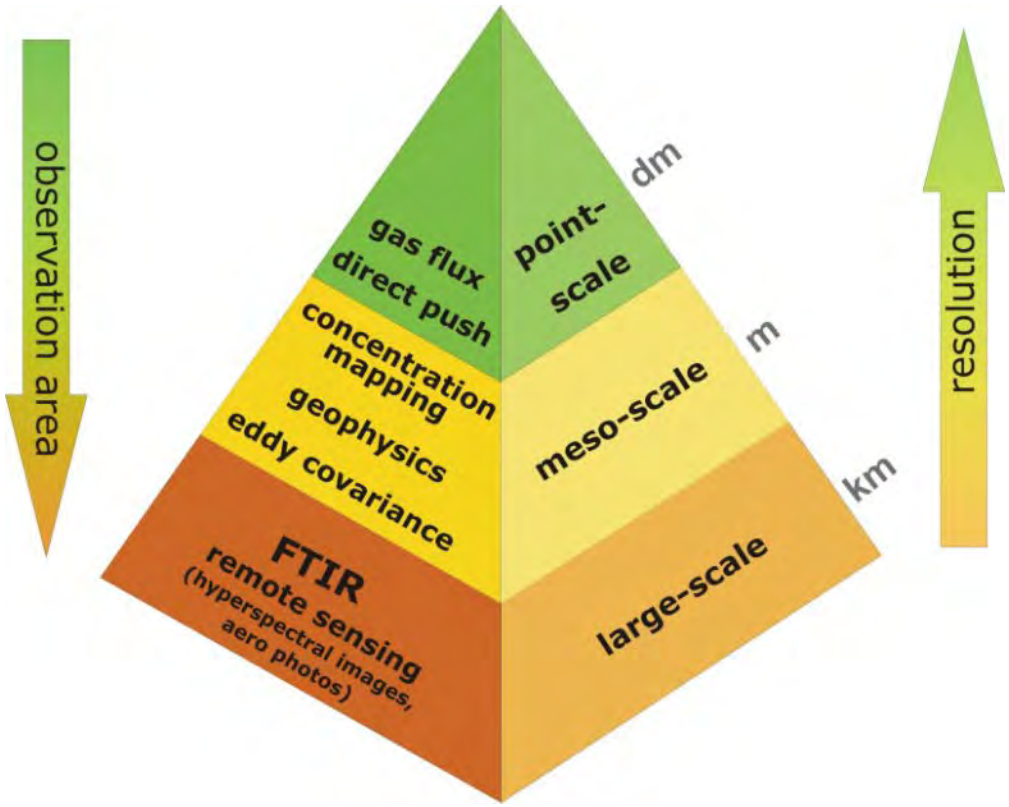

Fig. 1: Hierarchic monitoring concept

There are two main processes which should be monitored. Firstly, dissolved volatile CO_2 in the pore space has an impact on resistivity, which could be measured with Electrical Resistivity Tomography (ERT) and Electromagnetic Induction (EMI) methods. Secondly, fluid movements may lead to the occurrence of electro-kinetic effects (streaming potentials), measurable with self-potential (SP) mapping or monitoring. BYRDINA et al., 2009 showed that measured SP and electrical resistivity tomography results are related to the permeable fracture zone serving as a preferential pathway for soil gases and water. The combination of various kinds of geophysical information (such as resistivity, self-potential with surface-based measurements of CO_2 concentration and CO_2 flux) will provide more reliable insights, in order to constrain the extent of potential leakage systems and to understand patterns of fluid flow (FINIZOLA et al., 2009).

Naturally occurring CO_2 deposits provide unique natural analogues for evaluating and validating methods used for the detection and monitoring of CO_2 spreading and degassing into the atmosphere.

The investigation of natural CO_2 release sites can facilitate the attainment of valuable information that helps improve our understanding of the chemical and physical processes taking place and thus provide significant information for the development of new monitoring and assessment tools.

Furthermore, natural analogues are useful for providing dependable insights into processes related to CO_2 migration, trapping and leakage. Geological and hydrological structures of the Cheb Basin (NW Bohemia, Czech Republic), situated in the western part of the tectonically active Eger Rift, represent such a natural analogue for CO_2 leakage and offer a perfect location for the

verification of monitoring tools, concerning the direct investigation of processes along preferential migration paths (Figure 2).

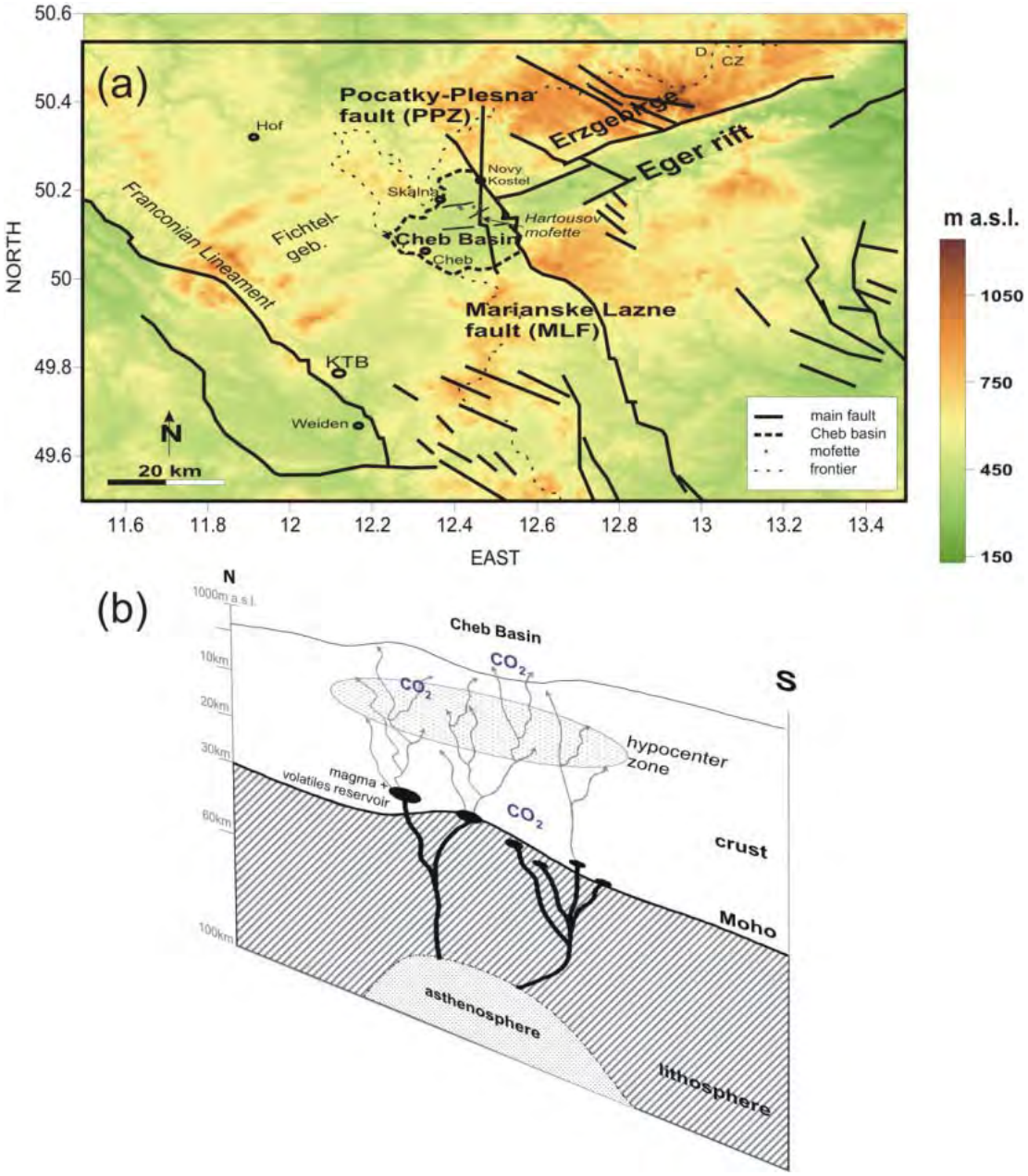

Fig. 2 (a): The border region Vogtland/NW Bohemia is one of the most tectonically active regions in Central Europe. The Cheb Basin is situated in the western Eger rift. The most important deepreaching N-S trending faults regarding the Cheb Basin are the Mariánské Lázně fault (MLF) and the Počatky-Plesná fault zone (PPZ) (after BANKWITZ et al., 2003). The elevation map is derived from STRM 90m Digital Elevation Data Base (JARVIS et al., 2008).
(b): Deep processes are responsible for the occurrence of CO_2 in the Cheb Basin (simplified according to GEISSLER et al., 2005). The CO_2-rich mineral springs and mofettes along the PPZ and MLF are an indication of preferential CO2 migration pathways.

This shallow basin of Tertiary age is characterized by up to 300 m thick Neogene sediment fillings and several tectonic active faults. The CO_2-rich mineral springs and mofettes along the major faults are an indication of preferential CO_2 migration pathways. They are supplied by fluids from a deep magmatic reservoir in the lithospheric mantle. The gas (up to 99,99 % CO_2) ascends via

tectonic fault zones directly from the upper mantle to the surface (BRÄUER et al., 2008, 2011). In this area, both focused small-scale CO_2 degassing sites (so-called mofettes) and larger areas with diffuse degassing behavior (see Figure 3b) are present.

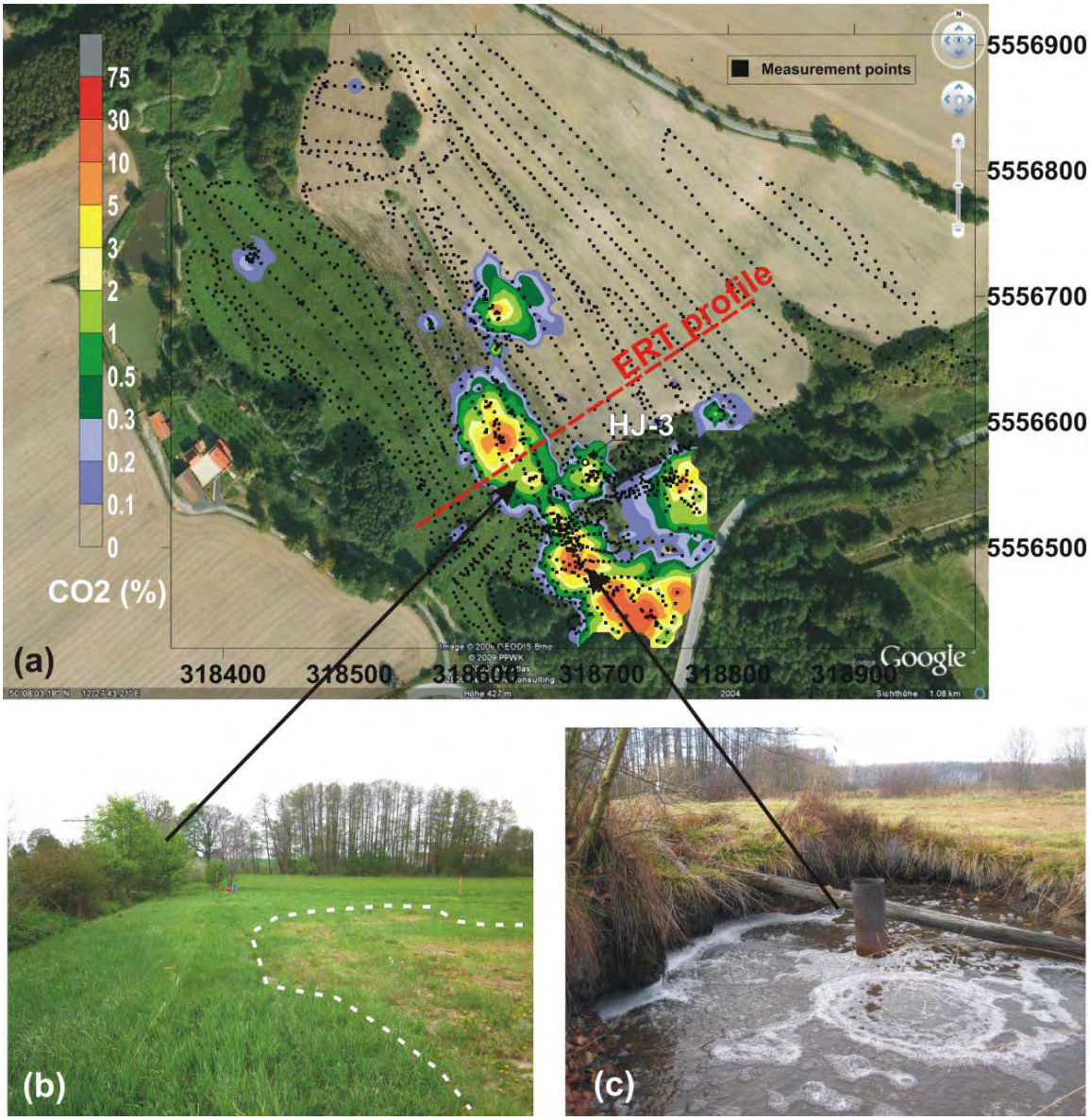

Fig. 3 (a)**:** Surface CO2 concentration patterns near the village Hartousov. Maximum CO2 concentrations of up to 75 % are observable in shallow soil horizons. The degassing area is supposed to be aligned along the trace of the Počatky-Plesná fault zone segment. The geoelectrical line (ERT profile) crosses the diffuse degassing anomaly in the northern region of the test site. (Source aerial photo: Google Earth).
(b): Diffuse CO2 degassing structure is often traceable due to anomalies in vegetation vitality.
(c): Focused degassing can be observed at the main mofette, seasonally filled with groundwater (SCHÜTZE et al., 2012).

At the test site in Hartouchov, we consider two anomaly zones – anomaly zone 1 with focused release and anomaly zone 2 with diffuse release. At both anomaly zones, CO_2 concentration measurements with a mobile gas analyzer ANSYCO GA94, CO_2 flux measurements with the Automated Soil CO_2 Flux System LI-8100A (LI-COR Biosciences), SP and ERT measurements were performed. Table 1 gives an overview of the first results of the measurements.
The SP measurements show a strong correlation between CO_2 degassing zones and SP anomalies. However, there are negative anomalies in the zone with focused release and positive anomalies in

the zone with diffuse release, which poses a significant challenge for interpretation. SP signal can be influenced by a combination of electrokinetic and junction potentials (MAINEULT et al., 2006), due to the presence of flow and concentration gradients, dissolution of volatile CO_2 in groundwater and movements of fluids (CO_2 and water). In further investigations, the main question relating to the basic self-potential driving processes must be solved.

	Anomaly zone 1 – focused release	**Anomaly zone 2 – diffuse release**
CO_2 concentration measurements	soil gas concentration up to 100%,	soil gas concentration up to 80%
CO_2 flux rates	flux rates up to 5000 g m^{-2} d^{-1}	flux rates up to 3800 g $m^{-2}d^{-1}$
SP measurement	negative SP anomaly minima of -30 mV	large positive SP anomaly up to 15 mV
ERT	ERT - anomaly with decreased resistivities	ERT – resistivity variations especially in near surface horizon

Tab. 1: General outcomes at the two degassing zones considered in our study.

Site-specific near surface geological features seem to exert great influence upon the degassing pattern. In this current study, the distribution and thickness of lowly permeable sediments at surface level are able to impede CO_2 discharge into the atmosphere. ERT data shows two distinct locations where the upper clay layer is only a few decimeters thin or nearly non-existent. Highest soil CO_2 concentrations and flux rates were observed at these locations. Furthermore, a correlation between the thickness of the upper clay layer and the flux rates needs to be discussed. It should be noted that agricultural usage can possibly create migration paths in the surface layer and therefore higher CO_2 concentrations can be observed.

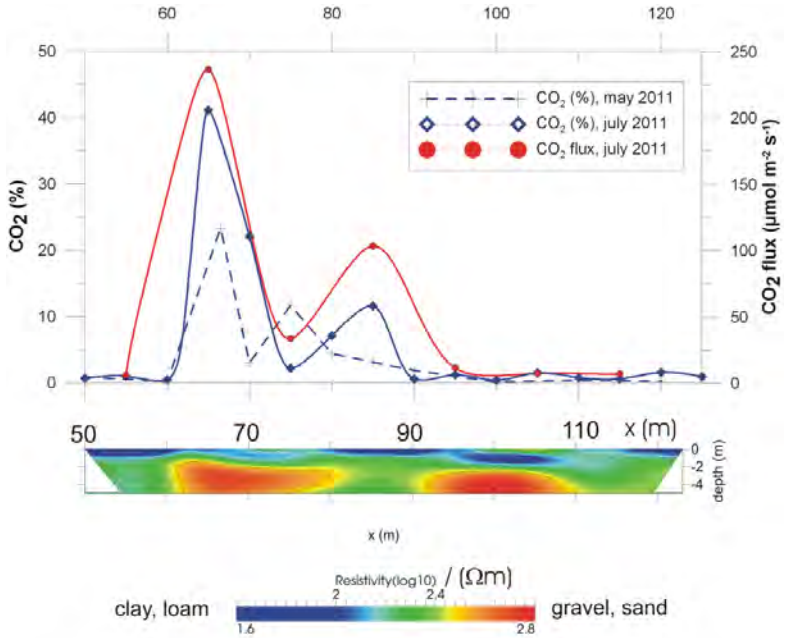

Fig. 4: Detailed soil gas and geoelectrical investigations characterizing a distinct degassing anomaly. Variations are observable in the CO_2 concentration values. This may be caused by the features of the upper soil horizons, in particular the pore water content, due to different meteorological situations in May and July. The structural features of the shallow subsurface (down to a depth of 5 m) can be described by a clay layer (lower resistivities) with variable thickness, followed by a gravel and sand layer (higher resistivities) (SCHÜTZE et al., 2012).

The first measurements indicate that the hierarchic monitoring approach represents a multidisciplinary modular concept working in different scales and resolutions. Soil gas surveys in combination with geoelectrical investigations have been proven to be a valuable tool for the characterization of structural near surface features controlling the degassing process. It is a non-destructive technique, which is relatively inexpensive to perform. Depending on the required spatial and temporal resolution, method combination is recommended for the characterization and observation of medium-scale to small-scale areas.

Natural analogues provide different geological and hydrological situations to test, adapt and validate appropriate monitoring technologies. Results of geoelectric and soil gas measurements clearly indicate subsurface structures and dynamic behavior of degassing areas. However, comprehensive investigations (including those on site-specific and temporal environmental conditions) will be necessary, so that a better understanding of leakage processes can be gained.

Acknowledgements

This research was carried out within the frame of the joint research projects “CO2 leakage test within a near surface aquifer” – support code 03G0785A and “MONACO – Monitoring approach for geological CO2 storage sites using a hierarchic observation concept” – support code 03G0785A. Financial support given by the GEOTECHNOLOGIEN Programm and the German Federal Ministry of Education and Research (BMBF) is gratefully acknowledged. We thank the native speaker Christopher Higgins for proof reading.

References

BANKWITZ, P., SCHNEIDER, G., KÄMPF, H. and BANKWITZ, E., 2003: Structural characteristics of epicentral areas in Central Europe: study case Cheb Basin (Czech Republic). – Journal of Geodynamics, **35**, 5-32.

BRÄUER, K., KÄMPF, H., NIEDERMANN, S., STRAUCH, G. and TESAR, J., 2008: Natural laboratory NW Bohemia: Comprehensive fluid studies between 1992 and 2005 used to trace geodynamic processes. – Geochemistry Geophysics Geosystems, **9**, Q04018, doi: 10.1029/2007GC001921.

BRÄUER, K., KÄMPF, H., KOCH, U. and STRAUCH, G., 2011: Monthly monitoring of gas and isotope compositions in the free gas phase at degassing locations close to the Nový Kostel focal zone in the western Eger Rift, Czech Republic. – Chemical Geology, **290**, 163-176.

BYRDINA, S., REVIL, A., PANT, S.R., KOIRALA, B.P., SHRESTHA, P.L., TIWARI, D.R., GAUTAM, U.P., SHRESTHA, K., SAPKOTA, S.N., CONTRAIRES, S. and PERRIER, F., 2009: Dipolar self-potential anomaly associated with carbon dioxide and radon flux at Syabru-Bensi hot springs in central Nepal. – Journal of Geophysical Research, Solid Earth, **114**, B10101, doi: 10.1029/2008JB006154.

FINIZOLA, A., AUBERT, M., REVIL, A., SCHÜTZE, C. and SORTINO, F., 2009: Importance of structural history in the summit area of Stromboli during the 2002-2003 eruptive crisis inferred from temperature, soil CO_2, self-potential, and electrical resistivity tomography. – Journal of Volcanology and Geothermal Research, **183**, 213-227.

FISCHEDIK, M., ESKEN, A., LUHMAN, H., SCHÜWER, D. and SUPERSBERGER, N., 2007: CO_2-Capture and Geological Storage as a Climate Policy Option. Technologies, Concepts, Perspectives. – Wuppertal Spezial 35 e, 32 S., Wuppertal Institute for Climate, Environment and Energy.

GEISSLER, W.H., KÄMPF, H., KIND, R., BRÄUER, K., KLINGE, K., PLENEFISCH, T., HORÁLEK, J., ZEDNÍK, J. and NEHYBKA, V., 2005: Seismic structure and location of a CO_2 source in the upper mantle of the western Eger (Ohře) Rift, central Europe. – Tectonics, **24**, TC5001, doi: 10.1029/2004TC001672.

JARVIS, A., REUTER, H.I., NELSON, A. and GUEVARA, E., 2008: Hole-filled SRTM for the globe Version 4, available from the CGIAR-CSI SRTM 90m Database (http://srtm.csi.cgiar.org).

MAINEULT, A., BERNABÉ, Y. and ACKERER, P., 2006: Detection of advected, reacting redox fronts fromselfpotential measurements. – Journal of Contaminant Hydrology, **86**, 32-52.

SCHÜTZE, C., SAUER, U., BEYER, K., LAMERT, H., BRÄUER, K., STRAUCH, G., FLECHSIG, CH., KÄMPF, H. and DIETRICH, P., 2012: Natural analogues – a potential approach for developing reliable monitoring methods to understand subsurface CO_2 migration processes. – Environmental Earth Sciences, DOI: 10.1007/s12665-012-1701-4.

Time Lapse/4D Data Inversion

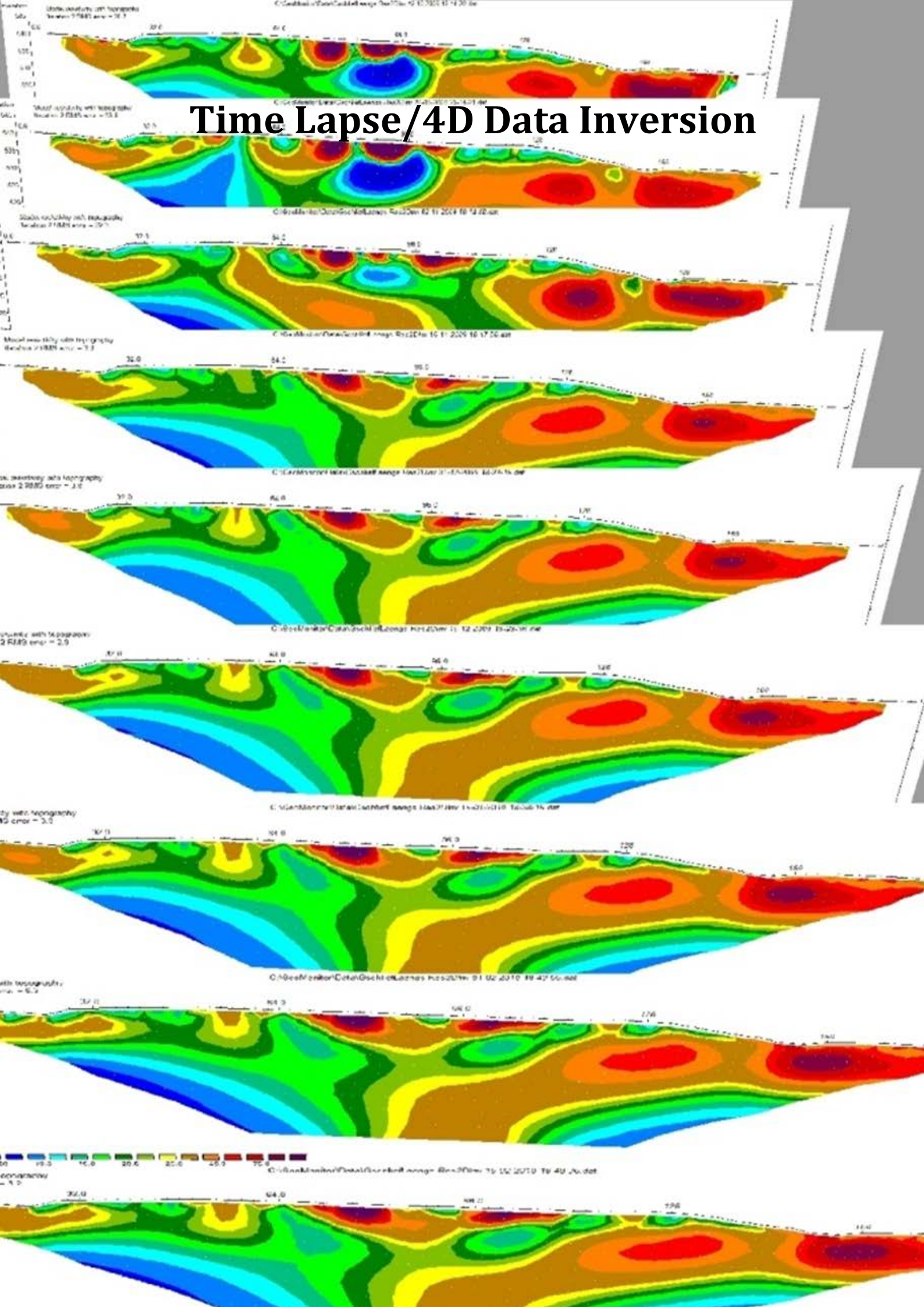

Timelapse ERT inversion approaches and their applications

THOMAS GÜNTHER

Leibniz-Institute for Applied Geophysics (LIAG), Hannover, Germany.

thomas.guenther@liag-hannover.de

Introduction

Aim of timelapse ERT is to image resistivity changes in the subsurface in such that plausible timedependent models fit the data. Since plausibility involves temporal changes, specific inversion and regularization schemes are to be found, particularly if quantitatively reliable measures as absolute water content or ground water velocity are of interest. ERT Inversion is usually ill-posed and non-unique and needs further restrictions. The question is how we can do it best?

There is a number of factors that influence the imaging and thus determine the applicability and performance of the existing approaches, i.e. (1) contrast and heterogeneity of background model, (2) shape and contrast of the changes, (3) reproducibility of electrode positions and arrays, (4) error structure overall and correlation between frames, (5) velocity of ongoing processes, and (6) target values, whether absolute or relative changes of ρ or secondary parameters (e.g. moisture content θ) are regarded.

Generally, five main types of minimization can be distinguished:

- individual inversion of single time frames: $\boldsymbol{d^n} = \{log\ \rho_a(t = t_n)\} \rightarrow \boldsymbol{m}^n = \rho^n$
- inversion of data ratios (Schütze et al., 2002): $\boldsymbol{d}^n = \rho_a^n / \rho_a^0 \rightarrow \boldsymbol{m}^n = \{\rho^n/\rho^0\}$
- inversion with $\mathbf{m}^0$ as reference constraining $\mathbf{m}^n$-$\mathbf{m}^0$ (or alternatively $\mathbf{m}^n - \mathbf{m}^{n-1}$)
- the so-called difference inversion after LABRECQUE and YANG (2001), which additionally corrects the misfit at t_0 so that $\boldsymbol{d}^n = \{\rho_a^n/\rho_a^0\}\boldsymbol{f}(\boldsymbol{m}^0)$ (or n-1 instead of 0).
- fully discretized (4D ERT) with constraints in space and time.

Furthermore there exist different regularization schemes for the absolute models or the model differences (in the usual logarithmic domain the ratio). Mostly smoothness constrains approximating a first or second order derivative are used, sometimes with direction-dependent penalties. Alternatively, minimum length, i.e. the total deviation independent on model cell neighbourhood can be used, or any combination of them.

Synthetic 1D experiments

In order to systematically investigate the role of different inversion and regularization techniques, we simulate synthetic time-lapse experiments with each two time-steps (frames). Therefore a discretisation in time does not have to be treated separately. To keep it simple, a 1d resistivity structure is considered, but it is inverted using a fixed discretisation as in 2d or 3d. A Schlumberger depth sounding is assumed, data are contaminated with 1% correlated and 1% uncorrelated noise. Regularization strength is varied iteratively such that the data are fitted within noise ($\chi^2 = 1$). Unless stated otherwise, smoothness of 1st order is used for both inversion of background and time-lapse data.

First scenario is a shallow infiltration, i.e. a decrease of resistivity by factor 2 in the very first layer of a three-layer model describing a profile of soil, vadose zone and aquifer.

The sounding curve (Fig. 2) of the second frame is lower but the maximum is down-shifted, which leads to an increase of apparent resistivity for deeper penetrations. The latter is known leading to artifacts of increasing resistivity at depth as reported by DESCLOITRES et al. (2003).

The absolute resistivities (Fig. 2 left) are all similar and show mainly the three-layer case in a smooth representation for both frames. Consequently, the ratio images are almost identical in showing a slight increase at medium depths, except the ratio inversion, which shows a strong increase at large depths but also bad values for intermediate depths (Fig. 2 right). Reason is the disregarded deviation in the sensitivity function, which is affected by the background resistivity. In the next scenario, the described infiltration front is moving down, i.e. only changing its layer thickness, which is represented by a thin decrease of factor 3 at 0.5 – 1 m depth. Again, the absolute resistivities (Fig. 3 left) describe the smooth background model. However the ratio curves all show the expected decrease. For ratio inversion it is too shallow and smoothed, similar to the difference inversion. Both independent and reference inversion exhibit a sharper image of the change, but produce severe artifacts at greater depths. In contrast to the last examples the ratio inversion shows least artifacts.

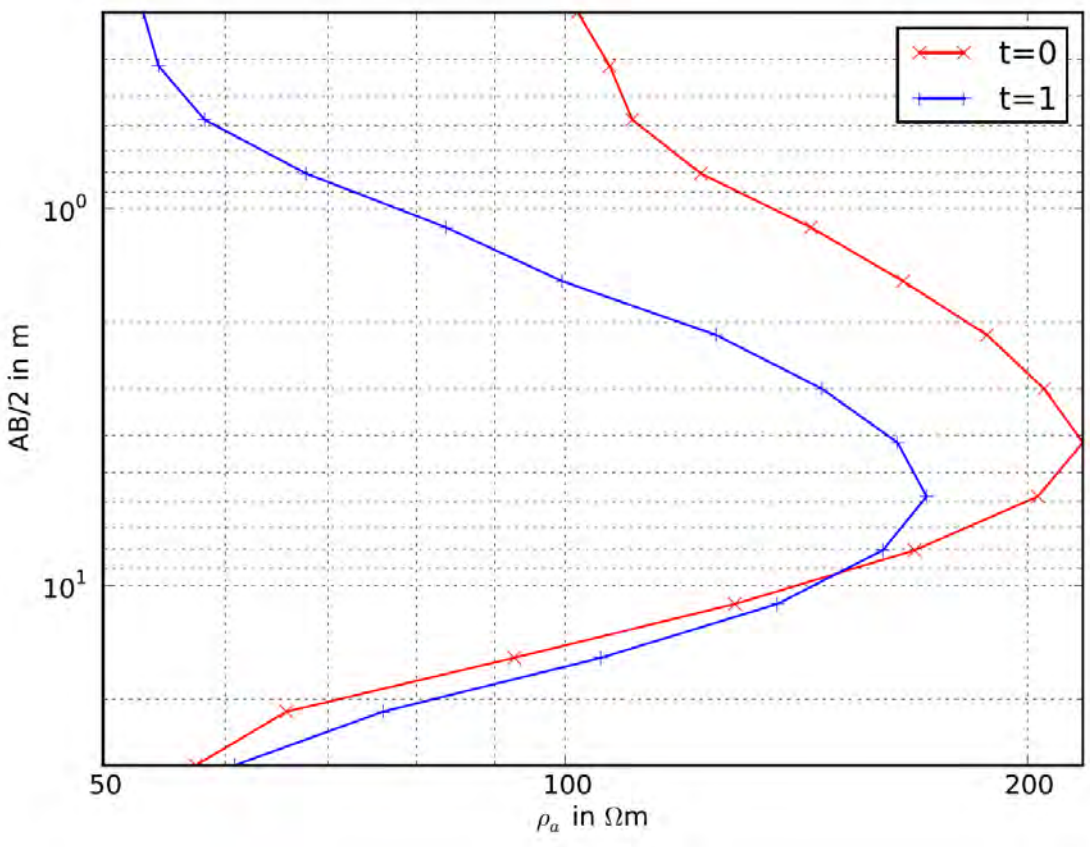

Fig. 1: Apparent resistivity curves of the two time steps for a shallow infiltration front.

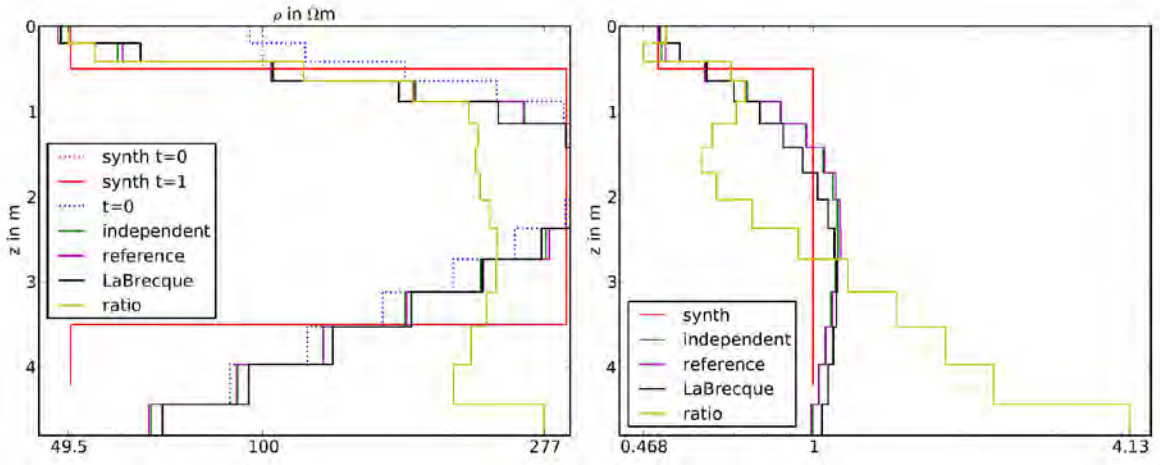

Fig. 2: Absolute resistivity (left) and relative changes (right) of different time-lapse strategies for a shallow infiltration front.

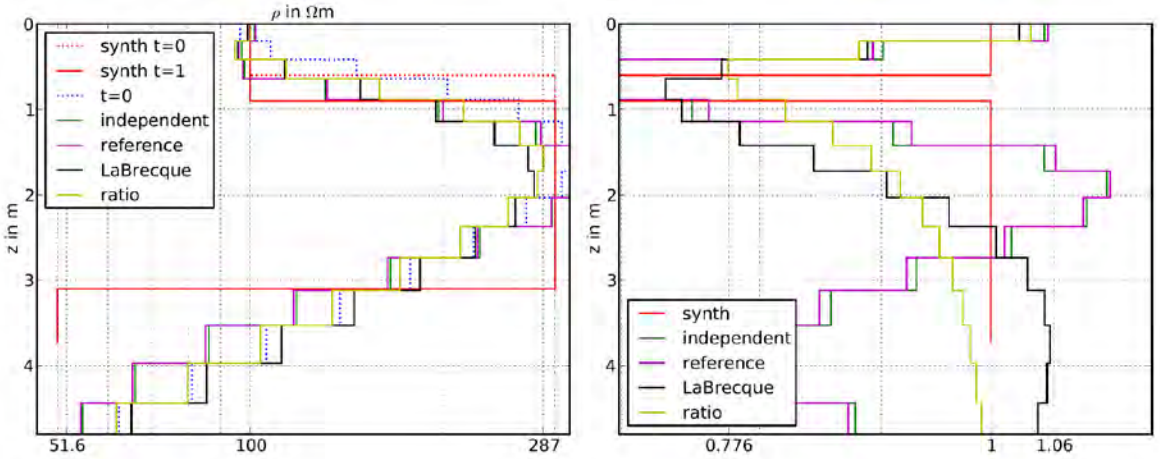

Fig. 3: Absolute resistivity (left) and relative changes (right) for the infiltration front moving down.

In the next example we consider a conductive tracer injection at a certain depth for the same three-layer case. The synthetic ratio is similar but inside the second layer and with a stronger contrast of 20. Therefore absolute and relative resistivity are similar. All methods are able to see the decrease but smoothed and too deep. At least the ratio inversion sees a sharper image.

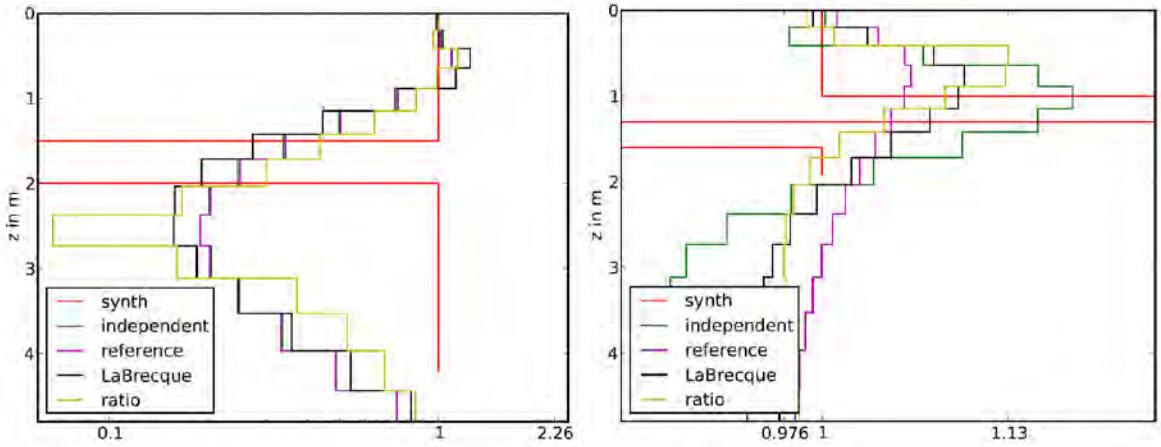

Fig. 4: Relative changes of a synthetic tracer injection (left) and movement (right).

Further, an already injected tracer is moving down, leaving a combined increase/decrease pattern. All methods can see the increase, but are shallow. The following decrease is observed and much too deep. Amazingly, the independent inversion yields the most realistic curve.
The difference inversion seems to be the most stable approach concerning imaging properties and artifacts, particularly if the amount of correlated noise is increased. However, if we use uncorrelated noise only, the method becomes very similar to reference inversion, but with higher smoothness due to the superposition of noise from both time steps.
Additionally to inversion techniques, we want to investigate how different regularization techniques affect the results of difference/reference inversion. The first time step is processed with smoothness of first order, whereas for the changes zero, first, second and combinations of zeroth with first and second order are considered (Fig. 5).

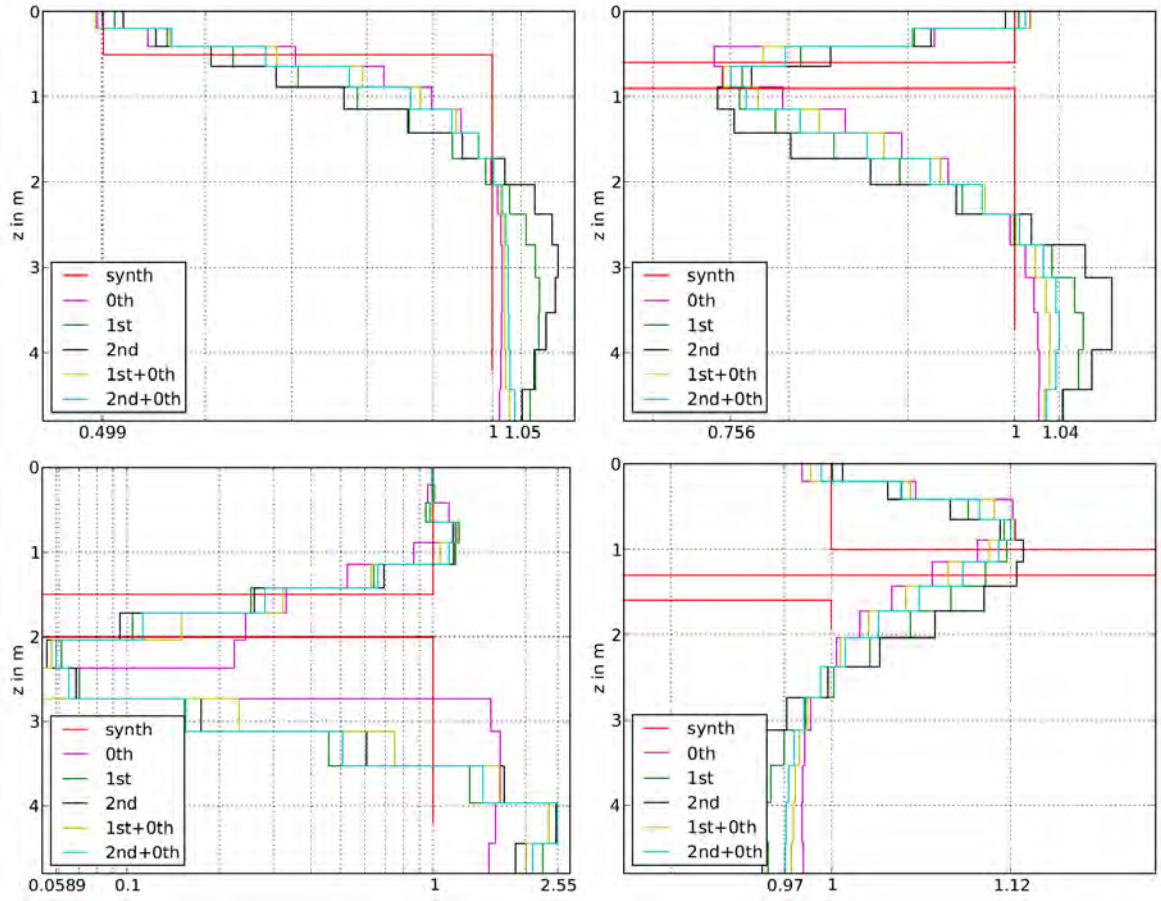

Fig. 5: Resistivity ratios of different time-lapse regularizations for shallow water (top) and tracer (bottom) infiltration (left) and movement (right).

For the shallow infiltration example we see that 0^{th} order alone or in combination does not lead to artificial increase due to smoothness. This holds also for the second example (moving infiltration), where 0^{th} order is showing the change too shallow and 2^{nd} order too deep. A combination of 0^{th} and 1^{st} (or 2^{nd}) order performs best.
In example three (tracer injection) 0^{th} order is too deep, although with least artifacts. The others are similar, but 0^{th} + 1^{st} order performs best. When the tracer moves down, 0^{th} order is too shallow again and 2^{nd} order shows the best agreement, although overly smoothing at depth.

Real data

We tested the methods for a tracer injection experiment presented by KURAS et al. (2009), a cross-hole ERT data set using 9 boreholes with 10 cm spaced electrodes. The BERT algorithm after GÜNTHER et al. (2006) with a regular discretisation of rectangular cells (5 cm x 5 cm) was used. Figure 6 shows the resistivity ratios for two time steps (4 hours and 12 hours) using different inversion and regularization techniques. Generally, the conducting tracer can be seen by all methods but with different imaging properties.

Individual inversion (first row) yields strong artifacts at the borehole electrodes, probably due to systematic error sources such as positioning inaccuracies. This effect was similarly observed in other reference inversions and therefore the misfit removal after LABRECQUE and YANG (2001) was used for the following inversions. Constraining the models to the predecessor (second row) leads to decreases followed by increases due to combination of two ratios.

From the inversions with regularization orders 0, 1 and 2 (lines 3-5) the classical smoothness constraints (1st/2nd with slightly decreased vertical weights) exhibit the largest effects, but also the largest artifacts above and below the tracer. Minimum-length regularization of the model difference does not show such artifacts but increases at the electrodes interrupting the tracer shape. If (isotropic) smoothness and pure deviation are combined (last line), the least artifacts are observed, but the shape of the tracer remains interrupted. Further tuning may lead to even nicer images, however it is not clear beforehand which method is best and how reality looks like.

Conclusions

There is a huge number of different timelapse approaches and options concerning minimization methods and regularization types. All schemes are generally similar, especially for small contrasts, but can produce significant artifacts, particularly when resistivity ratios are of interests. The best method is not clear beforehand and depends on the background model, shape and contrast of the changes, but also on noise conditions.

Difference inversion (LaBrecque's method) turns out to be a safe choice for all considered models but could decrease resolution in case of negligible systematic errors. The reference model inversion is most general and works with arbitrary measuring sequences and even electrode positions for the different time-steps. Ratio inversion achieved most contrasted models but can yield wrong depths and resistivities due to wrong sensitivity. Therefore it has to be treated with care and should only be used for quasi-homogeneous $\mathbf{m}^0$.

Different regularization schemes applying to the model differences can have significant impact on the results. After our experience, a mix of first order smoothness constraints and simple damping produces least artifacts. Movements of small units should not be constrained to each other (as in 4D approaches) but to a background model. In all cases, only with a good m0 model successfull time-lapse ERT can be performed. Synthetic studies should be carried out before the measurement and help interpreting the solutions by understanding the nature of imaging.

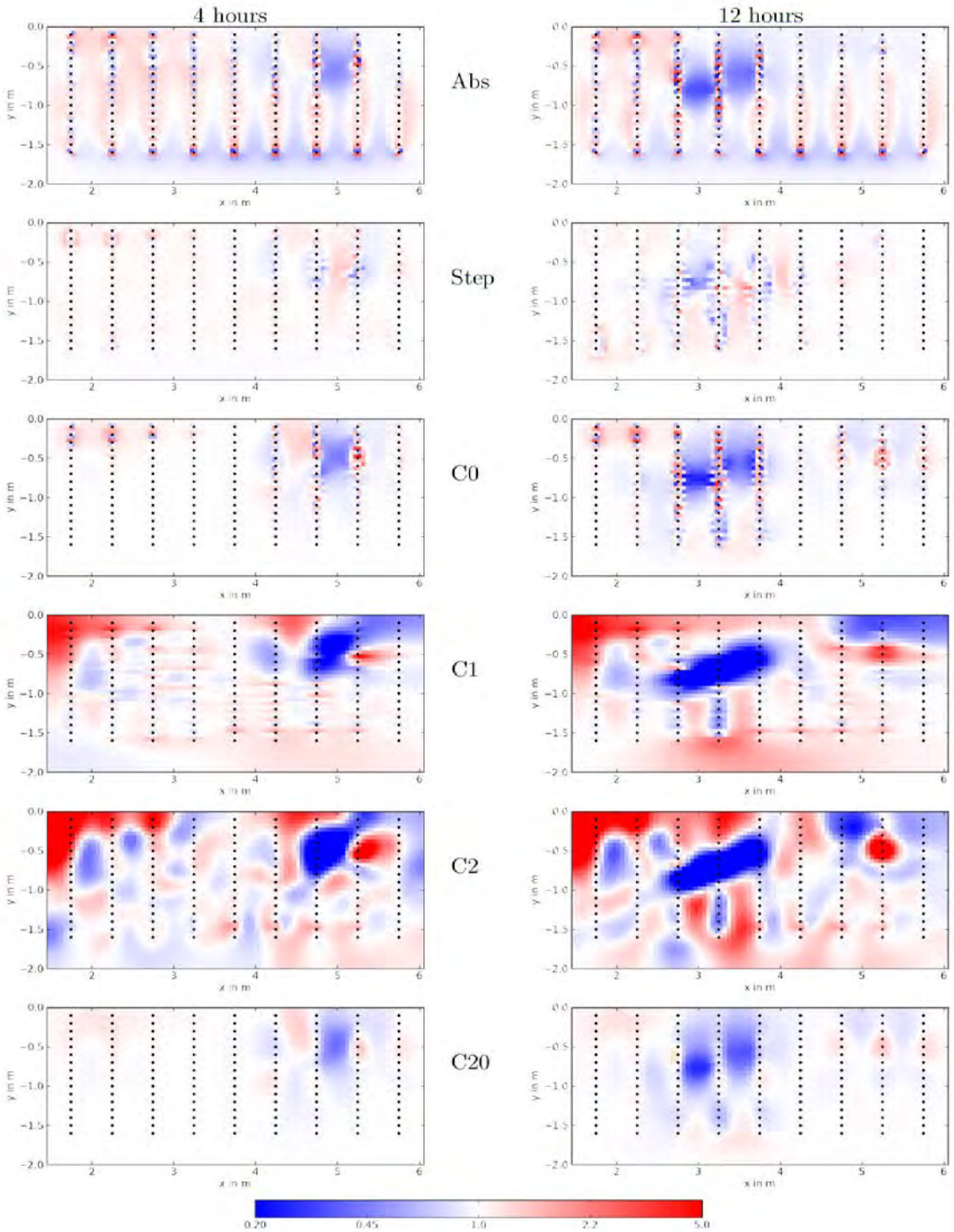

Fig. 6: Resistivity ratio for timesteps 4 hours (left) and 12 hours (right) and inversion schemes: individual inversion, step-wise constrained and difference inversion using constraint orders 0, 1, 2 and 0+2.

References

DESCLOITRES, M., RIBOLZI, O. and LE TROQUER, Y., 2003: Study of infiltration in a Sahelian gully erosion area using time-lapse resistivity mapping. – Catena, **53**, 229-253.

GÜNTHER, T., RÜCKER, C. and SPITZER, K., 2006: 3-d modeling and inversion of DC resistivity data incorporating topography - Part II: Inversion. – Geophysical Journal International, **166**, 506-517.

KURAS, O., PRITCHARD, J., MELDRUM, P., CHAMBERS, J., WILKINSON, P., OGILVY, R. and WEALTHALL, G., 2009: Monitoring hydraulic processes with automated time-lapse electrical resistivity tomography (ALERT). – Compte Rendus Geoscience, **341**, 868-885.

LABRECQUE, D. J. and YANG, X., 2001: Difference Inversion of ERT Data: a Fast Inversion Method for 3-D in Situ Monitoring. – Journal of Environmental and Engineering Geophysics, **6**, 83.

SCHÜTZE, C., FRIEDEL, S. and JACOBS, F. 2002: Detection of three-dimensional transport processes in porous aquifers using geoelectrical quotient tomography. – European Journal of Environment and Engineering Geophysics, **7**, 3-19.

Comparison of algorithms of Time-lapse ERT inversion

MARIOS KARAOULIS[1], PANAGIOTIS TSOURLOS[2] and JUNG-HO KIM[3]

[1] Colorado School of Mines, Dept. of Geophysics, Golden, CO, USA.
[2] Aristotle University of Thessaloniki, Greece.
[3] Geoelectric Imaging Laboratory, Korea Institute of Geoscience and Mineral Resources, Daejeon, South Korea.

jungho@kigam.re.kr

Abstract

Electrical resistivity tomography (ERT) is often used for monitoring dynamic subsurface processes like remediation tests and geothermal processes. ERT imaging in a time-lapse mode ideally involves permanent electrode installations to maximize the repeatability of the measurements. It is a natural tool to complement standard geochemical or hydrogeological in situ sampling in wells, in providing spatio-temporal infomation that cannot be reached by direct sampling. Several single time step inversion algorithms have been proposed to model and invert DC/IP data, but as shown by many authors, inversion may be contaminated with inversion artifacts. Therefore, new inversion algorithms have been proposed, to reduce time related artifacts. The introduction of time into the data set can be achieved with the use of time-lapse tomographic algorithm and a variety of inversion strategies. In this work we will make a comparative study of some of some of the time-lapse inversion strategies.

Introduction

Electrical resistivity is sensitive to salinity, porosity, saturation, pore shape, temperature, clay content, and biological activity (e.g., WAXMAN and SMITS, 1968; REVIL et al., 1998; ATEKWANA et al., 2004). Variability in any of these parameters can have an influence on resistivity and can be monitored by time-lapse electrical resistivity tomography (TL-ERT). In the recent literature, TL-ERT has started to be a popular method to monitor dynamic processes occurring in the shallow subsurface (typically the first hundred meters, see LEGAZ et al., 2009, MÜLLER et al., 2010 and references therein). TL-ERT imaging, often involving permanent electrode installations, has proven to provide information complementary to in situ geochemical measurements. Applications of TL-ERT include monitoring of subsurface flow (e.g., DAILY et al., 1992; RAMIREZ et al., 1993; PARK, 1998; DAILY and RAMIREZ, 2000; NIMMER et al., 2007), characterization of solute transport (e.g., SLATER et al., 2002; KEMNA et al., 2002; SINGHA and GORELICK, 2005; LOOMS et al., 2008), saturation and temperature (LEGAZ et al., 2009), and mapping of salt-water intrusion in aquifers (e.g., NGUYEN et al., 2009; OGILVY et al., 2009) just to cite few applications.

A standard approach is to independently invert the measured data acquired at each monitoring step and to reconstruct time-lapse images (e.g. DAILY et al., 1992; RAMIREZ et al., 1993; BINLEY et al., 1996). As suggested by several researchers, the independent time-lapse inversion images may be strongly contaminated with inversion artifacts due to the presence of noise in the measurements and independent inversion errors. LABRECQUE and YOUNG (2001) and KIM et al. (2009) presented time-lapse algorithms to minimize those artifacts, but as shown by KARAOULIS et al. (2011), these

algorithmes may also suppress real changes in the complex resistivity due to the spurious effect associated with the selection of the time regularization parameter in the cost function.

Inversion

In this section, we descibe the different inversion strategies that can be applied to ERT data. We briefly report the single-time step inversion that is used in this work. In this work, **X** denotes the model, **d** denotes data and G the forward operator. It is important to notice that the main inversion equations remain the same no matter of the choice of 2D or 3D modeling.

Single time-step inversion

Consider the misfit vector **e** between the observed and calculated data that we need to minimize. Among different techniques we choose to minimize the L_2-norm of the following objective function *S*,

$$S = \|\boldsymbol{GX} - \boldsymbol{d}\|^2 + \lambda^2 \|\boldsymbol{CX}\|^2, \quad (1)$$

where λ denotes the tradeoff parameter that controls the model regularization and **C** is the second derivative of the model. The first term of the objective functions, ensures the convergence of the recovered model with respect to the observed data. The second part of the objection function, is introduced to stabilize the inversion algorithm, and produce smooth models (Constable et al., 1987).

The solution to this objective function is found either with an iterative Occam's update Equation (23),

$$\boldsymbol{X}_{i+1} = (\boldsymbol{J}^T\boldsymbol{J} + \lambda\, \boldsymbol{C}^T\boldsymbol{C})^{-1}\boldsymbol{J}^T(G(\boldsymbol{X}) - \boldsymbol{d} + \boldsymbol{J}^T\boldsymbol{X}) \quad (2)$$

By using each each date set seperatley,

Difference inversion

LABREQUE and YANG (2001) presented the difference inversion algorithm in an attempt to minimize possible inversion artifacts. They process time-lapse resistivity data by inverting for the differences between the background and subsequent data sets.

$$\Delta\boldsymbol{D} = (\boldsymbol{d}_t - \boldsymbol{d}_0) - (G(\boldsymbol{X}_t) - G(\boldsymbol{X}_0)), \quad (3)$$

$$\boldsymbol{X}_{i+1} = \boldsymbol{X}_i + (\boldsymbol{J}^T\boldsymbol{J} + \boldsymbol{C}^T\boldsymbol{\Lambda}\boldsymbol{C})^{-1}\boldsymbol{J}^T\Delta\boldsymbol{D}, \quad (4)$$

where the vectors $\boldsymbol{d}_0$ and $\boldsymbol{X}_0$ are the background data and model, while $\boldsymbol{d}_t$ and $\boldsymbol{X}_t$ are the data and model of the reference time-step *t*.

The difference inversion approach is the most popular for inverting time-lapse geoelectrical data as suggested by several published works (KEMNA el al., 2000 CASSIANI et al., 2007; LEROUX and DAHLIN, 2006; OLDENBORGER et al., 2007; TSOURLOS et al., 2008; DE FRANCO et al., 2009; MILLER et al., 2008; OGILVY et al., 2009).

4D inversion and 4D-ATC inversion

The 4D model as described by KIM et al. (2009) defines the subsurface as a combined space-time model which encompasses all space models during the entire monitoring period. The entire monitoring data are defined as a data vector in the space-time domain as well. The space-time model is assumed to change continuously along the time-axis, which allows the change of the subsurface material property distribution during the measurement of the geophysical datum.

Since both the data and the model are defined using space-time coordinates, the 4D-ATC algorithm is able to adopt regularization in both the time and space domains to stabilize the inversion. Consequently, the objective function S to be minimized by the inversion process can be expressed as follows (ZHANG et al., 2005; KIM et al., 2009),

$$S = \|\boldsymbol{e}^T\boldsymbol{e}\|^2 + \lambda\Psi + \alpha\Gamma, \quad (5)$$

where Ψ and Γ are the two regularization functions. The function Ψ is used for smoothness regularization in space and the function Γ is used for flatness regularization in time. The two parameters λ and α are the tradeoff parameters for controlling these two regularizations terms. Regarding the space-domain smoothness constraint, a second order differential operator is applied to the model perturbation vector. In the time domain, KIM *et al.* (2009) applied a first order differential operator to the model vector itself. This is based on the realistic assumption that the change of the material properties in the time domain is small compared to the space domain and the basic subsurface structure would remain the same throughout the entire monitoring period.

The time-domain tradeoff parameter is expressed either as a constant value α (**A**=α**I**) or as a diagonal matrix ***A*** (KARAOULIS *et al*., 2011a).

Minimizing the objective function (5) with respect to the model perturbation vector yields the following normal equations (Kim *et al.*, 2009),

$$\widehat{\boldsymbol{X}}^{k+1} = \widehat{\boldsymbol{X}}^k + d\widehat{\boldsymbol{X}} = + (\widehat{\boldsymbol{J}}^T\widehat{\boldsymbol{J}} + \widehat{\boldsymbol{C}}^T\widehat{\boldsymbol{\Lambda}}\,\widehat{\boldsymbol{C}} + \boldsymbol{M}^T\boldsymbol{A}\boldsymbol{M})^{-1}(\widehat{\boldsymbol{J}}^T\left(G\left(\widehat{\boldsymbol{X}}^k\right) - \widehat{\boldsymbol{D}}\right) - \boldsymbol{M}^T\boldsymbol{A}\boldsymbol{M}\widehat{\boldsymbol{X}}^k). \quad (6)$$

where **M** is a square matrix.

Synthetic test

Modeled data obtained for 5 different time steps representing a hypothetical time-lapse induced polarization change are depicted in Figures 1. A total of 225 surface electrodes were used to obtain surface dipole-dipole data (inter-electrode spacing *a*=1 with maximum intra-dipole spacing *dn* = 7) with 945 measurements for each time-step. The background model had an resistivity of 10 Ohm m.

Figure 2 and 3 shows the difference images, when comparing the independent inversion, the difference inversion, and the 4D/4D-ATC inversion. We can observer that the difference inversion mimics better the actual change than the independent inversion, but the amplitude is smallest than the actual one. Besides that, the area of the actual change is shown more extensive than the modeled one, indication of artifacts. 4D/4D-ATC inversion shows the actual change best, both in position and actual amplitude. Figure 4 shows the model RMS error, where the 4D/4D-ATC invasion achieves the smallest misfit, indication that the modeled changes are closer to the actual one.

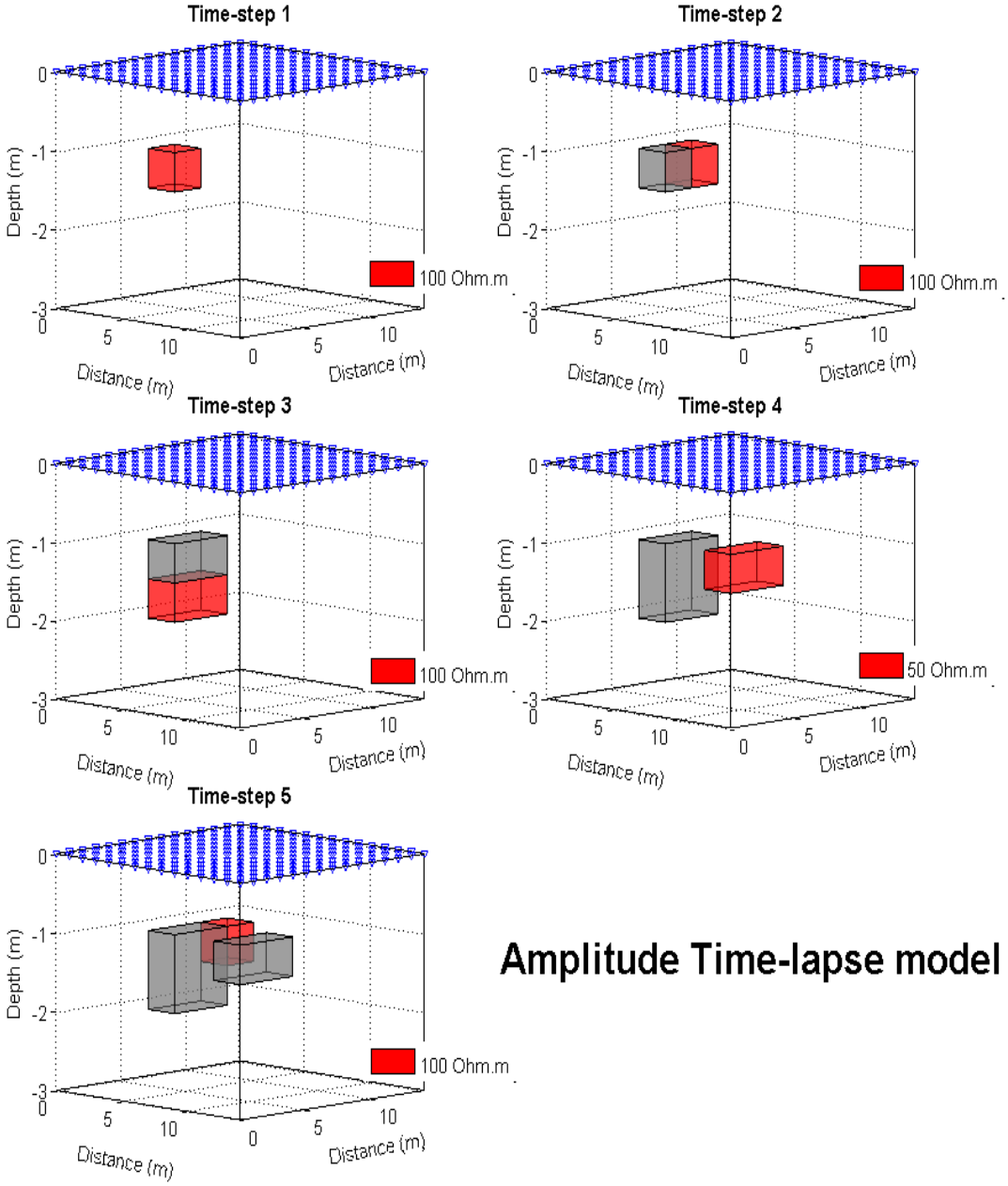

Fig. 1: The 4D resistivity model used in this work showing the changes in amplitude through time (five time-steps). The grey cubes denote the synthetic model used in the previous time-step. The red cubes show the change in that time-step with respect to the previous time-steps. The background model has a constant resistivity amplitude of 10 Ωm.

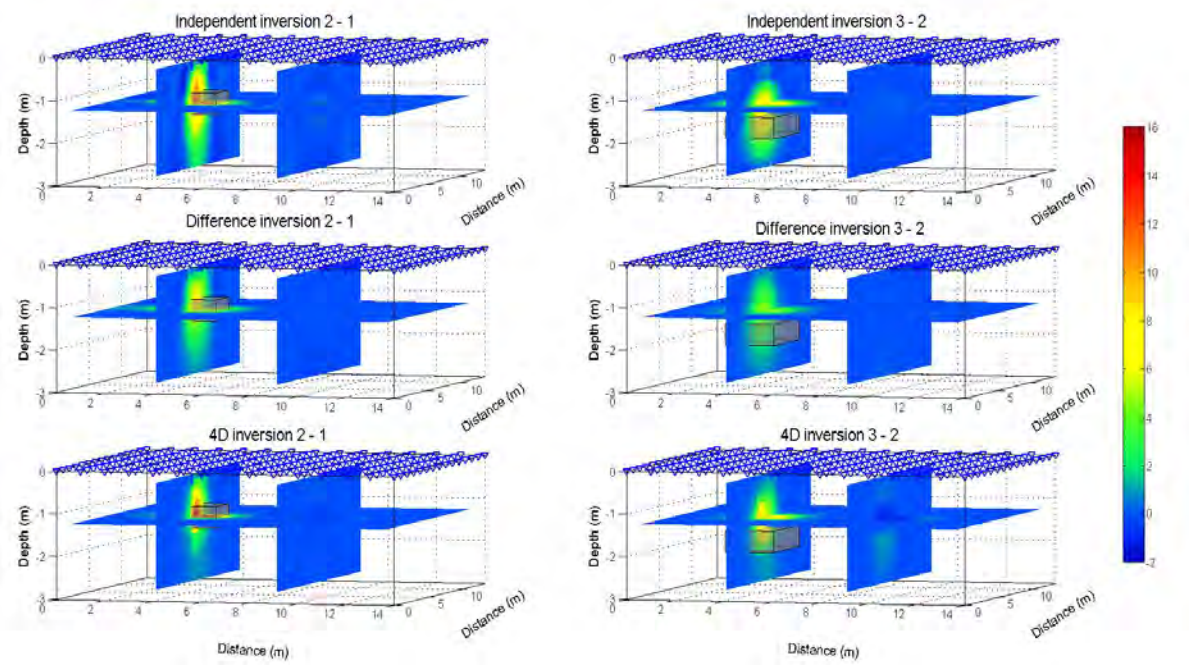

Fig. 2: Difference Images when using three different inversion algorithms for time steps 2-1 and 3-2. Grey cube denotes the area of the modeled change.

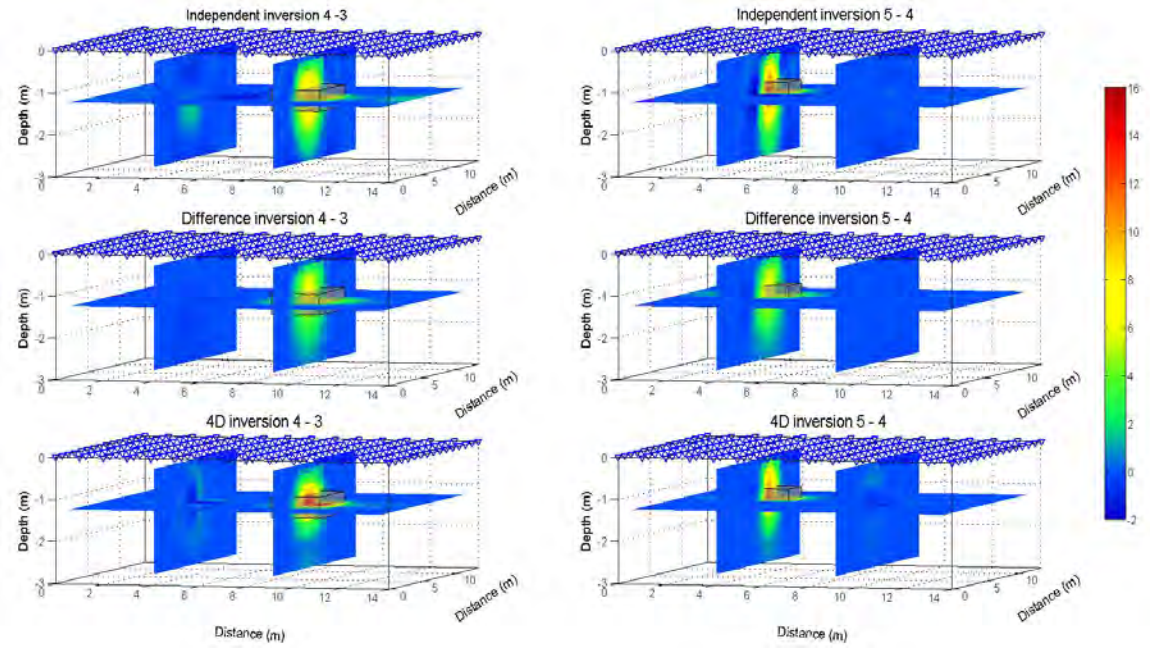

Fig. 3: Difference Images when using three different inversion algorithms for time steps 4-3 and 5-4. Grey cube denotes the area of the modeled change.

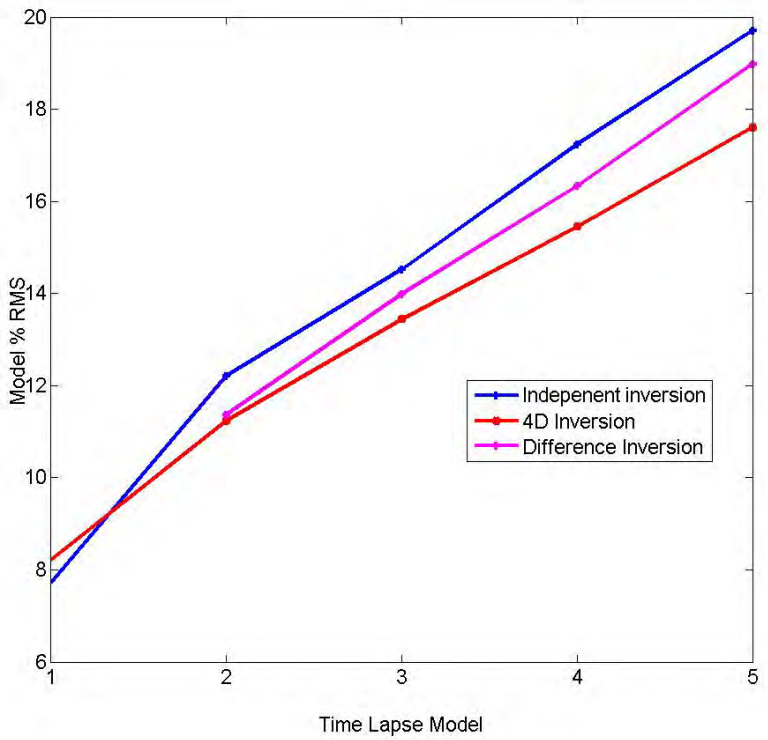

Fig. 4: The % model misfit from all tested algorithm. The smallest model rms error was observed by using the 4D/4D-ATC algorithm.

Conclusions

Independent inversion, as shown from numerical and real data, produces the most artifacts, which in some cases can lead to a false interpretation of the monitoring data. Difference inversion, seems to reduce those artifacts, but it does not eliminated them. 4D and 4D-ATC techniques have the least artifacts and produce the most realistic images.

References

BINLEY, A., HENRY-POULTER, S. and SHAW, B., 1996: Examination of solute transport in an undisturbed soil column using electrical resistance tomography. – Water Resources Research, **32**, 763–769.

CASSIANI, G., BINLEY, A. and FERRÉ, T.P.A., 2007: Unsaturated zone processes. – Applied Hydrogeophysics, **71**, 75-116.

CONSTABLE, S., PARKER, R. and CONSTABLE, C., 1987: Occam's inversion: A practical algorithm for generating smooth models from electromagnetic sounding data. – Geophysics, **52**, 289-300.

DAILY, W., RAMIREZ, A., LABRECQUE, D. & NITAO, J., 1992: Electrical resistivity tomography of vadose water movement. – Water Resources Research, **28**, 1429-1442.

DAILY, W. and RAMIREZ, A.L., 2000: Electrical imaging of engineered hydraulic barriers. – Geophysics, **65**, 83-94.

KARAOULIS, M., KIM, J.-H. and TSOURLOS, P.I., 2011: 4D Active Time Constrained Inversion. – Journal of Applied Geophysics, **73**, 25-34.

KEMNA, A., BINLEY, A., RAMIREZ, A. and DAILY, W., 2000: Complex resistivity tomography for environmental applications. – Chemical Engineering Journal, **77**, 11–18.

KIM, J.-H., YI, M.J., PARK, S.G. and KIM, J.G., 2009: 4-D inversion of DC resistivity monitoring data acquired over a dynamically changing earth model. – Journal of Applied Geophysics, **68**(4), 522-532.

LABRECQUE, D.J. and YANG, X., 2001: Difference inversion of ERT data: a fast inversion method for 3-D in situ monitoring. – Journal of Environmental and Engineering Geophysics, **5**, 83-90.

LEGAZ, A., VANDEMEULEBROUCK, J., REVIL, A., KEMNA, A., HURST, A.W., REEVES, R. and PAPASIN, R., 2009: Acase study of resistivity and self-potential signatures of hydrothermal instabilities, Inferno Crater Lake, Waimangu, New Zealand. – Geophysical Research Letters, **36**, L12306, doi: 10.1029/2009GL037573.

LEROUX, V. and DAHLIN, T., 2006: Time-lapse resistivity investigations for imaging saltwater transport in glaciofluvial deposits, Environmental Geology, **49**(3), 347-358.

LOOMS, M.C., JENSEN, K.H., BINLEY, A. and NIELSEN, L., 2008: Monitoring unsaturated flowand transport using cross-borehole geophysical methods. – Vadose Zone Journal, **7**, 227–237.

MILLER, C.R., ROUTH, P.S., BROSTEN, T.R., and MCNAMARA, J.P., 2008: Application of time-lapse ERT imaging to watershed characterization. – Geophysics, **73**, G7-G17.

MÜLLER, K., VANDERBORGHT, J., ENGLERT, A., KEMNA, A., HUISMAN, J.A., RINGS, J. and VEREECKEN, H., 2010: Imaging and characterization of solute transport during two tracer tests in a shallow aquifer using electrical resistivity tomography and multilevel groundwater samplers. Water Resources Research, **46**, W03502, doi: 10.1029/2008WR00.

NGUYEN, F., KEMNA, A., ANTONSSON, A., ENGESGAARD, P., KURAS, O., OGILVY, R., GISBERT, J., JORRETO, S. and PULIDO-BOSSCH, A., 2009: Characterization of seawater intrusion using 2D electrical imaging. – Near-Surface Geophysics, **7**(5-6), 377-390.

NIMMER, R.E., OSIENSKY, J.L., BINLEY, A.M., SPRENKE, K.F. and WILLIAMS, B.C., 2007: Electrical resistivity imaging of conductive plume dilution in fractured rock. – Hydrogeology Journal, **5**, 877-890.

OGILVY, R D., KURAS, O., MELDRUM, P I., WILKINSON, P B., CHAMBERS, J. E., SEN, M., GISBERT, J., JORRETO, S., FRANCES, I., PULIDO-BOSCH, A. and TSOURLOS, P., 2009: Automated time-Lapse Electrical Resistivity Tomography (ALERT) for monitoring Coastal Aquifers. – Near Surface Geophysics, **7**(5-6), 367-375.

OLDENBORGER, G.A., KNOLL, M.D., ROUTH, P.S. and LABRECQUE, D.J., 2007: Time-lapse ERT monitoring of an injection/withdrawal experiment in a shallow unconfined aquifer. – Geophysics, **72**(4), F177-F187.

PARK, S., 1998: Fluid migration in the vadose zone from 3-D inversion of resistivity monitoring data. – Geophysics, **63**(1), 41-51.

RAMIREZ, A., DAILY, W., LABRECQUE, D.J., OWEN, E. and CHESNUT, D., 1993: Monitoring an underground steam injection process using electrical resistance tomography. – Water Resources Research, **29**, 73-87.

SINGHA, K. and GORELICK, S.M., 2005: Saline tracer visualized with electrical resistivity tomography: field scale spatial moment analysis. – Water Resour. Res., **41**, W05023, doi: 10.1029/2004WR003460.

SLATER, L., BINLEY, A.M., VERSTEEG, R., CASSIANI, G., BIRKEN, R. and SANDLEBERG, S., 2002: A 3D ERT study of solute transport in a large experimental tank. – Journal of Applied Geophysics, **49**(4), 211–229.

ZHANG, Y., GHODRATI, A., BROOKS, D.H., 2005: An analytical comparison of three spatiotemporal regularization methods for dynamic linear inverse problems in a common statistical framework. – Inverse Problems, **21**, 357-382.

Inversion of multi-temporal geoelectrical data sets: insights from several case studies

FRÉDÉRIC NGUYEN[1], ANDREAS KEMNA[1], TANGUY ROBERT[1], THOMAS HERMANS[1] and DAVID CATERINA[1]

[1] University of Liège, Belgium, ArGEnCo, GEO³, Applied Geophysics.

f.nguyen@ulg.ac.be

Abstract

Time-lapse inversion of geoelectrical data is increasingly growing as remote monitoring systems are being used in more applications such as seawater intrusions, landslides, bioremediation of contaminated sites, landfill operations, shallow geothermal systems, or water resources. To date, several inversion strategies exist for taking into account the temporal dimension of the data. Among the most used ones are the independent inversion of multi-temporal data sets, the difference inversion, the temporally-constrained inversion, and the more recent process-based inversion. The success of a particular time-lapse inversion scheme depends on the validity of several assumptions made by these inversion schemes. Difference inversion schemes generally assume that part of the noise contained in the data cancels out when working with temporal data differences. Process-based inversion requires a more advanced knowledge of the system prior the inversion. Temporally-constrained inversion on the other hand assumes that the changes are localized and minor. We show in this paper using data sets with different time and spatial scales, and with different degrees of geological complexity and resistivity contrasts, that the particular success of a time-lapse inversion scheme is highly dependent on the temporal behaviour of the noise estimation in the time-lapse data set and of the model-dependent resolution pattern of the survey. We attempt to provide guidelines for successful quantitative interpretation of time-lapse data sets whenever possible.

4D inversion of L1 and L2 norm minimizations

JUNG-HO KIM[1, 3], PANAGIOTIS TSOURLOS[2] and ROBERT SUPPER[3]

[1] Korea Institute of Geoscience and Mineral Resources, 30 Gajeong-dong, Yuseong-gu, Daejeon 305-350, South Korea.
[2] Aristotle University of Thessaloniki, 54124 Thessaloniki, Greece.
[3] Geological Survey of Austria, Neulinggasse 38, 1030 Vienna, Austria.

jungho@kigam.re.kr

Abstract
A new 4-dimensional (4D) inversion algorithm is developed so that any of data misfits and model roughness in the space and time domains can be selectively minimized either in terms of L1 norm or in L2 norm. This study is motivated by the experiences that a 4D inversion adopting full L2 norm minimization may sometimes result in a model too smoothly varying with time. It is further encouraged by the realization that a particular criterion of either L1 or L2 norm cannot universally be the optimal approach for accurately reconstructing the subsurface condition. Along with this development of the algorithm, we try to overcome the difficulties of jointly choosing two optimal regularization parameters in the space and time domains. To achieve this, we devise automatic determination methods not only of the Lagrangian multipliers for the space-domain smoothness constraint but also of the regularization parameter for penalizing the model roughness along the time axis. Both kinds of the regularization parameters are actively updated as data misfits and model roughness vary at each iteration step. We conducted inversion experiments using synthetic and field monitoring data to test the proposed algorithms and further to compare the performance of L1 norm and L2 norm minimizations. Both of the synthetic and field data experiments proved that the automatic determination method developed in this study is very effective for calculating the ground changes that are closer to the ground truth than the approaches of using pre-determined parameter values. Synthetic data examples showed that L1 norm minimization of the time-domain roughness could cure the problem of unnecessary smooth model changes when the subsurface changes are locally confined, but at the same time, the L2 norm approach would be more reasonable when the changes are expected widespread.

Keywords: 4D, inversion; L1 norm; resistivity monitoring; geophysical monitoring.

Introduction

DC resistivity monitoring has widely been applied to many environmental and engineering problems (e.g., DAILY and RAMIREZ, 1995) and its application has recently been extended to the geological disaster mitigation (e.g., SUPPER et al., 2009). The ground condition changes are quantified and visualized by the difference of a pair of time-lapse images which frequently boosts up the artefacts; these artefacts amplified in the difference images may contribute to a misinterpretation of the ground condition change. KIM et al. (2009) proposed a four dimensional (4D) inversion algorithm where time dimension is included into inversion. The regularization in both the space domain and the time domain effectively reduce inversion artefacts. KARAOULIS at al. (2011) noted that the time regularization sometimes makes the inverted results too smooth in the time domain and proposed the 4D Active Time Constrained (4D-ATC) inversion where the

time regularization is allowed to vary depending on the degree of resistivity changes in the space-time domain.

Most of the studies on the inversion of electric monitoring data have adopted the L2 norm minimization of penalty values. It is known that the L2 norm minimization assumes a normal distribution, while a Laplace or exponential distribution is the basic assumption for the L1 norm inversion (MENKE, 1984). Therefore, a particular criterion of either L1 or L2 norm cannot universally be the optimal approach for accurately reconstructing the subsurface condition. We should flexibly select either L1 or L2 norm according to the behaviours of monitoring data and inverse model parameters in the 4D space. To address this, we develop a new inversion algorithm where any of the data misfits and two kinds of model roughness in the space and time domains can be selectively minimized either in terms of L1 norm or in L2 norm. Together with this, we note that it is very difficult to simultaneously determine regularization parameters which optimally control the two smoothness constraints both in the space and time domains. To solve the difficulties, we devise methods to automatically determine the regularization parameters that are actively updated as the data and model roughness vary at each iteration step. The newly developed methods are compared and their performances are demonstrated via synthetic examples as well as field data application for landslide monitoring.

4D inversion algorithm based on either L1 or L2 norm minimization

The 4D inversion defines the many subsurface models sampled in each monitoring time-laps as a single model vector in the space-time domain and the entire monitoring data sets as well:

$$\mathbf{P} = \{\mathbf{p}_1, \ldots, \mathbf{p}_i, \ldots, \mathbf{p}_o\} \text{ and} \tag{1a}$$

$$\mathbf{D} = \{\mathbf{d}_1, \ldots, \mathbf{d}_i, \ldots, \mathbf{d}_o\}, \tag{1b}$$

where o is the number of time-lapses. Owing to these definitions, the regularizations can be introduced both in the space domain and in the time domain. Accordingly, the objective function is expressed as

$$\Phi(\mathbf{P}+\Delta\mathbf{P}) = \Xi\,(\mathbf{P}+\Delta\mathbf{P}) + \Psi\,(\mathbf{P}+\Delta\mathbf{P}) + \Gamma\,(\mathbf{P}+\Delta\mathbf{P}). \tag{2}$$

$\mathbf{P}$ is a starting model or a model calculated in the previous iteration. $\Delta\mathbf{P}$ is the unknown model perturbation vector, i.e., $\Delta\mathbf{P} = \mathbf{P}_{j+1} - \mathbf{P}_j$, where j is the iteration number. Ξ, Ψ and Γ are the penalty functions of the data misfit, the model roughness in the space and that in the time domains, respectively. Any of these three functions are defined in either L1 or L2 norm which is to be minimized or penalized through an inversion process in a trade-off manner. Each penalty function is a measure of data misfit or model roughness and is quantified as its L1 norm or L2 norm:

$$\Xi(\mathbf{P}) = \left\|\mathbf{WE}(\mathbf{P})\right\|^p,\ \Psi(\Delta\mathbf{P}) = \left\|\sqrt{\boldsymbol{\Lambda}}\mathbf{C}^s\Delta\mathbf{P}\right\|^p, \text{ and } \Gamma(\mathbf{P}) = \left\|\sqrt{\alpha\mathbf{A}}\mathbf{C}^t\mathbf{P}\right\|^p, \text{ where } p = 1 \text{ or } 2. \tag{3}$$

$\mathbf{E}$ is the data misfit between the field and theoretically calculated data. The superscripts t and s imply space and time domains, respectively. $\mathbf{W}$ is a diagonal matrix of data weighting factors. $\mathbf{C}^s$ is a second order differential operator in the space domain. $\mathbf{C}^t$ is a difference operator to calculate the model roughness in the time domain.

The active constraint balancing (ACB) method (YI et al., 2003) is adopted to balance the smoothness constraints in the space domain; thus, the regularization parameter for controlling the contribution of the roughness term Γ is expressed as a diagonal matrix, $\mathbf{\Lambda} = \mathrm{diag}\ (\lambda_i)$, in the above equations. The model smoothness along the time axis is controlled by another regularization parameter α in the roughness term Ψ. These two different kinds of regularization parameters should optimally be chosen, which will be discussed later.

The time domain model roughness Γ includes a diagonal matrix, **A** = diag (a_i), which is called as the cross-time weighting matrix. It is introduced mainly to alleviate the problem that the 4D inversion of L2 norm minimization may result in an inverse 4D model too smoothly varying in the time domain (KARAOULIS et al., 2011). Another function of the matrix is to reduce the problem that the model parameters having less resolving power are more likely to be contaminated by inversion artefacts. Its diagonal elements (cross-time weighting factors) are automatically calculated so that a lower weighting factor can be assigned to an inverse model parameter which is more quickly changing with time, and vice versa. It should be noted that the average of the upper and lower bounds of the weighting factors is set as one on logarithmic scale. By doing this, the contribution of the time-domain roughness is systematically controlled by adjusting the regularization parameter α.

To numerically implement the L1 norm minimization of a particular penalty term, we adopt an algorithm of the iteratively reweighted least-squares inversion (FARQUHARSON and OLDENBURG, 1998). A merit of the algorithm is to easily implement the L1 norm minimization within the framework of commonly used least-squares inversion. By adopting the reweighting algorithm, the partial derivative of a penalty term with respect to the model perturbation vector is expressed in a similar form of L2 norm minimization but includes additional term of a reweighting matrix, **R** = diag (r_i). For example, the derivative of the L1 norm model roughness in the time domain, i.e., Γ, is expressed as following:

$$\frac{1}{2}\frac{\partial \Gamma}{\partial \Delta \mathbf{P}} \cong (\sqrt{\alpha}\mathbf{A}\mathbf{C}^t)^T \mathbf{R}_t (\sqrt{\alpha}\mathbf{A}\mathbf{C}^t)(\mathbf{P} + \Delta\mathbf{p}), \text{ and} \tag{4}$$

$$r_{i,i}^t = [\sqrt{\alpha a_i} \sum_{k=1}^{m \times o} C_{i,k}^t P_k + \varepsilon^2]^{-1/2}, \tag{5}$$

where the superscript T means the transpose of a matrix and ε is a small constant to avoid the division by zero. Note that the updated model and data misfits are necessary to calculate the reweighting matrices but they are actually not calculated yet. FARQUHARSON and OLDENBURG (1998) once calculated the model using a least-squares inversion and again used it for computing the reweighting matrices as an approximation of the updated model for L1 norm inversion. In this study, we simply use the solution at the previous iteration as equation (5) implies.

In such ways, we have the following normal equation for minimizing the L1 norms of all penalty terms:

$$\begin{aligned} &\{(\mathbf{W}\mathbf{J})^T \mathbf{R}^d \mathbf{W}\mathbf{J} + (\sqrt{\mathbf{\Lambda}}\mathbf{C}^s)^T \mathbf{R}^s (\sqrt{\mathbf{\Lambda}}\mathbf{C}^s) + (\sqrt{\alpha}\mathbf{A}\mathbf{C}^t)^T \mathbf{R}^t (\sqrt{\alpha}\mathbf{A}\mathbf{C}^t)\}\Delta\mathbf{P} \\ &= (\mathbf{W}\mathbf{J})^T \mathbf{R}^d \mathbf{W}\mathbf{E} - (\sqrt{\alpha}\mathbf{A}\mathbf{C}^t)^T \mathbf{R}_t (\sqrt{\alpha}\mathbf{A}\mathbf{C}^t)\mathbf{P} \end{aligned}, \tag{6}$$

where **J** is the partial derivatives of the data (apparent resistivity) with respect to the model parameters (resistivity), Jacobian matrix. $\mathbf{R}^d$, $\mathbf{R}^s$ and $\mathbf{R}^t$ are the reweighting matrices for the data

misfit functional and the two model roughness in the space and time domains, respectively. Note that we can have a normal equation of a mixed version of L1 and L2 norm minimizations of penalty measures, when a particular reweighting matrix is selectively replaced with a unit matrix. Solving the normal equation iteratively results in the final inverted subsurface model in the space-time domain.

Automatic determination of regularization parameters in the space and time domains

Our inversion algorithm includes two smoothness constraints in the space and time domains. Correspondingly, two different kinds of regularization parameters should optimally be chosen, but it is not easy since two constraints both in the space and time domains would be cross-related in an actual inversion process. Furthermore, the developed algorithm allows us to define the measure of each roughness in either L1 or L2 norm as we want. This in turn gives rise to more difficulties in selecting optimal Lagrangian multiplier values, since it is practically impossible to choose regularization parameter to be universally optimal for any arbitrary combination of penalty measures. These difficulties lead us to devise methods to automatically determine two different regularization parameters. The proposed methods are to calculate the parameter values by using of the relative value of each penalty measure with respect to the data misfit measure as follows.

The space-domain parameters, i.e., $\mathbf{\Lambda}$ = diag (λ_i), are computed so that the space-domain model roughness Ψ will be a constant fraction of the data misfit measure Ξ; the fraction value is given by the user and specified as a percentage with respect to the data misfit value Ξ. This is a practical implementation for maintaining the relative contribution of the space-domain model roughness with respect to the data misfits at a certain fixed level throughout the entire inversion process.

For automatically determining the time-domain parameter, we newly introduce a concept of the time-domain data roughness which is defined using the time differences of data misfits. This is introduced to realize that the amount of data misfits at each time-lapse should be almost constant along the time axis if an inverted 4D model would appropriately mimic the true subsurface model changes. The time domain regularization parameter α is computed to be inversely proportional to the relative value of the newly introduced data roughness with respect to the data misfit value. Actual computation of the parameter value includes the relative amounts of the model roughness in the time domain with respect to that in the space domain as well.

The devised method demands to optimally choose two predetermined proportional constants, but it is much more effective compared to regular approaches using pre-determined parameter values. Once optimal constants are chosen, then the value would be optimal to any combinations of penalty measures, since the penalty values themselves are used to compute the parameter. Furthermore, the regularization parameters are actively computed as the data and model roughness vary at each iteration step.

Numerical example

We conducted numerical experiments of surface resistivity monitoring firstly to verify the performance of the proposed algorithm and secondly to compare the performances of the L1 norm and L2 norm minimizations particularly of the time-domain model roughness. For convenience of discussion, let us denote “L1” and “L2” for the L1 and L2 norm minimization respectively. Similarly, “D”, “S” and “T” denote the data misfit, the model roughness in the space domain and that in the time domain, respectively. For example, L2D_L2S_L1T means the 4D

inversion of minimizing the L2 norm of both the data misfit and the model roughness in the space domain, and L1 norm in the time domain. In model studies discussed here, the adopted array was dipole-dipole and there were eight monitoring surveys. Synthetic data were calculated using the 2.5D finite element modeling code. Random electrical noise of 1 mV/A pea-to-peak amplitude was added to the synthetic potential difference data to simulate the field data.

Figure 1 illustrates inversion experiments using a subsurface model where the resistivity changes are spatio-temporally localized as shown in Figure 1a. The automatic determination method always resulted in the difference images much closer to the ground truth than the usual methods of using pre-determined parameter values. Comparing the L2 and L1 norm minimizations of the time-domain roughness, the L1 norm minimization is much superior to the L2 one in this test model experiments. The cross-time weighting positively affected the inversion results when adopting the L2 norm of the time-domain roughness (see Figure 1c and 1d), but negatively when the L1 norm was selected. Applying the cross-time weighting can be regarded as an attempt to partly introduce a L1 norm minimization concept into L2 norm inversion. The experiments using this type model seem to conclude that the L1 norm of the time-domain model roughness would be a way to achieve the best inversion results. We can find a good example of field application in KIM et al. (2010).

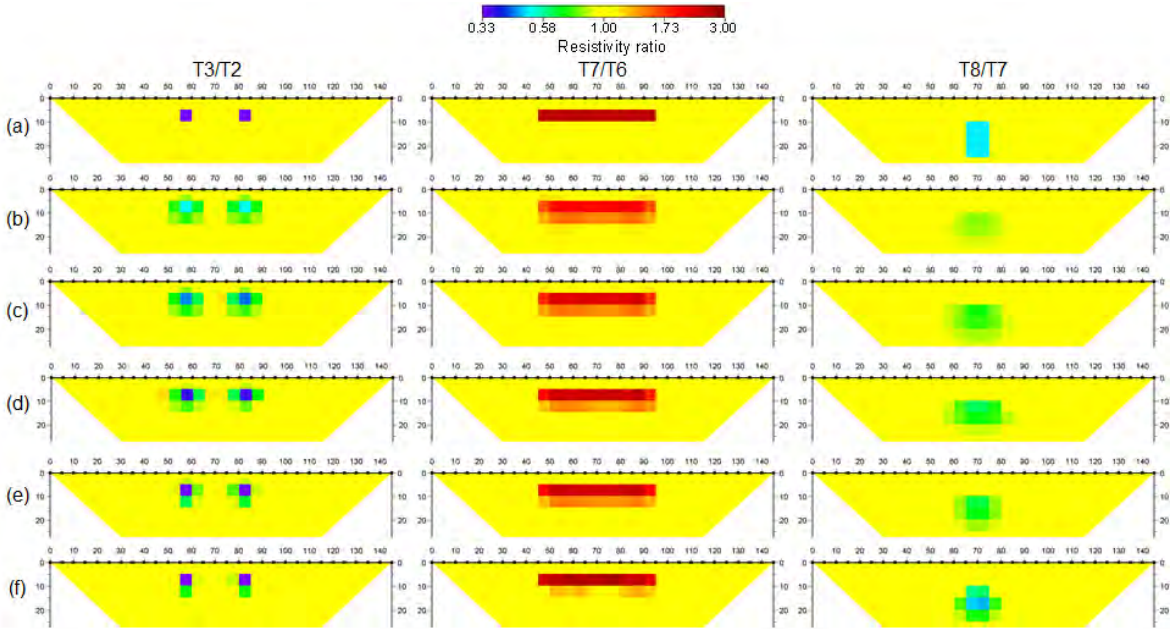

Fig. 1: Inversion experiments based on a model where the resistivity is changing very locally not only in the space domain but also in the time. (a) The true model changes between two sequential time steps. (b)-(d) are the results of L2D_L2S_L1T approach adopting (b) α = 0.1, and the automatic determination of regularization parameters (c) without and (d) with the cross-time weighting. (e) and (f) are those of L2D_L2S_L1T. (e) α = 0.1. (f) Automatic determination of regularization parameters without the cross-time weighting.

Figure 2 shows another test model in the case that the resistivity throughout the entire modeled region is always changing during the whole monitoring period. The characteristics of the assumed resistivity changes are completely different from those of the previous scenario that the resistivity changes are confined only at several particular 4D coordinates. As shown in Figure 3, the reconstructed difference images in this test case are relatively less accurate compared to the previous numerical experiments. In particular, discrepancies from the ground truth are more pronounced in deep depths, which are mainly due to the lower resolving power of deeper region.

The most important conclusion in this test case is that the L2 norm of the time-domain roughness is far better than the L1 norm approach; this is completely opposite to the previous experiments.

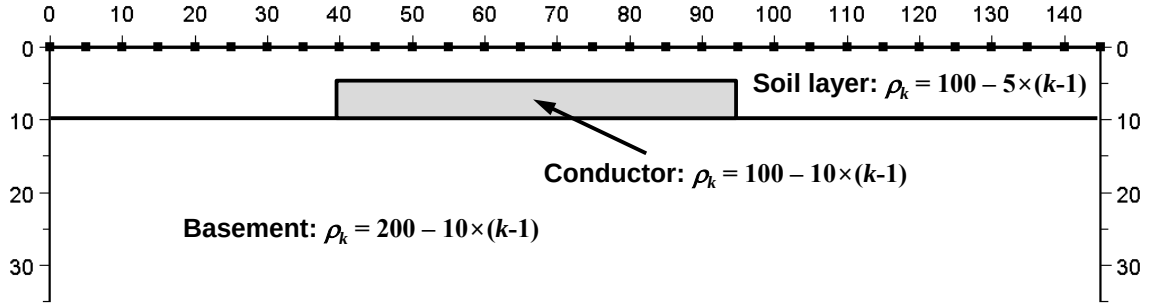

Fig. 2: A test model in which the resistivity throughout the entire modelled region is decreasing with time. ρ_k is the resistivity of each zone in Ωm at the monitoring time step *k*.

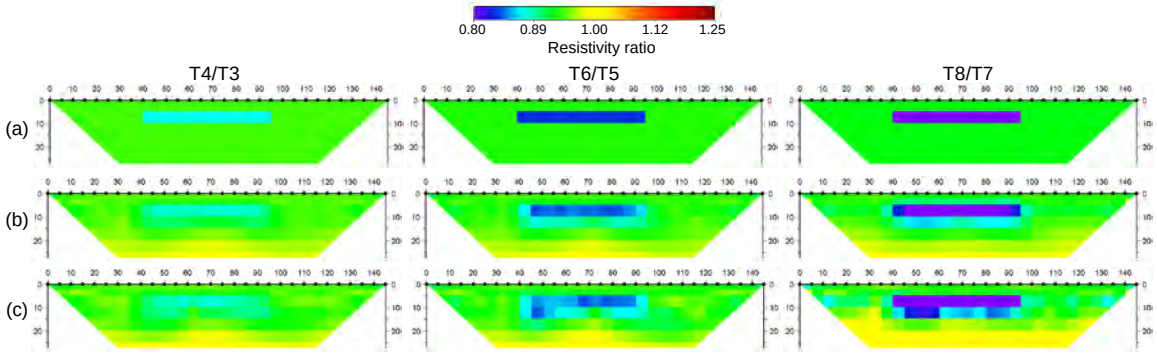

Fig. 3: Inversion experiments based on the test model of Figure 2. (a) The true model changes between sequential time steps. (b) L2D_L2S_L1T. (c) L2D_L2S_L1T. Regularization parameters were automatically determined.

As illustrated in the first model experiments, the problems of too smoothly varying model with time can be solved by minimizing the L1 norm of the time-domain roughness. However, numerous numerical experiments, for instance, the above two synthetic examples, led us not to conclude that a particular norm (L1 or L2) inversion would be the best choice for inverting monitoring data in a 4D inversion manner. Either L1 or L2 norm criterion should be selected through the careful consideration of the behavior of data and inverse model parameters in the 4D space. Particularly for the minimization of the time-domain model roughness, the L1 norm would be better when the subsurface changes are locally confined, while the L2 norm approach would be more reasonable when the changes are expected widespread.

Field application: landslide monitoring

Austrian Geological Survey has been operating six test sites for the monitoring of landslides for the TEMPEL project. DC resistivity data observed at the Bagnaschino site in the north-western Italy were chosen for the field application test of the developed algorithms. At the test site, significant displacements up to about 100 mm were recorded during the period of 15 to 18 March 2011, and we selected the 9 time-lapse data sets recorded from 14 March to 16 March (Figure 3). The reconstructed difference images illustrated in Figure 4 implies that the ground condition changes have mainly happened horizontally at the depth interval of 4-8 meters, which is expressed as conductivity increase. Movements of the changes with time are also recognizable; at

the monitoring step T3 the change started in the zone of about 90-110 meters and propagated leftwards along the slope until T5. At the T7 phase, the anomalous zone became more resistive; the original ground condition somehow started to be recovered. According to the displacements recorded by a high-precision borehole inclinometer, ground movements were dominant from the surface down to about 8 meter depth; the ground mass above the 8 meter depth slid. These observations well match the understanding of ground changes from the difference images.

Comparing the L1 norm minimization of the time-domain roughness with the L2 norm one, the anomalies in the L1 norm results look are more focussed, while the L2 ones are more horizontally elongated. Nevertheless, both results well agree with the observations of ground displacement. It is hardly concluded which particular approach would be superior to the other one, since the true changes are not precisely known and both reasonably match the known information.

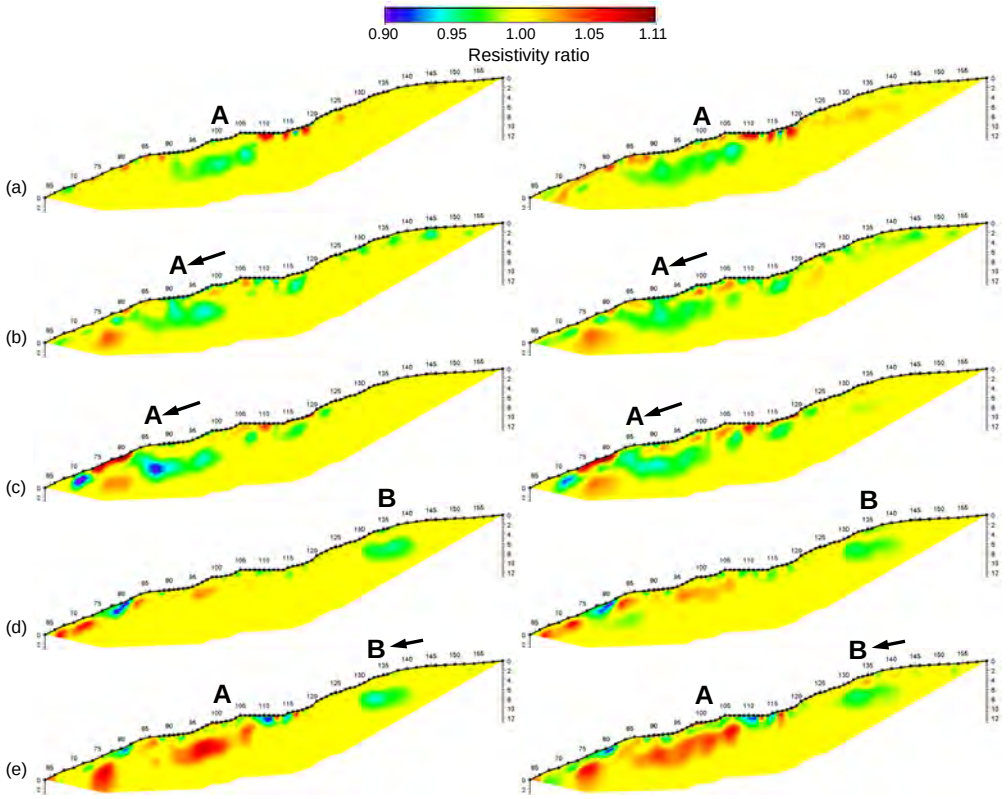

Fig. 4: Reconstructed difference images between two sequential time steps. The left column is the results by the L2D_L2S_L1T approach while the right is L2D_L2S_L2T. (a) T3/T2. (b) T4/T3. (c) T5/T4. (d) T6/T5. (e) T7/T6.

Conclusions

A new 4D inversion algorithm of resistivity monitoring data is presented for precisely estimating the ground condition changes. Through the developed method, we intend to provide a way to adopt either L1 norm or L2 norm minimization of any penalty values in the 4D inversion based on the characteristics of expected subsurface model as well as measured data. The most innovative aspect of the developed algorithm is that the optimal values of the regularization parameters controlling the two smoothness constraints can automatically be updated at each iteration step as the data misfits and the model roughness varies.

Comparisons with the inversion results adopting many different pre-determined values of the regularization parameters confirmed the effectiveness of the newly devised automatic methods.

The automatic determination method always resulted in the difference images much closer to the ground truth than the approaches of using pre-determined parameter values. The problems of too smoothly varying model with time can be solved simply by minimizing the L1 norm of the time-domain roughness. However, either L1 or L2 norm criterion should be selected through the careful consideration of the behavior of data and inverse model parameters in the 4D space. Particularly referring to the time-domain model roughness, the L1 norm minimization would be better when the subsurface changes are locally confined, while the L2 norm approach would be more reasonable when the changes are expected widespread.

References

DAILY, W. and RAMIREZ, A.L., 1995: Electrical resistance tomography during in-situ trichloroethylene remediation at the Savannah River Site. – Journal of Applied Geophysics, **33**, 239-249.

FARQUHARSON, C.G. and OLDENBURG, D.W., 1998: Non-linear inversion using general measure of data misfit and model structure. – Geophysical Journal International, **134**, 213-227.

KARAOULIS, M.C., KIM, J.-H. and TSOURLOS, P.I., 2011: 4D active time constrained resistivity inversion. – Journal of Applied Geophysics, **73**, 25-34.

KIM, J.-H., YI, M.-J., PARK, S.-G., and KIM, J.G., 2009: 4-D inversion of DC resistivity monitoring data acquired over a dynamically changing earth model. – Journal of Applied Geophysics, **68**, 522-532.

KIM, J.-H., YI, M.-J., AHN, H.-Y. and KIM, K.-S., 2010: 4-D Inversion of Resistivity Monitoring Data Using L1 Norm Minimization. – Proceedings of Near Surface 2010, A15, Zurich, Swiss, 6.-8. September.

MENKE, W., 1984: Geophysical data analysis: discrete inverse theory. – 260 p., Academic Press Inc.

SUPPER, R., RÖMER, A. and JOCHUM, B., 2009: Geoelectric measurements for natural hazard monitoring. – Proceedings of the 9th SEGJ International Symposium – Imaging and Interpretation, Sapporo, Sapan, 12.-14. Oct. 2009.

YI, M.-J., KIM, J.-H. and CHUNG, S.-H., 2003: Enhancing the resolving power of least-squares inversion with active constraint balancing. – Geophysics, **68**, 931-941.

Applications in Landslide Monitoring

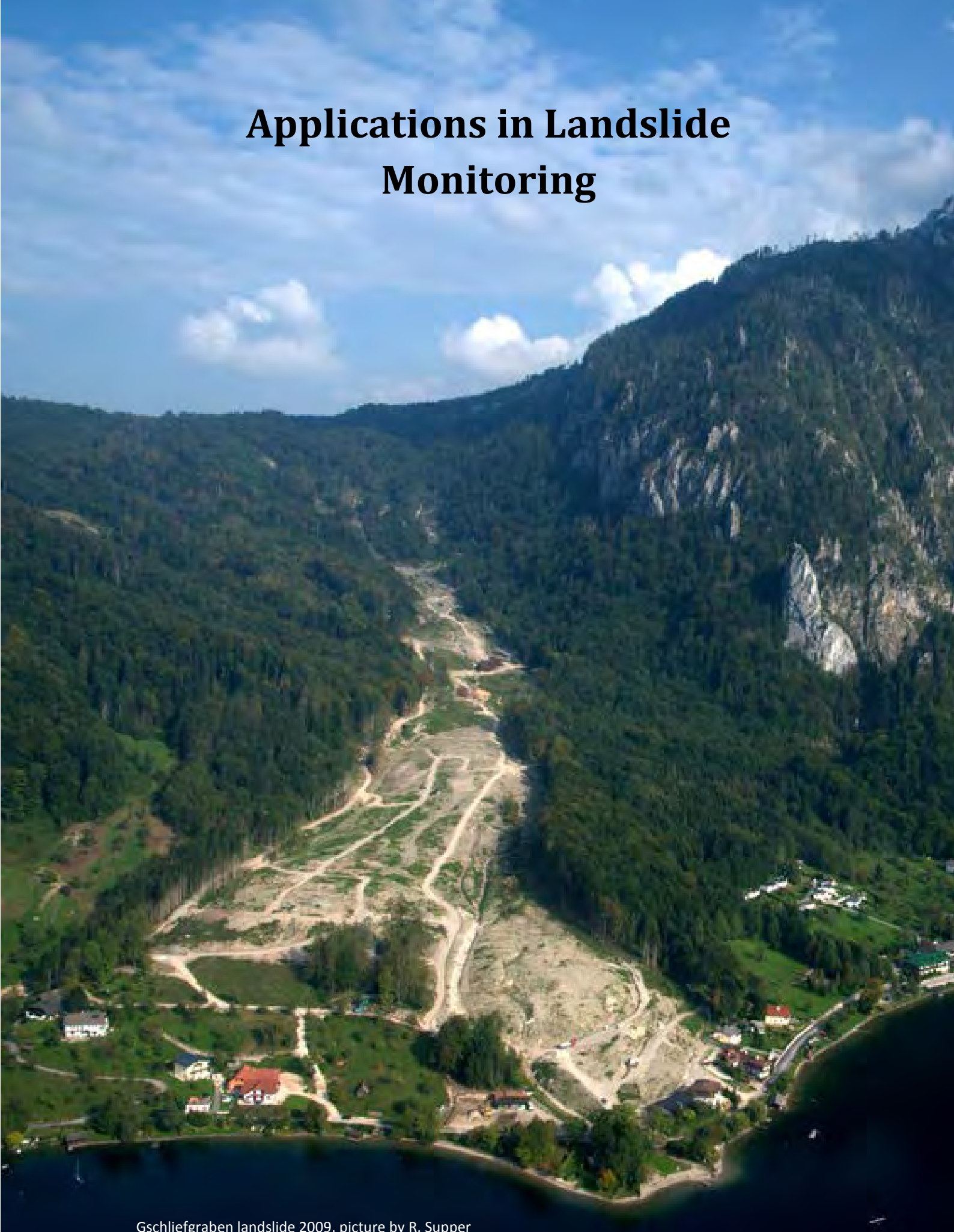

Gschliefgraben landslide 2009, picture by R. Supper

Geophysical-geotechnical sensor networks for slope stability monitoring

JONATHAN E. CHAMBERS[1], PHILIP I. MELDRUM[1], PAUL B. WILKINSON[1], DAVID A. GUNN[1], OLIVER KURAS[1], JOANNA WRAGG[1] and CHRIS MUNRO[1]

[1] British Geological Survey, Keyworth, Nottingham, NG12 5GG.

jecha@bgs.ac.uk

Abstract

Slopes, such as earth embankments, can be vulnerable to instability triggered by sustained wetting or drying events. The resilience of earth structures to these climatic stresses, particularly in the case of old waterway and railway embankments, can be difficult to determine due to the complexity of fill materials and the limitations of current approaches to characterisation and monitoring. For example, remote observation of change in surface morphology generally indicates late-stage failure, whilst point sensors provide insufficient spatial sampling density to adequately characterise, and therefore monitor, highly heterogeneous subsurface conditions.

Recent developments in geoelectrical imaging technology now enable full 3D characterisation and monitoring of earth structures to reveal compositional and moisture related variability. Here we describe a study in which automated time-lapse electrical resistivity tomography (ALERT) monitoring technology has been installed on a section of Victorian embankment on the Great Central Railway (Nottingham). Through establishing geophysical-geotechnical property relationships by laboratory testing, electrical resistivity tomography (ERT) monitoring has been used to characterise the internal structure of the embankment, and image moisture content changes and wetting front development at a high spatial resolution. These preliminary results indicate that ERT has the potential to identify structures and processes related to instability at an early stage in their development.

Introduction

Here we investigate the use of ERT for monitoring moisture content changes in an engineered earth structure. We consider methodologies for correcting ERT models for the effects of seasonal temperature changes, and the translation of resistivity into moisture content using laboratory derived resistivity-moisture content relationships. The resulting images show the spatial distribution of moisture content, which when considered alongside other geotechnical properties, including liquid and plastic limits, provide a basis for predicting the likely changes in stability associated with wetting and drying cycles within the embankment material.

Fig. 1: Location map showing the Great Central Railway, and the location of the test site.

Site Description

The study site is located on a section of Victorian Great Central Railway embankment between Nottingham and Loughborough (Figure 1), which is currently used as a freight and heritage line. The embankment runs approximately north-south, and is located on a natural slope dipping a few degrees towards the west. In the area of the study site the embankment is approximately 5.5 m high and 30 m wide, and is constructed from end-tipped Westbury Formation Mudstone, sourced from a cutting situated less than 1 km to the south. Investigations at the site have demonstrated that the embankment is highly heterogeneous, due to the end-tipping technique used in its construction, comprising re-worked mudstone gravel of angular lithoclasts of the Westbury Formation with sporadic cobbles of Blue Anchor Formation (GUNN et al., 2009). The embankment rests on Branscombe Formation Mudstone Bedrock.

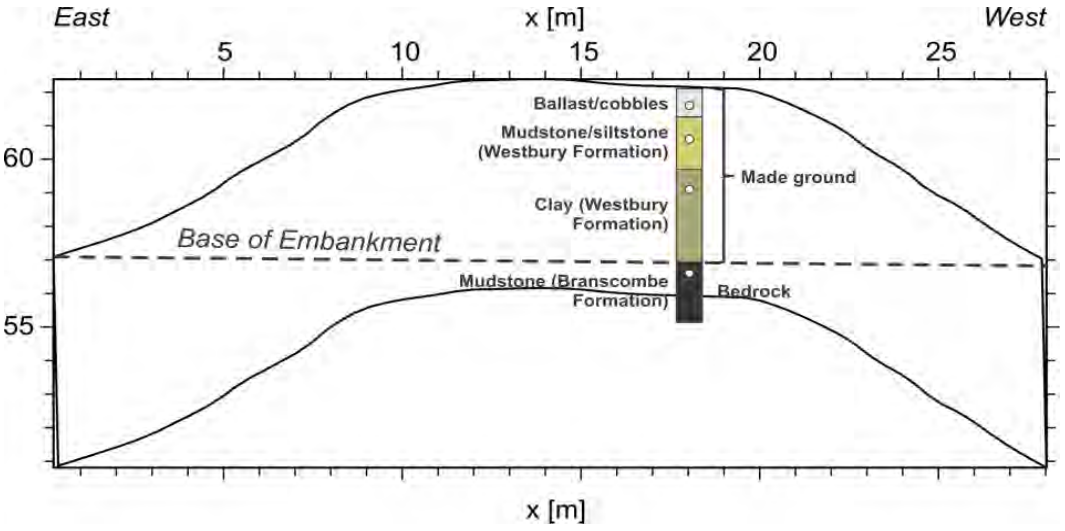

Fig. 2: Cross-section through the embankment at *y* = 12 m, showing topography, borehole log, depth to bedrock (dashed line), and temperature sensor locations (white circles).

Methodology

ERT Monitoring

Permanent ERT Monitoring arrays have been installed within a 22 m section of the embankment as a series of twelve lines at 2 m intervals running perpendicular to the rails. Each line comprised 32 electrodes at 1 m intervals, running from the toe of the eastern flank to the toe of the western flank. Initial 2D ERT measurements, which commenced during July 2006, were made on 2D arrays using a Super Sting R8/IP resistivity instrument during visits to the site. During August 2010 a semi-permanent resistivity system (ALERT, Figure 3; OGILVY et al., 2009) was installed along with additional 3D imaging arrays for automated remote monitoring of the embankment, thereby eliminating the need for repeat monitoring visits to the site and enabling significantly improved temporal resolution (i.e. a measurement frequency of hours as compared to weeks). The 2D imaging line (y = 12 m, x = 0 to 31m) is located within the 3D imaging area (y = 0 to 22 m, x = 0 to 31 m). The y-axis is parallel to the rails.

All resistivity data were collected using the dipole-dipole array configuration, with dipole sizes (a) of 1, 2, 3 and 4 m, and unit dipole separations (n) of 1 to 8. The dipole-dipole command sequences comprised full sets of both normal and reciprocal configurations; comparison of forward and reciprocal measurements provided a robust means of assessing data quality and determining reliable and quantitative data editing criteria.

The 2D and 3D ERT data were inverted using the regularized least-squares optimization method (LOKE and BARKER, 1995, 1996), in which the forward problem was solved using the finite difference method. Sequential time-lapse inversion of the 2D ERT data was carried out using the approach described by CHAMBERS et al. (2010). Good convergence between the observed and model data was achieved for both the 2D and the 3D models, as indicated by RMS errors of between 2.5 and 4.1%, and 6.9% respectively.

Fig. 3: Installation of ALERT monitoring instrumentation at the GCR(N) test site.

Temperature Modelling and Resistivity Model Corrections

Monitoring using multi-level sensors (Figure 2) has been undertaken at the test site to determine seasonal temperature changes in the subsurface (Figure 4); these data have been used to correct the time-lapse ERT images for temperature effects using a methodology similar to that described

by BRUNET et al. (2010). Seasonal temperature changes in the subsurface can be described by the following equation,

$$T(z,t) = T_{\text{mean}}(air) + \frac{A}{2} e^{-(z/d)} \sin(\omega t + \varphi - z/d) \qquad \text{Equation 1}$$

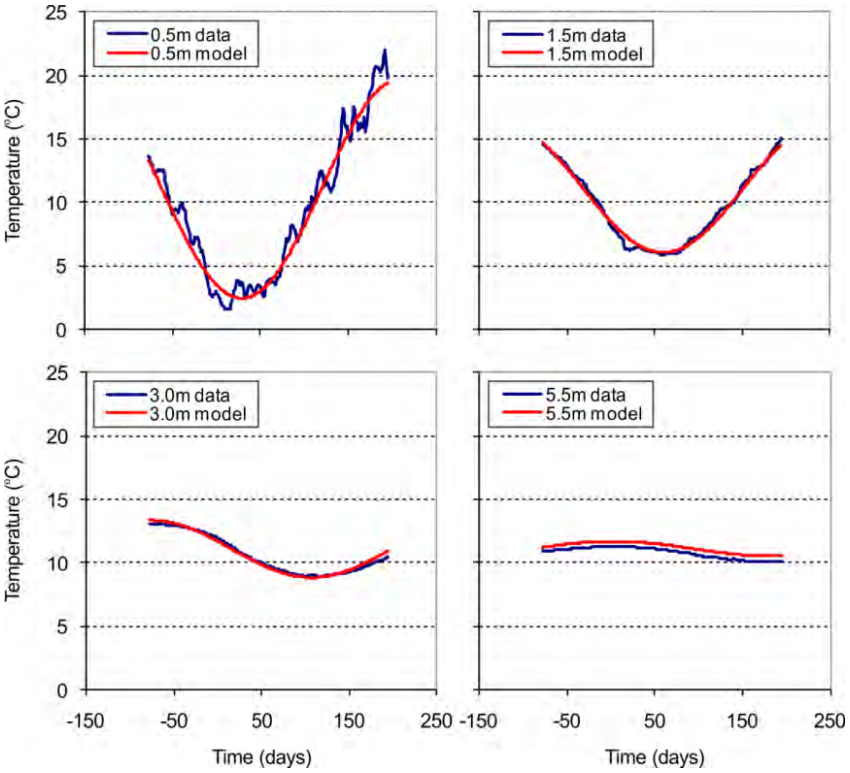

Fig. 4: Observed (October 2009-July 2010) & modelled ground temperatures, Great Central Railway test site.

where $T(z,t)$ is the temperature at day t and depth z, T_{mean}(air) is the mean yearly air temperature, A is the yearly amplitude of the air temperature variation, d is the characteristic penetration depth of the temperature variation, φ is the phase offset, $(\phi - z/d)$ is the phase lag, and ω is the angular frequency ($2\pi/365$). We fitted the temperature data (Figure 4) to Equation 1 using the FindMinimum[] function in the Mathematica computational algebra package. This is a Quasi-Newton method, which uses the Broyden–Fletcher–Goldfarb–Shanno algorithm to update the approximated Hessian matrix (PRESS et al. 1992). The modelled seasonal temperature variations with depth were used to correct the 2D and 3D ERT models, with the assumption that resistivity decreases by 2% per 1 degree C increase in temperature (HAYLEY et al., 2007). Resistivities for all ERT models were normalised to the mean air temperature (11.1°C).

Resistivity-Moisture Content Relationship

Laboratory measurements have been carried out to establish the relationship between resistivity and gravimetric moisture content in the material used to construct the embankment within the area of the study site. Core samples were gathered via drilling sorties in September 2005 and July 2006. The core was sub-sampled into 200 mm sections, which were used to determine a range of estimated values of porosity, density and moisture content for the fill and bedrock.

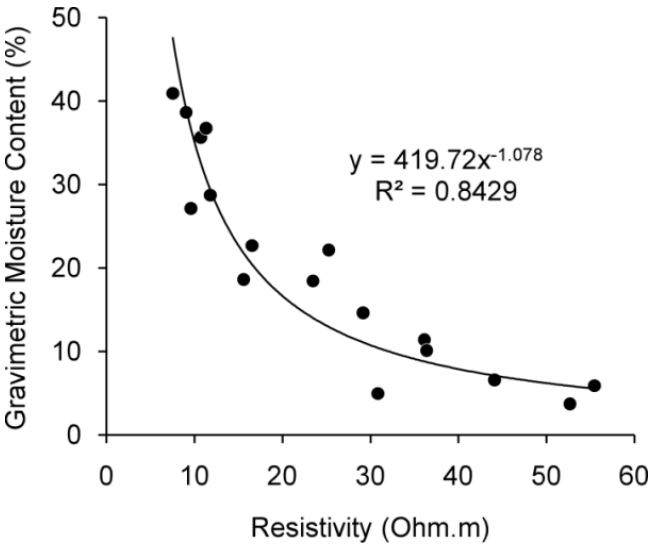

Fig. 5: Variation in resistivity with gravimetric moisture content in laboratory samples derived from Westbury Mudstone Formation embankment material taken from the Great Central Railway test site.

Samples were gently crushed to remove particles greater than 8 mm and re-saturated using distilled, deionised water to moisture contents ranging from below the shrinkage limit and up to the liquid limit - in practice this ranges from 5% to 40% w/w. The re-saturated materials were compacted into 100 mm diameter by 100 mm long core liners and sealed with plastic end caps. Sample moisture contents were verified on surplus material during preparation, and the sample masses were measured throughout testing to monitor moisture loss, which was less than 0.1%. Multiple samples of reworked Westbury Formation Mudstone taken from different locations within the study area were used for the tests to reflect the effects of the heterogeneity (e.g., mineralogical and geotechnical property variations) observed in the embankment into the results. Resistivity measurements were made using a non-contact, inductive logging tool (JACKSON et al., 2006). Prior to measurement, all samples were conditioned for at least 24 hours at a constant temperature in a temperature controlled cabinet. The electrical conductivity logging equipment was also conditioned at the same temperature, as were three additional fluid calibration samples of the same dimensions and of known resistivities 20, 200 and 2000 Ωm. At each selected measurement temperature, the internal temperature of a further water filled sample was used as a proxy to monitor any change in temperature within the test samples during the measurement phases. The temperature of the measuring head of the logger was also monitored to gauge the effect upon the test results. The relationship between resistivity and gravimetric moisture content is given in Figure 5.

Results

Temperature-corrected 2D resistivity and log resistivity ratio plots are shown in Figure 6 for a monitoring period between October 2009 and July 2010, which captures a complete seasonal wetting and drying cycle. ERT derived 2D moisture content and moisture content ratio plots for the same period are shown in Figure 7, and rainfall and air temperature records are shown in Figure 8. 3D baseline resistivity and moisture content images from September 2010 are shown in Figure 9. The 2D results are located on a vertical section located at *y* = 12 m relative to the 3D imaging area (Figure 9).

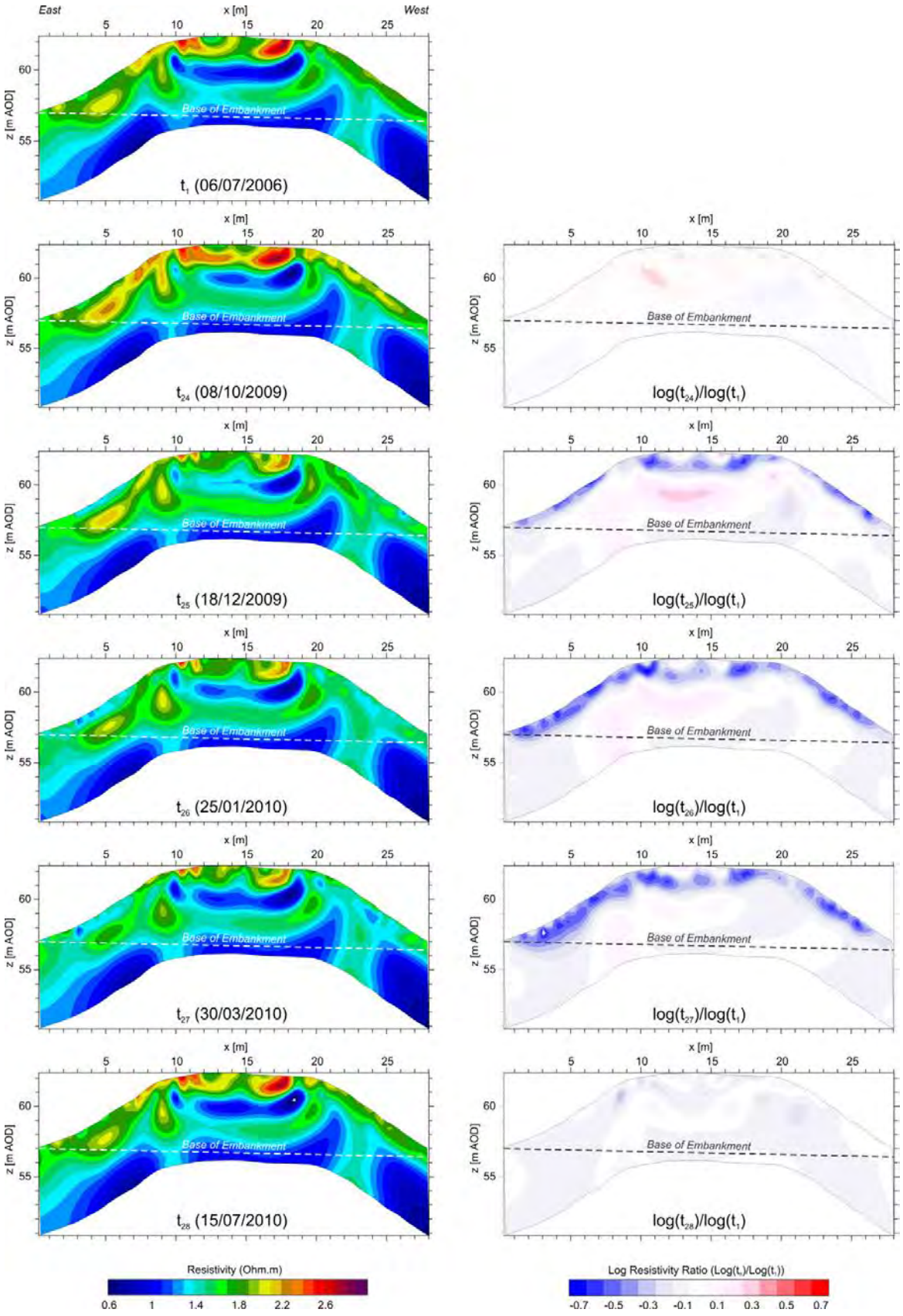

Fig. 6: Temperature corrected 2D ERT model sections (left) and log resistivity ratio plots (right) showing changes in resistivity relative to the July 2006 baseline (top left).

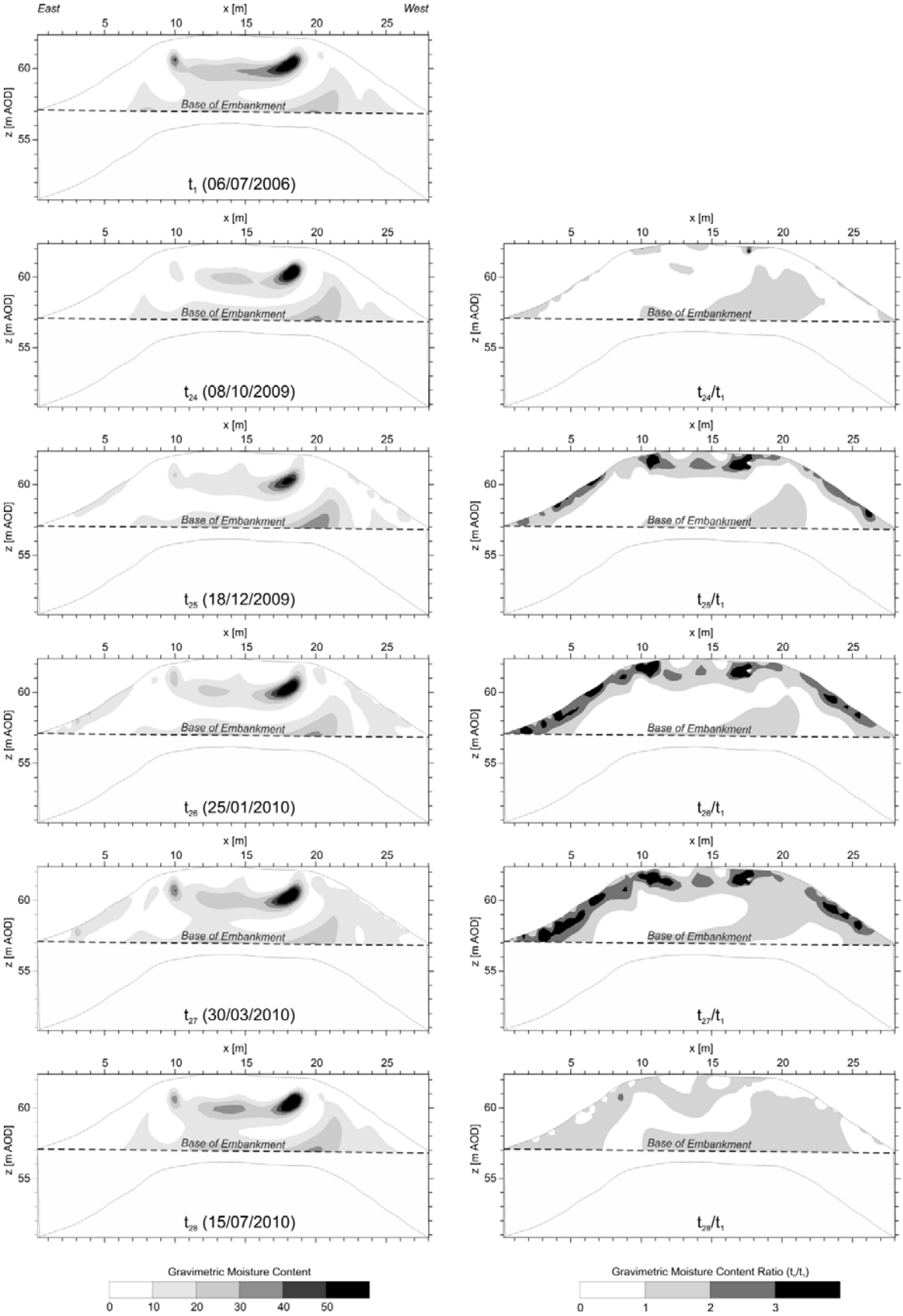

Fig. 7: ERT derived gravimetric moisture content (left) and ratio (right) plots calculated using the resistivity moisture content relationships determined from laboratory testing (Figure 5).

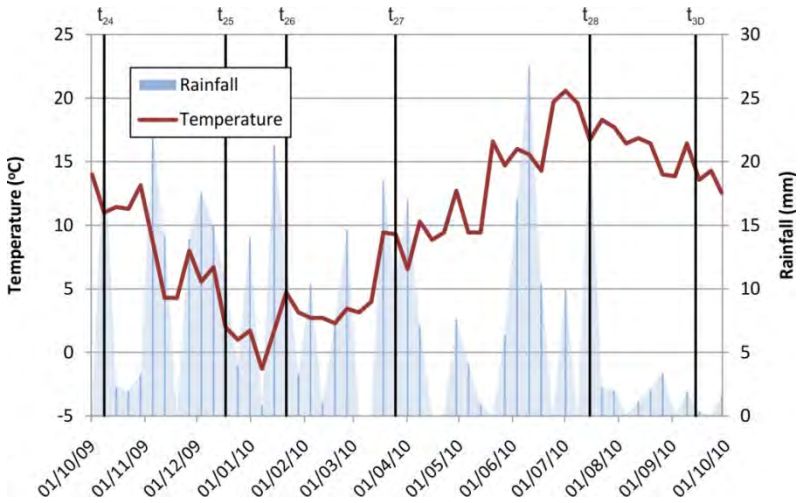

Fig. 8: Weekly rainfall and mean air temperature records (~8 km from the test site).

2D Time-lapse Imaging

The resistivity model sections display significant heterogeneity, consistent with the findings of intrusive sampling at the site (e.g. GUNN et al., 2009). In particular, a layered structure in the core of the embankment, and a temporally and spatially varying layer (~ 2 m thick) across the flanks and crest are apparent in the models. The internal layered structure is likely to be a function of both compositional and moisture content variations. Intrusive investigations in the form of borehole (Figure 2) and friction ratio logs (GUNN et al., 2009) indicate a ~ 2 m layer of granular material at the surface overlying more clayey fill, which is likely to account for the more resistive material on the crest. Lower resistivities at the base of the embankment may be related to elevated moisture contents resulting from water draining down slope from the east and perching on the bedrock.

The effects of temporal variations in moisture content are indicated in the log resistivity ratio plots, which show that changes are concentrated predominantly in the upper 2 m of the flanks and crest. These changes show the development of a wetting front during the winter months (indicated by a decrease in resistivity) associated with higher rainfall, lower temperature (Figure 8) and lower evapotranspiration.

The ERT derived gravimetric moisture content and moisture content ratio plots (Figure 7) have been masked below bedrock level. This is because the laboratory derived resistivity-moisture relationships used in the property translation are valid for Westbury Formation Mudstone embankment material, and not the Branscombe Formation Mudstone bedrock. The moisture content sections indicate that moisture levels are generally significantly below the liquid limit of the Westbury Mudstone Formation. The wettest zone (30-40%) is in the core of the embankment within a layer between ~2 and 4 m below the crest. This zone persists throughout the summer and winter months, and is located in the clayey fill materials, which may retain moisture more effectively than the more granular overlying materials.

Moisture contents associated with seasonal variations on the flanks and crest are relatively low (<20%), indicating that significant instability on the flanks or crest is unlikely even during the wettest periods of the year.

Volumetric (3D) Imaging

Baseline volumetric resistivity and moisture content images (Figure 9) reveal significant heterogeneity in the embankment. In the case of the moisture content image, the relatively wet core and dry flanks of the embankment are clearly shown. Ongoing monitoring efforts at the site are now focussing on automated remote monitoring and the collection of volumetric (4D) images.

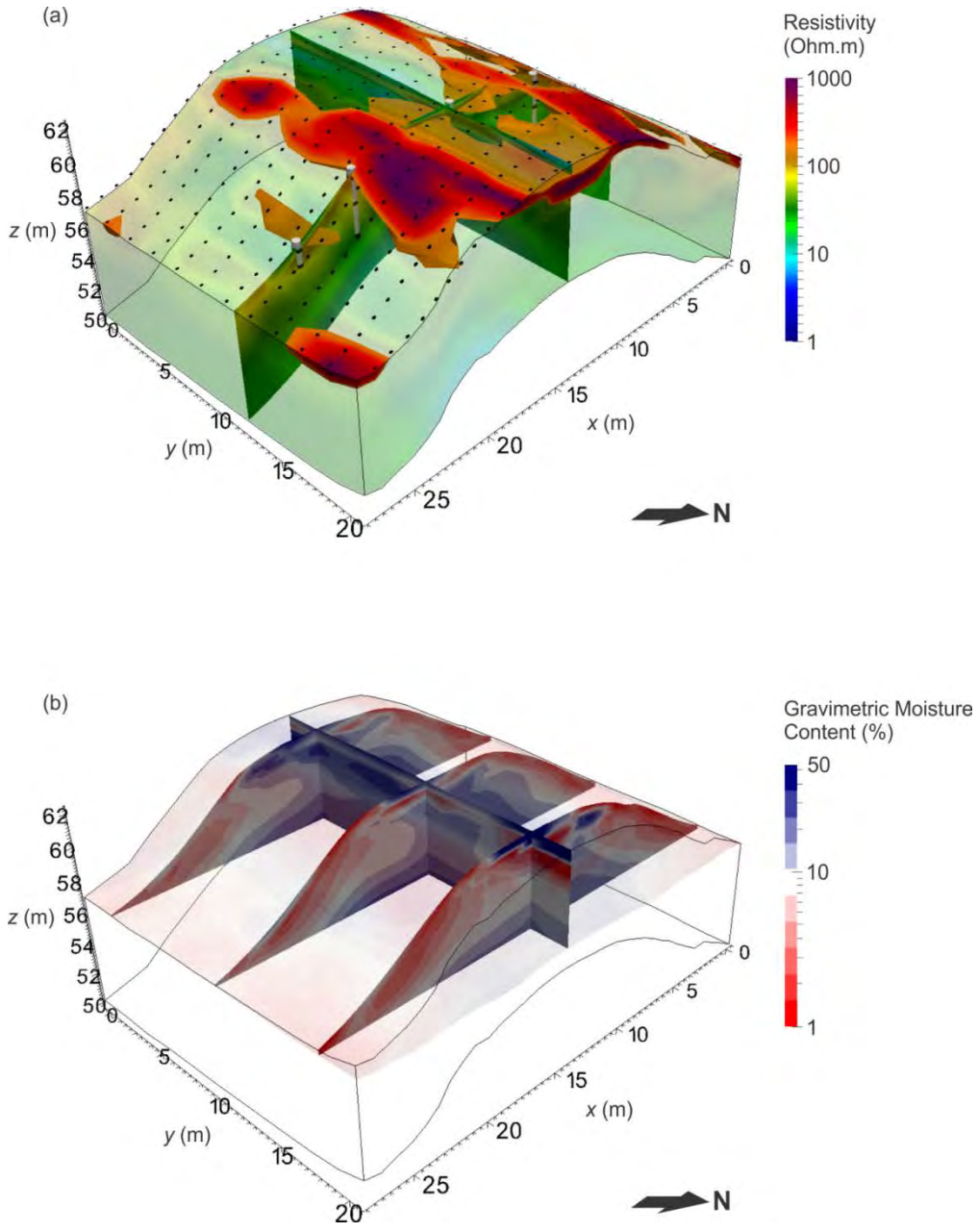

Fig. 9: Volumetric images of (a) resistivity and (b) ERT derived gravimetric moisture content, September 2010.

Conclusions

The use of 2D and 3D ERT as a means of estimating moisture content changes within an earth railway embankment has been demonstrated. A workflow has been described that incorporates the correction of resistivity models for seasonal temperature changes, and the translation of subsurface resistivity distributions into moisture content. Although the moisture content ranges

observed at this site are not a cause for concern, the methodology demonstrated here is applicable to other more vulnerable engineered earth structures and natural slopes. The results clearly demonstrate the potential of ALERT technology for the remote, real-time condition monitoring of slopes.

Acknowledgements

This paper is published with the permission of the Executive Director of the British Geological Survey (NERC). We also gratefully acknowledge the Great Central Railway (Nottingham) Ltd. for allowing access on to the East Leake embankment. This research has been supported by the East Midlands Development Agency (emda) via the Single Programme fund.

References

BRUNET, P., CLEMENT, R. and BOUVIER, C., 2010: Monitoring soil water content and deficit using Electrical Resistivity Tomography (ERT) – A case study in the Cevennes area, France. – Journal of Hydrology, **380**, 146-153.

CHAMBERS, J.E., WILKINSON, P.B., WEALTHALL, G.P., LOKE, M.H., DEARDEN, R., WILSON, R., ALLEN, D. and OGILVY, R.D., 2010: Hydrogeophysical imaging of deposit heterogeneity and groundwater chemistry changes during DNAPL source zone bioremediation. – Journal of Contaminant Hydrology, **118**, 43-61.

GUNN, D.A., HASLAM, E., KIRKHAM, M., CHAMBERS, J.E., LACINSKA, A., MILODOWSKI, A., REEVES, H., GHATAORA, G., BURROW, M., WESTON, P., THOMAS, A., DIXON, N., SELLERS, R. and DIJKSTRA, T., 2009: Moisture measurements in an end-tipped embankment: Application for studying long term stability and ageing. – Proc. 10th Int. Conf. Railway Engineering, London.

HAYLEY, K., BENTLEY, L.R., GHARIBI, M. and NIGHTINGALE, M., 2007: Low temperature dependence of electrical resistivity: Implications for near surface geophysical monitoring. – Geophysical Research Letters, **34**, L18402.

JACKSON, P.D., LOVELL, M.A., ROBERTS, J.A., SCHULTHEISS, P.J., GUNN, D., FLINT, R.C., WOOD, A., HOLMES, R. and FREDERICHS, T., 2006: Rapid non-contacting resistivity logging of core. – In: ROTHWELL, R.G. (Ed.): New techniques in sediment core analysis. – Geological Society Special Publication SP **267**.

LOKE, M.H. and BARKER, R.D., 1995: Least-Squares Deconvolution of Apparent Resistivity Pseudosections. – Geophysics, **60**, 1682-1690.

LOKE, M.H. and BARKER, R.D., 1996: Practical techniques for 3D resistivity surveys and data inversion. – Geophysical Prospecting, **44**(3), 499-523.

OGILVY, R.D., MELDRUM, P.I., KURAS, O., WILKINSON, P.B., CHAMBERS, J.E., SEN, M., PULIDO-BOSCH, A., GISBERT, J., JORRETO, S., FRANCES, I. and TSOURLOS, P., 2009: Automated monitoring of coastal aquifers with electrical resistivity tomography. – Near Surface Geophysics, **7**, 367-375.

PRESS, W.H., TEUKOLSKY, S.A., VETTERLING, W.T. and FLANNERY, B.P., 1992: Numerical Recipes in C: The Art of Scientific Computing, 2nd edition, Cambridge University Press, Cambridge.

Resistivity monitoring of a landslide in the Swabian Alb, Germany

HEINRICH KRUMMEL[1], MARKUS JANIK[1], HEIKO WIEBE[1] and RAPHAEL HOLLAND[1]

[1] geoFact GmbH, Bonn, Germany.

h.krummel@geofact.de

The study area is located at the Jurassic escarpment and generally consists of impermeable clays and marls underlying limestone. The investigated slope (approx. 0,5 ha) is periodically active and part of a larger landslide (approx. 3 ha).
In the course of an integrative landslide early warning system (ILEWS research project, sponsored by the German Federal Ministry of Education and Research) a remote controlled resistivity monitoring system with two perpendicular profiles (48 and 30 electrodes, 3 m electrode spacing) was installed. Furthermore an automated procedure for collecting and processing the data was developed. The resistivity data were combined with climate data, in-situ soil moisture measurements (Time-Domain-Reflectometry-probes) and inclinometer measurements gained on location by other partners of the ILEWS project.
Due to variations in resistivity data toward soil moisture and precipitation we mainly pursued two approaches: time lapse inversion and single data point analysis.
The first one detects the reaction of whole regions to rainfall events. The second approach allows the correlation between resistivity data (raw values from pseudo section or inverted data points) and soil moisture content or precipitation. Nevertheless the relationships are non-linear but correlations of resistivity variations and rainfall events are cleary seen.

Pluri-annual time lapse survey applied to landslide monitoring: new highlights on short and long term dynamics

THOMAS LEBOURG[1], CLARA LEVY[1] and SWANN ZERATHE[1]

[1] Geoazur Lab CNRS UNS, 250 rue A. Einstein 06560 Valbonne, France.

lebourg@geoazur.unice.fr

Abstract

This study reports the results from 4 years of multi-parametric time laps survey on the "Vence" landslide (South eastern France). This landslide is active since the 1970s, jeopardinzing the safety of more than 20 houses. It develops in a sandy-clay Eocene layer overlying a highly fractured and faulted Jurassic limestone discordantly. The actual survey combined Electrical Resistivity Tomography (2 daily acquisitions), many boreholes monitoring of groundwater levels as well as inclinometer and temperature measurements, rainfall records and water spring chemistry measurements (available only for the last 2 years). Gaps in the data represent about 20% of the survey duration. However, the amount of data is sufficiently significant to address the question of the long term behavior of the sliding mass. Thus, we were able to study the landslide dynamic at various time scales.

At short time-scale (few days), the time laps survey enables us to follow mean resistivity variations after rainfall events in correlation with the consecutive rises of the groundwater level within the sliding mass. Firstly, the statistical data analysis highlights a global correlation between the rainfall rate, the piezometric elevation and the mean resistivity decrease. Secondly, by analyzing the resistivity variations of each tomogram point, we observed a time-dependant vertical clustering, representative of two hydrogeological answers to rainfalls events:

1. A few hours later, near the surface: small resistivity variations related to subsurface water infiltrations,
2. about 2 days later, deeper: strong variations highlight the influence of the drained limestone fault systems in the landslide water supply.

During some very strong rainfall events, irreversible deformation was recorded by inclinometers. However, it is necessary to consider the landslide answer at longer time scale as the amplitude of deformation is strongly dependent on the massif state prior the rainfall event (e.g. piezometric levels).

At long time-scale, we show a clear annual hysteris. The landslide behavior follows a cycle directly linked to the seasonal state of the geological system. Using Principal Component Analysis, we observed periods characterized by stable relations between all physical parameters (summer and winter) punctuated by short transitional phases (autumn and spring). During stable periods, the landslide dynamic answer (ground deformation) will follow the same pattern for rainfall events.

Understanding this long term behavior represent the main challenge to define the precursors of landslide re-activation and thus to provide safety alarm systems.

Electrical resistivity tomographies for landslide monitoring: a review

ANGELA PERRONE[1], SABATINO PISCITELLI[1] and VINCENZO LAPENNA[1]

[1] Istituto di Metodologie per l'Analisi Ambientale, CNR, c.da S. Loja, Tito Scalo (PZ).

perrone@imaa.cnr.it

Abstract

This work aims at summing up and presenting both the current state of the art of the electrical resistivity tomography (ERT) technique for the landslide monitoring and its new emerging applications within this framework. In particular, we are overviewing and discussing the most noteworthy results obtained by applying this technique in different geographical areas affected by wide and diffuse hydrogeological instability phenomena. The attention will be focused on the contribution that this technique can give to the different phases (pre-vent, emergency and post-event) of a landslide disaster cycle. The analysis of the results points out the main advantages of this technique and the efforts to be made in order to improve and expand its application fields. Great attention is paid to the use of the time-lapse ERT as a promising monitoring tool to be used during the emergency phase.

Introduction

Landslides are complex phenomena whose study necessarily requires a multidisciplinary approach based on a wide range of observations including geological and geomorphological mapping, geotechnical and geophysical investigations, geodetic surveys, satellite observations and meteorological data analysis (PERRONE et al., 2006; CASTELLANOS ABELLA and VAN WESTEN, 2008; KAWABATA and BANDIBAS, 2009; DE BARI et al., 2011). The integration of different techniques should allow us to obtain useful information for all the phases of the landslide disaster cycle, overcoming the drawbacks of each single method applied.

Different geophysical techniques (seismics, geoelectrics, magnetometry, gravimetry, thermometry, GPS, etc.), which have led to significant results and provided useful information concerning both the landslide geometry reconstruction and the site hydrological characterisation (JONGMANS and GARAMBOIS, 2007), can be applied for the investigation of landslides. Among these the geoelectrical (electrical resistivity tomography, self-potential, induced polarization) and seismic methods play the most important role. In particular, the Electrical Resistivity Tomography (ERT) technique, based on the measurement of the electrical resistivity values and their spatial distribution in the subsoil, has been largely applied in order to investigate landslide areas (LAPENNA et al., 2005, MERIC et al., 2005, GODIO et al., 2006). This technique provides useful data to be used during the pre-event and post-event phases, thanks to its capability of giving information both on the lithostratigraphic sequences and the geometry of the landslide body (lateral extension and thickness), identifying the sliding surfaces between the slide material and the underlying bedrock, and individuating high water content areas. Indeed, during the pre-event phase, it is very important to gather information both on the geological setting of the potentially unstable area (electro-stratigraphy, tectonic lineaments, etc) and the presence of water tables that could trigger

off the phenomenon. After the event, it is important to know the geometry of the landslide body and estimate the volume of the slide material, in order to plan the mitigation activities and interventions (drainage system installation, stabilization structures, etc). The application of 2D and 3D ERT, even if indirectly, can provide this information.

Recently, novel algorithms for tomographic data inversion, robust models for the description of the hydrogeophysical processes and new sensor networks for the field data acquisition have turned this method into a powerful and cost-effective tool for the geo-hazard monitoring. These technological and methodological improvements are opening the way to a broad spectrum of interesting and challenging applications in geo-hazard monitoring, as well as the use of time-lapse ERT for the mapping of the time-dependent changes of water content in the vadose zone of a landslide area. Although the literature reports only few examples of the application of time-lapse ERT for landslide investigation (LEBOURG et al., 2010; NIESNER, 2010) the preliminary results seem to encourage the possibility to apply this technique during the emergency phase. This is due to its capability of monitoring the dynamic behaviour of a physical parameter indirectly connected to the triggering factors of a landslide so as to provide important information during the emergency phase. The aim of this work is to describe the evolution of the ERT technique application for landslide investigation, from the 2D acquisition to the time-lapse ERT, paying particular attention both to some examples of 2D and 3D ERT carried out in certain Italian landslide areas and the preliminary results coming from the time-lapse 2D ERT application.

2D and 3D ERT in landslide areas

This work reports a review of the results obtained by applying the 2D and 3D ERT technique during the pre and post landslide events with the aim to reconstruct the geometry of landslide bodies, individuate the sliding surface, estimate the thickness of slide material, approximate the volume of the body investigated and highlight the areas with high water content. The interpretation of the ERT was frequently supported by the comparison with stratigraphical data from direct boreholes performed in the same area.

Figure 1 reports an example of comparison between an ERT carried out longitudinally to the accumulation zone of Varco d'Izzo landslide (Basilicata region, Italy) and the stratigraphies from three direct boreholes (PERRONE et al., 2004). The ERT HH' highlights a clear resistivity contrast between a low-resistivity zone ($\rho < 20$ ohm-m), associated with the mobilized body, and a relatively high zone ($\rho > 30$ ohm-m) related to the compact deposits (alluvial and clayey material) not involved in the landslide. These results are in accordance with the stratigraphic and inclinometric data from boreholes B24, B23, and B22, which show a sliding surface at depths of about 21, 30, and 32 m, respectively. The relatively high resistivity nucleus ($\rho > 50$ ohm-m) located at about 110 m from the origin of the profile is due to a railway tunnel involved in the landslide.

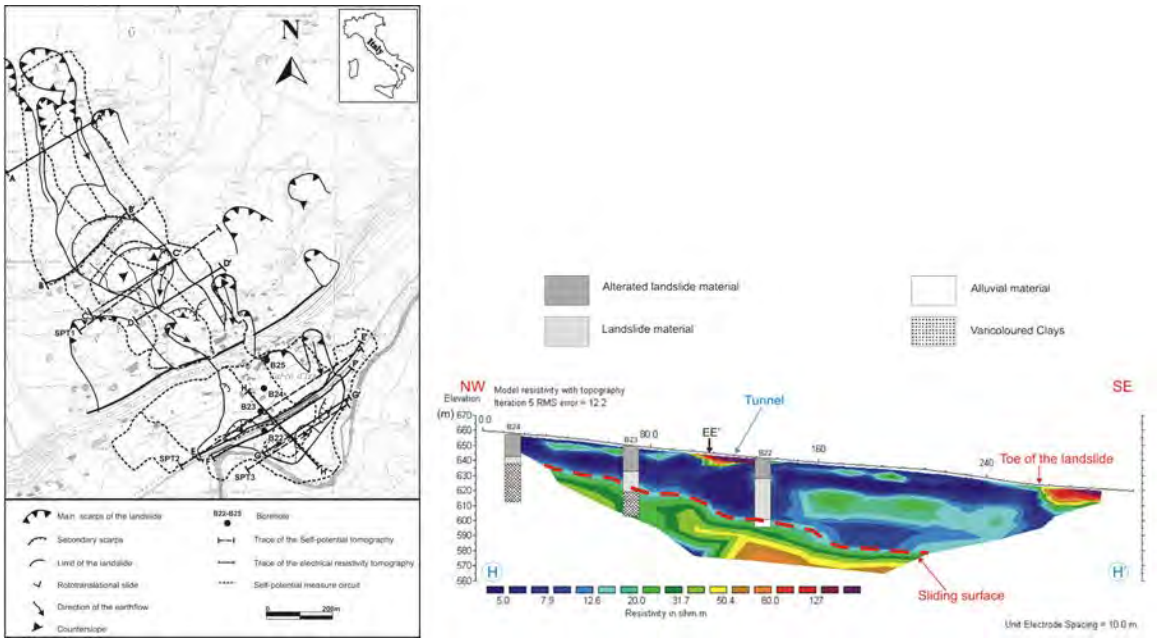

Fig. 1: Comparison between HH' ERT carried out on Varco d'Izzo landslide (Basilicata region) and stratigraphical data (from PERRONE et al., 2004)

Figure 2 reports the comparison of the electrical resistivity and seismic refraction tomography results obtained along the profile 1 in a landslide area located in the Altındağ district of İzmir (Turkey) (GÖKTÜRKLER et al., 2008).

Both the electrical resistivity and the P-wave velocity images show very similar results and highlight the geometry of failure surface. Low resistivity values (<100 Ωm) and low velocities (400-1600 m/s) characterize the landslide material mainly composed of (by) clay material with high water content. Both the images clearly define the landslide bedrock characterized by consolidated clastic rocks and by high resistivities (100-400 Ωm) and high velocities (2000-3000 m/s).

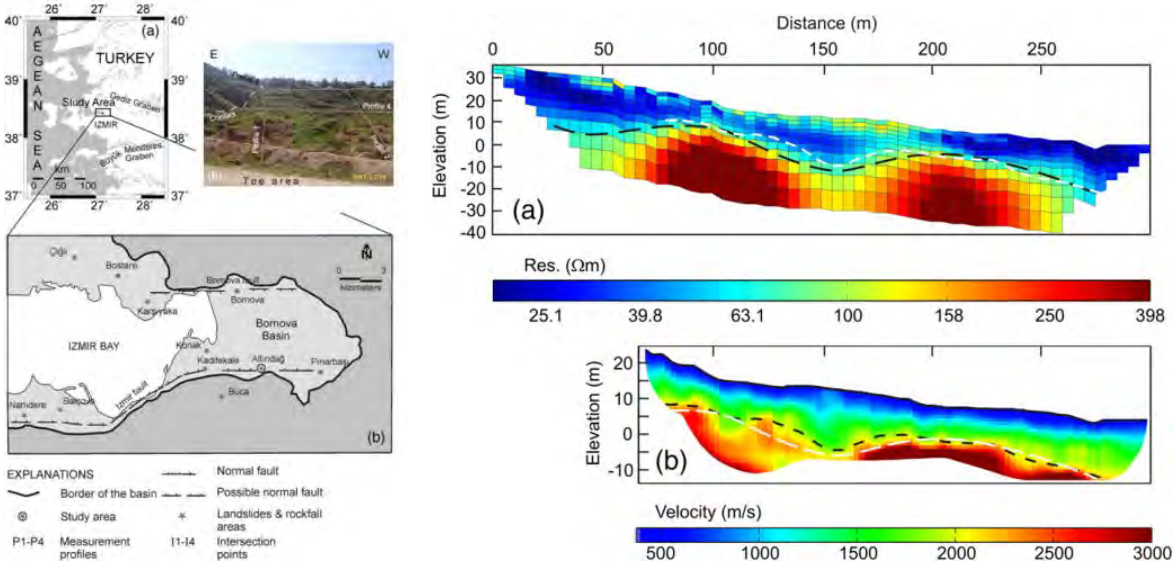

Fig. 2: Left: landslide area located in the Altındağ district of İzmir (Turkey). Right: (a) Resistivity tomogram together with the failure surface interpretations from the resistivity (black dashed line) and seismic data (white dashed line). (b) Velocity tomogram together with the failure surface interpretations from the resistivity (white dashed line) and seismic data (black dashed line) (modified from GÖKTÜRKLER et al., 2008).

Figure 3 reports an example of 3D fence diagram of all resistivity data acquired along parallel profiles in a landslide located on the Quesnel River in British Columbia (Canada), (BICHLER et al., 2004).

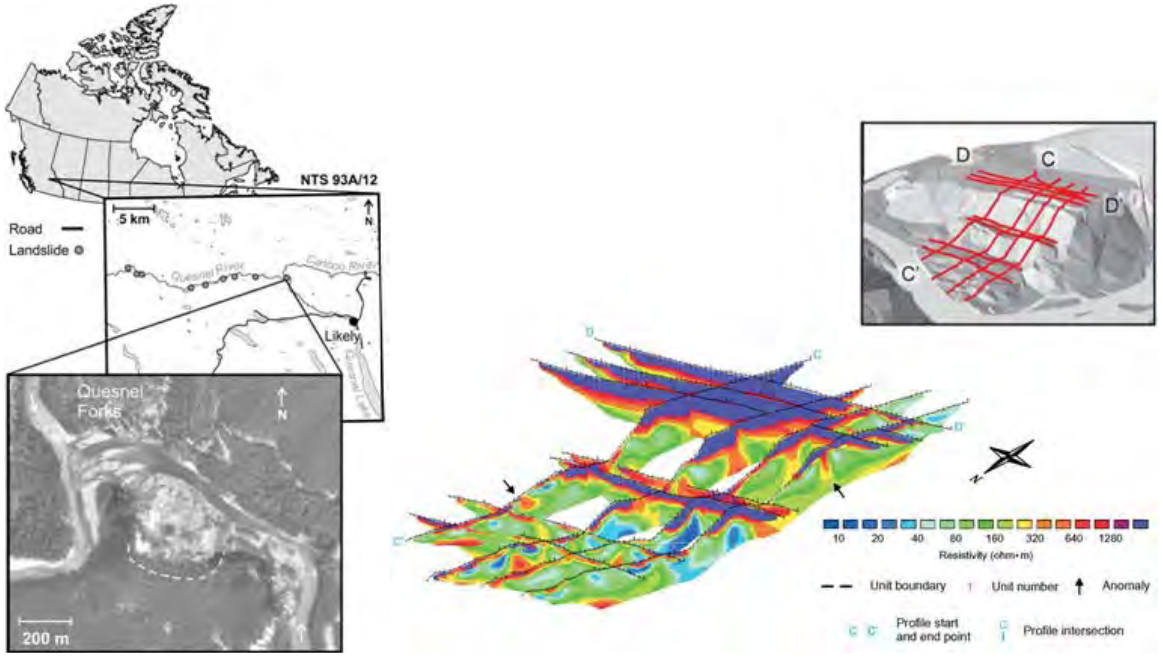

Fig. 3: Left: Landslide on the Quesnel River in British Columbia (Canada); right up: DTMs with DC electrical resistivity survey lines superimposed onto its surface; right bottom: 3D fence diagram of all resistivity data (modified from BICHLER et al., 2004)

Six different lithological units are identified. The 3-dimensional model of the terrace and landslide constructed from the 2D ERT aids in the understanding of landslide processes. The model suggested that increased pore water pressures in the clay unit and artificial loading of terrace due to a perched water table played a role in the instability of the terrace but was not necessarily the trigger. It is much more likely that fluvial erosion of the terrace face was responsible for the loss of shear strength and subsequent collapse of the terrace (BICHLER et al., 2004).

Time-lapse ERT in landslide areas

Time-lapse ERT have recently been applied in landslide areas with the aim to test a new powerful tool for mapping the time-dependent changes of water content in vadose zones. This is a very innovative application that could allow us to use the ERT also during the emergency phase of a landslide disaster cycle.

Figure 5 reports the initial results of the ALERT system located on an active landslide in Malton (North Yorkshire, UK). In particular, the subsurface resistivity variations that occurred between static conditions and an active phase of slope failure are highlighted by analyzing time-lapse resistivity results (CHAMBERS et al., 2009). The two times, August 2008 (t_1) and February 2009 (t_2) were chosen as they represent a dry period (t1) and a wet period (t2) during which movement was occurring. The authors (CHAMBERS et al., 2009) concluded that only at depths (i.e. > 5-10m) where the influence of seasonal air temperature variations is minimal, changes in resistivity could be attributed to changes in moisture content.

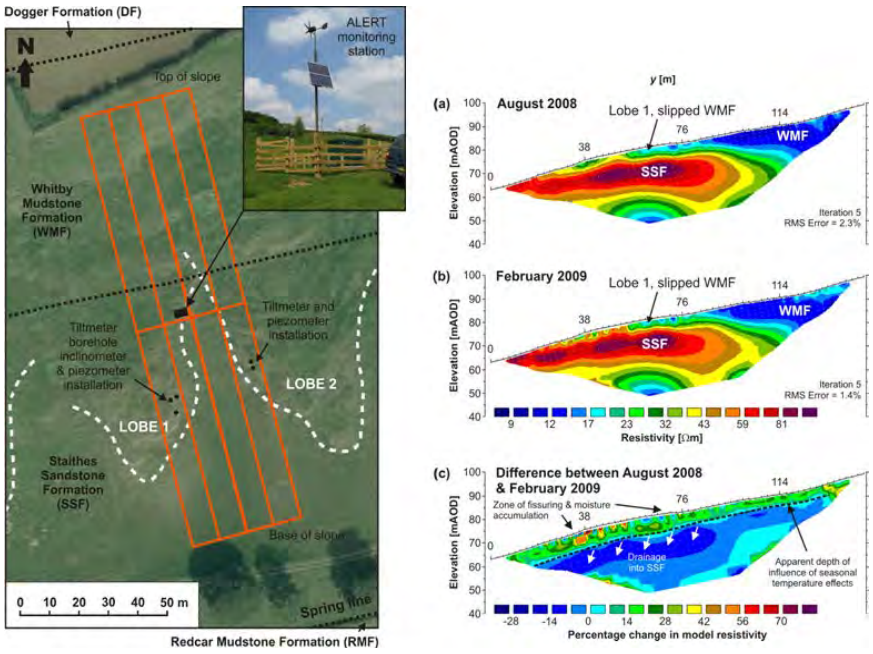

Fig. 4: Left: location of the ALERT station and ERT monitoring arrays (red lines); right: (a) August 2008 and (b) February 2009 ERT models, and (c) resulting differential resistivity image (modified from CHAMBERS et al., 2009).

Conclusions

The results reported in literature and obtained over the last ten years from the application of the 2D and 3D ERT method to study several landslide areas located in different geographical contexts make us consider the ERT method as a very suitable tool for investigating landslides during the pre-event and post-event phases of a disaster cycle.

Indeed, during the pre-event phase the resistivity contrasts which characterize the 2D ERT make it possible to define the subsoil geological setting. They permit to identify high water content areas that could be responsible for events of reactivation. In the post-event phase 2D and 3D ERT allow us to reconstruct the landslide body providing information also about the volume of the material involved in the movement. This information can contribute to better plan future mitigation activities.

The biggest drawback of this method for landslide investigation is the fact that it does not provide time-continuous acquisitions which makes it unsuitable for the study of the landslide dynamic nature. This is also the reason why it cannot be used during the emergency phase of a landslide disaster cycle. Fortunately, the development of systems for the time-continuous acquisition of electrical resistivity and software for data inversion and time-lapse tomographic acquisitions are paving the way for testing this method also during the emergency phase. The possibility to use ERT to monitor the water content changes in the first layers of a landslide area will add important information during the emergency phase. At now, the preliminary results obtained when applying time lapse ERT for this purpose are very encouraging.

References

BICHLER, A., BOBROWSKY, P., BEST, M., DOUMA, M., HUNTER, J., CALVERT, T. and BURNS, R., 2004: Three-dimensional mapping of a landslide using a multi-geophysical approach: the Quesnel Forks landslide. – Landslides, **1**, 29-40.

CASTELLANOS ABELLA, E.A. and VAN WESTEN, C.J., 2008: Qualitative landslide susceptibility assessment by multicriteria analysis: a case study from San Antonio del Sur, Guantánamo, Cuba. – Geomorphology, **94**, 453–466.

CHAMBERS, J.E., MELDRUM, P.I., GUNN, D.A., WILKINSON, P.B., KURAS, O., WELLER, A.L. and OGILVY, R.D., 2009: Hydrogeophysical Monitoring of Landslide Processes Using Automated Time-Lapse Electrical Resistivity Tomography (ALERT). – Near Surface – 15th European Meeting of Environmental and Engineering Geophysics Dublin, Ireland, 7.–9. September 2009.

DE BARI, C., LAPENNA, V., PERRONE, A., PUGLISI, C. and SDAO, F., 2011: Digital photogrammetric analysis and electrical resistivity tomography for investigating the Picerno landslide (Basilicata region, southern Italy). – Geomorphology, **133**, 34–46.

GODIO, A., STROBBIA, C. and DE BACCO, G., 2006: Geophysical characterisation of a rockslide in an alpine region. – Engineering Geology, **83**, 273–86

GÖKTÜRKLER, G., BALKAYA, C. and ERHAN, Z., 2008: Geophysical investigation of a landslide: The Altındağ landslide site, İzmir (western Turkey). – Journal of Applied Geophysics, **65**, 84-96.

JONGMANS, D. and GARAMBOIS, S., 2007: Geophysical investigation of landslides: a review. – Bulletin of the Geological Society of France, **178**, 101–12.

KAWABATA, D. and BANDIBAS, J., 2009: Landslide susceptibility mapping using geological data, a DEM from ASTER images and an Artificial Neural Network (ANN). – Geomorphology, **113**, 97–109.

LAPENNA, V., LORENZO, P., PERRONE, A., PISCITELLI, S., RIZZO, E. and SDAO, F., 2005: Case history: 2D electrical resistivity imaging of some complex landslides in Lucanian Apennine (Southern Italy). – Geophysics, **70**, B11–B18.

LEBOURG, T., HERNANDEZ, M., ZERATHE, S., EL BEDOUI, S., JOMARD, H. and FRESIA, B., 2010: Landslides triggered factors analysed by time lapse electrical survey and multidimensional statistical approach. – Engineering Geology, **114**, 238–250.

MERIC, O., GARAMBOIS, S., JONGMANS, D., WATHELET, M., CHATELAIN, J.L. and VENGEON, J.M., 2005: Application of geophysical methods for the investigation of the large gravitational mass movement of Sechilienne France Can. – Geotechnical Journal, **42**, 1105–15.

NIESNER, E., 2010: Subsurface resistivity changes and triggering influences detected by continuous geoelectric monitoring. – The Leading Edge, **29(8)**, 952-955.

PERRONE, A., IANNUZZI, A., LAPENNA, V., LORENZO, P., PISCITELLI, S., RIZZO, E. and SDAO, F., 2004: High-resolution electrical imaging of the Varco d'Izzo earthflow (southern Italy). – Journal of Applied Geophysics, **56**, 17-29.

PERRONE, A., ZENI, G., PISCITELLI, S., PEPE, A., LOPERTE, A., LAPENNA, V. and LANARI, R., 2006: Joint analysis of SAR interferometry and electrical resistivity tomography surveys for investigating ground deformation: the case-study of Satriano di Lucania (Potenza, Italy). – Engineering Geology, **88**, 260–273.

Stability Analysis of Pyroclastic Covers by a new Geoelectrical-Hydrogeological Approach

ROSA DI MAIO[1], ESTER PIEGARI[1] and SOLANGE SCOGNAMIGLIO[1]

[1] Department of Earth Sciences, University of Naples "Federico II", Italy, Largo San Marcellino 10 - 80138 Naples (Italy).

rodimaio@unina.it

Abstract

Debris-flows hazard is strictly correlated to the water content of loose deposits mantling a slope. Obviously, many other factors predispose and influence a slope to landsliding (such as the slope morphology, the geological setting, the soil thickness, etc.), but in most cases a water content variation is the most frequent triggering factor of debris-flows. Thus, it would be helpful to define water content thresholds, which may be critical for debris-flow mobilization.

In this framework, we propose geoelectrical measurements as an important tool for seepage analysis and landslide hazard assessment. By means of in-situ resistivity tomography surveys, we define the stratigraphical setting, which is needed to create a synthetic slope model. By means of laboratory resistivity measurements, we link electrical resistivity to the percentage of water content in order to obtain the water content distribution within the surveyed slope in a specific period of the hydrological year. Such a distribution is used to validate the synthetic water content distribution resulting from steady-state seepage analysis, which is realized by using geotechnical parameters. Next, we perform a transient-state seepage analysis by imposing to the achieved synthetic water content distribution the daily rain rate of the rainfall occurred before a catastrophic landslide event of the past. Transient analysis provides the critical water content distribution of the surveyed cover for the considered debris-flow event. Finally, by converting critical water content in resistivity values, we obtain information about the stability condition of the surveyed slope by calculating the previously introduced geophysical safety factor, defined in terms of slope angle and resistivity.

An application of the proposed tool in a test area located on the Sarno Mountains (Campania region, southern Italy) is presented. The main finding of the shown example is the identification of saturated conditions of the shallowest pyroclastic layer of the cover on the day when a calamitous landslide event occurred.

Introduction

Peri-Vesuvian area encloses a portion of the Campania region (southern Italy) characterized by ash-fall deposits resulting from the volcanic activity of the Mt. Somma-Vesuvius, which overlap a carbonate basement. Geological, structural and hydrogeological conditions of this area may often trigger very rapid landslides as debris-slides and debris-flows.

Many authors currently study how to evaluate the water content of such loose deposits and its variations over time. In particular, due to the well-known dependence of the soil matric suction from the water content, most of recent researches (e.g., CASCINI and SORBINO, 2004) are focused on monitoring the soil suction values at various depth from the slope surface. These values are used to realize a synthetic suction (or equivalently water content) model of the slope

(SORBINO, 2005) and to get information about its hydrological status. However, suction measurements give local information about soil condition around porous probes and down to a depth of 3 m at most.

Alternatively, we propose an innovative tool for groundwater seepage analysis substantially founded on laboratory and in-situ geoelectrical measurements, whose aim is the definition of effective early warning thresholds for debris-flow landslide initiation. The main advantages of our proposal are: the non-invasiveness of the measurement technique and the possibility to take into account the local changes of soil properties on considerable volumes by means resistivity tomography surveys, which in turn provide the water content distribution within the whole surveyed volumes.

In order to verify the potentiality of the proposed tool, we present an application in a test area of the Campania region (southern Italy), where debris-flow phenomena of pyroclastic soils are very often induced by critical rainfall events.

A combined geoelectrical-hydrogeological approach

Figure 1 shows a schematic diagram of the proposed geoelectrical-hydrogeological approach. We use the results of high-resolution 2D resistivity tomographies (*ERT*) to obtain a stratigraphical model of the slope and the results of geotechnical measurements to define the hydraulic behavior of the pyroclastic cover. Once we have realized a synthetic slope model, a steady-state representative of in-situ soil conditions is achieved by using a *trial and error* approach. This consists in comparing the synthetic water content distribution within the cover, resulting from seepage analysis, with that resulting from a joint interpretation of the in-situ and laboratory resistivity measurements (DI MAIO and PIEGARI, 2011). Next, we use rainfall data of real storms to simulate the in-situ condition preceding a catastrophic past landslide event occurred close to the survey area. The applied conditions provide the 2D critical water content distribution within the investigated cover on the day when the landslide occurred.

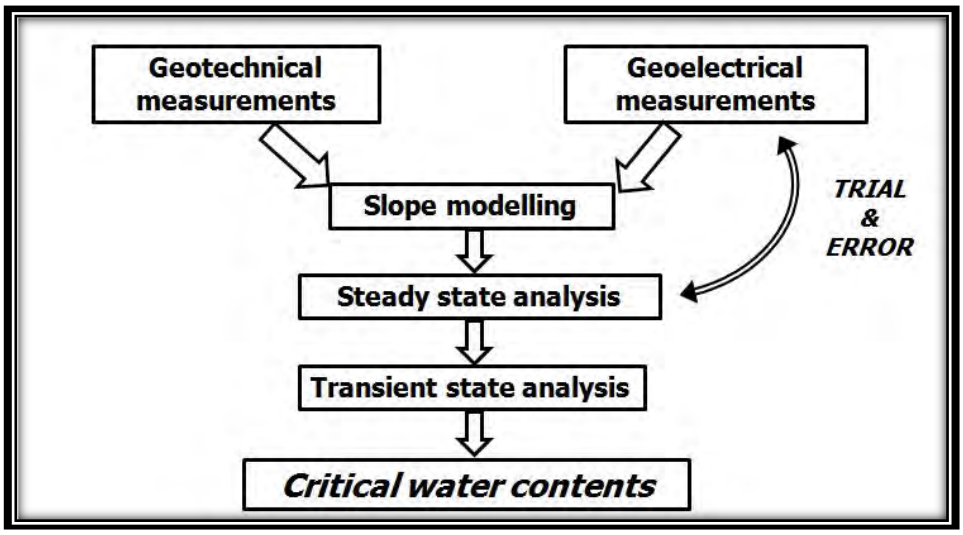

Fig. 1: Schematic diagram of the proposed geoelectrical-hydrogeological approach.

Application to the Sarno landslide event of May 5, 1998

The proposed approach has been implemented on a test area localized on the S-W slope of Mts. Sarno (Campania region, southern Italy). These mountains are covered by ash-fall deposits

characterized by pumice and ashy layers, resulting from the volcanic activity of the Mt. Somma-Vesuvius, which overlap a carbonate basement. Such deposits may be occasionally mobilized from the slope and produce huge and very rapid rainfall-induced debris flows, which may cause significant property damage and loss of human life in the tows located at the foothill of the slopes. The most serious event occurred on May 5th, 1998, when severe rainfall-triggered landslides devastated the cities located at the foothill of Mt. Pizzo D'Alvano, causing more than 150 casualties. The test area is localized upstream the initial detachment area of two landslides occurred on May '98 (Figure 2).

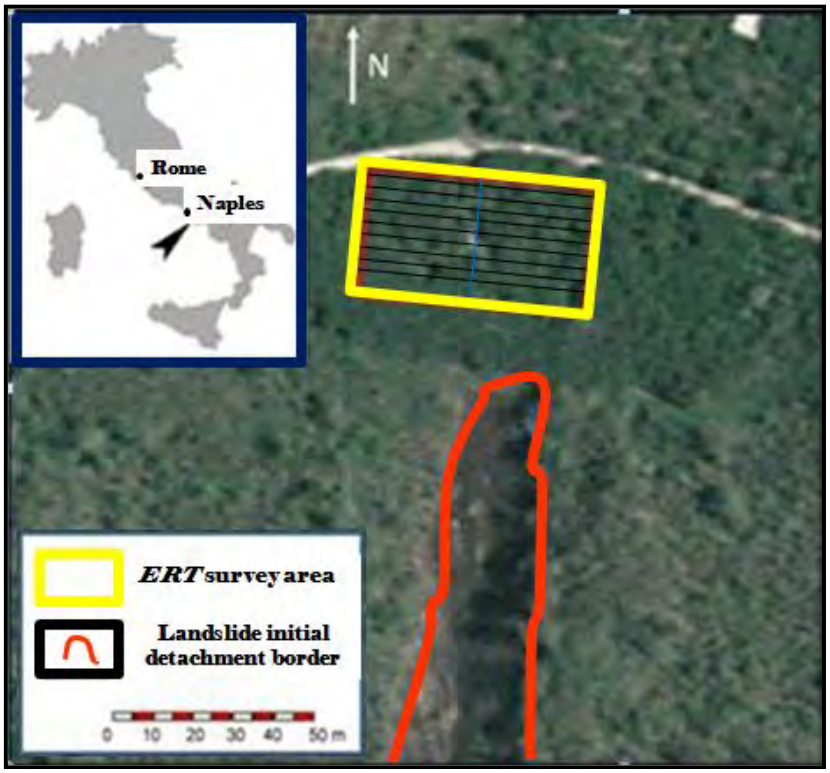

Fig. 2: Map showing the location of the survey area. Black lines indicate the 2D resistivity profiles; blue line specifies the orientation of the synthetic slope model.

In the test area, we performed 2D resistivity tomography surveys along 9 W-E profiles (black lines in Figure 2), 58 meters long and 4 meters spaced, by using a Wenner-Schlumberger array (DI MAIO and PIEGARI, 2011). As an example, figure 3a shows the resistivity section obtained along one of the investigated profiles. Looking at the figure, the cover appears sketchily described by a shallow resistive layer overlapping a wide conductive layer; both deposits may be ascribed to pyroclastic materials. Conversely, the deepest resistive layer that emerges at about 5 m below ground level (b.g.l.) is likely correlated to the limestone bedrock. The geoelectrical measurements were carried out both in the autumnal and spring season and, by using the 3D data inversion algorithm of LOKE and BARKER (1996), 3D resistivity distributions within the pyroclastic cover were obtained.
By comparing geoelectrical and geotechnical laboratory measurements performed on pyroclastic samples collected in the test area, a more detailed stratigraphy of the surveyed area was attained (Figure 3a). Such a stratigraphical setting was used to realize the synthetic slope model, approximately N-S oriented (blue line in Figure 2), which is required for the seepage analysis. The slope modelling was based on two main steps: the first consists on the discretization of the slope

by using a finite element mesh and the second one consists on assign the hydraulic properties to each layer characterizing the pyroclastic cover. About the first step, the synthetic stratigraphical model is illustrated in Figure 3b. The thickness of each layer was obtained from the results of the high-resolution 2D resistivity surveys previously mentioned. In particular, 7 regions were defined, 6 for each layer of the pyroclastic cover and one for the limestone bedrock. To characterize the hydraulic behavior of pumice and ashy layers, we used two different types of curves retrieved from literature geotechnical data: hydraulic conductivity vs. suction (CASCINI et al., 2000) and suction vs. water content (i.e., retention curves) (SORBINO, 2005; DE VITA et al., 2012).

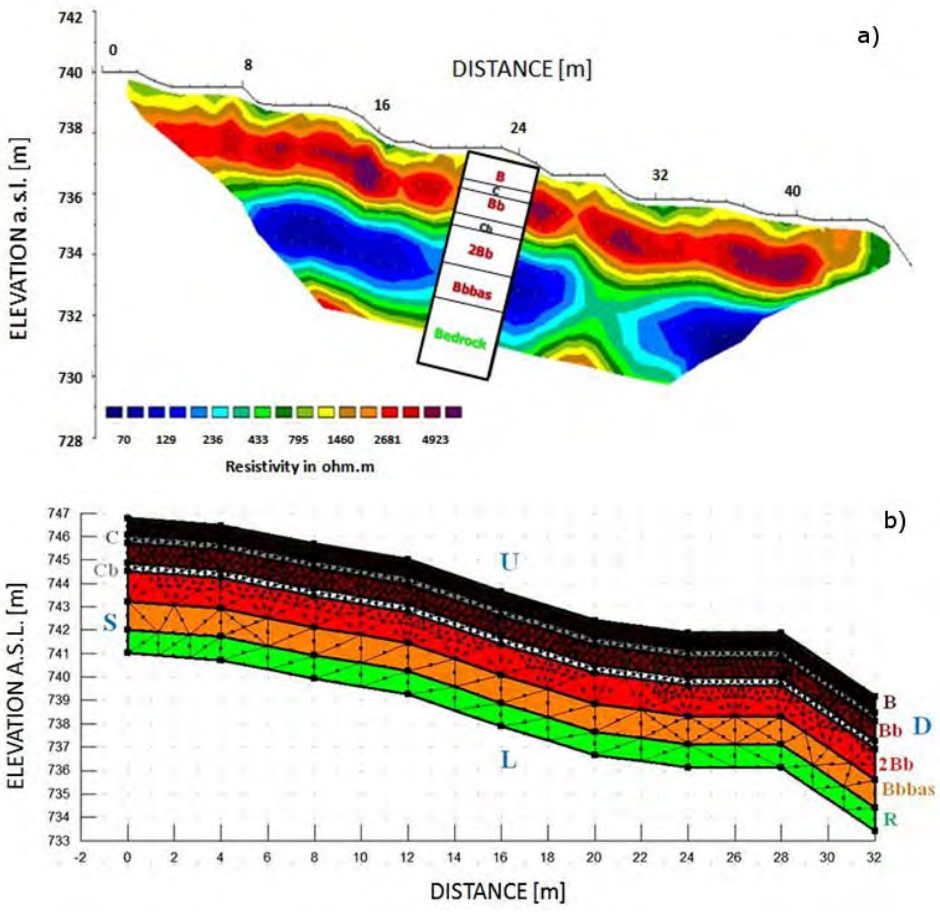

Fig. 3: a) An example of resistivity section obtained along one of the 9 investigated ERT profile. The superimposed stratigraphic column indicates the layers of the cover that overlaps the bedrock R (after DI MAIO and PIEGARI, 2011). b) Slope model used to perform seepage analyses. The 7 regions represent the 6 layers of the surveyed pyroclastic cover and the limestone bedrock. On the left and right sides of the model is indicated the name of each layer, while the blue letters designate the upper (U), lower (L), right (D) and left (S) edges of the model.

Steady-state seepage analysis

Steady-state analysis is aimed at providing in-situ soil condition of the investigated cover in a specific period of the hydrological year. To achieve it, we propose to apply a *trial and error* routine based on geoelectrical measurements. First, we assign to the top of the slope model a steady (over time) rain rate. As result of the steady-state seepage analysis, we obtain a synthetic 2D water content map within the pyroclastic cover. Subsequently, such synthetic water content

values are compared with the water content distribution resulting from laboratory geoelectrical characteristic curves (DE VITA et al., 2012), which link resistivity values to the corresponding water content. If there is a good agreement between the two distributions, then the synthetic 2D water content map resulting in output from steady-state analysis is really representative of in-situ conditions. Otherwise, it is necessary to re-iterate the routine by applying a different input unit flux at each iteration until a good agreement is found. To perform the steady-state analysis, we considered the top, bottom and right borders of the model as open edges. This means that water can pass through them, while the left edge is closed to ensure that water exits from the system only through the bottom and the right edge.

It is worthwhile noticing that geoelectrical measurements are used as innovative and effective tool in seepage analysis, since they validate the steady-state representative of in-situ soil conditions.

Transient-state seepage analysis

Transient-state analysis is aimed to simulate soil conditions on the day of a specific landslide event and then to define water contents that might be critical for the stability of the surveyed pyroclastic cover.

In detail, as transient boundary conditions, we applied to the spring steady-state of the investigated area the daily rain rates of the rainfalls occurred before the ’98 landslide event. The resulting synthetic water content map showed highest water content values in the ashy layers and downstream the model, thus indicating this part of the slope as mainly susceptible to debris-flow phenomena. To perform a more detailed analysis, we plotted for each one of the 6 pyroclastic layers the water content vs. time (Figure 4). For shallow ashy layer the water content trend over time follows the rain rate trend, while the deepest layers reach maximum water contents gradually over time and slower than *B* layer. The shallowest layer (*B*) has a water content value of about 46% on the day when the landslide event occurred. This means that the *B* layer was in a saturated condition as deduced by the resistivity laboratory analyses. Moreover, the water content peak of this layer corresponds to the day when landslide occurred. So, we can suppose that the slope stability was affected by the water content of both the shallower and the deeper layers; but most likely, the landslide triggering was caused by the water content of the shallowest layer.

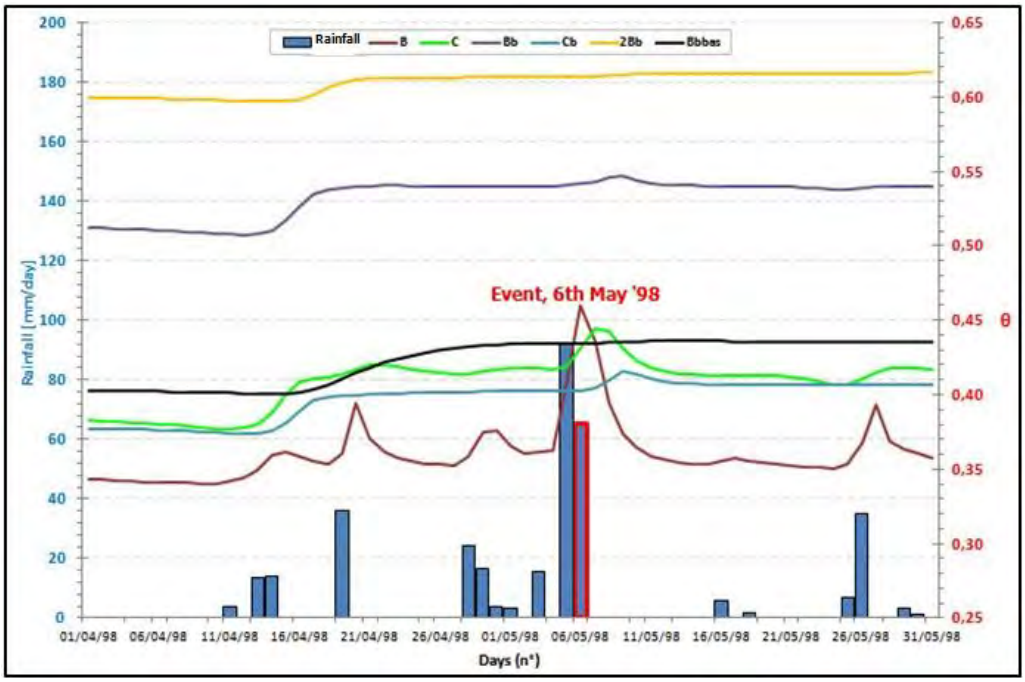

Fig. 4: Water content (θ) vs. time for each layer of the pyroclastic cover. The curves are correlated with the daily rainfall histograms (blue rectangles). The rectangle marked with the red edge indicates the rainfall occurred on May 6th, 1998.

Finally, to assess the stability condition of the surveyed slope we use the geophysical safety factor (FS) previously introduced by PIEGARI et al. (2009) in terms of resistivity values and slope angles. The *FS* map of the test area was calculated by using resistivity values at a depth of 70 cm b.g.l. (corresponding to the thickness of the *B* layer). The *FS* values are found everywhere greater than 1. This means that the slope during the spring season is stable. Converting the critical water contents values, resulting from the transient seepage analysis, into resistivity values by using the characteristic electrical curves of the upper ashy layer (DE VITA et al., 2012), we evaluate the FS distribution at the same depth b.g.l. on the day when the considered landslide event occurred. As expected, FS values are still greater than 1 (Figure 5) for the investigated area of figure 2, which was not involved in the landslide event. Interestingly, by calculating FS with a rigid shift downstream, within initial detachment area, its values (that here we do not show for brevity) are found lower than one, confirming that the downstream part of the slope was effectively unstable on the day of the considered past landslide event.

Anyway, it is worth to underline that looking at the map of Figure 5 it is possible to recognize an elongated strip, approximately N-S oriented, where FS values are lower than surrounding. This area might be associated to a structurally weak sector of the investigated slope. In fact, we have observed that the elongated strip is at the centre of the initial detachment area of the considered landslide event, which is located downstream of our survey area (Figure 5). So we can hypothesize that such a buried structural weakness might be related to the landslide trigger zone that extends upstream the initial detachment area.

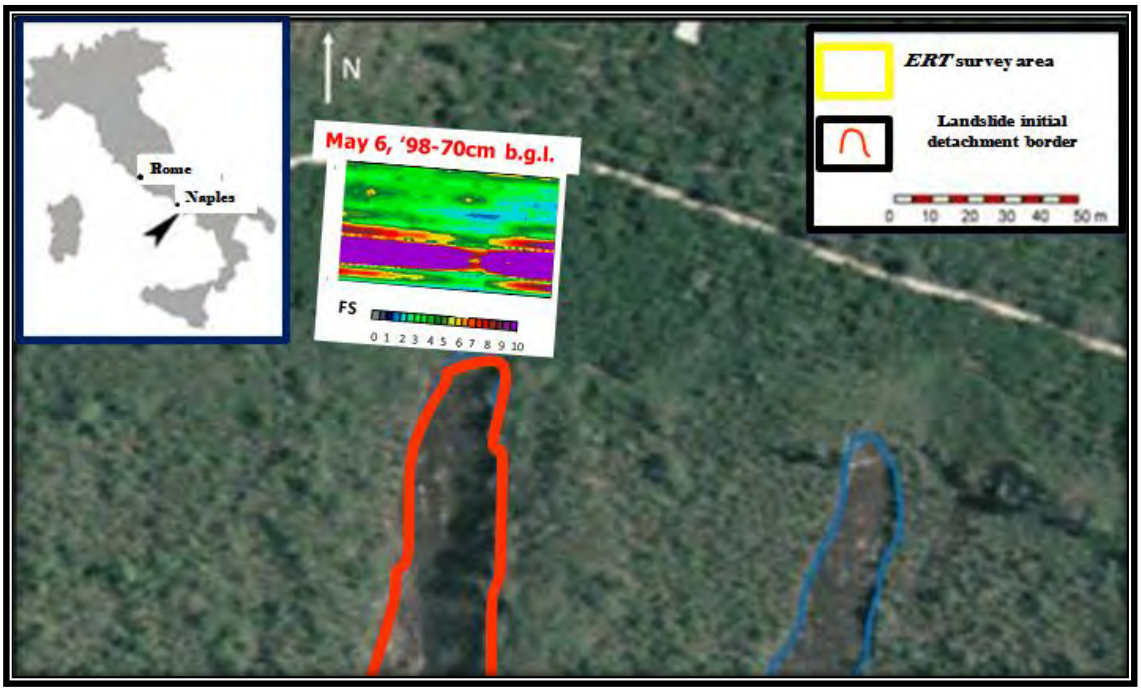

Fig. 5: Geophysical FS map of the survey area on May 5th, 1998, when the considered debris-flow event occurred. The FS values refer to a depth of 70 cm b.g.l. Note that the elongated strip characterized by FS values lower than surrounding is at the center of the initial detachment area marked with the red line.

Conclusions

A new geoelectrical-hydrogeological approach has been developed to estimate the water content distribution within pyroclastic covers, which could be critical for the stability condition of the investigated slopes. The proposed approach has been applied to a test area on Sarno Mountains, where intense rainfall events periodically trigger landslides. The analysis has identified a saturated condition of the shallow layer and a quasi-saturated condition for the deepest layers on the day when a landslide occurred. These results encourage studying critical conditions of any other slope mantled by loose deposits and hence subjected to debris-flow mobilization. We point out that the proposed approach could be a useful tool to both monitor the evolution over time of the water content distribution within loose deposits and determine alarm water content thresholds for each considered slope in support of short-term landslide forecast.

References

CASCINI, L., GUIDA, D., ROMANZI, G., NOCERA, N. and SORBINO, G., 2000: A preliminary model for the landslides of May 1998 in Campania Region. – Proc. 2nd Int. Symposium on "Geotechnics of Hard Soil-Soft Rock", Napoli, Balkema, **3**, 1623-1649.

CASCINI, L. and SORBINO, G., 2004: The contribution of soil suction measurements to the analysis of flowslide triggering. – In: PICARELLI, L. (Ed.): Proc. International Workshop on "Occurrence and Mechanisms of Flow-like Landslides in Natural Slopes and Earthfills". – 14.-16. May 2003, Sorrento, Italy. Bologna: Pàtron Editore, 77-86.

DE VITA, P., DI MAIO, R. and PIEGARI, E., 2012: A study of correlation between electrical resistivity and matric suction for insature ash-fall pyroclastic soils in the Campania region (Southern Italy). – Environmental Earth Sciences, doi: 10.1007/s12665-012-1531-4 (in press).

DI MAIO, R. and PIEGARI, E., 2011: Water storage mapping of pyroclastic covers through resistivity measurements. – Journal of Applied Geophysics, **75**, 196-202.

DI MAIO, R. and PIEGARI, E., 2012: A study of stability analysis of pyroclastic covers based on electrical resistivity measurements. – Journal of Geophysics and Engineering, 9(2), 191.

LOKE, M.H. and BARKER, R.D., 1996: Practical techniques for 3D resistivity surveys and data inversion. – Geophysical Prospecting, **44**, 499-523.

PIEGARI, E., CATAUDELLA, V., DI MAIO, R., MILANO, L., NICODEMI, M. and SOLDOVIERI, M.G., 2009: Electrical resistivity tomography and statistical analysis in landslide modelling: A conceptual approach. – Journal of Applied Geophysics, **68**, 151-158.

SORBINO, G., 2005: Numerical modelling of soil suction measurements in pyroclastic soils. – In: TARANTINO, ROMERO and CUI (Eds.): "Advanced experimental unsatured soil mechanics" Proceedings of the International Symposium on Advanced Experimental Unsaturated Soil Mechanics, Trento, 541-547.

Electromagnetic Induction (EM) for monitoring of soil-moisture pattern at the hill-slope scale

STEFFEN POPP-HOFMANN[1], DANIEL ALTDORFF[1], UTA SAUER[1], HENDRIK PAASCHE[1] and PETER DIETRICH[1]

[1] Helmholtz Centre for Environmental Research – UFZ, Permoserstrasse 15, 04318 Leipzig, Germany.

steffen.popp@ufz.de

Knowledge about spatially distributed soil-moisture pattern and its temporal dynamics is a key issue for understanding and modelling hydrologically triggered landslides. Because traditional measurements based on soil samples probe are very limited area or volume of the subsurface, 2D electrical resistivity tomography (ERT) is more frequently used for qualitatively monitoring soil-moisture variability. However, the effort for ERT increases significantly with increasing field sizes. Furthermore, cultivation of land can hamper the installation of permanent electrode arrays.
Ground-based electromagnetic induction (EM) methods have proven to be an efficient technique for a quick and area-wide mapping of soil electrical conductivity. We conducted several EM mapping surveys at the Heumöser site in Vorarlberg, Austria, which is a complex and slow-moving landslide area. EM surveys focus on the open space areas, which are used as pasture in summer and ski slope in winter. Using the EM-Profiler (EMP-400, GSSI), we repeatedly collected data over one year. Due to changing weather conditions over the period of EM monitoring, raw data have to be standardized to an equivalent conductivity at a reference temperature of 25°C. Furthermore, any unwanted external influences on the EM response have to be eliminated or corrected. As a result, we obtained standardized maps of interpolated electrical conductivity that allow for calculating differences between selected surveys, the delineation of slope areas with different dynamics, or the zonation of the slope area based on statistical cluster method. When assessing the EM maps, one should keep in mind that apparent electrical conductivity is a sum parameter, influenced by various soil components such as soil texture, water content, and mineral content. Since soil texture and mineral content are static features, variations in apparent electrical conductivity can be attributed to relative soil-moisture variability. EM monitoring is thus a suitable tool for the characterization or partitioning of the survey area prior to the installation of data logger, or monitoring relative changes in soil conditions.

The TEMPEL geoelectrical monitoring network for landslides: highlights of recent monitoring result

ROBERT SUPPER[1], BIRGIT JOCHUM[1], JUNG-HO KIM[2], DAVID OTTOWITZ[1], STEFAN PFEILER[1], IVO BARON[1], ALEXANDER RÖMER[1], MARIO LOVISOLO[3] and GÜNTHER MOSER[4]

[1] Geological Survey of Austria, Neulinggasse 38, 1030 Wien.
[2] KIGAM, 30 Gajeong-dong, Yuseong-gu Daejeon 305-350 Korea.
[3] C.S.G., Via Cazzulini 15A, 15010 Ricaldone, Italy.
[4] ZT Moser/Jaritz, Münzfeld 50, 4810 Gmunden , Austria.

robert.supper@geologie.ac.at

Introduction

In the frame of the FP7 project SafeLand, which was funded by the European Commission, the Geological Survey of Austria (in cooperation with several different European partners) started to set up a European landslide monitoring test site network (SUPPER et al., 2012a, b, c). This network setup was supported and further continued within the TEMPEL project, which was funded by the Austrian Science Fund (TRP 175-N21). Currently, the active network, which is attended by the Geological Survey of Austria, consists of five landslide monitoring sites in Austria (Gschliefgraben, Laakirchen), France (Super-Sauze) and Italy (Bagnaschino, Ancona) and one permafrost monitoring site in Austria (Magnetköpfl). Three further monitoring sites in Austria have already been abandoned (Sibratsgfäll, Mölltaler Glacier, Ampflwang-Hausruck) and one monitoring system will be installed in summer 2012 in Italy (Rosano). In the following, the results of two test sites of the Austrian network are described in detail.

Case Study Gschliefgraben

The Gschliefgraben site is one of the most prominent and extensively studied slope failures in Central Europe. The area of Gschliefgraben (Fig. 1) is a 2.85 km long and 0.85 km wide valley along the foot of the Northern Calcareous Alps and comprises a large complex of geologically controlled slides, earth flows, topples, rockfalls and deep-seated gravitational deformations.

In late November 2007, an earth flow of about 3.8 million m^3 of colluvial mass was reactivated in the central and western parts of the valley. The displacement velocity was up to 4.7 m/day at the beginning. Consequently, in the frame of the first emergency measures, 55 buildings had to be evacuated. Recently, the Gschliefgraben landslide has been a test site of the European FP7 project SafeLand where new techniques have been tested for rapid mapping monitoring and effective early warning, consisting of, e.g., airborne and ground-based geophysical surveys and the GEOMON4D (continuous geoelectrics) and D.M.S. (automatic inclinometer) monitoring systems.

After a first phase of mitigation in 2008, where major measures were focused on property and infrastructure protection and slow-down of the moving mass (drainage of the sliding mass, removal of sliding material), multi-disciplinary investigations including drilling, borehole logging and complex geophysical measurements (e.g. geoelectric, seismic and GPR surveys), were performed to investigate the structure of the landslide area in order to evaluate maximum hazard scenarios as a basis for planning further measures. Based on these results, a complex monitoring

system was installed, where geoelectric monitoring was coupled with high resolution DMS. Two perpendicular geoelectric profiles of 120 m length (electrode separation 3 m, 41 electrodes) and 192 m length (electrode separation 4 m, 49 electrodes) were installed. The DMS was installed at their intersection point.

The monitoring started in September 2009 and the system has been operating since that time with only one short interrupt due to a torrential rain event, which flooded the retention channels and damaged the geoelectrical cables.

Fig. 1: General setting of the Gschliefgraben site: (A) Position within Austria, B) Airborne photo of the Gschliefgraben valley and Mt. Traunstein from the west (Photo by: R. Supper, 2009).

Figure 2 clearly highlights the correlation of the geoelectric pattern with areas of different displacement characteristics. The low resistivity structure at the top correlates with the most active top layer, whereas the region with higher resistivity below exhibits only a slowly creeping behaviour. The sliding plains detected by the DMS inclinometer are clearly marked by high gradients of resistivity.

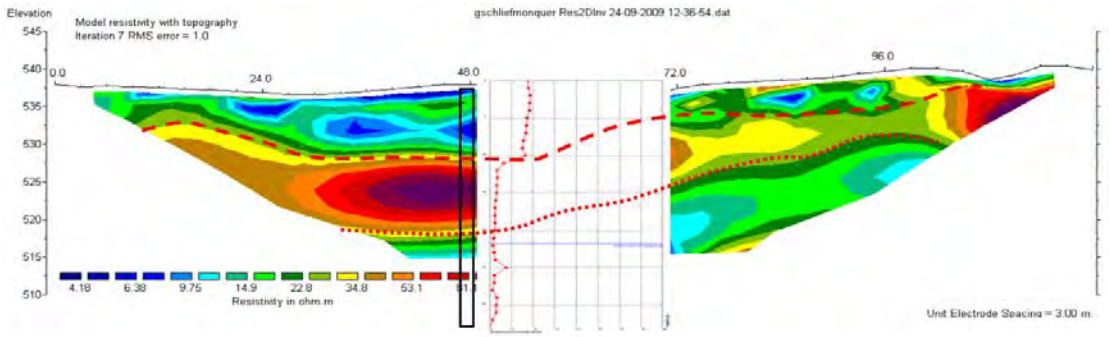

Fig. 2: Correlation of resistivity layers with sliding surfaces determined by a permanent inclinometer (red curve) in the area of Gschliefgraben.

During the whole survey only one small triggering event (1st of May 2010; acceleration from approx. 2 mm/12 days to 6 mm/12 days) with longer lasting aftermaths could be detected.
Consequently a correlation of resistivity anomalies with landslide acceleration is not possible and we can only focus on a correlation with very small changes in displacement velocity, which in fact are not relevant for early warning purposes, but might help to understand the dynamics of the landslide under "normal" conditions and to derive information on the background variations of subsurface resistivity.
Fig. 3 shows the variation of some selected values of apparent resistivity over the whole survey period. It can be recognised that the major variations of resistivity, which are very small (+/- 3 Ohmm), are due to seasonal temperature variations. In some cases, sudden resistivity changes correlated with major rainfalls (resistivity increase or decrease), depending on the sensitivity of the respective array and on the absolute apparent resistivity value. Fig. 4 zooms in on the 1st of May event. In the presented cases the rainfall event and the connected acceleration of the landslide was correlated with a (very small, but detectable) decrease in apparent resistivity (below 2 Ohmm!). The response times are difficult to calculate, since the starting time of acceleration cannot exactly be determined. However the results suggest a delay between 6-24 hours between the onset of the resistivity decrease and the initiation of the acceleration.

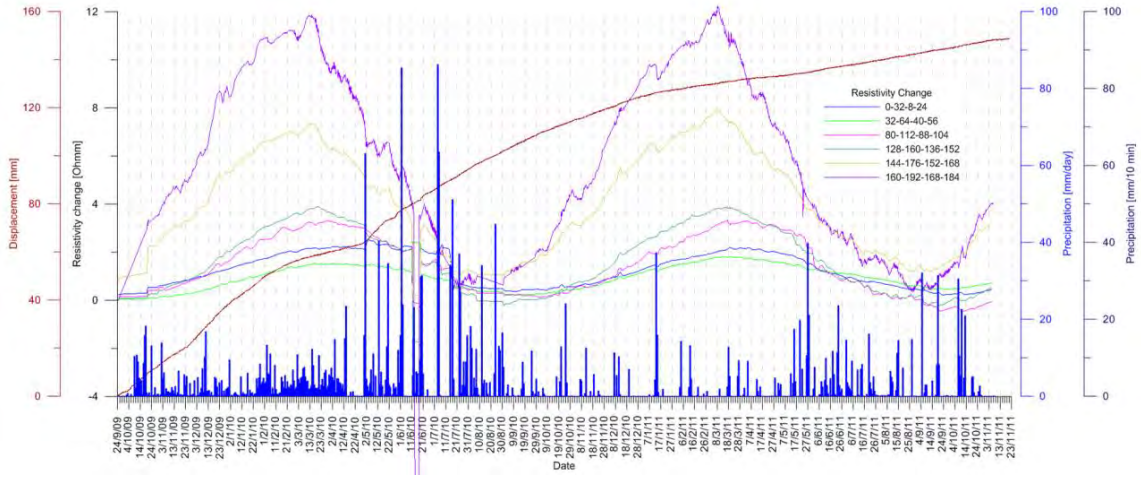

Fig. 3: Correlation of selected apparent resistivity data with displacement and precipitation for the entire survey period.

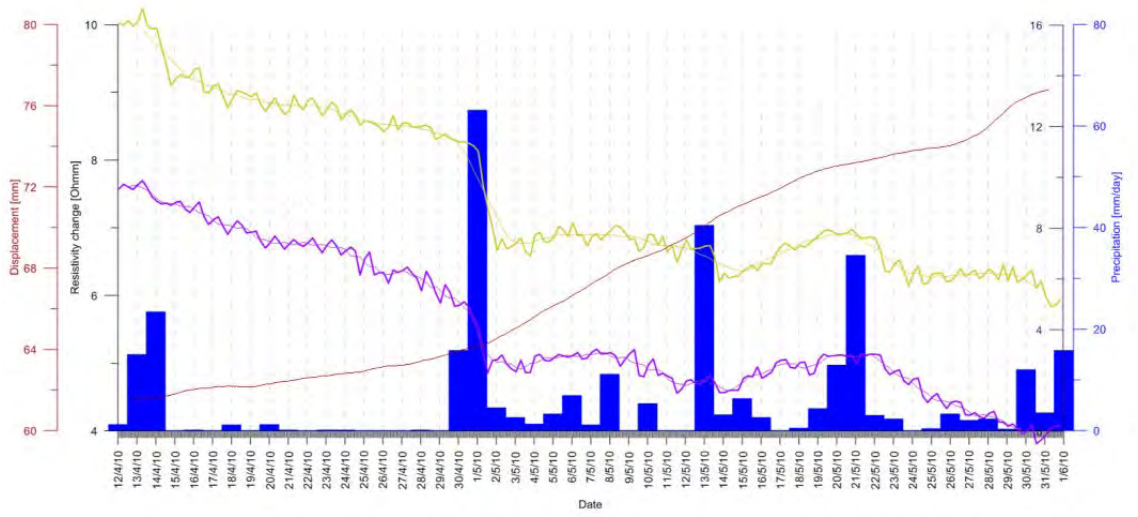

Fig. 4: Correlation of selected apparent resistivity data (yellow, purple) with displacement and precipitation for the event on March 1st, 2010.

We can conclude that resistivity monitoring helped to understand the process that led to a minor acceleration of the landslide in May 2010. However, apart from that, no significant changes of subsurface resistivity took place over the whole survey period. Most variations can be associated with seasonal temperature changes or short time precipitation events. Since no major triggering event happen during the entire survey period, no detailed correlation between resistivity and displacement could be investigated. Longer survey periods have to be envisaged.

Case Study Ampflwang/Hausruck

The Ampflwang monitoring site (Fig. 5) is situated in the Hausruck Hills in NW Austria, where a recent landslide was activated in March 2010 within the area of an old deep-seated landslide, following snow melting and heavy rainfalls. The old dormant landslide is about 650 m long, 900 m wide and has an estimated depth of failure of about 20-30 m b.g.l. The reactivated part, as recognized by topographic changes and inclinometric data, is about 40 m long, 40 m wide and about 4 m thick. It is a shallow rotational-translational landslide of an elliptic shape and quite smooth topography. It is rather in initial evolution stage. However, a newly constructed family house was partly damaged by the crown of the landslide in 2010.

Therefore, a geoelectric and DMS monitoring system was implemented in cooperation with the geotechnical bureau of Moser/Jaritz, C.S.G. and the Geological Survey of Austria in order to investigate the behaviour of the landslide and its triggering in more detail and to develop an optimized strategy for site specific remediation measures.

Two D.M.S. columns were installed, which consisted of tilt/displacement, temperature and piezometric sensor modules and they hourly registered displacement data down to the depth of 5 and 7 m b.g.l., respectively. The transversal geoelectric GEOMON4D profile comprised 60 electrodes at a spacing of 1 meter. Precipitation data was taken from the weather station of Wolfsegg, courtesy of the Central Institute for Meteorology and Geodynamics (ZAMG) in frame of the cooperation contract between GSA and ZAMG. The monitoring data were sent via GPRS to the GSA and C.S.G. office in order to be analysed and interpreted.

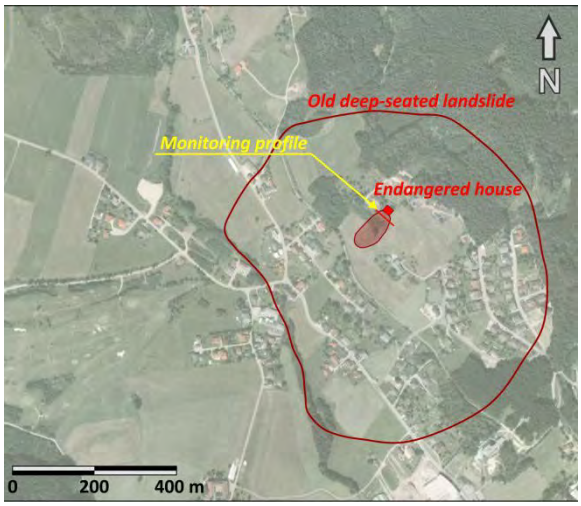

Fig. 5: Orthophoto with the marked landslides and geoelectric monitoring profile. Source of map: GoogleEarth.

Resistivity measurements were performed along one profile close to the DMS column 2. One set of data comprising around 4000 gradient-type measurements was taken every 4 hours. For power supply a connection to the local power grid was installed. The data was sent every day to the GSA office, where the results were checked for quality and time sequences of apparent resistivity and inversions were automatically generated each day. Fig. 6 shows the time series of selected apparent resistivity values in correlation with precipitation and displacement, whereas Fig. 7 gives a closer up look at the winter and spring period, during which all major displacement events took place. From these figures it is obvious that most major rain events were accompanied by a resistivity decrease.

Fig. 8 shows details of the period of the major displacement event which took place on the 13th of January 2011. Resistivity values already start to decrease around the 8th of January most probably due to additional inflow of water from snow melting. In the period after this trend continues until a first short rainfall on January 12th after which the decrease accelerated. After the start of an intense rainfall after midnight of January 12th, apparent resistivity decreased further until around 4 o´clock, when the landslide successively started to move with increased speed. Around 16 o´clock, after the main acceleration phase, resistivity started to increase rapidly although precipitation continued with less intensity for almost one day.

Data from the events 2 and 3 in February (cp. Fig. 7) show a quite similar behaviour. Resistivity started to decrease in the afternoon of February 4th and 5th, thus starting to speed up the landslide on the 5th, without any influence of rainfall. Again the reason could be melting of snow. The resistivity decrease took place before and during the acceleration phase. During the period of constant (but increased) speed, also resistivity remained approximately constant until the first rainfalls had taken place in the morning of February 11th. Interestingly, during the first hours of rainfall on the 12th, the landslide slowed down, indicated also by a short increase of resistivity. After that, resistivity started to decrease significantly until 14 o´clock, when the landslide started to speed up again. During the acceleration phase resistivity values became almost constant and started to increase again after the major acceleration phase on February 13th.

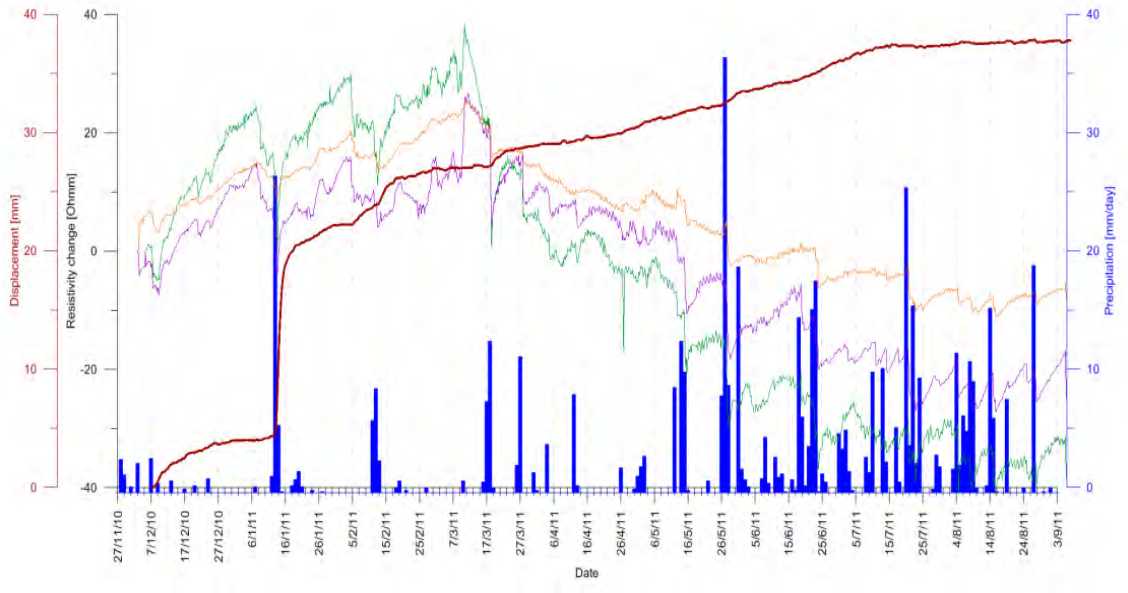

Fig. 6: Display of displacement (red), precipitation (blue; courtesy of the Central Institute for Meteorology and Geodynamics (ZAMG)) and apparent resistivity at different relative apparent depths (green: 1 m; purple: 2 m; orange: 4 m) for the whole survey period.

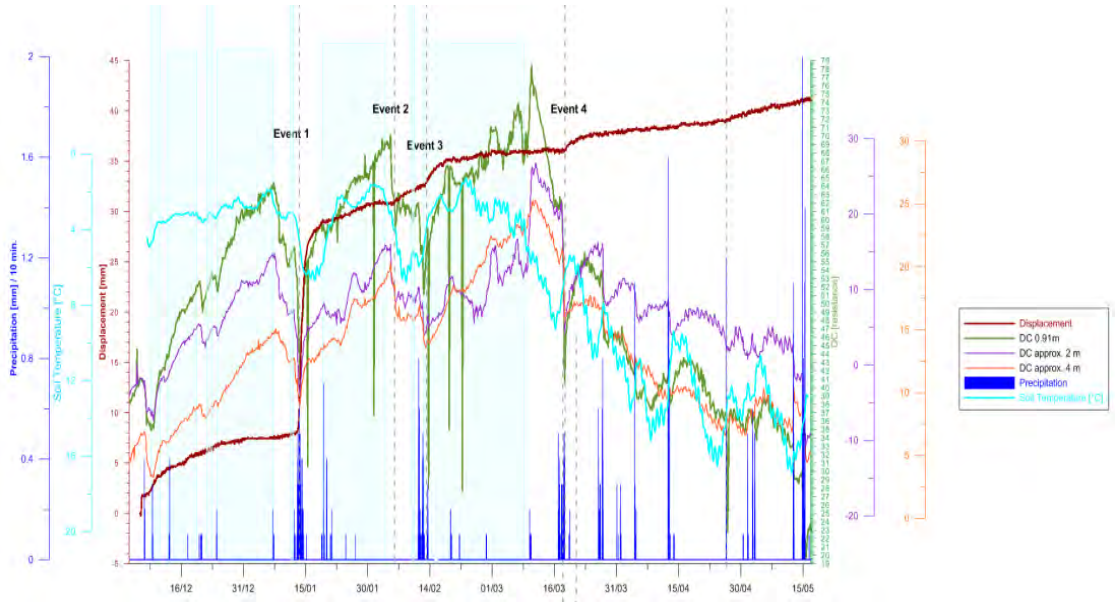

Fig. 7: Display of displacement (red), precipitation (blue; courtesy of the Central Institute for Meteorology and Geodynamics (ZAMG)) and apparent resistivity at different relative apparent depths (green: 1 m; purple: 2 m; orange: 4 m) in the winter/spring period.

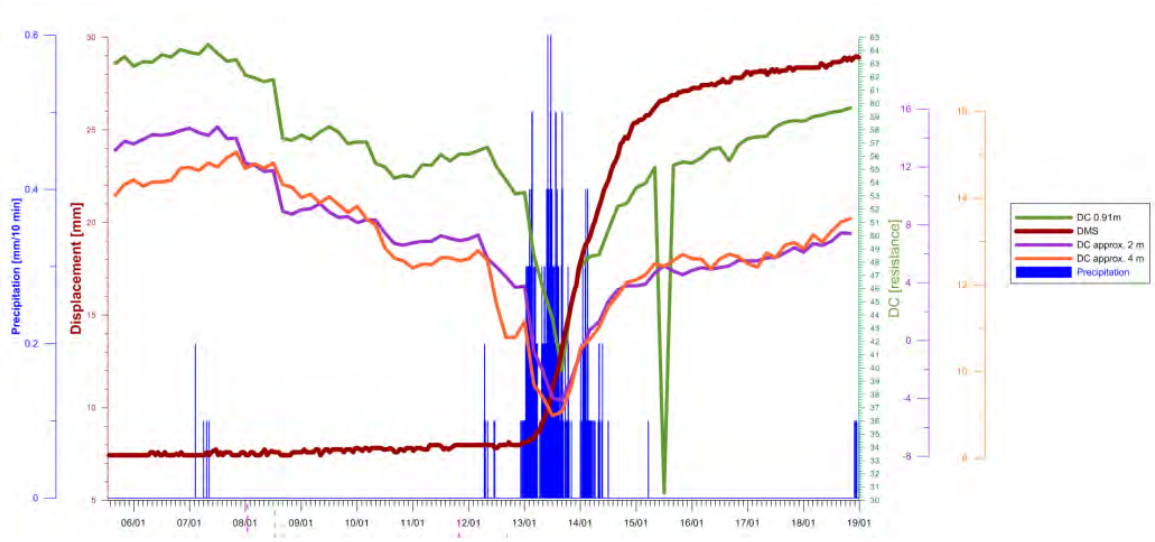

Fig. 8: Display of displacement (red), precipitation (blue; from the station Wolfsegg, courtesy of the Central Institute for Meteorology and Geodynamics (ZAMG)) and apparent resistivity at different relative apparent depths (green: 1 m; purple: 2 m; orange: 4 m) for the time around the major displacement event ("event1") in January 2011.

Based on the results described above we can conclude that decreasing values in the time series of apparent resistivity definitely correlate with the penetration of wetting fronts into the subsurface due to rainfall or snow melt events. However no information could be derived under which circumstances a movement of the landslide is triggered in case of rainfalls, since no acceleration event could be monitored in late spring and summer time, when even more intense rainfalls took place. However the reason for that could be that the landslide generally stabilised during that period. Further facts to understand this behaviour could only be derived if the monitoring would be continued for another year, which, in this case is not possible.

Conclusion

Results from the landslide monitoring studies, which were carried out in the frame of the SafeLand and TEMPEL projects, provide a solid basis for further research of landslide triggering events and early warning parameters. As mass movement events happen rarely, longer observation periods will be necessary. Real progress will only be possible, if many triggering events in different geological settings are analysed.

Even though, some conclusions concerning landslide monitoring and early warning can already be drawn:

- Almost all of the observed events were triggered by rainfall or melting water.
- Important parameters of landslide monitoring are displacement, velocity and acceleration, groundwater level fluctuations, pore-water pressure and micro seismicity, electrical resistivity, induced polarization and self-potential.
- For detailed interpretation of the results and to establish correlations, a high data sample interval of at least one hour or even less is necessary, depending on the velocity of the mass movement.

Acknowledgements

The study was supported by the 7th FP project "SafeLand – Living with the landslide risk in Europe" and the project "TEMPEL – **Temp**oral changes of geo**el**ectrical properties as possible indicator of future failure of high risk landslides", funded by the Austrian Science Fund (FWF)-TRP 175-N21 in frame of the Translational Brainpower Program. The authors would further like to thank W. Gasperl, Torrent and Avalanche Control (WLV), Section Upper Austria, for providing additional funding for the installation of the DMS system in Gschliefgraben, supplying a lot of additional data and for the excellent cooperation and their logistical and infrastructural support. We further acknowledge the support of F. Zott, Institute of Mountain Risk Engineering, Department of Civil Engineering and Natural Hazards, BOKU - University of Natural Resources and Life Sciences, Vienna, who supplied the meteorological monitoring data of Gschliefgraben and R. Potzmann, Central Institute for Meteorology and Geodynamics (ZAMG) for allocating the meteorological data from the station Wolfsegg i. Hausruck. We would also like to thank the family Gaisbauer for their support at the test site Ampflwang.

References

SUPPER, R., JOCHUM, B., OTTOWITZ, D., BAROŇ, I., VECCHIOTTI, V., PFEILER, S., RÖMER, A., LOVISOLO, M. and KIM, J-H., 2012a: Case histories – Analysis of real monitoring data: Bagnaschino. – In: BARON, I. and SUPPER, R. (Eds.): The Safeland Project, Deliverable 4.6, Report on evaluation of mass movement indicators, p. 191-220, Vienna.

SUPPER, R., JOCHUM, B., BAROŇ, I., OTTOWITZ, D., PFEILER, S., RÖMER, A., LOVISOLO, M. and MOSER, G., 2012b: Case histories – Analysis of real monitoring data: Ampflwang-Hausruck. – In: BARON, I. and SUPPER, R. (Eds.): The Safeland Project, Deliverable 4.6, Report on evaluation of mass movement indicators, p. 150-173, Vienna.

SUPPER, R., BARON, I., JOCHUM, B., OTTOWITZ, D., PFEILER, S., KAUER, S., RÖMER, A., ITA, A., MOSER, G., LOVISOLO, M. and KIM, J-H., 2012c: Case histories – Analysis of real monitoring data: Gschliefgraben. – In: BARON, I. and SUPPER, R. (Eds.): The Safeland Project, Deliverable 4.6, Report on evaluation of mass movement indicators, p. 191-220, Vienna.

Applications in Engineering

Monitoring of tunnel stability, Arzberg, 2006; picture by G. Bieber

Electrical resistivity monitoring of simulated piping and hydraulic fracturing within a dam structure

HEE-YOON AHN[1], HUEI-DAE LIM[2], HEE-BOK AHN[3] and JUNG-HO KIM[4]

[1] Heesong Geotek. Co., LTD, Daejeon, Korea.
[2] Dept. of Civil Eng., Chungnam National University, Daejeon, Korea.
[3] Korea Water Resources Corporation, Daejeon, Korea.
[4] Korea Institute of Geoscience and Mineral Resources, Daejeon, Korea.

ayoony1014@gmail.com

Introduction

There are about 20,000 large dams world-wide. In the 20th century, around 200 dam failures have occurred in the world. And the accidents caused a large of property damage and killed about 11,000 people (LIM et al, 2004). In generally, the causes of failures are over flow, seepage and piping of the dam, substructure, slide activity and earthquake. Especially, overflow and piping account for 49.6 % and 47.0 % of the failures, respectively (FORSTER and MACDONALD, 1998). It is difficult to prediction the failures in dam caused by piping.

Piping has been the main cause of fill dam failure and generated by the various causes. The reason why the dam failure was piping by concentrated seepage leakage and backward erosion. Piping by concentrated seepage leakage frequently occur a dam designed with modern technology. Cracks in the dam and locally vulnerable permeable layer formed a seepage flow. But this is not a cause of piping at all times. In addition, the concentrated seepage flow may erode fine soil particles, and carry these fine particles up to the surface. As the erosion process continues, a piping may form through the top stratum. UNSW (Univ. of New South Wales) dam laboratory suggested 4-steps of the progress in piping. Generally, the progress is ①Initiation→②Continuation→③Progression→④Failure (FOSTER et al, 1999). If it is possible to estimated change of resistivity values for a piping, we could prevent the failures of a dam and ensure a safety of a dam.

In this study, we attempted to monitor the changes in electrical resistivity values of earth dam material while a saddle dam is dismantled for the construction of emergency spillways of Dae-chung dam. Two artificial sub-horizontal boreholes were drilled into the embankment structure to simulate piping along the two artificial flow channels. And, after the simulated piping test was finished, we were carried out using injecting with grouting cement fluids on the dam crest. One was to develop a piping detection technique measuring electrical resistivity of earth dam by monitoring, and the other was to estimate reinforcement of dam by grouting, which electrical resistivity lower enough to yield resistivity contrast.

The spatial distribution of the artificial region by leachate was visualized in space using the electrical resistivity change ratio of 2-D resistivity distribution before and after the simulated piping test and hydraulic fracturing.

Site Description

Dae-cheong Dam is located at 150 km upstream from the estuary of the Geum River which flows into the Yellow Sea from the middle part of the Korean peninsula. The saddle dam was planned to

be dismantled due to reconstruction of emergency spillway. The saddle dam under consideration is an earth dam with central clay core and it has a dimension of 244 m in length and 8m in height. From the geologic investigation performed before the reconstruction of emergency spillway, it was covered with weathered surface soils for mica schist around of saddle dam. Bedrock consists of quartz schist with biotite, amphibole quartz schist, and quartz porphyry.

Simulated Piping Test and Hydraulic fracturing Test

We should try to approach for the various aspects of the situation. First, two artificial sub-horizontal boreholes with diameter of 75.7 mm were drilled into the dam structure to simulate piping along the two artificial flow channels. The boreholes were installed with open-holes, each one at different level (Figure 1(a)). It was tried to identify for resolution of electrical resistivity data. And we had installed the PVC pipe for preventing progressive collapse in the filter zone (Figure 1(b)). The piping test had been conducted for 72 hours, except replacing flow-meters. And it was measured an injection charges, discharge and turbidity during piping test.

Second, four vertical boreholes were drilled at the crest, and hydraulic fracturing carried out. We injected pillar-shaped with cement milk about 10 minutes for hydraulic fracturing. The effect of hydraulic fracturing was visually identified after applying phenolphthalein solution.

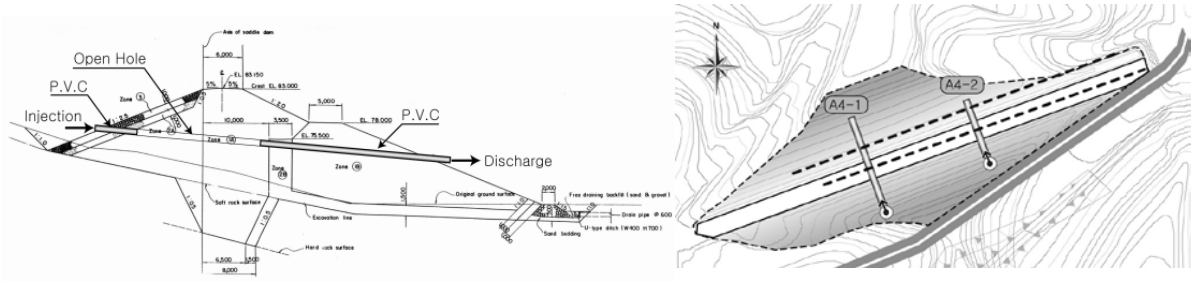

(a) (b)

Fig. 1: The boreholes were installed for simulated piping test in saddle dam, (a) Plan map, (b) Cross-section of the saddle dam.

Resistivity Monitoring

The electrical resistivity measurements were performed at the dam crest and the downstream slope. The resistivity data were collected with a survey system of SuperStingR8/IP^{TM} by AGI, USA. The length of the survey line was 160m, and the electrodes were spaced 2m. The electrode arrays used were dipole-dipole and modified pole-pole systems. The depth of investigation was extended by increasing the dipole separation to 4m. The resistivity data were collected using both electrode array system form each survey line and both data sets from each survey line were incorporated as one data set for each survey line in order to enhance the quality of the data.

All the electrical resistivity data was first processed and interpreted by DIPRO for Windows, the 2.5-D resistivity interpretation software package. The processing includes bad data elimination, 2.5-D inversion, and drawing 2-D resistivity color images. In the 2.5-D inversion, we adopt the active constraint balancing method (YI et al., 2003) to enhance the resolving power of the least-squares inversion.

The total number of the electrical resistivity monitoring data was performed 7 times during the simulated piping test. The measurement conditions of the electrical resistivity are listed in Table 1. According to this table, the electrical resistivity measurements were carried out in 11 stages,

Phase 1 before the drilled boreholes, and Phase 2 to Phase 9 are during simulated piping test. And we conducted a hydraulic fracturing test in October 18.

To monitor the changes in the dam resistivity before and during simulated piping test, surface survey has been conducted. The result of electrical resistivity survey in dam crest and the downstream slope ranged 100~230 Ωm and 100~180 Ωm, respectively. The electrical resistivity values in dam crest were bigger than these of the downstream slope. It is observed that a low resistivity zone lies in the upper area from the surface to a depth 4m, zone shows a higher resistivity, greater than 150 Ωm. According the boring data at the crest, the upper area of the soil unit consists of mostly silt soil with granule. Therefore we thought that the anomaly in the upper area is attributed to the silt soil and granule with low resistivity.

Monitoring stage	**Acquisition date**	**Description**	
Phase 0	16. Sep. 2008	N=12	A preliminary survey
Phase 1	17. Sep. 2008	N=16	
Phase 2	04. Oct. 2008	N=16	Injection of water
Phase 3	04. Oct. 2008	N=16	During piping test
Phase 4	05. Oct. 2008	N=16	
Phase 5	05. Oct. 2008	N=16	
Phase 6	06. Oct. 2008	N=16	
Phase 7	06. Oct. 2008	N=16	
Phase 8	07. Oct. 2008	N=16	
Phase 9	07. Oct. 2008	N=16	Finished piping test
Phase 10	20. Oct. 2008	N=16	2 days before hydraulic fracturing test

Tab. 1: History of simulated tests and electrical resistivity monitoring.

But there were a certain difference the result of Phase 0 and Phase 1 (Figure 2). As a whole, resistivity distribution aspect of profiles for Phase 2 to Phase 9 looks similar results. The ranges of electrical resistivity values were 100-400 Ωm around boreholes, and the RMS error was 4.6-7.5% ranged each phases in the crest. Phase 1 showed the better image than Phase 0 in lower depth zone. The data acquired in Phase 1 unfortunately showed too little electrode separation index to get subsurface image from them. Therefore, one set of monitoring data was assembled using the data from Phase 2 to 10 excluding Phase 1.

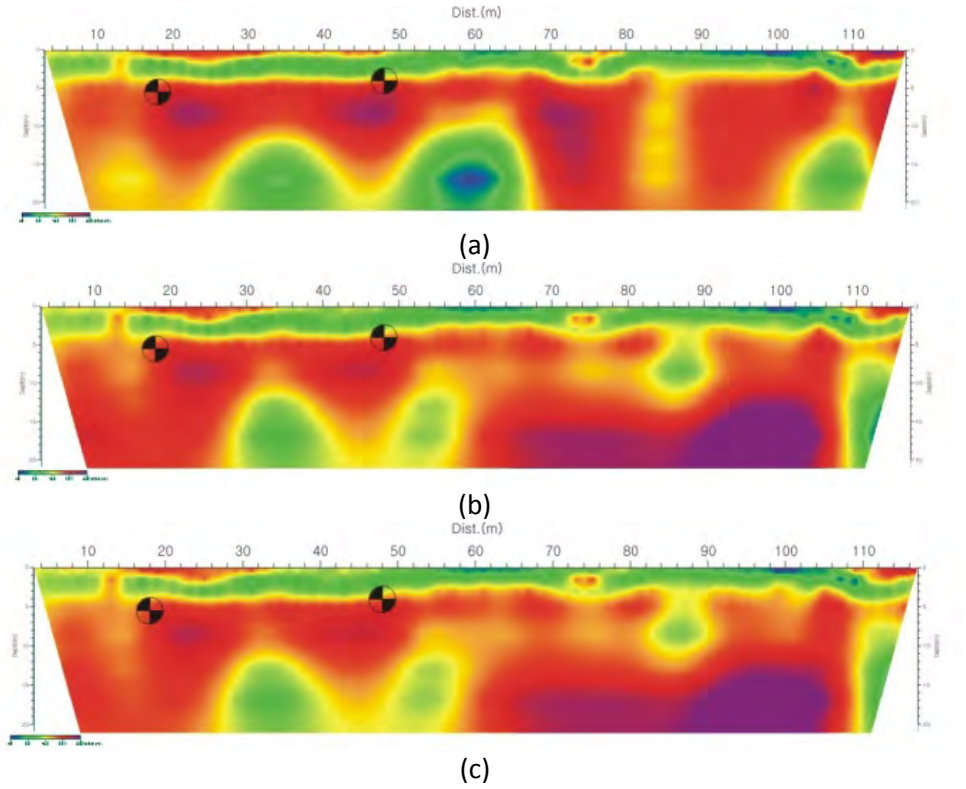

Fig. 2: Time-lapse images of electrical resistivity survey of Phase 0 in the crest (a), and the measurement of Phase 2 (b), and when Phase 9 measurement was completed (c).

In order to image around boreholes, the different images were analyzed for each phases. Figure 3 show the ratio of resistivity changes for Phases 2 to 9 divided by Phase 1. This ratio was calculated simply by dividing every resistivity values for each grid of one profile by that of corresponding grid of the other. If the resistivity change ratio is 1, it is never any change in the phases. And less 1 indicates a decrease in resistivity values, while above 1 indicates an increase. There wasn't changed a ground condition during piping test. Therefore the boreholes area must be imaged as an anomalous zone having the value less than 1 during piping test. We could easily recognize that the electrical resistivity ratio showed many artifacts, while difference images appeared with false anomalies of resistivity increasing. These figures indicate the ratio of resistivity change around the boreholes is very low, less than 5%. So it is really difficult to detect leakages, since the ratio of resistivity change is less than RMS error by inversion.

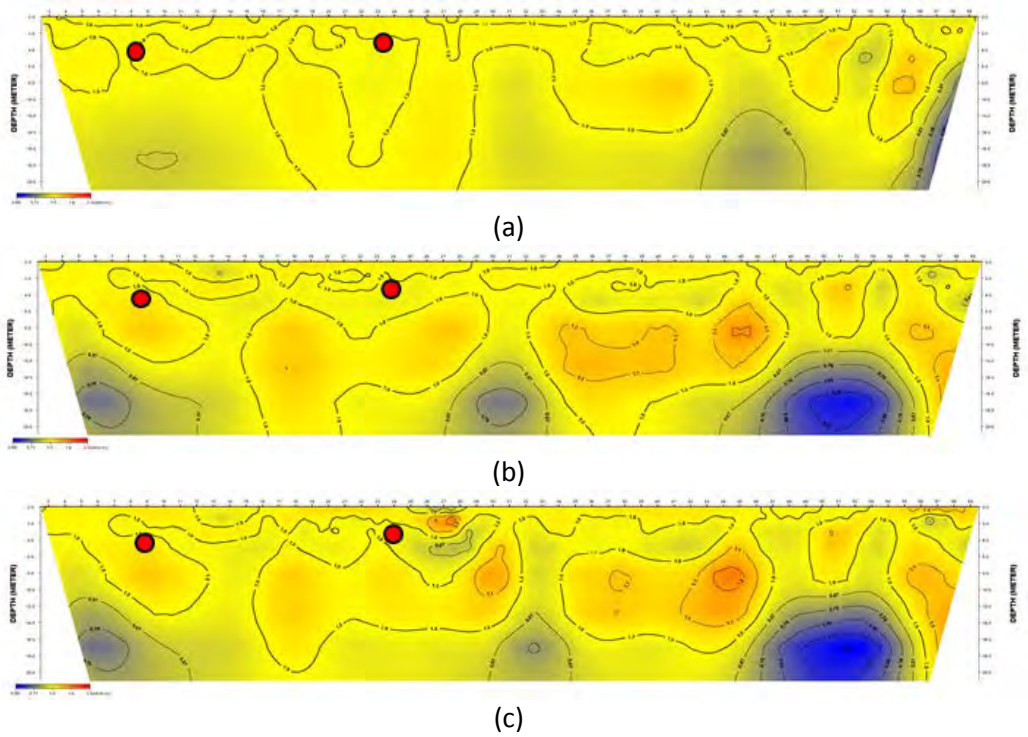

Fig. 3: Resistivity changes of Phase 3 (a), Phase 6 (b), Phase 8(c) expressed in terms of the resistivity ratio between each phase and Phase 1.

The ratio of resistivity change was very low until Phase 6. Therefore, we changed two kind of ground condition for a big change of resistivity. First, Phase 8 was saturated around 24 hours in the boreholes for piping test. Second, we collapsed the right borehole. Figure 4 shows the resistivity change ratio of Phase 8/Phase 6 on the dam crest. White rectangle indicates the zone of borehole was collapsed by water injection, and left borehole isn't collapse. The resistivity change ratio is 1~3 % range around borehole (A4-1), but white rectangle area is decreasing with 28%. The detection of leakage could be difficult to conclude that the resistivity change ratio was decreased. Because the resistivity change ratio was appeared that increasing or decreasing of resistivity value during piping test.

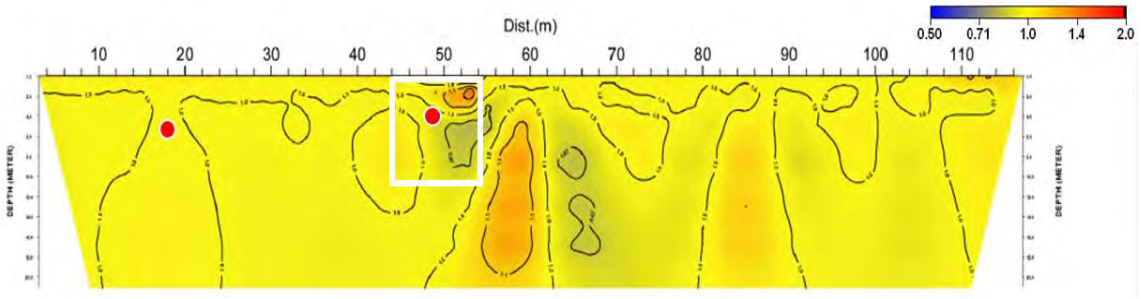

Fig. 4: The resistivity change ratio of the Phase 8/Phase 6 on the dam crest.

After the simulated piping test was finished, we was analysed the resistivity change ratio for the hydraulic fracturing test. Figure 5 shows the resistivity change ratio of Phase 10/Phase 1 on the dam crest after hydraulic fracturing. The most obvious change of ground condition is observed near to the location of 47 m, while little change near 16 m and 112 m. The anomalies of resistivity

decrease on and the surface are mainly attributed to the overflow of ground material which was observed in field. The effect of hydraulic fracturing was visually identified after applying phenolphthalein solution since the solution changes its color after reacting with grouting cement. An injected cement of pillar-shaped would be turned magenta by applying phenolphthalein solution. The scale of the grout materials wasn't big, but it was confirmed to spread widely in around injected boreholes during destruction from the saddle dam.

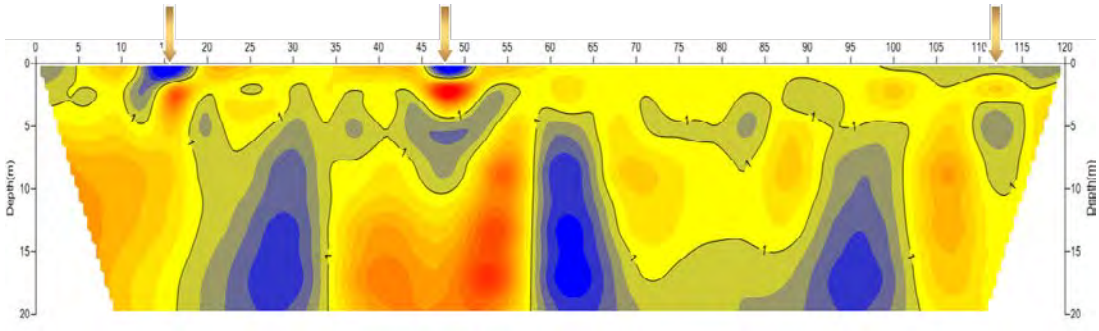

Fig. 5: The resistivity change ratio for Phase 10/Phase 1 on the dam crest after hydraulic fracturing.

Conclusion

The electrical resistivity monitoring of piping in a dismantled saddle dam provided an excellent opportunity to evaluate potential for detecting piping. We were able to obtain high-quality resistivity along-dam profiles of total 8 phases for 4 days during piping. This is demonstrated by low RMS error (2.5~7.5%). However, the decreased resistivity due to injection of water is not apparent. This is probably because the decreased resistivity is within the range of RMS error. Therefore, resistivity monitoring may not be suitable for the detection of piping especially at early stages. We suggest tighter spacing of electrodes for future studies. For artificial hydraulic fracturing experiments; it is found that the extent of propagation of grout material is identified by resistivity monitoring.

References

FORSTER, I.R. and MACDONALD, R.B., 1998: Post-Earthquake Response Procedures for Embankment Dams – Lessons from the Loma Prieta Earthquake. – ANCOLD Bulletin No. **109**, 46-64, Australian National Committee on Large Dams.

FOSTER, M.A., FELL, R. and SPANNAGLE, M., 1999: A Framework for Estimating the Probability of Failure of Embankment Dams by Internal Erosion and Piping using Event Tree Methods. – UNICIV Report R-377, UNSW, Sydney, Australia.

LIM, H.-D., KIM, K.-S., KIM, J.-H., KWON, H.-S. and OH, B.-H., 2004: Leakage Detection of Earth Dam Using Geophysical Methods. – ICOLD 72nd Annual Meeting ,May 16-22, 2004 Seoul, Korea, pp.26.

YI, M.-J., KIM, J.-H. and CHUNG, S.-H, 2003: Enhancing the resolving power of least-squares inversion with active constraint balancing. – Geophysics, **68**, pp. 931-941.

Resistivity monitoring for the detection of leakage zones in earth fill dams

IN-KY CHO[1], IK-SOO HA[2], KI-SEOG KIM[3], HEE-YOON AHN[3], SEUNGHEE LEE[4] and HYE-JIN KANG[1]

[1] Department of Geophysics, Kangwon National University, Chuncheon, Korea.
[2] Department of Civil Engineering, Kyungnam University, Changwon, Korea.
[3] Heesong Geotech , Daejeon, Korea.
[4] Geoems, Anyang, Gyenggido, Korea.

choik@kangwon.ac.kr

Abstract

We applied the resistivity monitoring at an embankment dam to effectively identify the leakage zones or their expansion with time. We first analyzed the three-dimensional (3D) effects caused by 3D dam structure through 3D finite element modeling. Through numerical tests, we demonstrated the effectiveness of time-lapse inversion for the detection of leakage zone at embankment dams. Applying the resistivity monitoring system devised for dam surveillance to a test dam site, resistivity monitoring data were acquired. Noise characteristics of collected resistivity data were analyzed and a processing procedure was proposed to establish a proper reference model for the time-lapse inversion of future monitoring data.

Introduction

More than 16 percent of 18,000 reservoir dams in Korea are reported to have leakage problems and need to be repaired. Recently, resistivity monitoring has been applied to wide range of engineering and environmental problems with the help of automatic/rapid data acquisition, data communication and effective interpretation software. Resistivity survey and long term monitoring at an embankment dam can provide helpful information about leakage zones.

Resistivity monitoring is based on the fact that a change in the porosity leads to the changes in water content and fine particles, which alter the electrical resistivity. At every embankment dam, internal erosion always occurs as time passes. The internal erosion generally develops into piping over a long time by backward erosion and concentrated leak, and finally leads to dam failure. Thus internal erosion and piping are major cause of embankment dam failure. Internal erosion initially results in an increased porosity due to loss of fine particles in the core. Resistivity is known to be very sensitive to the changes in porosity in embankment dams. Thus resistivity monitoring is a reasonable method to find out the leakage zone. However, resistivity is strongly influenced by seasonal variation of temperature, TDS of reservoir water and water level (SJÖDAHL et al., 2008). Also, various noises prevent accurate measurement of resistivity. These make it very hard to accurately interpret resistivity monitoring data.

In the resistivity monitoring, significant challenges still remain in data acquisition system, noise suppression and time-lapse inversion for more detailed and quantitative interpretation. Here, we will present various problems occurring in the resistivity monitoring for the detection of leakage zones at embankment dams.

3D effect

Generally, 2D data acquisition and interpretation is widely used in the survey of embankment dams because of convenient field work and fast inversion. In the 2D survey, constant physical property and topography are assumed along the strike direction. Also, survey line has to be perpendicular to geological strike direction. But 2D resistivity survey along the dam crest violates this 2D assumption. Topography also does not fulfill the 2D condition and 3D effects caused by the 3D dam structure distort apparent resistivity data (SJÖDAHL et al., 2006; CHO and YEOM, 2007). Consequently, inverted 2D resistivity section does not represent the true resistivity distribution of the embankment dam. This is another problem of 2D resistivity survey at embankment dams. However, 2D survey is still one of the most widely used methods since it provides very useful information about leakage zones.

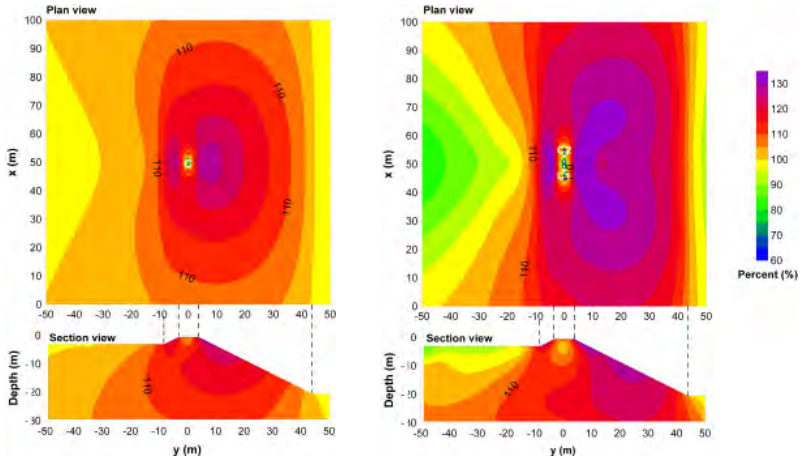

(a) (b)

Fig. 1: Distortion of potential distribution by 3D effect caused by 3D dam structure when a homogeneous dam is excited by a pole (a) and dipole (b) source.

To investigate the 3D effect in the resistivity survey at embankment dams, we carried out 3D numerical modeling. We assumed a homogeneous dam model in which all the component of embankment dam have constant resistivity. Figure 1 shows the distortion of potential at an embankment dam when one ampere current is injected into the ground through a pole and dipole source. From Figure 1, we can see that apparent resistivity is differently influenced according to the location of survey line. If a survey line is located on the crest, measured apparent resistivity is always larger than that of homogeneous half-space model even in the case of dipole-dipole measurement. Not shown here, we calculated dipole-dipole sounding data and plot sounding curve. We set station spacing to 5 m and water level to 10, 13.5 and 17 m. The calculated apparent resistivity is larger than that of homogeneous half-space model by 10 to 30 percent. This means that the apparent resistivity data are distorted by 3D effect caused by 3D dam structure.

Resistivity monitoring

When long term resistivity monitoring is performed, change in resistivity with time can be assessed by simply carrying out independent inversion. To understand how much resistivity

change occurs when leakage takes place at an embankment dam, we conducted 3D modeling. Figure 2 shows a leakage model. The physical dimension and resistivity are set empirically. We assumed that damaged core shows increasing resistivity and saturated downstream shell shows decreasing resistivity.

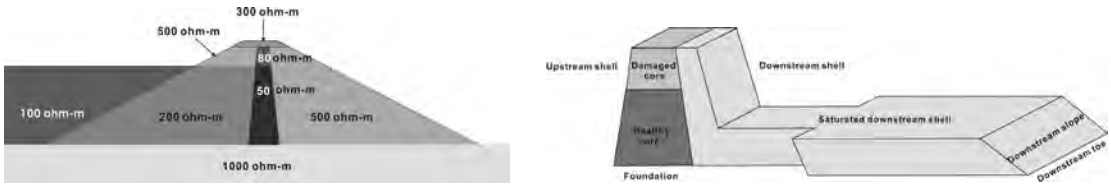

(a) (b)

Fig. 2: A healthy (a) and damaged dam model (b).

Figure 3(a) and (b) are comparison of inversion results for a healthy and damaged dam. Two sections are nearly identical. The damaged zone is not defined in the inverted section because changes in apparent resistivity data are too subtle to identify leakage zones. Figure 3(c) is the percent resistivity ratio section. The damaged zone in the core is clearly defined as an increasing resistivity zone in the ratio section. Low resistivity zone at depth is the effect of saturated downstream shell. Monitoring is a reasonable tool to identify the leakage zones in the dam although the section does not exactly represent the saturated downstream shell.

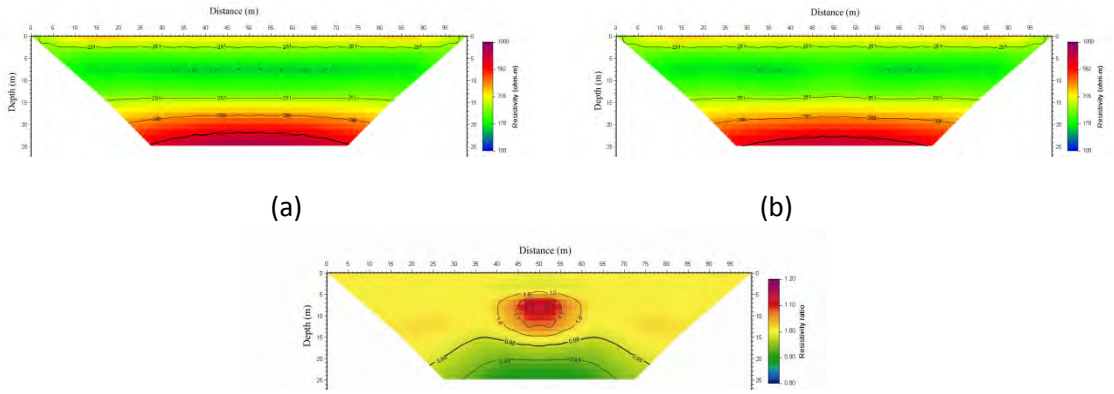

(a) (b)

(c)

Fig. 3: Independent inversion results for a healthy dam (a) and damaged dam (b), and resistivity ratio section (c).

However, the independent inversion does not guarantee that the changes in resistivity are due to actual changes in the subsurface resistivity with time and does not take into account the reference model or prior information. Accordingly, independent inversion is not effective to identify small changes in resistivity (LOKE, 1999). In order to accurately identify changes in resistivity at particular locations and different times, time lapse inversion is required. Time lapse inversion of long term monitoring data is generally based on the conventional least-squares

method, but time or cross-model constraint is added in the object function (OLDENBORGER et al., 2007, KIM and CHO, 2011).

Resistivity monitoring system

We devised a resistivity monitoring system. The system is divided into two parts: the field system and office system. Two systems are connected by bidirectional CDMA communication. Office system is composed of three parts; system control unit, data processing unit and data base. The system control unit remotely controls the data acquisition unit and receives acquired data through CDMA communication. Received monitoring data are stored in the data base and processed whenever it is needed.

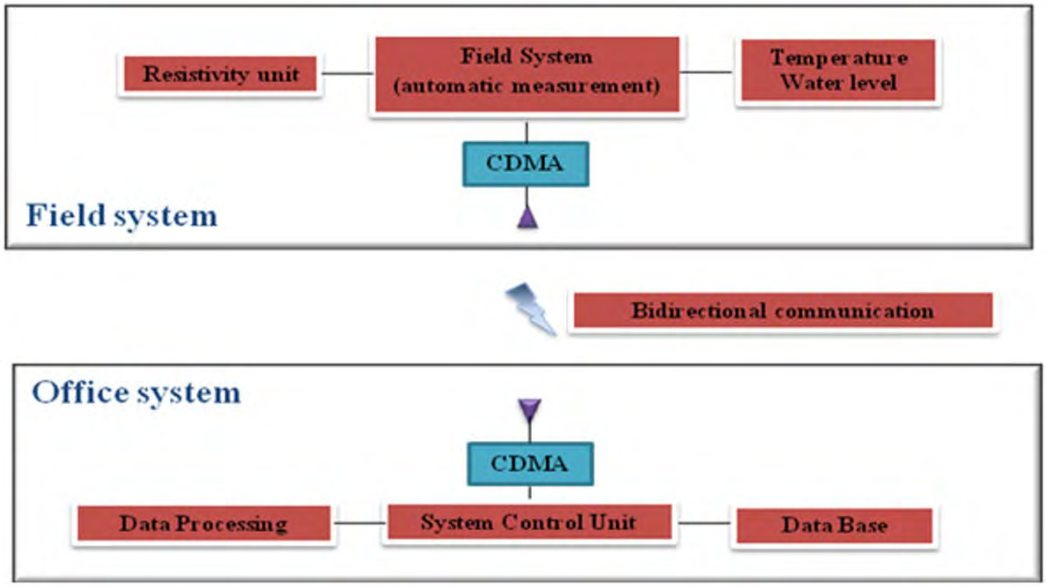

Fig. 4: Resistivity monitoring system devised for the leakage detection in embankment dams.

Resistivity data acquisition system is remotely controlled by system control unit in the office system through CDMA communication. The system is PC based one. Thus the system is composed of embedded main CPU, transmitter, switch box, 24 bit AD converter, 8 Giga bytes memory and modem for CDMA communication. Afterward, we will add other sensors to monitor temperature, water level, etc.

Data processing

We acquired resistivity monitoring data at a test dam site that is located at the southern part of Korean peninsula. The dam is 390 m long and 39.3 m high. We first installed electrodes permanently at the center of the crest. The total length of the survey line was set to 200 m and station spacing to 5 m. Dipole-dipole resistivity data set acquired every 6 hours form Aug. 30, 2011 to Sep. 6, 2011.

Generally, noises are divided into two groups; coherent and random noise. However, in this case appears a mixed type noise repeating non-periodically. Figure 5 represents typical pseudo-sections obtained in the monitoring. As a whole, these 3 sections look to be similar. But there are lots of noises. The red circles seem to be mixed type noise and black circle coherent noise. At this

dam, high voltage power line pass over the dam. Also street lights and steel fence are installed along the crest. These are the major noise sources in this dam. Thus data quality is not good and noise contaminated data should be rejected before the inversion.

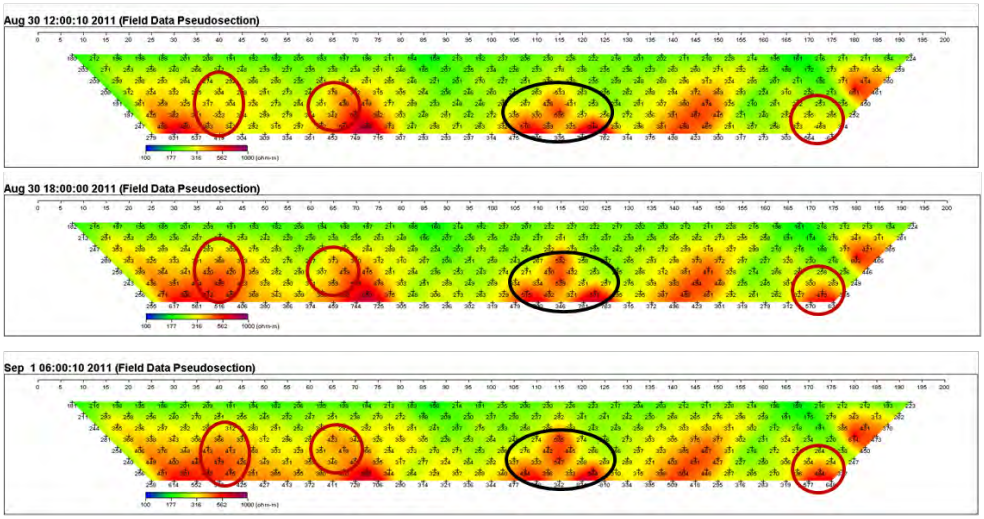

Fig. 5: Typical pseudo-sections obtained in the monitoring. The red circles seem to be mixed type noise and black circle coherent noise.

Before the time lapse inversion of long term monitoring data, a proper reference model should be established. We assumed no changes in resistivity since variation of water level and temperature is negligible over this short period. In such a case, the model obtained from independent inversion of data set at a particular time can be used as a reference model. But each data set has its own noise. Thus it is risky to use the independent inversion result as a reference model since the model estimated is not a true one. To estimate an optimal reference model, noise should be effectively suppressed before the inversion. A possible method is the median filtering that effectively suppresses random and mixed type noise. Of course, coherent noise does not be eliminated. Therefore, coherent noise should be rejected by data editing. Mixed type noise produces higher deviation and coherent noise low deviation. This deviation can be used as data weighting in future study of time lapse inversion.

Through median filtering and data editing, we established a filtered data and inverted the filtered data to build a reference model. The reference data was theoretically calculated from the modeling for the reference model. This model is accepted as the representative model at the period from Aug. 30 to Sep. 6, 2011.

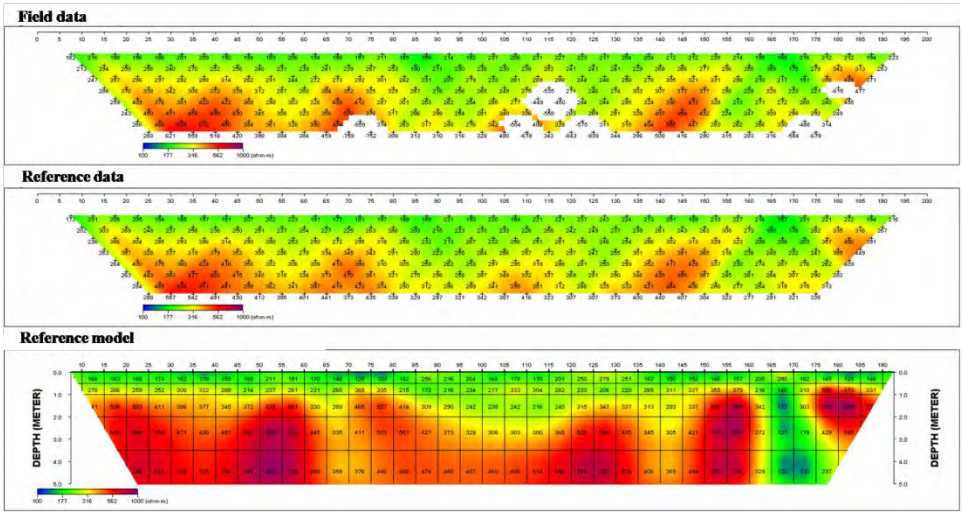

Fig. 6: Filtered data, estimated reference data and model from the inversion of the data set by the median filtering and data editing.

We carried out time lapse inversion using the estimated reference model, for a data set collected at Aug. 30, 18:00. The inversion result has to be the same as the reference model because we assumed no changes in resistivity over a short period. Furthermore many data showing larger deviation than 20% are rejected in the inversion process. However, difference ratio is larger than expected and maximum value reach 10%. Thus, we think that the method to estimate a reference data and model should be more refined in the future.

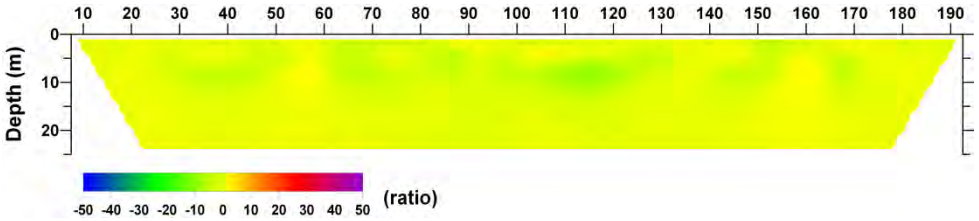

Fig. 7: Resistivity ratio section obtained from the time lapse inversion of a data set acquired at August 30, 18:00.

Discussion

We reviewed the resistivity monitoring at embankment dams and proposed lot of problems in the interpretation of monitoring data; First, more stable and accurate data acquisition system are required to effectively suppress noise. Stable data communication is also necessary. Second, 3D effects caused by 3D dam structure distort the 2D inversion result. This means that the inverted section does not represent the true resistivity section. Data processing, especially to automatically reject the contaminated data, is also the important part of monitoring. Finally, time lapse inversion is a crucial part in the interpretation of long term monitoring data. In the time lapse inversion, optimal choice of model, time and data constraint is also another challenge we have to overcome. We are sure that the resistivity monitoring will be a reliable geophysical tool to find out subsurface changes in time, if we make consistent effort to overcome the problems listed above.

Acknowledgements

This research was supported by Basic Science Research Program through the National Research Foundation of Korea (NRF) funded by the Ministry of Education, Science and Technology (2010-0002440).

References

CHO, I.K. and YEOM, J.Y., 2007: Crossline resistivity tomography for the delineation of anomalous seepage pathways in an embankment dam. – Geophysics, **72**, G31-G38.

KIM, K.J. and CHO, I.K., 2011: Time-lapse inversion of 2D resistivity monitoring data with a spatially varying cross-model constraint. – Journal of Applied Geophysics, **74**, 114-122.

LOKE, M.H., 1999: Time-lapse resistivity imaging inversion. – Proceedings of the 5th Meeting of the Environmental and Engineering European Section, Em1.

OLDENBORGER, G.A., KNOLL, M.D., ROUTH, P.S. and LABRECQUE, D.J., 2007: Time-lapse ERT monitoring of an injection/withdrawal experiment in a shallow unconfined aquifer. – Geophysics, **72**, F177-F188.

SJÖDAHL, P., DAHLIN, T. and ZHOU, B., 2006: 2.5D resistivity modeling of embankment dams to assess influence from geometry and material properties. – Geophysics, **71**, G107-G114.

SJÖDAHL, P., DAHLIN, T., JOHANSSON, S. and LOKE, M.H., 2008: Resistivity monitoring and internal erosion at Hallby embankment dam. – Journal of Applied Geophysics, **65**, 155-164.

Monitoring the Chemical Grouting in Sandy Soil by Electrical Resistivity Tomography (ERT)

PHAM HUY GIAO[1], NGUYEN QUOC CUONG[1] and MENG HENG LOKE[2]

[1] Geo-Exploration and Petroleum Geoengineering (GEPG) Program, Asian Institute of Technology (AIT), Bangkok, Thailand.
[2] Adjunct faculty of AIT & Geotomo Software, Malaysia.

hgiao@ait.asia

Abstract

An experimental study was carried out to investigate the applicability of Electrical Resistivity Tomography (ERT) in monitoring the changes brought by the injection of chemical permeation grouting into a sandy soil. First, a sand tank was constructed in the laboratory for the grouting injection test. The tank is of 30x30x60 cm size and filled with a sandy soil compacted to optimum moisture of 9%. To make the grouting solution, sodium silicate (Na_2SiO_3) was mixed with a reactant of formamide ($HCOONH_2$) and water by the ratio 25:3:2, respectively, to form a gel. 3D forward modeling and model-based inversion were conducted to understand the behavior of the injected soil and to find out the most suitable electrode configuration. Monitoring by ERT was then conducted using crosshole bipole-bipole and four gradient electrodes arrays. Even though the correction for the finite size effect of the tank was not yet applied to the measured data, the resistivity inversion results could accurately delineate the grouted part. The findings from this geotechnical-geophysical experimental study are useful for the implementation of a larger scale ERT monitoring of chemical grouting process in the field conditions in Bangkok.

Introduction

Grouting is the process in which a liquid is forced under pressure into the voids of soils, where the liquid will solidify by physical or chemical action. The injection of grout into the void space is used to block water movement and increase the strength of the treated material. Grouting is applicable mainly to cohesionless soils that are relatively permeable. However, one problem with grouting is that there is no good way to control the shape and location of the grout body, and injection of the grout often turns out to be a random operation. Therefore, in many occasions leakage occurs because the grout body is not in the right location. Other failures are linked to the fact that the grout body is too thin or not strong enough, or the grout body is discontinuous. So monitoring and mapping are useful to check the quality of grouting and provide an early warning for failure of geotechnical works (EWANIC et al., 1999). Although Electrical resistivity tomography (ERT) is not an easy technique to be applied it can be quite useful for geoengineering applications (WILKINSON et al., 2008; ZHOU and GREENHALGH, 1997, 2000). In this study a laboratory experimental model using the sand tank was built to simulate the grouting process and ERT was employed to monitor and assess the behavior of the grouted space.

Preparatory tests

A series of geotechnical and chemical tests were conducted in precedence of the main experiment as described below:

Grain size distribution test: Sand was selected as the soil to be grouted. The grain size distribution of this testing sandy soil was found by the sieve analysis as shown in Fig. 1.

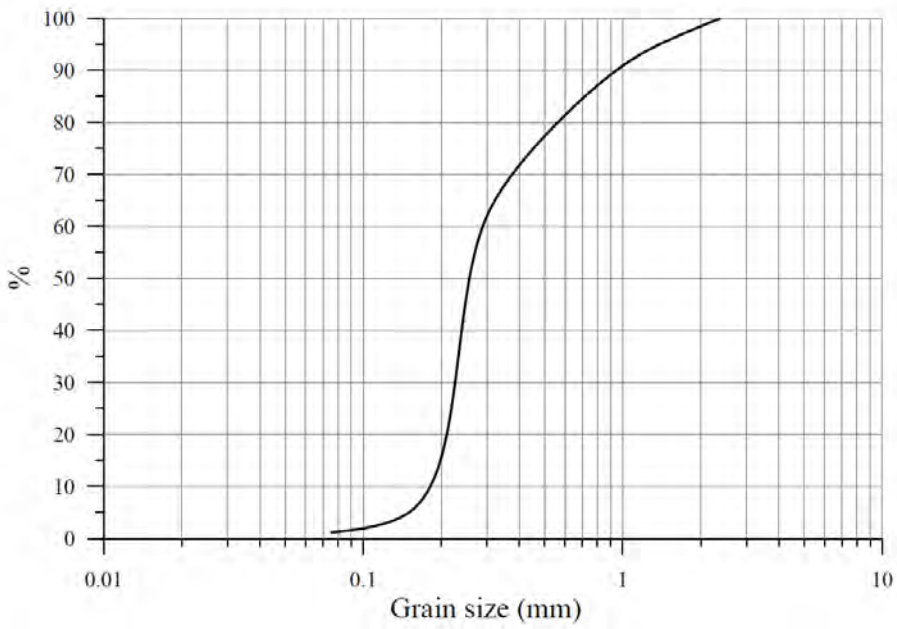

Fig.1: Grain size distribution of the sandy soil.

Compaction test: The standard proctor test with a mold having a volume 943.4 cm^3 was conducted to obtain the maximum dry unit weight and the optimum moisture content. The results are shown in Fig. 2.

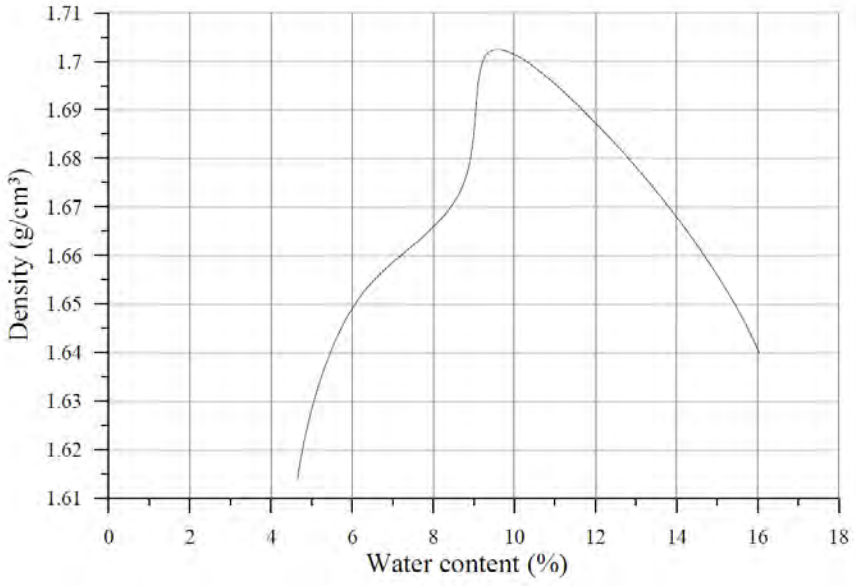

Fig. 2: Results of compaction test.

Preparation of grouting solution: The grouting solution mainly consists of sodium silicate as the gel-forming material and formamide ($HCOONH_2$) as the reactant. Two solutions are prepared and mixed thoroughly in the so called one-solution process. Sodium silicate is alkaline that is neutralized by the reactant, and colloidal silica will aggregate to form a gel. The main properties of Sodium silicate (Na_2SiO_3) N44 include: mole ratio from 3 to 3.2; percentage of Na_2O: 10 to 11%; percentage of SiO_2: 30 to 32%; specific gravity at 20°C: 1.420-1.450; density at 20°C: 1.38 g/cm^3; pH: 11.3; viscosity: 180cps;

Measuring the grouting material resistivity

Information on electric resistivity of sand, grout and grout-sand mixture are of primary importance in analysis of ERT data. The grout material is made of Sodium silicate mixed with formamide ($HCOONH_2$) and water by the ratio: 25:3:2. The gel time is 6 hours. For measurements of resistivity the grout material is prepared in form of core samples. The measuring scheme follows the setup shown in Fig. 3.

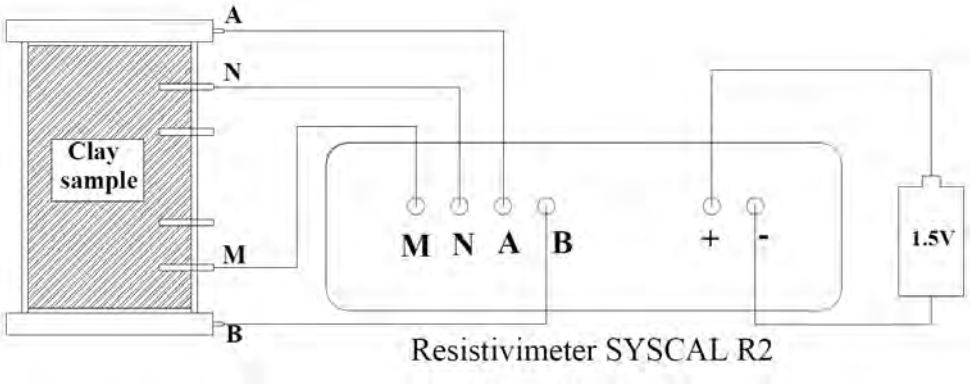

Fig. 3: Setup to measure electric resistivity on a core sample (GIAO et al., 2003).

The resistivity test results are plotted in Fig. 4 that shows the change of grout resistivity with time. At the beginning the resistivity was 0.3 Ωm, and then it has gradually increased to 0.55 Ωm after 15 hours, and remained almost constant after that.

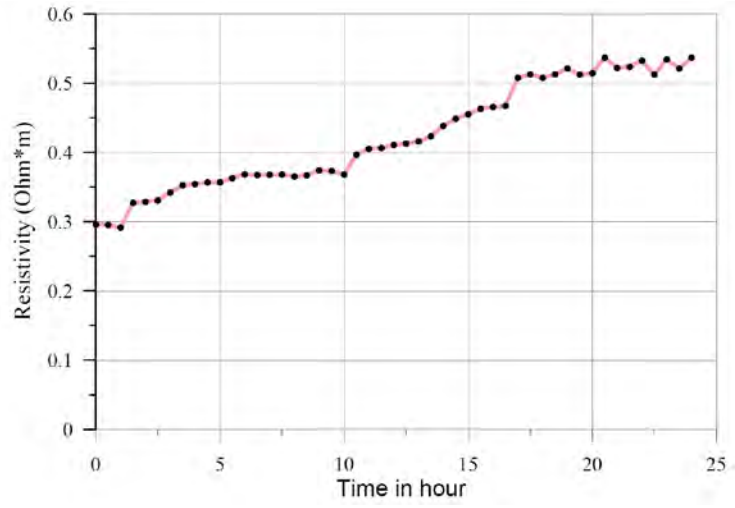

Fig. 4: Resistivity of grouting material vs. time.

Measuring the grouting material conductivity

The conductivity meter HI 9835 was used to directly measure the electrical conductivity of the grouting solution that was poured in a glass. The conductivity unit σ is in $S.m^{-1}$. As the reciprocal of the conductivity is the resistivity one could determine the resistivity as follows:

(1) $\rho = 1/\sigma$

Where: ρ is the resistivity (Ω.m) and σ is the conductivity (S/m).

The measurements were conducted during 24 hours for different states of solution, from liquid gel to solid. The resistivity values converted from conductivity measurements are plotted in Fig. 5, where the grout resistivity is found as the 0.55 Ωm, similar to the value obtained by measurements performed on the cores.

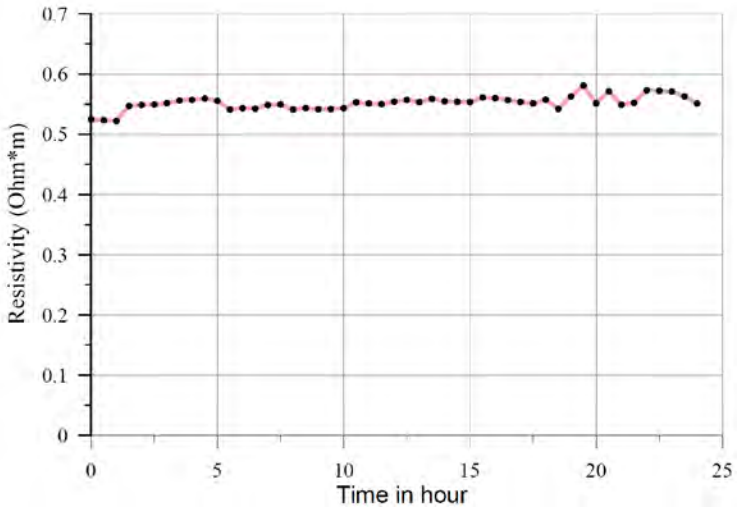

Fig. 5: Resistivity measured by conductivity meter.

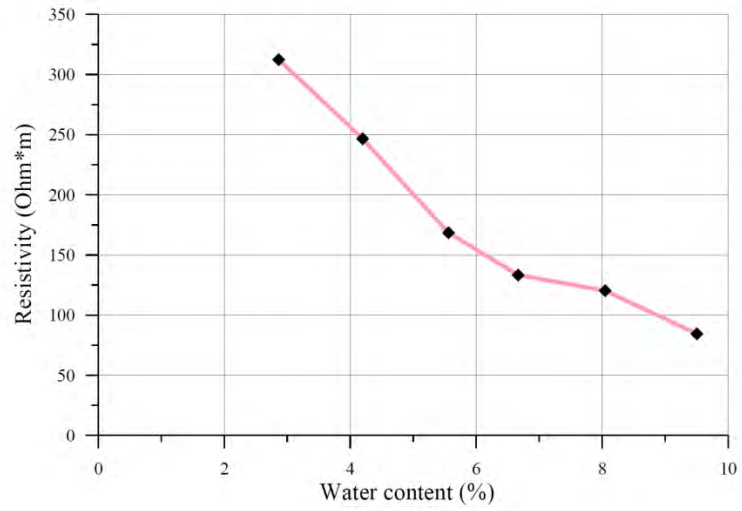

Fig. 6: Resistivity of compacted sand

The to-be-grouted sand is compacted in a PVC mold having a 43-mm diameter and a l00-mm length. Samples were prepared for different water contents, from 3 to 10% with the increment of 1.5%. The sand resistivity was measured by the setup shown in Fig. 3 and the measurements are

plotted in Fig. 6, which shows a decreasing sand resistivity with the increasing water content. At the optimum water content of 9% (Fig. 2) the resistivity is about 100 Ωm as seen in Fig. 6.
Before conducting the real experiment of grouting injection and its accompanied monitoring by ERT a series simulations were performed to investigate the response of the tank model and, finally, to find out the number of electrodes and type of electrode array to be employed. Details and results of such forward and inverse analyses are presented in the following section.

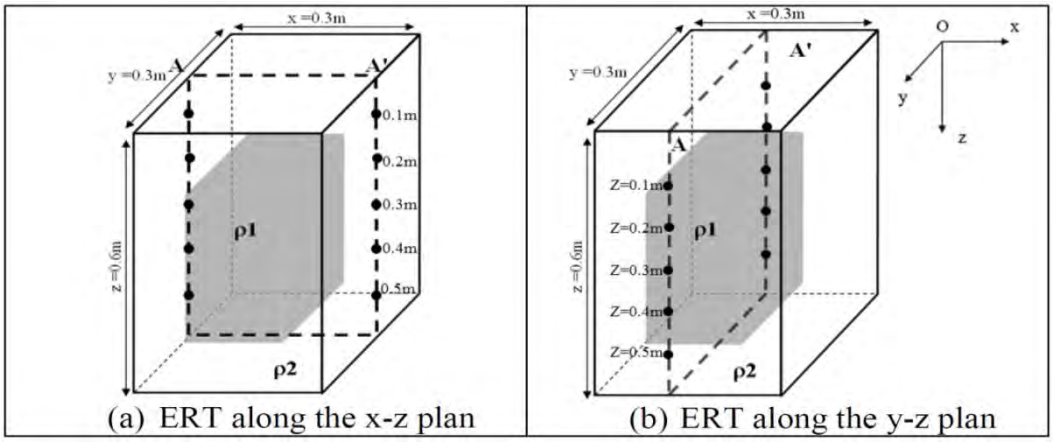

Fig. 7: Simulation of ERT monitoring on the synthetic grouting model.

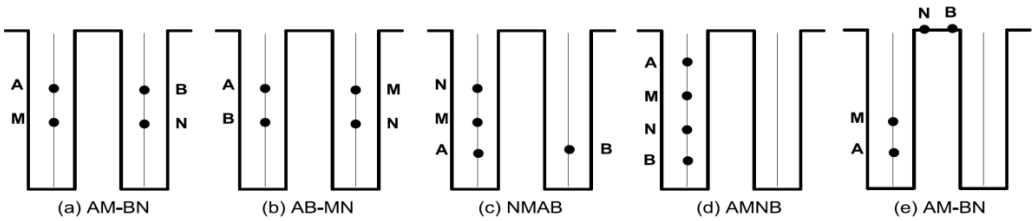

Fig. 8: ERT electrodes arrays: (a-b) Bipole–bipole; (c) Four-electrode gradient array; (d) Wenner – Schlumberger in the same borehole; (e) Surface-to-borehole.

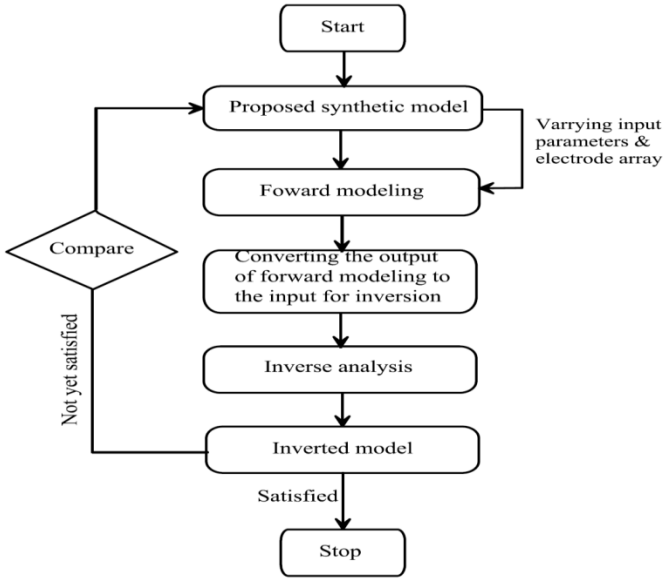

Fig. 9: Flowchart of model-based resistivity inversion.

Synthetic model	Array type	Electrode spacing (m)	Resistivity (Ωm)	Nos. of electrode per line	Number of ERT points	Plane	Abs. Error (%)
1	Bipole–Bipole AM-BN	AM = BN = 0.1, 0.2, 0.3	ρ_1= 0.55; ρ_2=100	5	120	XZ	1.20
						YZ	1.18
2	Bipole–Bipole AB-MN	AB = MN = 0.1, 0.2, 0.3	ρ_1= 0.55; ρ_2=100	5	111	XZ	3.69
						YZ	3.45
3	Four- electrode gradient array NMAB	MN = 0.1, 0.2, 0.3	ρ_1= 0.55; ρ_2=100	5	50	XZ	10.90
						YZ	6.98
4	Borehole to Surface AM-BN	AM = BN = 0.1, 0.2, 0.3	ρ_1= 0.55; ρ_2=100	5	160	XZ	1.06
						YZ	0.81
5	Bipole–Bipole AM-BN	AM = BN = 0.1, 0.2, 0.3	ρ_1= 0.55; ρ_2=100	11	1532	XZ	0.76
						YZ	0.64
6	Bipole–Bipole AB-MN	AB = MN = 0.1, 0.2, 0.3	ρ_1= 0.55; ρ_2=100	11	1036	XZ	4.86
						YZ	0.75
7	4-electrode gradient array NMAB	MN = 0.1, 0.2, 0.3	ρ_1= 0.55; ρ_2=100	11	1037	XZ	0.77
						YZ	0.45
8	Wenner–Schlumberger in the same borehole AMNB	a = MN= 0.1, 0.2, 0.3	ρ_1= 0.55; ρ_2=100	11	45	XZ	1.71
						YZ	0.98
9	Borehole to Surface AM-BN	AM=BN = 0.1, 0.2, 0.3	ρ_1= 0.55; ρ_2=100	11	1320	XZ	0.99
						YZ	0.69

Tab. 1: Synthetic models for forward modeling and model-based inversion.

Simulation of ERT monitoring

The material properties tested in the first part of the experiment as mentioned before were used to construct a synthetic grouting model as shown in Fig. 7. The tank sizes are of 0.3 x 0.3 x 0.6 m in the x, y and z directions, respectively. Resistivity of the grouting material (i.e., Sodium silicate mixed with formamide) is taken as ρ_1 = 0.55 Ωm. Resistivity of grouted sand is taken as ρ_2 = 0.55 Ωm. Two pairs of boreholes were employed for ERT monitoring in the model, one in the X-Z plane and another one in the Y-Z plane as seen in Fig. 7a and 7b, respectively. The electrode arrays of Bipole-bipole, four-electrode gradient, Wenner-Schlumberger and surface-to-borehole as shown in Fig. 8 were considered. The array that gives the best ERT response can be assessed based on a model-based inversion (see Fig. 9) that included the following steps: i) firstly, a synthetic model was constructed, having the same sizes of the real tank to be tested in the grouting experiment; ii) the forward modeling was then run to simulate the ERT monitoring of the grouting process using RES3DMOD software (LOKE, 2011a); iii) the resistivity values computed from the forward modeling are used as the synthetic measurements (model responses) in the input file for the inversion using RES3DINV software (LOKE, 2011b); iv) input parameters and electrode array type

can vary and the best inverted resistivity distribution is the one that resembles the constructed grouting model the most.

Various scenarios of simulation with 5 and 11 electrodes as presented in Table 1 were conducted. Some of the simulation results of ERT monitoring with 5-electrode array are shown in Figs. 10a-d. It was found out that the bipole-bipole (AM-BN) and four gradient electrodes (MNAB) gave the best response. Thus, they were elected to be employed in the subsequent monitoring experiment phase in the laboratory.

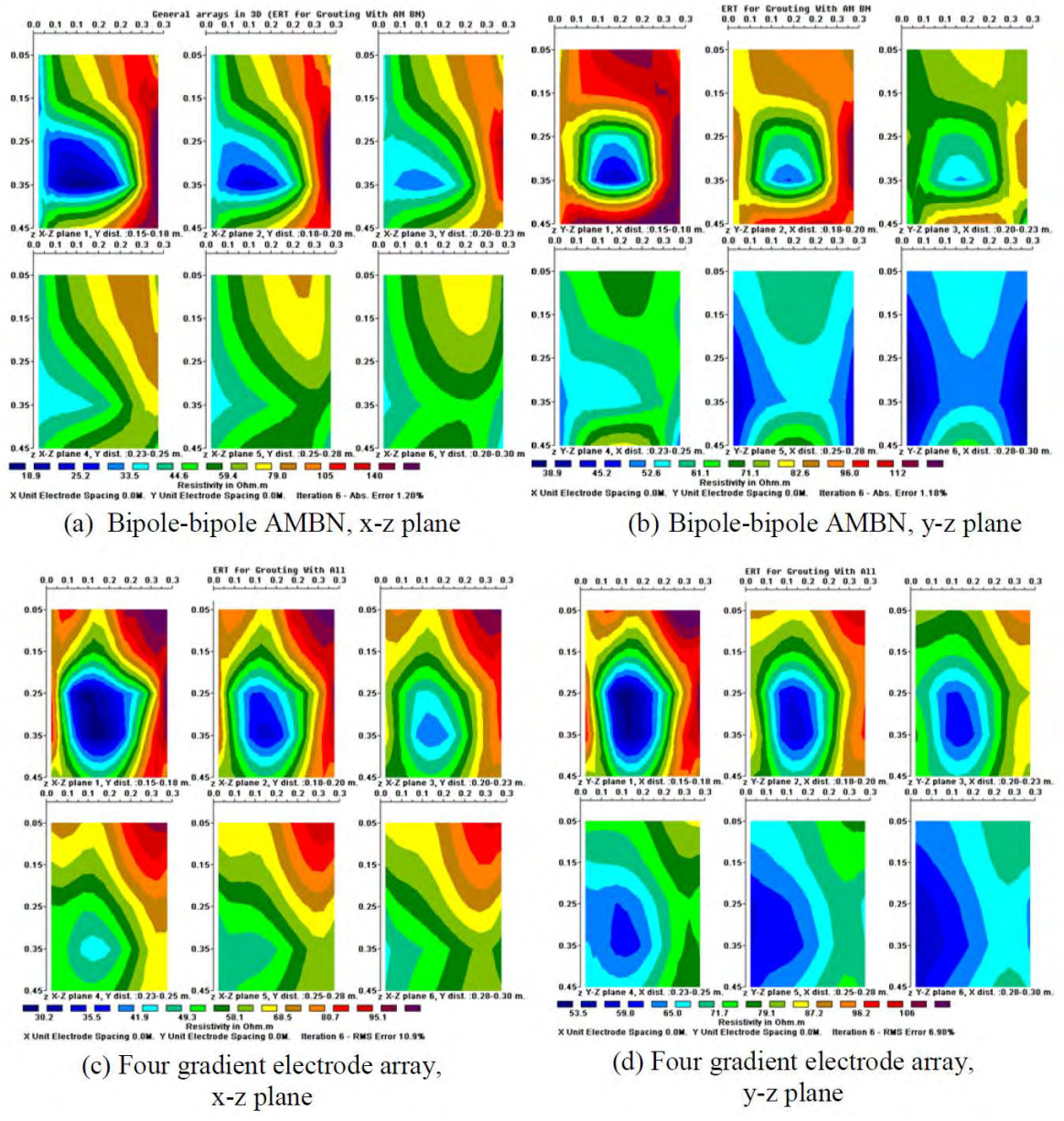

(a) Bipole-bipole AMBN, x-z plane

(b) Bipole-bipole AMBN, y-z plane

(c) Four gradient electrode array, x-z plane

(d) Four gradient electrode array, y-z plane

Fig. 10: Model-based inversion of the synthetic measurements simulated by forward modelling.

Laboratory experiment of grouting injection and ERT monitoring

Grouting Injection Test

The test setup can be seen in Figs. 11 and 12, respectively. Sand was volumetrically compacted to 90% of that found from the compaction test. The main operations included: (i) mixing one litter of grout of sodium silicate, formamide (reactant) and water at the ratio of 25:3:2 and pouring it into

the chamber; (ii) connecting the tube between the chamber and air pressure and steel chamber with injection tube; (iii) installing the injection tube into the sand tank and make sure that it does not touch the bottom of the tank. The air release valve and shut-off valve are used to control the pressure pumping the grout into the sand. Sodium silicate grout with low viscosity will fill the voids without disturbing the structure of sandy soil.

ERT Monitoring

Electrodes are installed on the four sides of the sand tank with 5 electrodes per one side and 10 cm apart as viewed in Fig. 12. Firstly, the measurements on two opposite sides were conducted, and then the measurements were repeated in a similar way on the other opposite sides. The cross-hole bipole-bipole AM–BN was employed in the experiment.

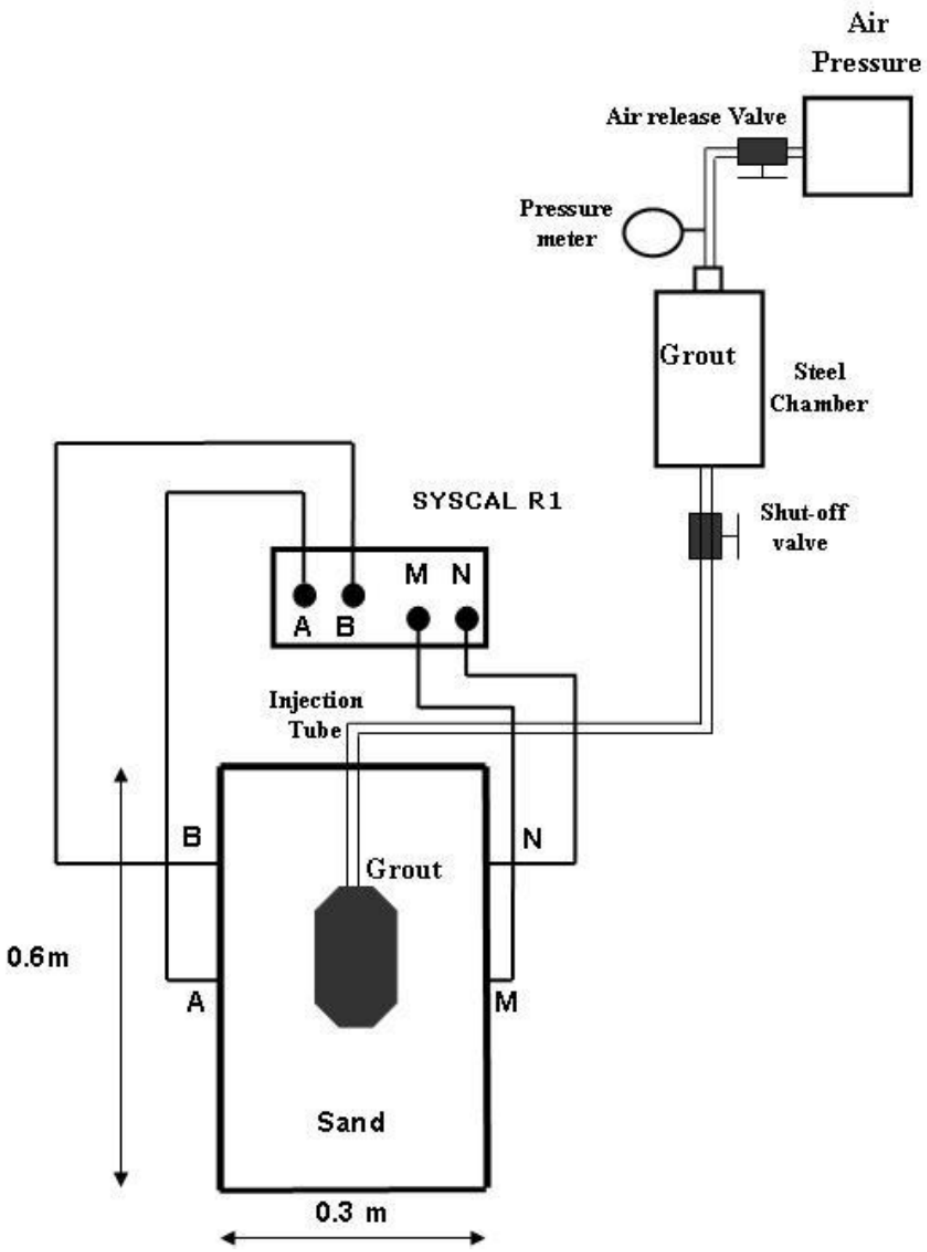

Fig. 11: Setup of grouting and ERT test.

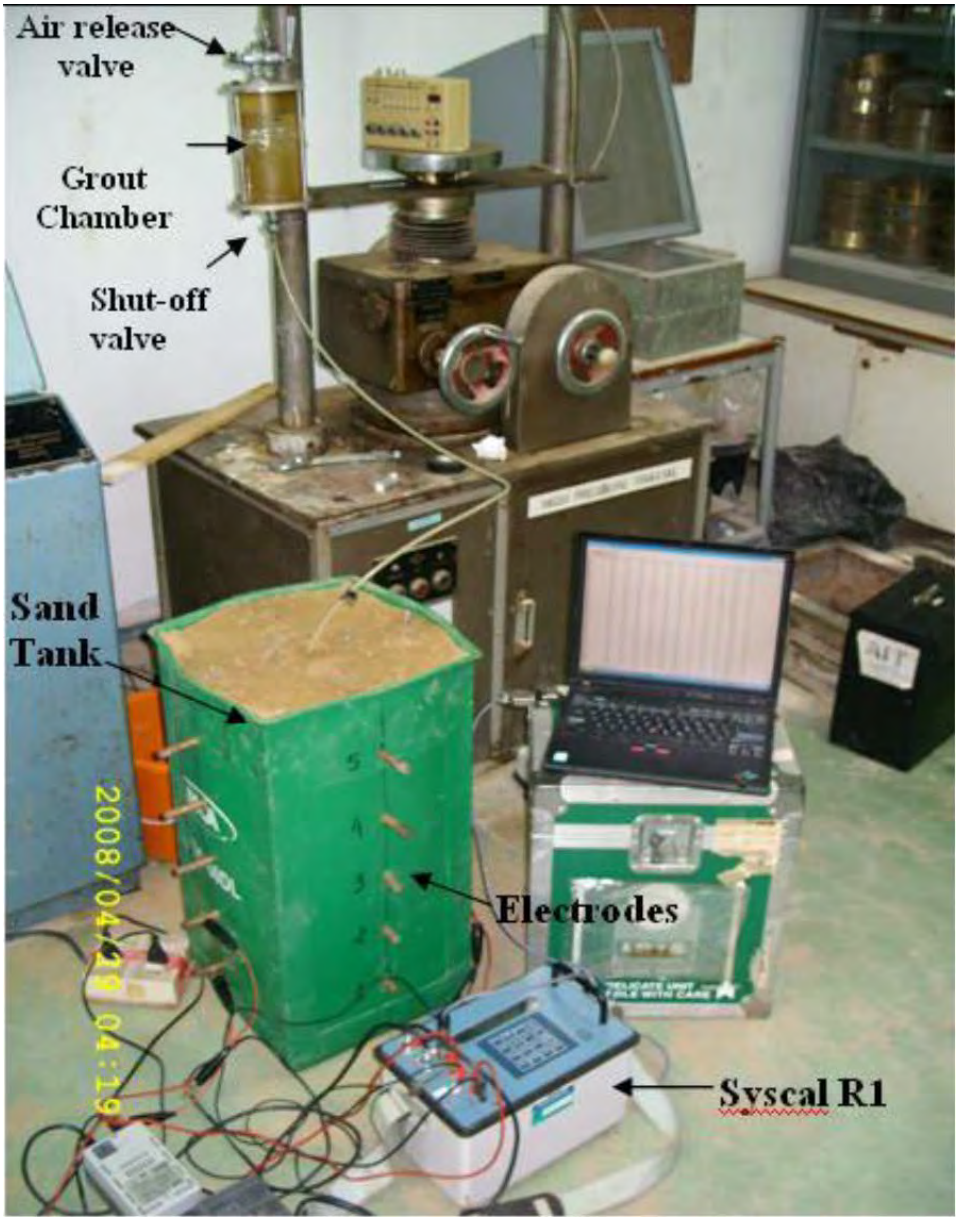

Fig. 12: View of the grouting and ERT setup.

The inversion was done using RES3DINV program (LOKE, 2011b). The inverted resistivity slices are shown in Fig. 13 for different ERT times of grouting, i.e., at the beginning, after 4 hours and after 12 hours. Each figure (Fig. 13a, b and c) displays slices of X-Z plane cut at different Y-coordinate values, i.e., 0.15m, 0.18m, 0.23m, 0.25m, 0.28 m and 0.30m, respectively. The best results of ERT monitoring were obtained by the bipole-bipole AMBN array, which show that in the first period when the grouting was just injected to the sand tank, the grout body of very low resistivity is quite clearly seen with a good resistivity contrast in comparison to the base material. After four hours the grouted body sank down towards the bottom of the tank due to the gravity. After 12 hours, the grouted sand body continued moving down to the bottom of the tank until it become solid and gets a well-defined shape as seen in Figs. 13a-c, respectively.

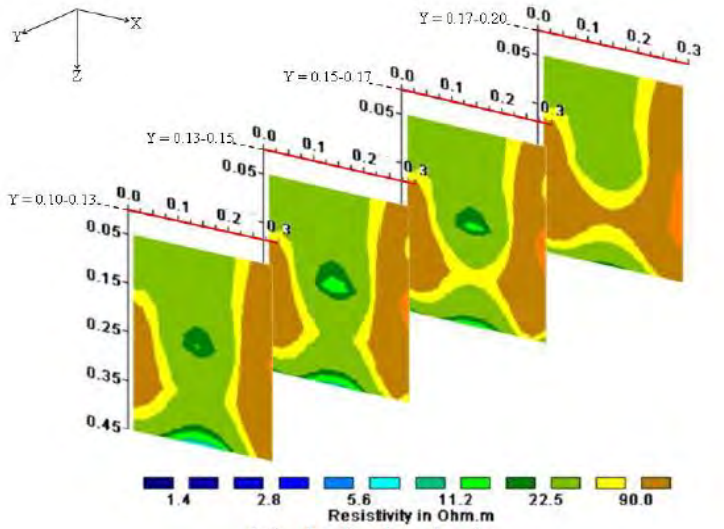

(a) At the beginning

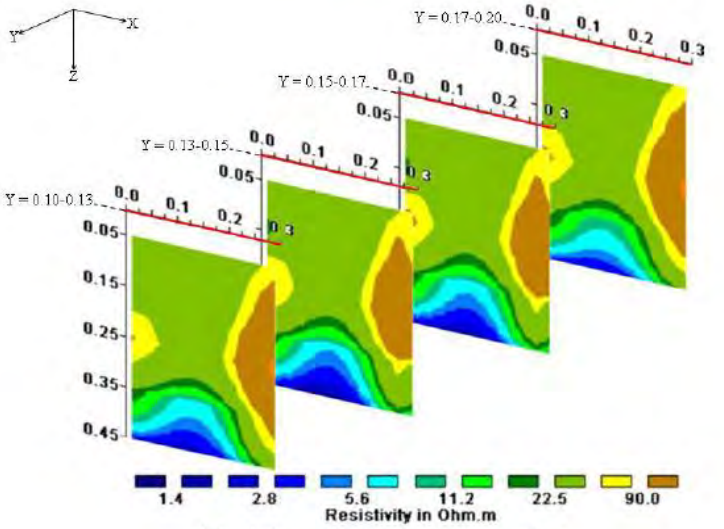

(b) After 4 hours of grouting

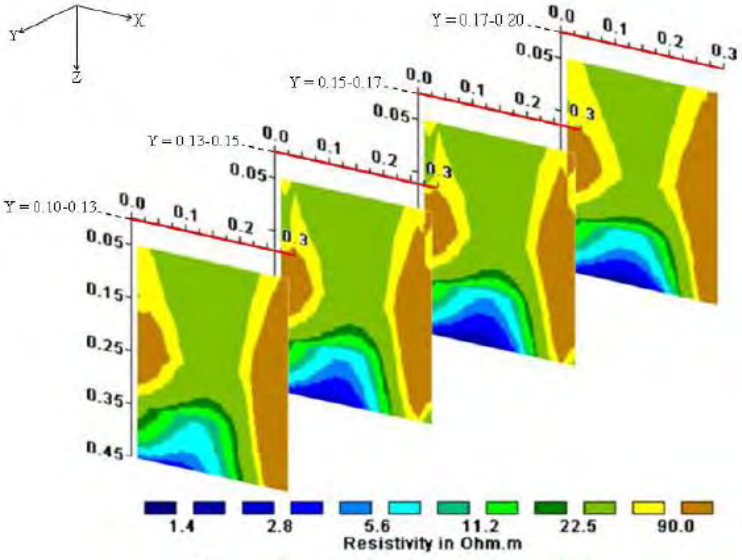

(c) After 12 hours of grouting

Fig. 13: Results of inversion of real resistivity data by bipole-bipole AMBN array.

Conclusions

Electrical Resistivity Tomography (ERT) proved to be effective in monitoring the chemical permeation grouting in a sand tank due to the clear contrast in resistivity between the grouting material and the base material. In this study experiment, the grouting material is a mixed of sodium silicate (Na_2SiO_3), formamide ($HCOONH_2$) and water by the ratio: 25:3:2 and has a low resistivity of 0.55 Ωm. The base sandy soil has a resistivity of about 100 Ωm at the optimum water content of 9%. A number of electrode arrays were used in ERT and it was found that the cross-borehole bipole-bipole configuration is good to determine the shape of the grout body and the movement of the grout solution inside the sand. As the measurements of resistivity on the tank model were clearly affected by its finite sizes of the tank the resistivity values need to be corrected before being input for inversion, which can be practically solved. It is recommended that similar setup of ERT will be further developed and applied in the field conditions in geotechnical practice in Bangkok.

References

GIAO, P.H., CHUNG, S.G., KIM, D.Y. and TANAKA, H., 2003: Electric imaging and laboratory resistivity testing for geotechnical investigation of Pusan clay deposits. – Journal of Applied Geophysics, **52**(4), p. 157-175.

EWANIC, M., REICHHARDT, D. and BRUNETTE, B.S., 1999: Electrical Resistivity Tomography Imaging of a Colloidal Silica Grout Injection. – U.S. Department of Energy (DOE).

LOKE, M.H., 2011a: RES3DMOD, 3D resistivity forward modeling using the finite difference and finite element methods, http://www.geotomosoft.com

LOKE, M.H., 2011b: RES3DINV, 3D resistivity inversion using the finite difference and finite element methods, http://www.geotomosoft.com

WILKINSON, P.B., CHAMBERS, J.E., LELLIOT, M., WEALTHALL, G.P. and OGILVY, R.D., 2008: Extreme Sensitivity of Crosshole Electrical Resistivity Tomography Measurements to Geometric Errors. – Geophysical Journal International, **173**, 49-62.

ZHOU, B. and GREENHALGH, S.A., 1997: A synthetic study on cross-hole resistivity imaging with different electrode arrays. – Exploration Geophysics, **28**, 1-5.

ZHOU, B. and GREENHALGH, S.A., 2000: Cross-hole resistivity tomography using different electrode configurations. – Geophysical Prospecting, **48**, 887-912.

Development of Tunnel Electrical Resistivity Prospecting System and its Applicaton

HEE-HWAN RYU[1], GYE-CHUN CHO[2], SUNG-DON YANG[3] and HYUN-KANG SHIN[4]

[1] Professor, Korea Advanced Institute of Science and Technology (KAIST), Daejeon, South Korea.
[2] Post Doctor, Korea Advanced Institute of Science and Technology (KAIST), Daejeon, South Korea.
[3] General Manager, POSCO E & C, Incheon, South Korea.
[4] Section Manager, POSCO E & C, Incheon, South Korea.

fbgmlghks@kaist.ac.kr

Abstract

The detailed knowledge of ground conditions ahead of the tunnel face is necessary for safe and economical tunnel construction. The Tunnel Electrical resistivity Prospecting System (TEPS) has been developed to accurately detect the geological, hydro-geological, and geotechnical conditions such as the location, the size, the state of anomalies, cavities, weak zones, improved zones, high permeability water or gas bearing zones, or faults/fractures existing ahead of the tunnel face by measuring a series of electrical resistances and performing back analyses. The TEPS are composed of several electric sensors (electrodes), an in-situ resistance measurement system, an automated data acquisition system, inversion programs for back analyses, and closed form solutions for electric field analyses of jointed rock masses. Although the detectability of the TEPS is dependent upon the size and state of an irregular zone, its reliable penetration depth ranges in about 4~5 times of the tunnel size. It takes about 30 minutes to complete a test for one section of a tunnel. As practical applications, this paper presents several case studies for the ground condition estimation of collapsed tunnel zones using the TEPS. Overall, the ground conditions predicted by the TEPS are in accordance with the ground conditions measured during construction, verifying the TEPS.

Introduction

Rapid urbanization has increased the necessity of new spaces such as underground structures and long tunnels. For successful underground and long tunnel construction, it is very important to have a detailed understanding of the ground conditions at the design stage. As such, a site investigation such as boring and geophysical exploration surveys must be performed in order to ascertain the conditions of ground around the tunnel scheduled for construction. Nevertheless, there have been many reports of tunnel accidents that are caused by unexpected occurrence of anomalies, such as weak zones, fault zones, and cavities (CHO et al., 1999; KIM et al., 2000; HASEGAWA et al., 1993). So, technology that can be used to attain an accurate understanding of the ground conditions ahead of tunnel face and to predict even minute anomalies existing ahead of tunnel face is needed.

Measurement of electrical resistivity, used to attain information on the ground conditions of a tunnel region, facilitates understanding of the electrical characteristics and configuration of media (BOYCE, 1968; CHOI et al., 2004). In practice, electrical resistivity based exploration techniques are widely used in a variety of fields, from predicting the particle size in a discrete medium at a small

scale to detecting anomalies or geological structures under the ground at a large scale (JACKSON et al., 1978; KIM et al., 2005). The conventional nondestructive method of using apparent electrical resistivity at a large scale is suitable for understanding the general ground conditions, but is not suitable for close-range exploration within a range of 3 times the tunnel diameter ahead of tunnel face, where the stability of the tunnel is most significantly affected and most tunnel accidents occur. In this paper, a method to predict ground conditions in the area ahead of tunnel face using electrical resistivity (Tunnel Electrical resistivity Prospecting System: TEPS) is developed in order to improve the reliability and efficiency of site investigations under tunnel construction (Figure 1).

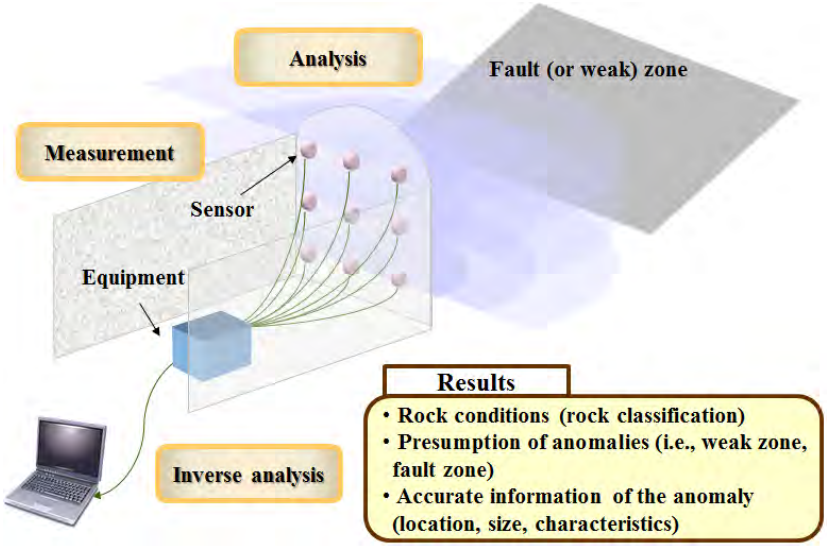

Fig. 1: Tunnel Electrical resistivity Prospecting System (TEPS).

TEPS

A TEPS consists of the analytical equation, the rock mass classification system, the inverse program, the control system, and the measurement system (RYU, 2010).

Analytical equations

Analytical equations are obtained by the electric field analysis using Gauss' law and Laplace equation. Those consists of the electrical resistance equation (R_{rm}) at jointed rock mass, the electrical resistance equation ($R_{rm\text{-}sa}$) at jointed rock mass with a spherical anomaly, and the electrical resistance equation ($R_{rm\text{-}pa}$) at jointed rock mass with a platy anomaly, as follows:

$$R_{rm} = f(\sigma_{ir}, \sigma_j, d, t, a) \tag{1}$$

$$R_{rm-sa} = f(\sigma_{rm}, \sigma_{sa}, x_{sa}, y_{sa}, z_{sa}, x_s, y_s, x_r, y_r, r_{sa}, K_{sa}, a) \tag{2}$$

$$R_{rm-pa} = f(\sigma_{rm}, \sigma_{pa}, A, B, C, D, x_s, y_s, x_r, y_r, t_{pa}, K_{pa}, a) \tag{3}$$

where σ_{ir} is the electrical conductivity of joints, σ_j is the electrical conductivity of intact rock, d is the thickness of intact rock, t is the thickness of joints, a is the radius of sensors, σ_{rm} is the electrical conductivity f surroundings possible to obtain from Equation (1), σ_{sa} is the electrical conductivity of a spherical anomaly, (x_{sa}, y_{sa}, z_{sa}) is the locational coordinate of a spherical anomaly, (x_s, y_s) is locational coordinate of source sensor, (x_r, y_r) is locational coordinate of

receiver sensor, r_{sa} is the radius of a spherical anomaly, K_{sa} is the ratio of dielectric permittivity, σ_{pa} is the electrical conductivity of a platy anomaly, ($Ax+By+Cz=D$) is the plane equation of a platy anomaly, t_{pf} is the thickness of a platy anomaly, and K_{pa} is the ratio of dielectric permittivity.

Rock mass classification system

In order to estimate the rock conditions by using electrical resistivity, the Q-system and RMR, used as the rock mass classification, were correlated with electrical resistivity (CHOI et al., 2006; RYU, 2010). The parameters of Q-system and RMR are correlated with the electrical resistivity by using the equation (1), and the specific relationship between rock mass classification and electrical resistivity could be obtained using the certain field information (Figure 2).

Inverse programs

The inverse programs of TEPS can predict the location, size, and characteristics of anomalies that exist ahead of tunnel face by using the developed analytical equation and electrical resistance values measured in the fields. The inverse procedures consist of the Monte Carlo method and the Genetic Algorithm method.

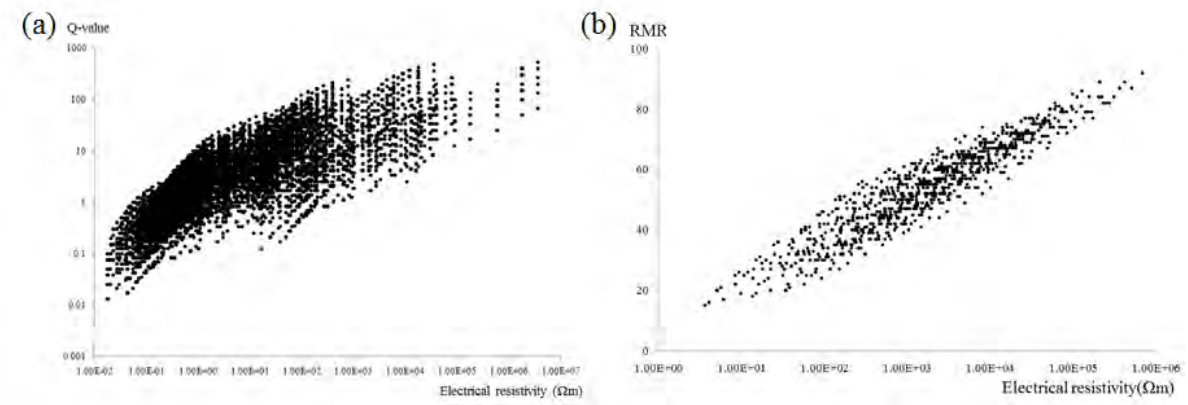

Fig. 2: The relationship between rock mass classification and electrical resistivity. (a) Q-system and electrical resistivity. (b) RMR and electrical resistivity.

Control system and measurement system

The control system can control the measurement of electrical resistance values in the fields, and the measurement system is organized for measuring the electrical resistance values in the fields. The measurement system consists of a data acquisition (DAQ), a digital multimeter (DMM), a power supply, a switch controller, a terminal block, and sensors.

Field applications

In order to verify the applications of Tunnel Electrical resistivity Prospecting System (TEPS), the field tests are performed at several field sites. The representative field tests are like followings:

OO western detour roads (OO tunnel)

Field experiments were performed in order to distinguish the existence of anomaly ahead of tunnel face, predict the possibility of the adding collapse, and estimate the rock condition around a collapsing section, in regards to the collapse of side wall under construction. In prediction results of tests, the weak zone (the height is 5m ~ 10m, the radius is about 2.6m, the depth is

0.5m, and electrical resistivity values are 0.2 times than one of surroundings) was predicted at the location near to the tunnel face (Figure 3a). This means that the larger region than the collapsed zone is put as the reinforcement region in order to prevent the adding collapse. Also, the strong zone (electrical resistivity values are relatively 3 times than one of surroundings) is predicted at 1m ~ 1.5m ahead of tunnel face and the left of tunnel face. The field mapping data in ○○ tunnel shows the accuracy of predicted results.

<u>○○ national highway – zone 2 (○○ tunnel)</u>

Field experiments were performed in order to distinguish the existence of anomaly ahead of tunnel face, predict the possibility of the adding collapse, and estimate the rock condition around the collapsing section, in regards to the collapse of tunnel face under tunnel construction. Prediction results are shown in Figure 3(b). Based on predicted results, the excavation work was performed after fixing the rock-bolt and the anchor at the bedrock for no more collapsing at ceiling part of tunnel. The adding collapse didn't happen.

All things taken together, although the detectability of the TEPS is dependent upon the size and state of an irregular zone, its reliable penetration depth ranges in about 4~5 times of the tunnel size. It takes about 30 minutes to complete a test for one section of a tunnel.

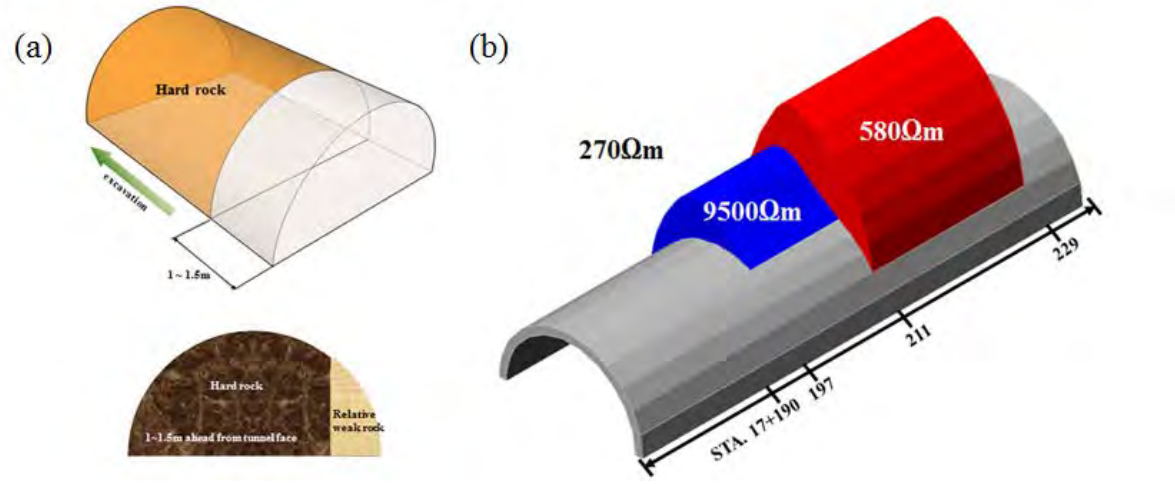

Fig. 3: Field test results. (a) ○○ western detour roads (○○ tunnel). (b) ○○ national highway – zone 2 (○○ tunnel).

Conclusions

A TEPS (Tunnel Electrical resistivity Prospecting System), which was developed as a tunnel-ahead prediction technology for preventing previously economic and social damage caused by the unexpected occurrence of anomalies under tunnel construction, consists of the analytical equation, the rock mass classification system, the inverse program, the control system, and the measurement system. Field tests were performed for field applications of the TEPS and field test results show the accuracy and reliability of TEPS.

References

BOYCE, R.E., 1968: Electrical resistivity of modern marine sediments from the Bering sea. – Journal of Geophysical Research, **73**(14), 4759-4766.

CHO, H., LIM, J.S., CHUNG, Y.Y. and CHOI, S.Y., 1999: A case study on the ground reinforcement method and effect of the failed tunnel. – Proceedings of the Korean Geotechnical Society Conference, Seoul, 293-300.

CHOI, J.S., SONG, K.I., CHO, G.C. and LEE, S.W., 2004: Characterization of unsaturated particulate materials using elastic and electromagnetic waves. – Key Engineering Materials, **270/273**(2), 1653-1658.

CHOI, J.S., RYU, H.H., LEE, I.M. and CHO, G.C., 2006: Rock Mass Classification using Electrical Resistivity – an analytical study. – Key Engineering Materials, **321/323**(2), 1411-1414.

HASEGAWA, M., USUI, M. and GOTOH, K., 1993: Geological prognosis ahead of tunnel face. – Engineering Geology, **35**(3-4), 229-235.

JACKSON, P.D., TAYLOR SMITH, D. and STANFORD, P.N., 1978: Resistivity-porosity-particle shape relationships for marine sands. – Geophysics, **43**(6), 1250-1268.

KIM, N.Y., KIM, S.H. and CHUNG, H.S., 2000: Analysis of collapse and cause in the highway tunnel. – Journal of Korean Tunnelling Association, Tunnelling Technology, **2**(3), 13-23.

KIM, J.H., YI, M.J. and CHO, S.J., 2005: Application of high-resolution geoelectric imaging techniques to geotechnical engineering in Korea. – Geosystem Engineering, **8**(2), 25-34.

RYU, H.H., 2010: Development of a tunnel electrical resistivity prospecting system and its application. – Doctor thesis, KAIST, Daejeon, Korea.

Geoelectrical monitoring of the tunnel boring at lot H3-4, section Kundl/Radfeld-Baumkirchen

† KNUT SEIDEL[1], ULRICH SERFLING[1], MANFRED KÖHLER[2] and CHRISTOPH SEDLACEK[2]

[1] Bautzner Str. 67, 04347 Leipzig, Germany, Tel: +49 341 2421 310, Fax: +49 341 2421 311, email: info@ggl-gmbh.de
[2] ÖBB Infrastruktur AG, Geschäftsbereich Unterinntal, Industriestraße 1, 6134 Vomp, Austria, email: manfred.koehler@oebb.at

Introduction

For the tunnel construction at lot H3-4 in the Inn Valley, Austria, a tunnel boring machine (TBM) was used which was stabilized by a bentonite shield. In the case of increased hydraulic permeability of the sediments, the bentonite suspension could be blown out and, as a result, an uncontrollable collapse of the ground could happen, even a damage of the TBM. As no method was known at this time to control the spreading of the bentonite suspension from the surface, a methodological investigation should test high resolution 2D geoelectrical measurements for monitoring the tunnel boring. This technique was the most promising one because on the one hand the geological conditions in the Inn Valley were suited for resistivity measurements (the water level is close to the surface, and cohesive and non-cohesive material can change in short distance) and on the other hand it could be presumed that there is a contrast in resistivity between the bentonite and the pore liquid.

Investigation programme

A comprehensive investigation programme has been carried out, comprising the following phases:

- Test measurements for the selection of the most suitable electrode array
  These measurements should help to determine which electrode array would provide the best results with regard to robustness, time consumption, and resolution at the planned exploration depth (Wenner-α, Wenner-β and Schlumberger-array were tested).
- Reference measurements along the tunnel section
  This recording of the resistivity conditions before the passage of the TBM provides information about the geological situation and reference data for comparison.
- Measurements at the positions of escape shafts
  As bentonite suspension was used for the construction of the escape shafts, such measurements should investigate the influence of the bentonite suspension on the geoelectrical data. At the same time, the influences of installations on geoelectrical measurements should be determined.
- Measurements during and after the passage of the TBM
  The final goal of the investigations was the monitoring of the passage of the TBM and the detection of changes after the passage.

Altogether more than 5000 profile metres were measured.

Results of the investigation

Assessment of the electrode arrays

The measurements at very different conditions have shown that the Wenner-α-array produces the most reliable data under disturbed conditions. In the case of undisturbed, layered conditions the results of the different arrays are very similar and here the Wenner-α-array requires the least expenditure of time. When Wenner-α- and Wenner-β-data were acquired, a joint inversion of both data sets could improve the resolution.

For the exploration depth of 15 m to 30 m (the depth of the tunnel), an electrode spacing of 5 m was the optimum with regard to resolution and required measuring time.

Results of the reference measurements

The reference measurements along the tunnel route provided a very detailed picture of the different sediments in the ground. These geoelectrical results displayed the complicated sedimentation in the Inn Valley better than the drillings alone. The three vertical resistivity sections in figure 1 show material changes at short distances (the profiles have only a distance of 10 m to each other) – low resistivities (green to yellow) correlate with cohesive material and high resistivities (red to purple) correlate more to sandy or gravelly material or to reduced water content (e.g. near the surface). Thus, such areas with high resistivities in deeper ground indicate areas of possibly increased hydraulic permeability.

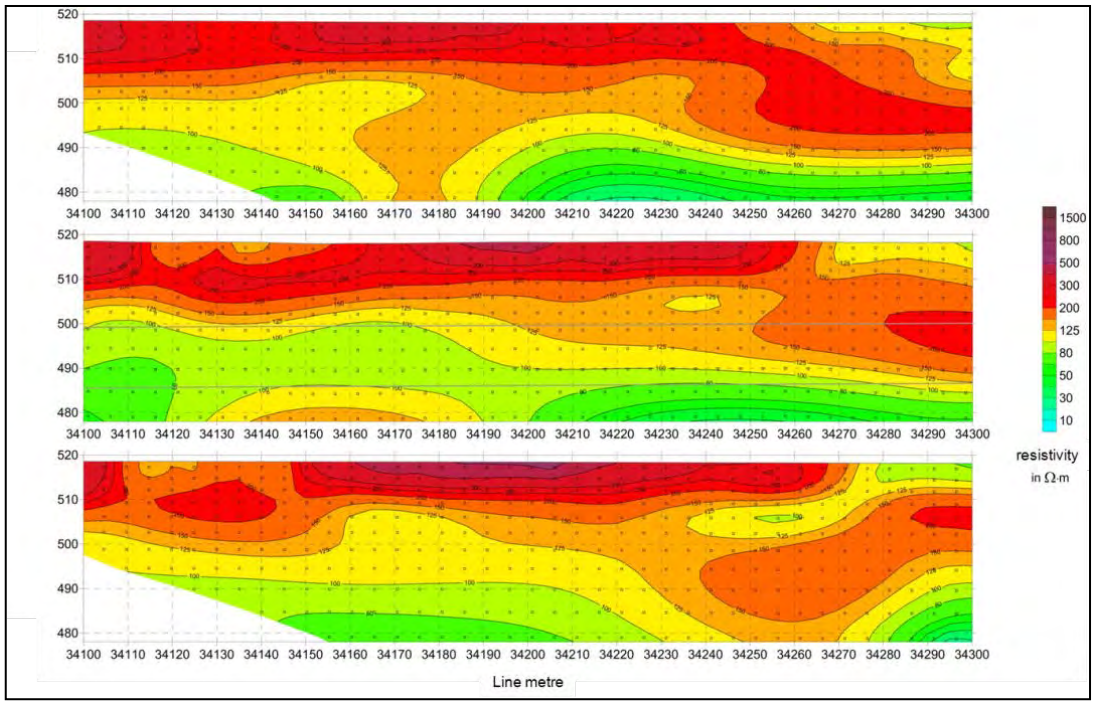

Fig. 1: Vertical sections of the calculated resistivity distribution along three parallel profiles (the middle is above the planned tunnel, the others 10 m left and right of it).

When five parallel profiles were measured, the data could be inverted in 3D. This kind of interpretation provided the best picture of the sedimentation along the tunnel route but it required a lot of computer capacity to build a sufficiently detailed model of the ground. Figure 2 presents different views at the resulting resistivity model. The three-dimensional variation of the

sedimentation can clearly be seen. Choosing a presentation of the resistivity model as an iso-surface (like on the right side in figure 2), it is even possible to predict where the TBM will pass areas with increased hydraulic permeability.

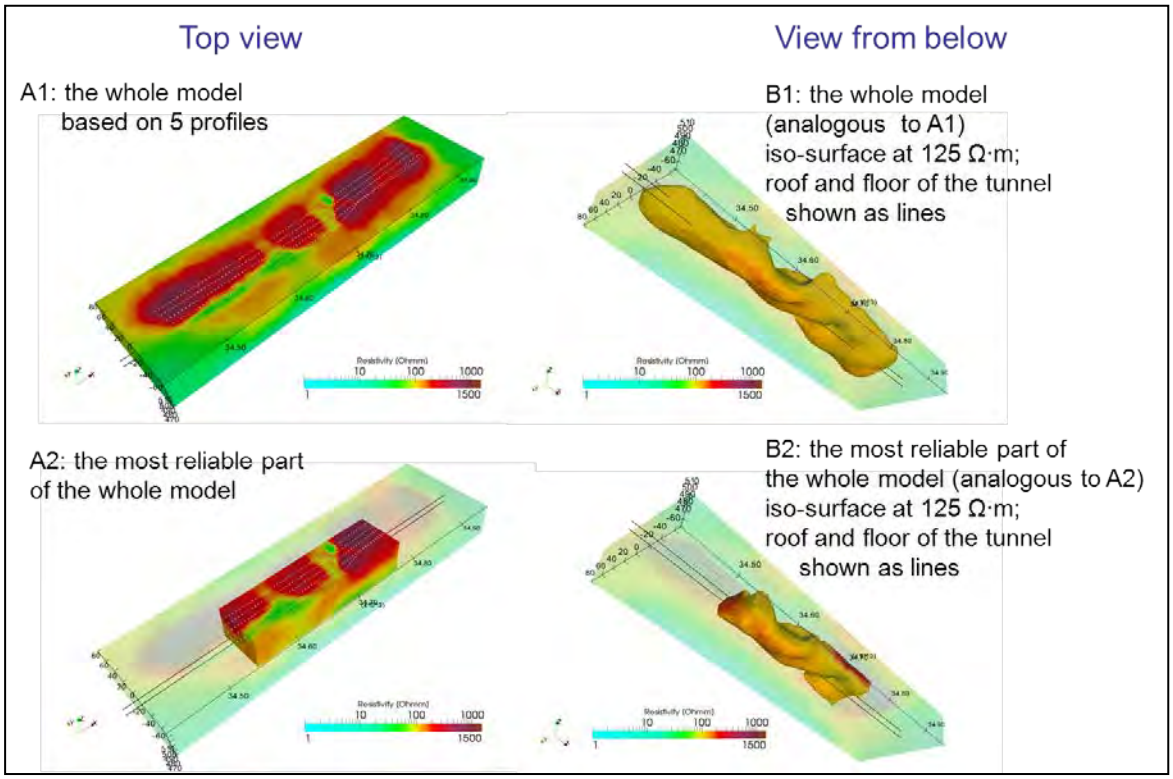

Fig. 2: Different views at the 3D model of the calculated resistivity in an area where five parallel profiles were measured (the electrode positions are marked by grey dots at the surface).

Results of the monitoring

The most interesting question was, of course, if the progress of the TBM and the spreading of the bentonite suspension could be monitored. To answer this question, an almost continuous measurement of the resistivity was carried out over about a week during the passage of the TBM. Some exemplary results of that investigation are shown in figure 3 as resistivity sections after inversion. The uppermost section presents the resistivity conditions before the arrival of the TBM (picture A: reference measurement in Nov 2007). The first measurement while boring on 10 March 2008 (picture B) shows principally the same resistivity distribution like the reference measurement, but two changes can clearly be seen: the resistivity left of the marked position of the cutting head of the TBM is much lower due to the spreading of the bentonite. Right of the cutting head a resistivity maximum is developing. As this maximum always occurs at this position (see also pictures C and D), it is assumed that this is an artefact caused by the influence of the steel wheel of the cutting head. With the progress of the tunnel boring the resistivity section changes accordingly. There are no indications for an uncontrolled spreading of the bentonite (the tunnel boring runs without any problems at this time). However, the results of the resistivity sections indicate that the bentonite is sinking downwards with time. These measurements proved impressively that a monitoring is possible by the technology applied.

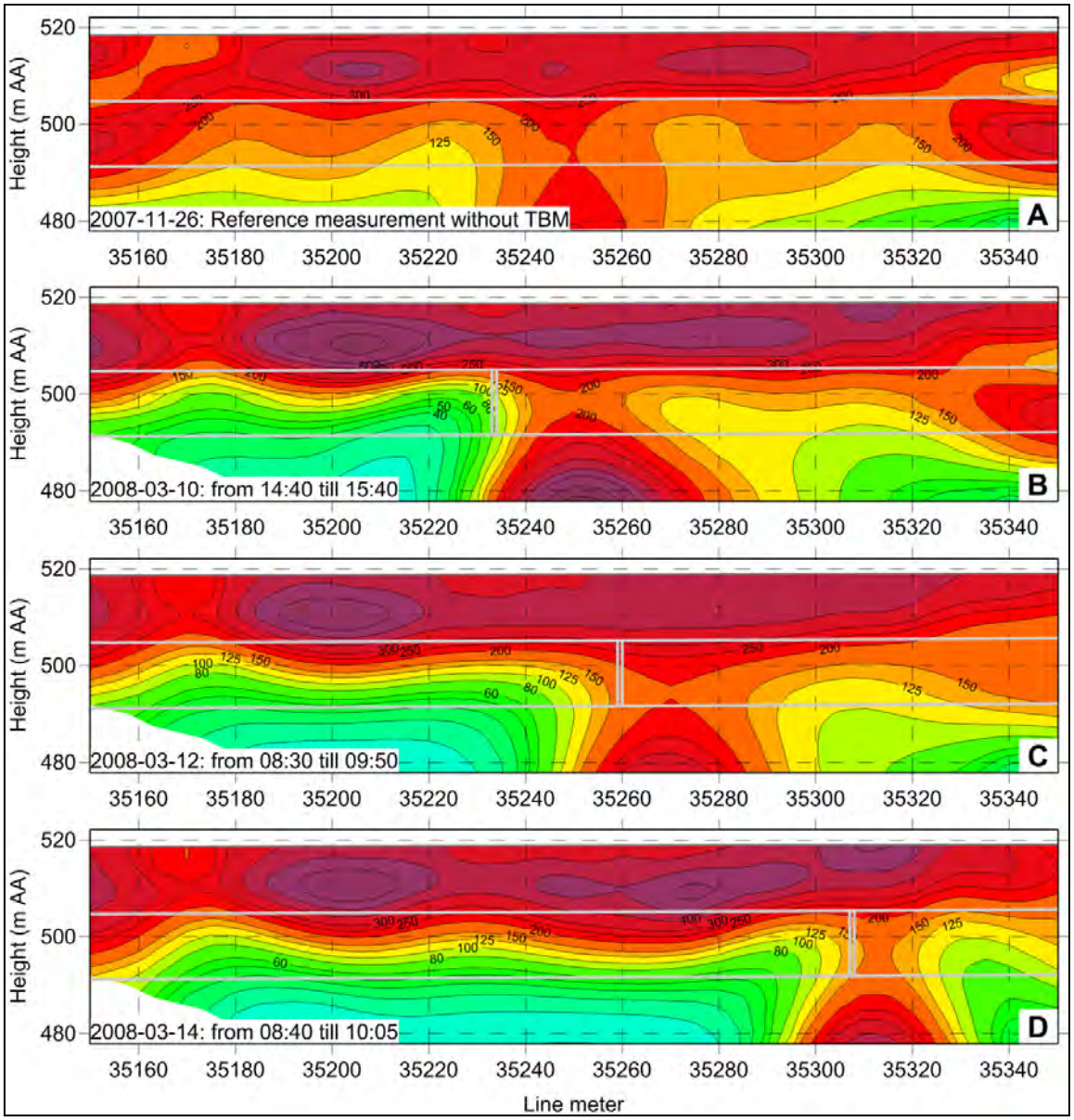

Fig. 3: 2D resistivity sections at different periods of time during the passage of the TBM (the position of the cutting head is marked in the sections B to D).

An assessment of the changes on the basis of the pseudo-sections alone would be much more complicated and it is not expected that small extrusions of bentonite can be detected only by the interpretation of measured differences without inversion.

The detectability of an uncontrolled extrusion of bentonite could not be checked during this monitoring. But this was possible at a position of the tunnel route where, after the maintenance of the cutting head during the restart of the TBM, bentonite was blown out to the surface resulting in a sinkhole. The resistivity measurements could not be done directly above the sinkhole for safety reasons. Therefore two profiles 10 m apart were measured after this event.
The result at one profile is shown in figure 4 – the reference measurement on top and the resistivity section after the outflow below. The resistivity in the depth range of the tunnel is clearly reduced after the passage of the TBM due to the bentonite spreading into the ground. The position of the sinkhole region is also clearly marked at 34780 m by a local range of low resistivity.

But it can also be seen that in the area where the bentonite extruded to the surface the resistivity in the depth range of the tunnel is remarkably higher than in the areas before and behind. This example demonstrates that even local events of extreme bentonite spreading can be detected by 2D resistivity measurements, in particular, when reference data are available.

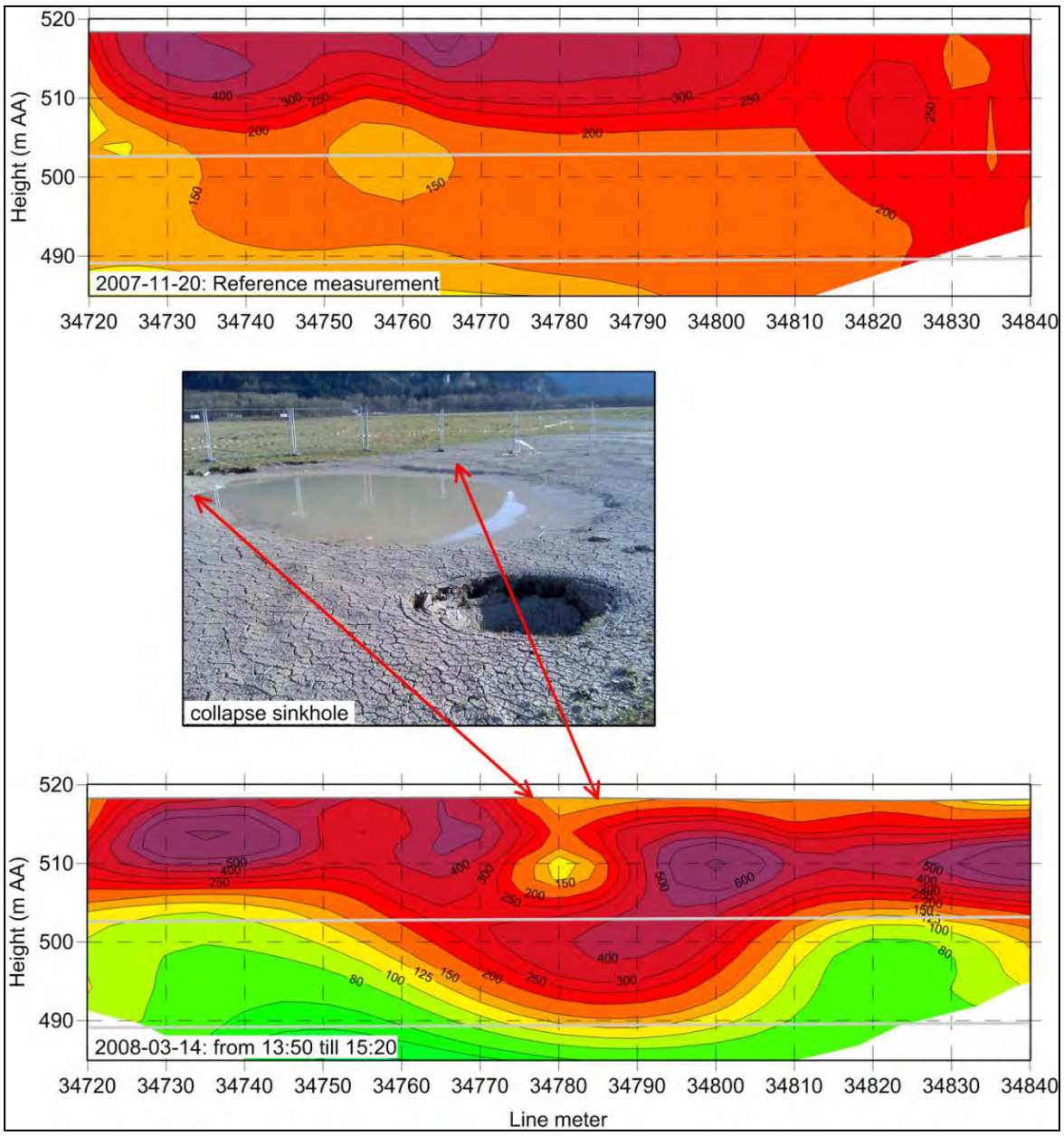

Fig. 4: 2D resistivity sections before and after the passage of the TBM; after maintaining the cutting wheel, bentonite was blowing out when restarting the TBM.

Conclusions

The very comprehensive methodological investigations regarding the monitoring of the tunnel boring in the sediments of the Inn Valley by 2D geoelectrical methods allow the following conclusions to be drawn:

- Geoelectrical measurements before the passage of the tunnel boring machine (TBM) could describe the partly complicated geological conditions more detailed than the results of drillings alone.
- The best interpretation of these reference measurements was achieved by 3D-inversion on the basis of five parallel 2D-profiles.
- According to the results achieved, it can be estimated that such a geoelectrical monitoring is useful for a maximum depth range of 15 m to 25 m to the top of the tunnel.
- Finally, this methodological investigation could prove that for tunnel boring with a bentonite shield the selected geoelectrical technique:
  - can provide information about the spreading of the bentonite suspension into the surrounding rock,
  - can detect local events as e.g. in the case of the sinkhole.

The one-week measurement on the central profile just above the route of the TBM showed the feasibility of the applied techniques for the monitoring of the tunnel boring but also the necessity to improve the technology of the measurement. Such improvements could be the acceleration of the measurement itself (e.g. by the application of multi-channel instruments) and the development of 'online'-interpretation and imaging tools which would allow the recognition of an uncontrolled spreading of the bentonite suspension almost in real-time.

Poster and Company Presentations

ERT pollution monitoring in areas of olive oil mills' wastes (OOMW): Preliminary results from a disposal site in Crete (Greece)

NIKOS PAPADOPOULOS[1] and STEFANOS CHATZIATHANASIOU[1]

[1] Laboratory of Geophysical – Satellite Remote Sensing & Archaeo-environment, Institute for Mediterranean Studies, Foundation for Research & Technology, Hellas (F.O.R.T.H.), Rethymno 74100, Crete, Greece.

nikos@ims.forth.gr

Introduction and Problem Statement

The Mediterranean region accounts for no less than 97% of the world's olive oil production due to the favourable climatic conditions. Especially, Greece holds the third place worldwide in olive oil production and the island of Crete contributes approximately 5% to the total world olive oil production. The production procedure of olive oil generates large volumes of Olive Oil Mill Wastes (OOMW) with high organic load and rich in-inorganic constituents which lead to pollution of soil and water resources and therefore environmental degradation

The OOMW are usually disposed in evaporation ponds which are rarely of proper size and wastewaters often overflow affecting neighbouring systems (soil, surface and groundwater) and other professional activities of the residents (agriculture, livestock farming). The base of the ponds is permeable and thus, the probability for groundwater and deep soil contamination is high.

Consequently long-term disposal of waste, without necessary monitoring and protective measures may cause changes in the physico-chemical parameters of the surrounding ecosystems, with the risk of future non-tissue degradation of the environment. Moreover, older waste sites often lack reliable geological or artificial barriers and depositional information, to minimize the possibilities of further environmental damages. The problem of environmental degradation and waste management are of major concern of earth scientists and the local authorities.

Geophysical methodologies in terms of Electrical Resistivity Tomography (ERT) can be used for monitoring the changes of the physical characteristics of the subsoil over time and identify the diffusion of the contaminants. An ERT monitoring experiment was conducted for the first time in an OOMW disposal site located in a test site in Crete. The purpose was to validate the resolvable capabilities of the method in capturing the spatial-temporal pollution caused by the low conductivity material of phenolic compounds.

Test Site, Crete (Greece)

Crete is the largest island of Greece and is situated at the south of the country. The test site where the ERT measurements were conducted is located in the countryside of the island and specifically in the village of Roustika, 21 km south-west of the city of Rethymno. The ERT monitoring experiment focused on a private property at the west of road connecting Rethymno and Roustika. Within the property there are two evaporation ponds, a larger one at the west and a smaller at the east, where the OOMW are stored. The property has also some scattered oil trees and is used as hosting place of sheep and goats (Fig. 1).

The Google Earth satellite image corresponding to the area of interest was extracted and rectified to the Greek Geodetic Reference System based on widely distributed ground control points, taken with a GPS with accuracy less than 1m. The ERT field data were gathered from flat area of almost 70 square meters at the east of the larger tank. The arrow indicates the location where the borehole was drilled (Fig. 1).

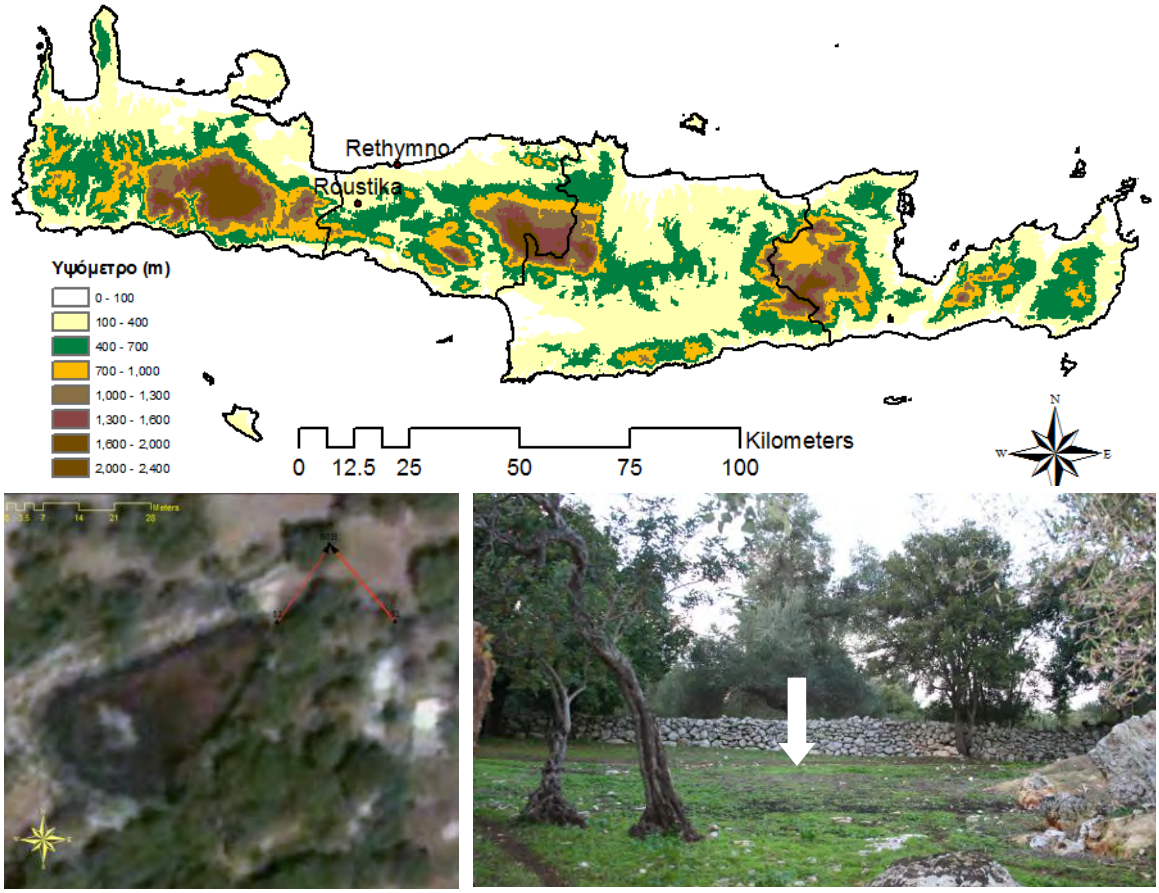

Fig. 1: (up) The island of Crete (southern Greece) where the monitoring experiment was conducted. (down) Satellite image of the larger evaporation pond of the OOMW site where the geophysical ERT monitoring measurements were conducted. The white arrow in the right picture indicates the place where the borehole was drilled.

Field Strategy & Methodology

A drill hole was opened close to the larger evaporation pond and a plastic piezometer was installed inside the borehole that reached the depth of 16 meters from the ground surface. A custom made multi-clone cable was manufactured which could drive simultaneously up to 48 outputs. The cable was attached on the outer surface of the plastic piezometer gradually during its installation in the borehole (Fig 2).

The cable outputs were placed on the plastic tube every 0.4 m, the lead leaf covered each output by surrounding the tube. Each lead leaf was tightly fixed with plastic clamp ensuring the maximum connection between the cable output and the lead leaf. Totally 36 electrodes were placed inside the borehole starting from the depth of 2 m and the reaching the bottom of the borehole (Fig 2).

The ERT monitoring measurements were made in terms of surface-to-borehole mode. Stainless steel electrodes were used for the surface measurements and the length of the surface branch of the survey was 18.8 meters. The surface electrodes were placed along the vertical lines S1-BR and

S2-BR in equal spaces every 0.4 meters. A dipole-dipole and gradient array configurations were employed to capture the surface, borehole and surface-to-borehole apparent resistivity measurements (Fig. 3). The gradient data were measured in a forward and reverse mode to evaluate and assess the noise level of the measurements. The time lapse resistivity data from totally 5 monitoring phases were collected from January 2011 until May of the same year.

Fig. 2: (left) Installation of the multi-node cable on the outer surface of the plastic piezometer that was placed inside the borehole. (right) Custom made multi-node cable with 48 electrode outputs and lead leaves that were used as borehole electrodes.

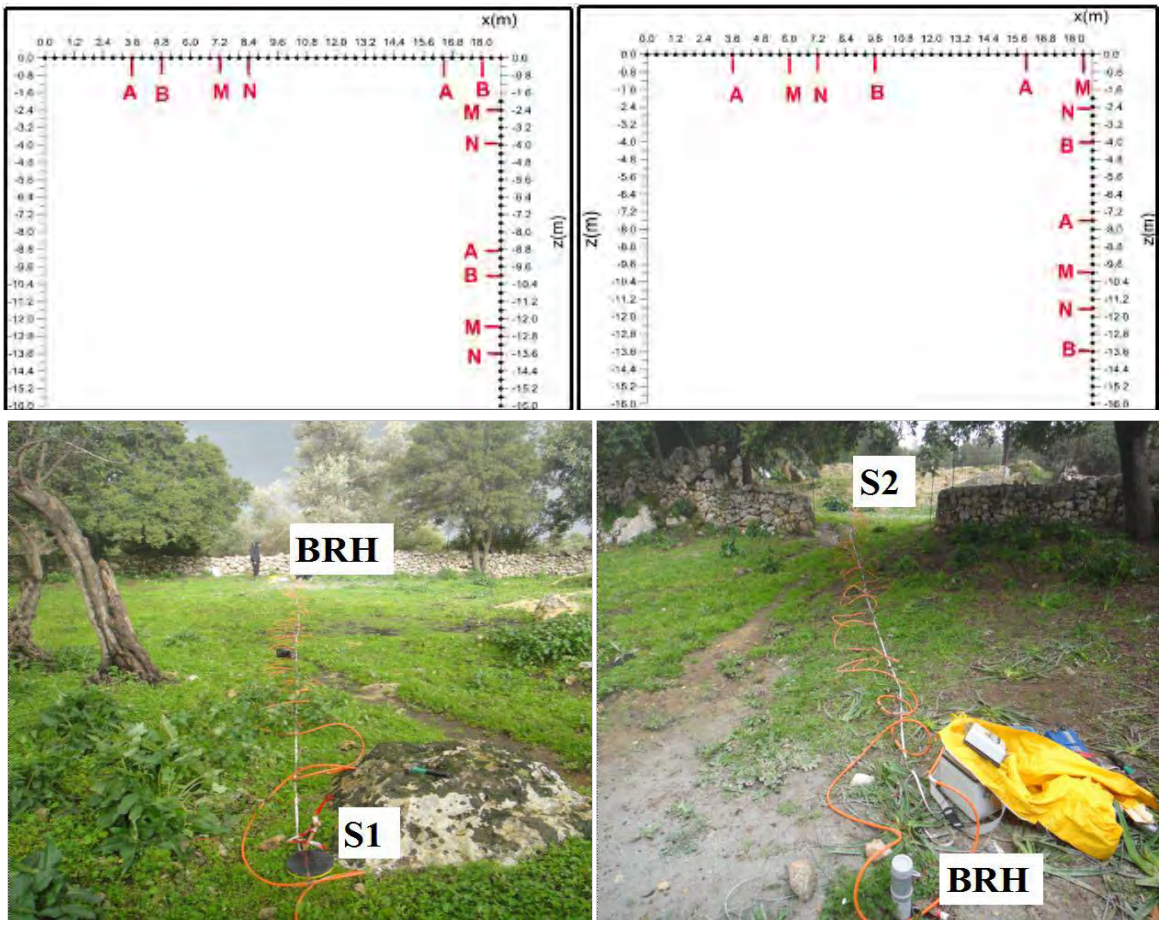

Fig. 3: (up) Dipole-Dipole (left) and gradient (right) electrode configurations for the surface, borehole and surface-to borehole measurements. (down) Arrangement of the surface electrodes along the lines S1 - BRH and S2 - BRH, where BRH shows the location of the borehole.

Preliminary Results

The relative error between the forward and reverse potential readings measured with the gradient array of each of the monitoring phases was plotted against the corresponding forward potential measurements in logarithmic plot. These plots gave a clearer indication regarding the level of noise that contaminates the resistivity measurements which has an average level of almost 2 %. Furthermore these plots were used in the pre-processing stage by removing totally less than 6 % of the monitoring data that exhibited unrealistic high or low resistivity values.

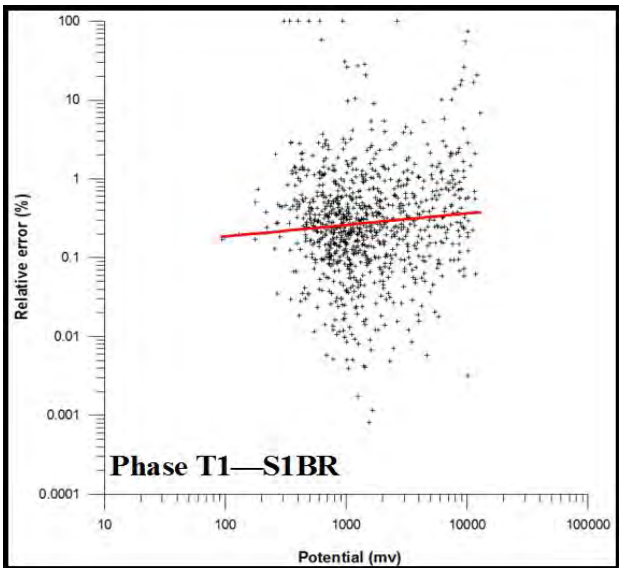

Fig. 4: Logarithmic plots of potential error from normal and reverse Gradient measurements for phase T1 and the S1-BR measurements.

Each phase of the ERT monitoring data were processed individually with a standard inversion algorithm that could account for the surface-to-borehole field measuring mode (LOKE and BARKER, 1996). Similar parameters were used in the inversion of the data where the program converged to a resistivity model after 5-7 iterations and RMS less than 4 %. In general, the reconstructed models of all the phases and the two vertical directions showed comparable results. A thin surface high resistivity layer (~20 cm/backfill material) is overlain by a more conductive layer (clay and marl) and a deeper resistance layer (clay with sand). The image inside the borehole shows generally a conductive material.

In order to have a better insight regarding the time-lapse variation of the subsurface resistivity, difference images were extracted between the first phase (reference phase) and the remaining ones based on the simple formula $\frac{T_x - T_1}{T_1}$, where T_1 is the resistivity inverted model of the first phase and T_x the inversion models for phases 2, 3, 4 and 5.

The preliminary ERT inversion models indicate a resistivity variation of +/-30% through the different monitoring phases. The decrease in resistivity values could be attributed to the movement of the conductive pollutant though the sandy marl of the area. These preliminary results signify that ERT could be a modern alternative in the original stage of monitoring and mapping the environmental pollution in OOMW areas providing solutions to address such environmental problems (Fig. 5).

Future Work

Future actions of this project include the conduction of controlled ERT experiments in non-metallic tank simulating the real conditions of an OOMW. The tank will be filled with porous material of known physical properties and composition and ERT will be used to monitor the pollutant flow within the tank using diverse electrode configuration and inversion strategies. Establishment of correlation factors between the geophysical and chemical properties.

The geophysical modelling results will be complemented with flow modelling codes (FeFLOW or MODFLOW) employing stochastic models that calculate the pollutant diffusion. Physico-chemical

analysis to soil and water samples that will be collected from the surface and the borehole and correlation between the chemical and geophysical parameters to improve the already established correlation functions that have been created in lab experiments which will significantly enhance and complement the existing methods of detection and monitoring of subsurface contamination.

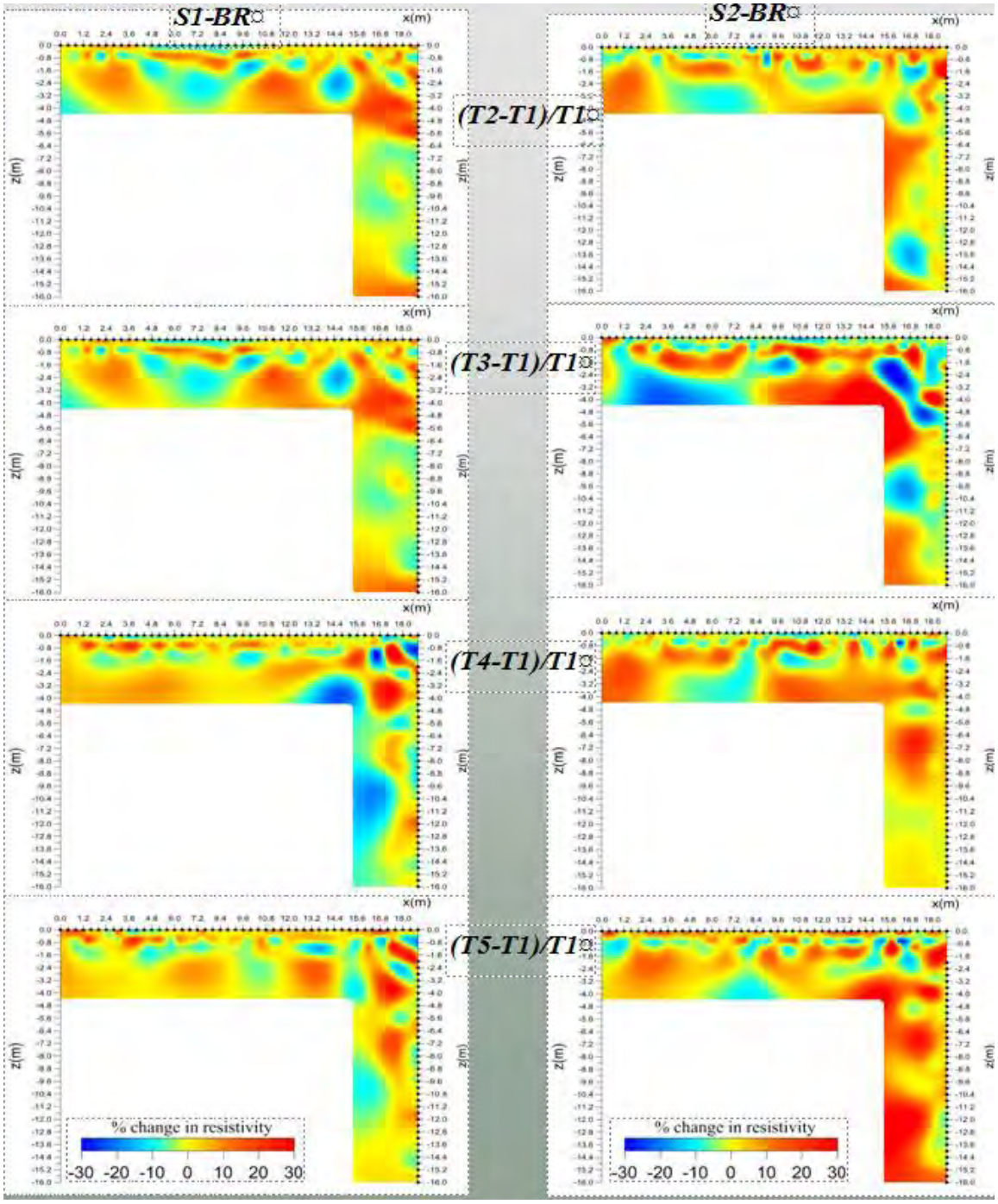

Fig. 5: Preliminary results of the difference inversion of the ERT data collected along lines S1-BRH and S2-BRH for the five time phases. The results are plotted in terms of percentage relative change of the model resistivity of each phase with respect to the reference phase.

References

LOKE, M.H. and BARKER, R.D., 1996: Rapid least-squares inversion of apparent resistivity pseudo-sections using quasi-Newton method. – Geophysical Prospecting, **48**, 181-152.

Geoelectrical imaging of slope deformations – towards repeated measurements, effective electrode array and limitations

PETR TÁBOŘÍK[1, 2], TOMÁŠ PÁNEK[2], JAN LENART[2], ROBERTA PROKEŠOVÁ[3], ALŽBETA MEDVEĎOVÁ[4]

[1] Institute of Hydrogeology, Engineering Geology and Applied Geophysics, Faculty of Science, Charles University in Prague, Czech Republic.
[2] Department of Physical Geography and Geoecology, Faculty of Science, University of Ostrava, Czech Republic.
[3] Landscape Research Institute, Faculty of Natural Sciences, Matej Bel University, Banská Bystrica, Banská Bystrica, Slovakia.
[4] Department of Geography, Geology and Landscape Ecology, Faculty of Natural Sciences, Matej Bel University, Banská Bystrica, Slovakia.

petr.taborik@post.cz

Abstract

Use of geophysical methods within the research of the slope deformation became a standard during last decades. Electrical resistivity tomography (ERT), as one of the advanced geoelectrical methods, experiences boom in its utilization in numerous scientific fields, such as archaeology, geomorphology, engineering geology or hydrogeology. The presented contribution deals with utilization of ERT on the various types of mass movements. Recognition of the processes that affect slope stability, predispose or trigger slope movements, is fundamental for both understanding of the slope development and effective rehabilitation of failing slopes or sliding mass. Contribution points out (dis)advantages of the method, its limitations and related electrode array selection that can be crucial considering the required results. The choice of the appropriate electrode configuration always depends on the demanded resolution, depth range, and sensitivity to vertical/horizontal structures and, of course, on the overall purpose of each measurement. Repeated measurements on landslides include range of difficulties that needs to be resolved. On the other hand, these practical experiences can help us to design a monitoring system based on repeated measurements.

Repeated ERT measurements on active landslide

Repeated ERT measurements were performed in the Ľubietová landslide (Central Slovakia), which is a large (320, 000 m^2) and relatively deep-seated (depth of the sliding plane is from 10 to 25 m) landslide body reactivated in 1977.

Four transversal ERT profiles were carried out repeatedly in different seasons of year with varying actual meteorological (humidity, precipitation) and hydrogeological (water saturation) conditions. As a whole, four sets of measurements were performed (Fig. 1) and figured as “1” (April 2008), “2” (November 2009), “3” (April 2010) and “4” (July 2010). Due to extremely slow movements (up to 1-2 cm per year) in the investigated landslide, observed changes in the resistivity pattern of the landslide substratum can be related rather to the slope saturation regime than deformation of the substratum.

Measured apparent resistivity (AppR) evaluated with respect to groundwater levels (measured in close monitoring wells, Fig. 1) and local precipitation data indicate that actual hydro-climatic conditions (actual weather, saturation of the near-surface layers) are affecting the extreme values of AppR (particularly the maximum), while the mean value of AppR (affected by actual weather) calculated from resistivity model probably responded to the combination of the long-term precipitation and actual rainfalls. The highest correlations among long-term hydrological condition (and ground water levels) are related to the lowest values of apparent resistivity (values close to minimal).

Repeatedly measured profiles thus gave us the opportunity to study relative changes in apparent resistivity distribution below the landslide body surface.

Simultaneously, we had an opportunity to test the method (ERT) and its various configurations (electrode arrays and spacing) in order to determine suitable (effective) parameters and limits for possible time-lapse ERT measurement. ERT proved a relative high potential as a method suitable for geoelectrical monitoring of active landslides (PROKEŠOVÁ et al., in review).

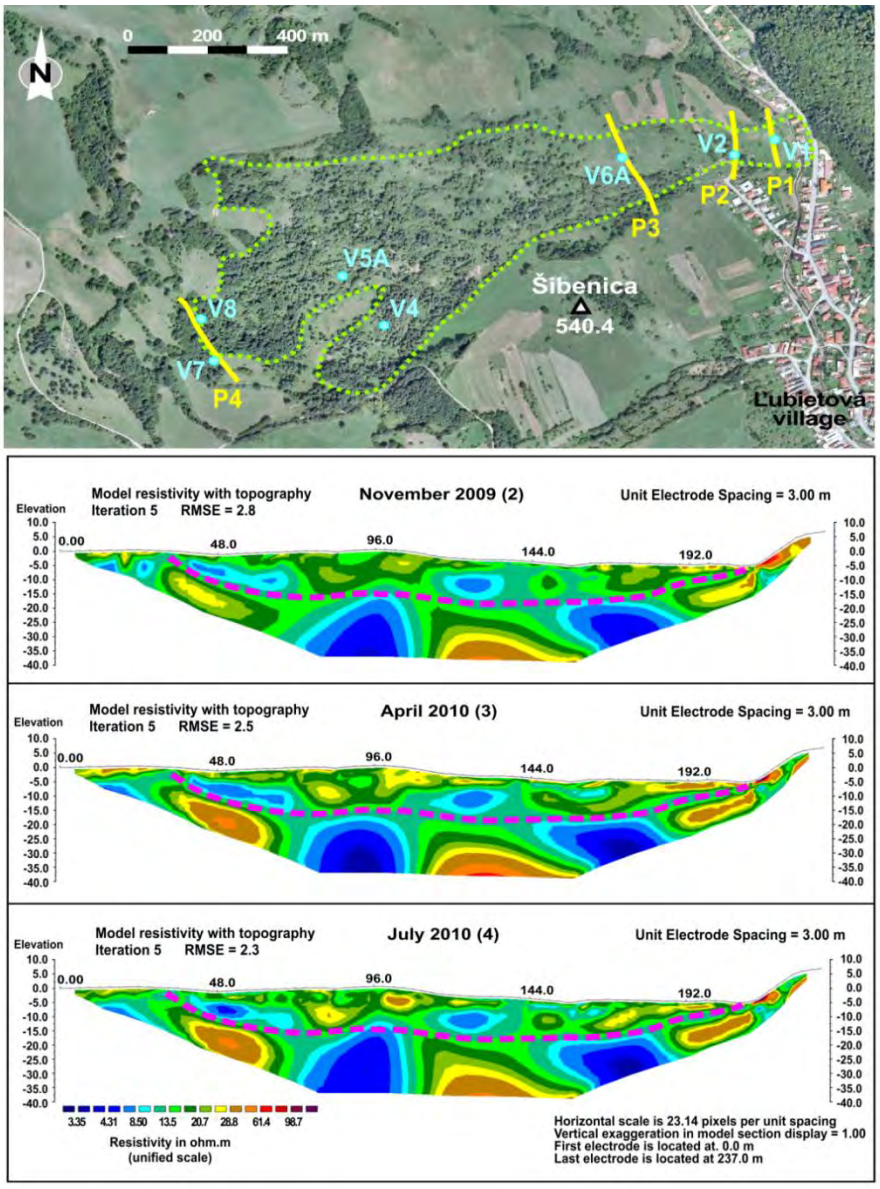

Fig.1: ERT monitoring on the Ľubietová active landslide.

Selection of effective electrode array and electrode spacing and its effect on final resistivity model

A detailed research of the Ondřejník Ridge collapse (Podbeskydská pahorkatina Hillyland, Czech Republic) revealed high intensity of flysch bedrock disruption caused by gravitational mass movements. Also tectonics (faults, crevices) and structure-geological conditions predispose this disintegration.

A number of 2D geoelectrical profiles were performed within subsurface survey. At the same time, different electrode arrangements (different arrays and variable electrode spacing) were tested. ERT survey also helped to extend valuable information - that we got from direct trenching - to deeper parts of the Ondřejník massif (Fig. 2, A).

The selection of the appropriate measuring method (electrode array) we consider as a crucial parameter of the measurements. We tested three most commonly used arrays that are Dipole-Dipole (D-D), Wenner-Schlumberger (W-S) and Wenner Alpha (W).

Our testing confirmed the presumption that W-S and W array offers similar results in depiction of horizontal and vertical structures. Nevertheless, W-S array has a deeper range and it is slightly more detailed as the W array. On the other hand, W array is less sensitive to geoelectric noise and also it offers lower RMS error.

Configuration of D-D differs in detection/depiction of horizontal and vertical structures. We use it particularly for vertical structure detection (widened crevices, tension cracks or vertical caves). Despite the best resolution (in comparison with the W-S and W arrays) based on higher number of the measured points, the D-D array is the most sensitive to geoelectric noise and higher near-surface resistivity and it is often affected by high RMS error. Higher depth range of the method can be very valuable. On the other hand, deeper range can cause a complication with higher electric noise. (PÁNEK et al., 2011)

Our evaluation of effective electrode array is in the case of the Ondřejník Ridge disintegration (flysch-type bedrock) slightly ambiguous. The W-S array seems to be a universal method with good resolution, very good depth range with slightly higher sensitivity to geoelectric noise. This method is a good compromise in detection of both vertical and horizontal structures. But, sometimes this compromise causes unclear imaging of some (sub-) vertical structures.

In this case, we consider the D-D electrode array as a more sufficient method - it is suitable rather for vertical structures and also it is more detailed (e.g. in case of narrow crevices). The disadvantage of high sensitivity to noise and higher near-surface resistivity was described above (PÁNEK et al., 2011).

If we have to deal with very high near surface resistivity (debris, block fields, etc) and, at the same time, we do not need a detailed survey or we are not focused primarily on vertical structures, we can employ the W method.

Similarly, we tested electrode configuration on an artificial embankment (Průhonice site, Praha, the Czech Republic). On the contrary to the Ondřejníks ridge, final resistivity model of the Průhonice embankment shows, that horizontal structures are better displayed with use of D-D configuration while the vertical ones are strongly depicted on model of W-S (or W) (Fig. 2, B).

This unexpected opposite depiction of subsurface structures could be a result of very steep slopes in combination with very narrow embankment body.

Higher resolution of the ERT results we can easily gain by variations of electrode spacing. Denser electrode configuration brings more detailed imaging, of course. On the other hand, technical

equipment is often also limited (e.g. number of simultaneously connected electrodes) so with smaller electrode spacing we get shorter profile and then also shallower depth range.

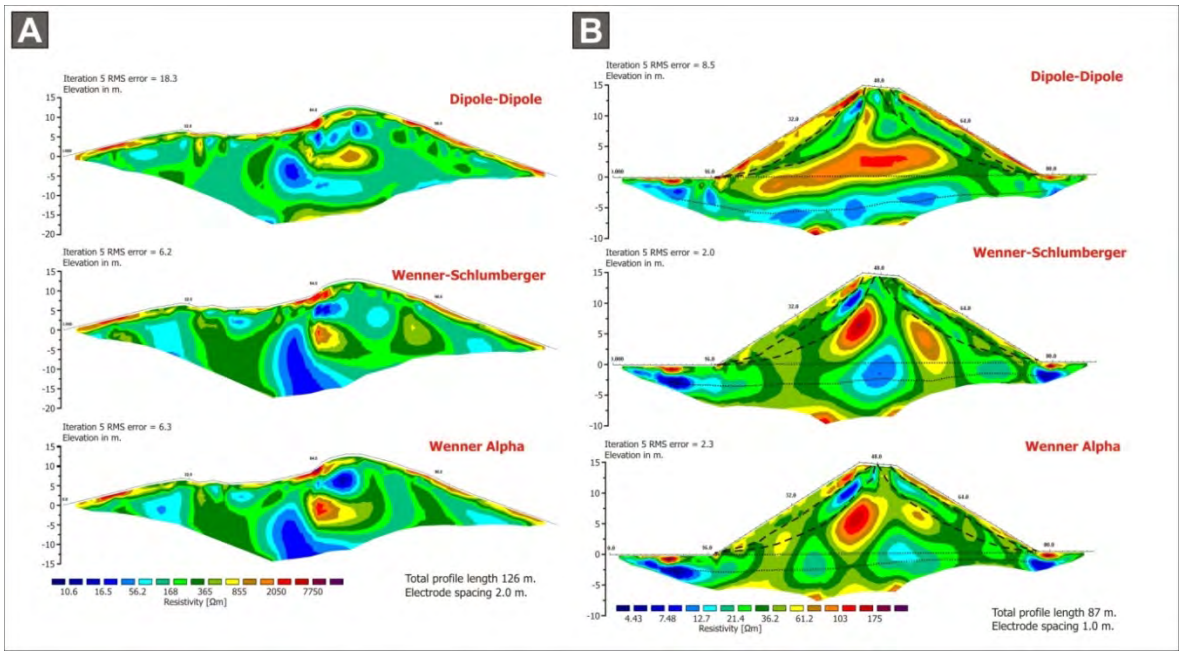

Fig.2: ERT electrode array testing: A. the Ondřejník ridge, B. the Průhonice artificial embankment (both localities are situated in the Czech Republic).

Geoelectrical modelling in electrode array selection

Selection of suitable electrode array is one of the most important things during the measurement. Besides the obvious problems with final resolution (depended mainly on electrode spacing), there are numerous measuring methods (arrays) which differs in the way of measurement, so, it can have an essential effect on final resistivity model. Each of the arrays is specific and brings different results in horizontal/vertical resolution and depiction of subsurface structures. Complex lithological structure of landslide bodies often requires information on both horizontal and vertical direction. Selection of the effective electrode array can be realized either by repeated measurement with application of various arrays or with use of geoelectrical modelling (LOKE, 2002).

Because we are not able to include all possible parameters of measured subsurface substratum, final result of forward modelling is only the simplified model. However, it has given to us valuable information on used arrays and it can help us to choose the most suitable method.

In case of mountain ridge disintegration (PÁNEK et al., 2010, 2011) we dealt with initial forms of deep seated slope deformations which are often represented by widening crevices and crevice-type (fissure) caves, open tension cracks and block subsidence, toppling, or lateral spreading of rock massifs. Rock disrupted by sets of crevices is, of course, more vulnerable to slope deformation, so detection of disintegrated zones is crucial for determination of possible subsequent development of the slope. Despite the complexity of the anisotropic flysch rock massif, forward geoelectrical modelling brings valuable information on suitability of the particular array, its resolution and depth range and also on distortion of depicted structures.

Forward modelling can be also used as an interpreting tool. For example, unclear boundaries in the final resistivity model of which strong expression were expected from direct survey (caving,

trenching) can be specified by simplified model which is less affected by anisotropy of rock massive and upper laying colluvial sediments. Also the evidence of a very narrow crevice can be only indirect and we cannot distinguish the crevice in the model as a separate structure. But, the existence of it influences the final image (Fig. 3).

Nevertheless, the application of forward geoelectrical modelling requires deeper knowledge of the modelled structures and it needs as much additional information as possible (e.g. lithology, structural geology aspects, tectonics, ground water level, etc.) gained from direct survey – mapping, drilling, trenching or caving.

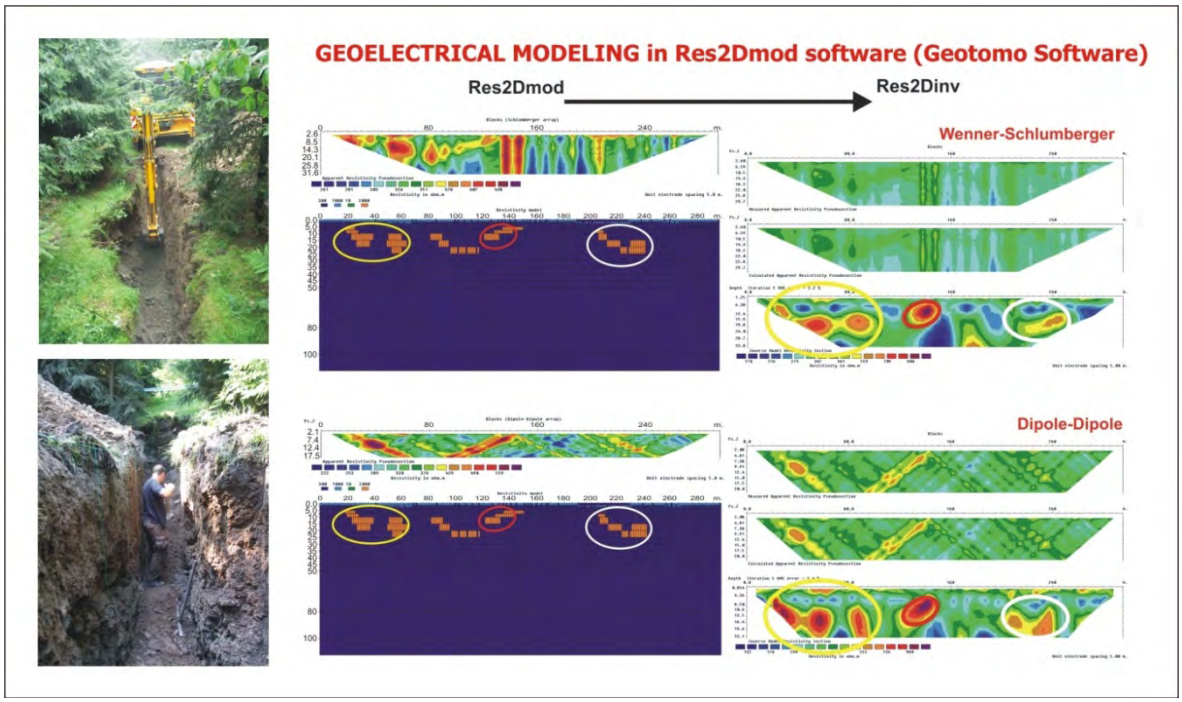

Fig.3: Directly investigated structures (e.g. from trenching) can be modelled and the model can help with selection of suitable method for further non-invasive ERT survey within wider area.

Conclusion

Suitability of resistivity methods (e.g. ERT) for geoelectrical imaging of slope deformation depends on various lithological, structural-geological and hydrogeological conditions. Slope stability is also affected by tectonics. Besides these natural conditions, we have to consider different result gained from different electrode array and spacing. So, for the optimisation of any geoelectrical monitoring, it is very valuable to test various electrode array with various electrode configuration. Repeated measurements bring knowledge on observational potential of each method and also help to set optimal interval of measurement (if it is not time-lapse).

In case, we are not able to test electrode configuration directly, we can use a forward resistivity modelling. This modelling tool is very effective, and even we are not able to include all possible parameters and conditions, final model is very useful in selection of the most effective electrode array. We can also create an approximate model of known situation below the surface (e.g. known cave system). Geophysical evidence of known structures can be used as an interpretation model for supposed similar structures (e.g. non-discovered cave chamber).

Acknowledgements

Research was supported by project VEGA 1/0157/10 and by Internal grant of University of Ostrava – SGS6/PřF/2011 – Deep-seated slope deformations, recent landslides and development of valley floors.

References

LOKE, M.H., 2002: RES2DMOD ver. 3.01: Rapid 2D resistivity forward modelling using the finite difference and finite-element methods. – Software manual.

PÁNEK, T., MARGIELEWSKI, W., TÁBOŘÍK, P., URBAN, J., HRADECKÝ, J. and SCIURA, C., 2010: Gravitationally-induced caves and other discontinuities detected by 2D electrical resistivity tomography: Case studies from the Polish Flysch Carpathians. – Geomorphology, **123**, 165-180.

PÁNEK, T., TÁBOŘÍK, P., KLIMEŠ, J., KOMÁRKOVÁ, V., HRADECKÝ, J. and ŠŤASTNÝ, M., 2011: Deep-seated gravitational slope deformations in the highest parts of the Czech Flysch Carpathians: Evolutionary model based on kinematic analysis, electrical imaging and trenching. – Geomorphology, **129**, 92-112.

PROKEŠOVÁ, R., MEDVEĎOVÁ, A., TÁBOŘÍK, P. and SNOPKOVÁ, Z., 2012: Towards hydrological triggering mechanisms in large deep-seated landslides. – Landslides, **9**(35), (in review).

Monitoring of water content, water displacement and freeze-thaw processes in alpine rock walls using geoelectric survey lines

MATTHIAS RODE[1] and OLIVER SASS[2]

[1] Institute for Geography and Regional Sciences, Karl-Franzens-University Graz, Austria.
[2] Institute of Geography, University of Innsbruck, Austria.

matthias.rode@uni-graz.at

Abstract

The detachment of rock fragments from alpine rockwalls is mainly assigned to frost weathering. However, the actual process of frost weathering as well as the contribution of further weathering processes (e.g. hydration, thermal fatigue) is poorly understood. Rock moisture distribution during freeze-thaw events is the key to understanding weathering. As freeze-thaw cycles of different duration and intensity can contribute to rock shattering, these events can only be adequately investigated by means of a continuous monitoring program. To achieve this aim, small-scale geoelectric survey lines have been installed in three study areas (Gesäuse, Dachstein, Kitzsteinhorn) in the framework of the initiated ROCKING ALPS project. The here presented results of geoelectric measurements at the Kitzsteinhorn point to high importance of hydrostatic pressures and the generated pore water movement during freezing for the process of freeze-thaw weathering in rock.

Introduction

Rockfall generation is not uniform in space and time and rockfall of all magnitudes is concentrated along pre-formed clefts and faults. Small scale joint density and differences in moisture supply are highly important for debris fall patterns. Furthermore, the presence of permafrost in the rock promotes frost weathering.

According to HUDEC (1980), water displacement during freezing and the resulting adsorption and desorption processes are responsible for "frost" damage in limestones. MCGREEVY and WHALLEY (1985) also favoured ice formations causing hydrostatic pressure in the unfrozen rock as being the main agent of frost weathering; this viewpoint was supported by e.g. FAHEY and LEFEBURE (1988) and COUTARD and FRANCOU (1989). ISHIKAWA et al. (2004) directly observed crack widening caused by water supply and subsequent freezing. High-resolution electrical conductivity measurements (SASS, 2004) showed heightened pore water contents near the margins of ice lenses, which also indicates that hydrostatical pressure is an important factor in frost weathering. Contrastingly, WALDER and HALLETT (1986) postulated that rock shattering is achieved by slow formation of ice lenses (segregation ice) similar to frost heave in soil. The critical point of all these theories is the lack of data on water contents of natural rock and on moisture fluctuations during freezing (MCGREEVY and WHALLEY, 1985; MATSUKURA and TAKAHASHI, 2000; REGMI and WATANABE, 2009).

Recent investigations use 2D-resistivity for monitoring ice in bedrock (e.g. HILBICH et al., 2009; KRAUTBLATTER et al., 2010). Applying this technique to bedrock using drilled-in electrodes is a relatively new approach (SASS, 2003; KRAUTBLATTER et al., 2007). This present paper is focusing on

frost weathering and debris fall and by the smaller scale of measurement. This small-scale approach has been only carried out by SASS (2003, 2004) and SASS and VILES (2006, 2010).

Study sites

In the framework of the ROCKING ALPS project investigations are carried out in three areas of the Eastern Alps (Figure 1) of different elevation and lithology. The first study area is the Gesäuse as part of the north-eastern Limestone Alps. The prevailing rock types are the Dachstein limestone and the Wetterstein dolomite. The study sites are at an elevation of 800-1200 m. The Dachstein area is situated west of the Gesäuse and reaches a summit height of up to 2.995 m. The rockwalls are also built up of Dachstein limestone. The existing permafrost in the north-facing rockwalls is a highly interesting comparison area to the geologically similar Gesäuse. The third area is the Kitzsteinhorn (3203 m) in the Hohe Tauern range consisting of calcareous mica-schist with permafrost.

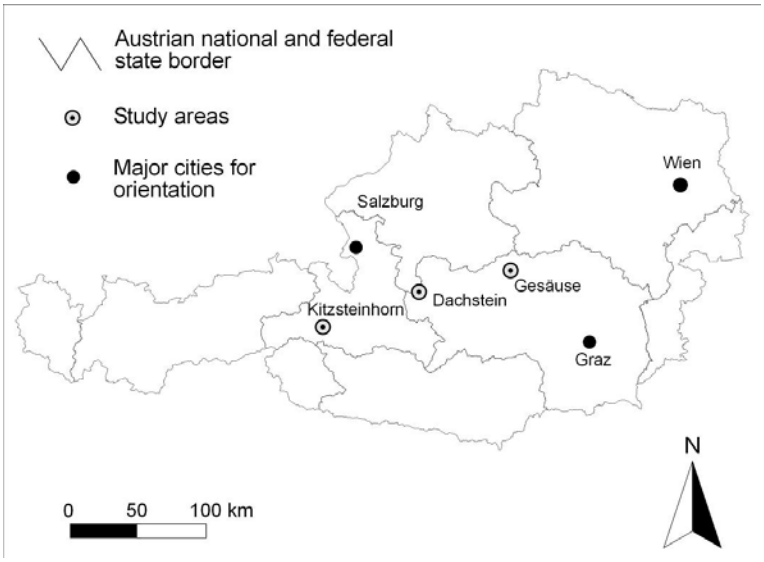

Fig. 1: Study sites of the ROCKING ALPS project.

Project methods

The aims of ROCKING ALPS are (1) to get information on rock moisture at high temporal and spatial resolution, (2) to monitor the pore water movement during freeze-thaw events and (3) to connect moisture and rockfall data obtained by TLS. Therefore, the 2D-resistivity measurements will be combined with rockfall monitoring.

Monitoring of water content, water displacement and freeze-thaw processes is achieved by permanently installed geoelectric survey lines (ERT). The ERT method enables an interesting, graphic general view of the small-scale moisture distribution and allows the assessment of moisture fluctuations during freezing.

Very short-term moisture fluctuations (e.g. those induced by freeze-thaw events) cannot be accurately recorded by geoelectric profiling. Thus, additional temperature and moisture measurements at higher temporal resolution are carried out. Two techniques are applied - transitional resistivity and heat capacity measurements. For investigating the impact of observed moisture fluctuations on weathering, regular laser scans (TLS) are carried out at several monitoring sites in the vicinity of the geoelectric instruments. The datasets allow assessing the dominant controlling factors of rockfall. While datalogger and geoelectrical measurements are

performed at fixed sites at high temporal resolution, TLS offers the spatial rockfall distribution within the test sites of some 100 m². To tie these two approaches closer together, georeferenced infrared photos are taken at regular intervals. This enables to visualize temperature patterns and amplitudes. The cross-check with TLS data offers interesting insights into the relevant drivers of weathering.

As freeze-thaw cycles of different duration and intensity can contribute to rock shattering, these events can only be adequately investigated by means of a continuous monitoring program. The design of the survey lines enables detailed observation of small-scale water movement during wetting, drying and freeze-thaw events (50 electrodes, spacing 0.06 m, Wenner-array) while additional longer profiles at the Dachstein will record the presence of frozen rock to a depth of c. 3 m (25 electrodes, spacing 0.5 m, Wenner-Array). The survey lines will be maintained over a period of at least one year each. Considerably different freezing behaviour between north- and south-facing sites, as well as between permafrost and non-permafrost sites is to be expected.

ERT-setup

Several geoelectric measurements were performed on the Magnetköpfl summit (2900 m), in the Kitzsteinhorn area from 27-04-2011 to 29-04-2011 (Figure 2). In the course of this field trip two geoelectric profiles, both equipped with 50 electrodes and a spacing of 0.06 m were drilled into a rock wall. This instrument setup enables to investigate the external layers of the rock wall to c. 0.5 m depth.

Fig. 2: ERT measurements at two profiles on a rock wall at the Magnetköpfl (Kitzsteinhorn).

On both survey lines measurements were taken on 28-04 from 09:00 to 20:00 and on 29-04 from 06:00 to 09:00. In the following, two data sets per profile are presented: the condition before freezing inside the rock wall (t1 – 28-04-2011, 19:30) and the frozen condition in the next morning (t2 – 29-04-2011, 07:30). During this time, the air temperatures decreased continuously from +1.8°C at t1 to -4.3°C at t2 (Figure 3).

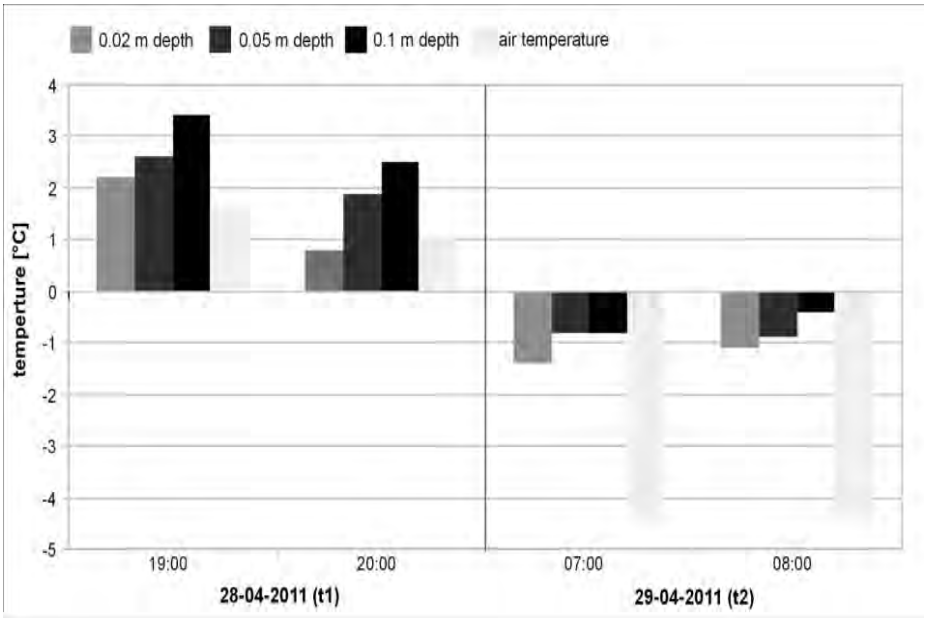

Fig. 3: Mean rock and air temperature at the two measurement dates t1 and t2.

First results

At profile 1 (Figure 4), increasing resistivity values between t1 and t2 are recognizable near the surface which is due to freezing of the pore water. However, at c. 1.92 m and at a depth of about 0.2 m, a decrease of resistivity values can be observed. This resistivity drop (blue zone) is caused by heightened pore water content underneath the frozen layer. This presumably indicates displaced pore water during freezing.

Profile 2 (Figure 4) yielded similar results. This profile was installed along a horizontal fissure in the rock wall. During the day, melted snow impounded in this fissure. Due to the night frost this water got frozen. This phenomenon is clearly mirrored by the increase in resistivity between t1 and t2. Due to freezing heat, caused by a higher amount of water at the surface than in dryer layers deeper inside the rock, not the entire surface got frozen. The RMS error of both profiles is fairly low in the unfrozen state (3.6-4.1%) and is markedly higher at subzero temperatures (4.8-14.2%). This is due to the extreme contrast between frozen and unfrozen rock areas.

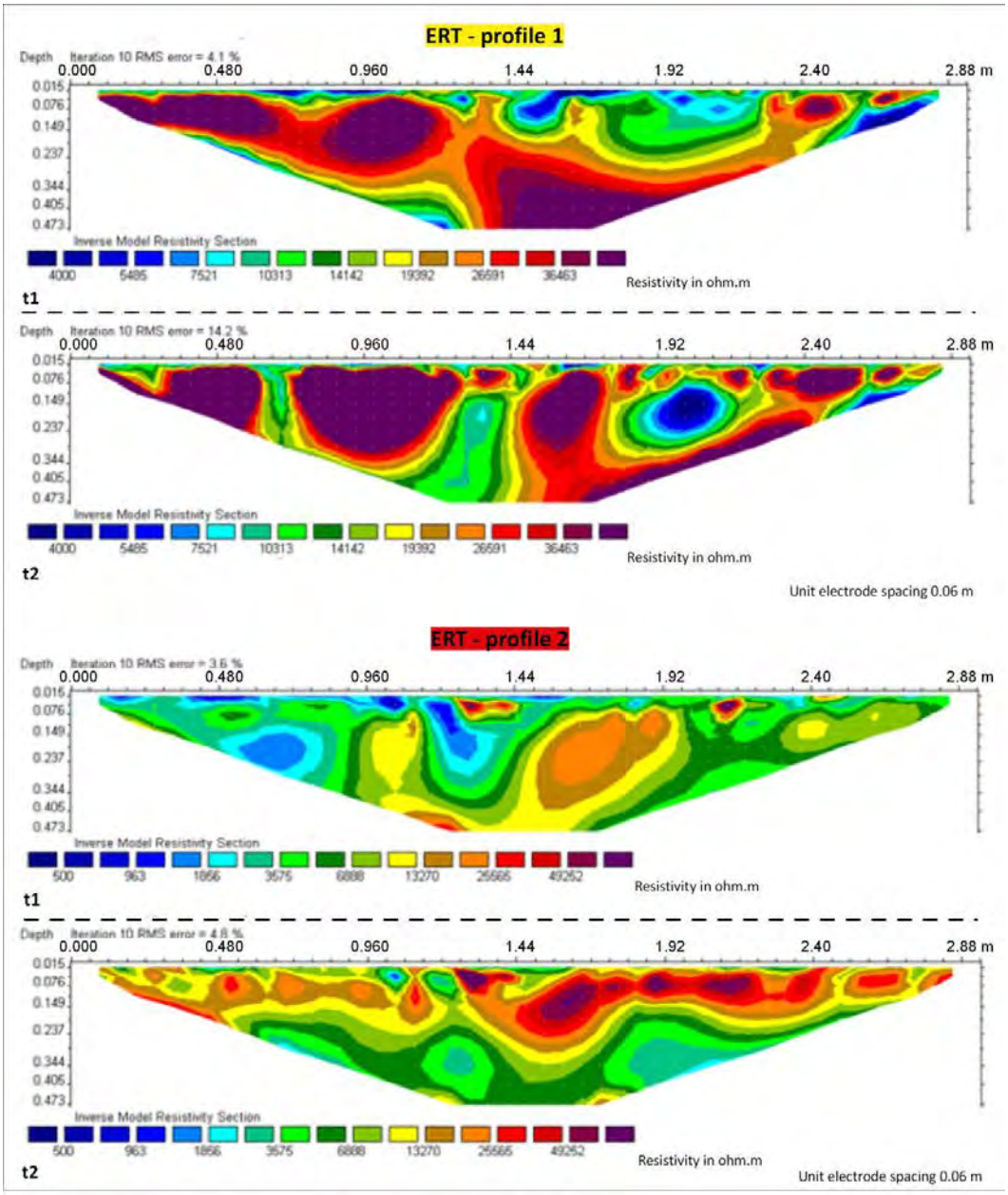

Fig. 4: Inversion models (Wenner-array) of the resistivity values at profile 1 and 2. RMS error: (root-mean-squared-error) = Difference between the calculated and the apparent measured resistivity.

To assess the change in resistivity between t1 and t2, a time-lapse inversion model was calculated in *Res2Dinv*. Thereby, the visual interpretation could be underpinned by relative numerical values. Time-lapse inversion models of the same measurements (Figure 5) also show an increase in resistivity near the surface and a decrease deeper inside the rock. The colors green to purple of the color bar represent the percentage decrease or increase, respectively, of the resistivity values. At 1.94 m of profile 1, pore water freezing could be clearly recognized by the observed increase of 160% at 0.15 m depth. At greater depth the percentage increase gets smaller, until at 0.25 m a decrease of the resistivity values becomes apparent.

The percentage increase in resistivity at profile 2 amounts 189% on average for nearly the whole section down to 0.14 m. The depth of freezing reaches down to 0.3 m. This pronounced increase is caused by the large amount of water impounded during the day in the horizontal fissure.

From 0.3 m depth on, a decrease of 35% of the resistivity values between t1 and t2 was observed. It is concluded that similar to profile 1, pore water was displaced during freezing.

The time-lapse inversions clearly show that the spatial patterns of resistivity changes is quite heterogeneous for both profiles, which is mainly due to the different geomorphic situation between the two profiles. The highly jointed surface of the rock wall at profile 2 caused a higher moisture level inside the rock than the compact and plain rock surface at profile 1.

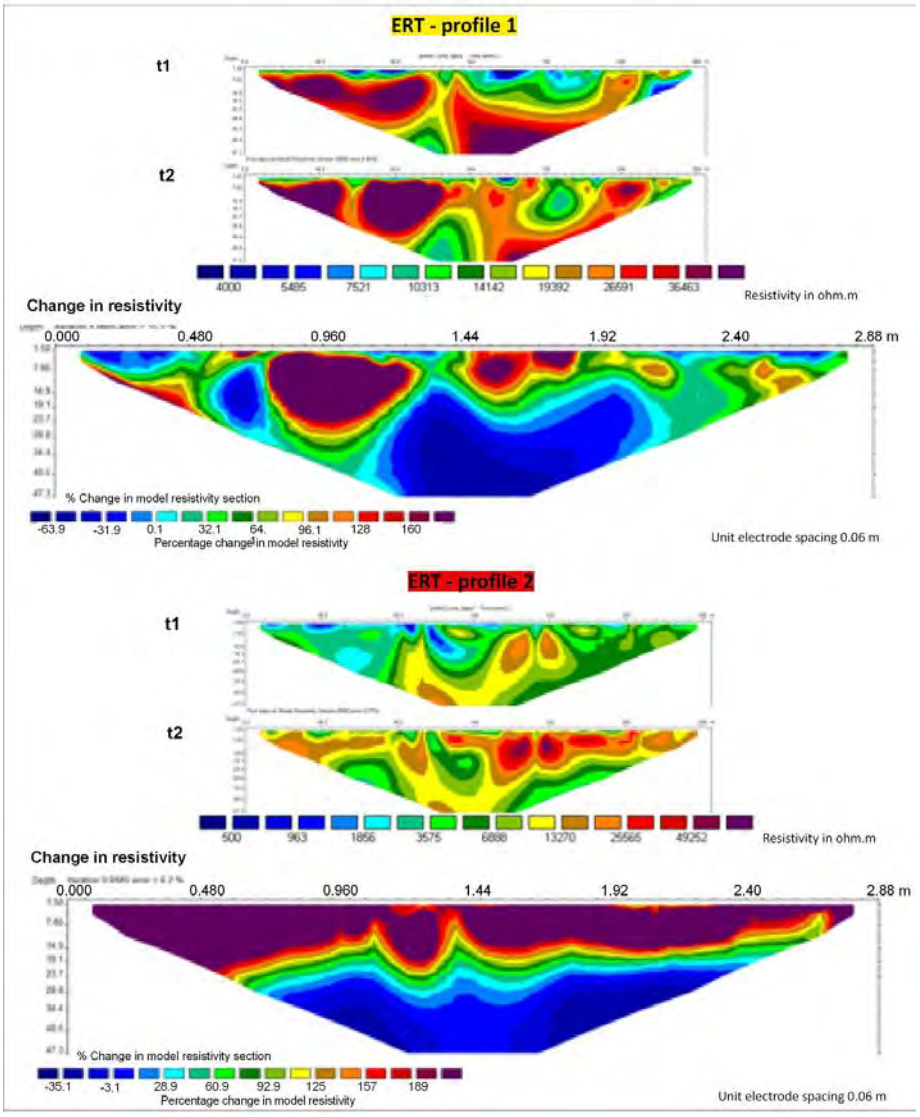

Fig. 5: Time-lapse inversion models at t1 and t2, as well as the percentage change of resistivity between t1 and t2 of the profiles 1 and 2.

To get a better quantitative overview of the change in resistivity at certain depths it is helpful to consider the numerical values. Figure 6 shows the mean resistivity values at different depths at t1 and t2. At a depth of 0.1 m the increase in resistivity in the morning (t2), comparing to the evening before (t1), is plain to see in both profiles. A slight increase of the mean resistivity values happened at a depth of 0.3 m at profile 2. Once again, this pattern is due to freezing near the surface and increased water content underneath the frozen layer.

Comparing t2 to t1, increasing resistivity down to about -0.23 m is evident at both profiles, which represents the frost penetration depth during the night and the freezing of moisture. In contrast, from -0.28m depth on, the resistivity values at t2 are getting lower than at t1. The decrease in

resistivity was particularly evident at profile 1 at about 0.47 m depth. Considering the assumed frost penetration depth, the moisture in those deeper layers should be frozen, but the results again indicate heightened pore water pressure under the freezing front. At profile 2 the decrease in resistivity values was not that pronounced, but in principle, the same phenomena of frozen and unfrozen moisture in different rock layers occurred.

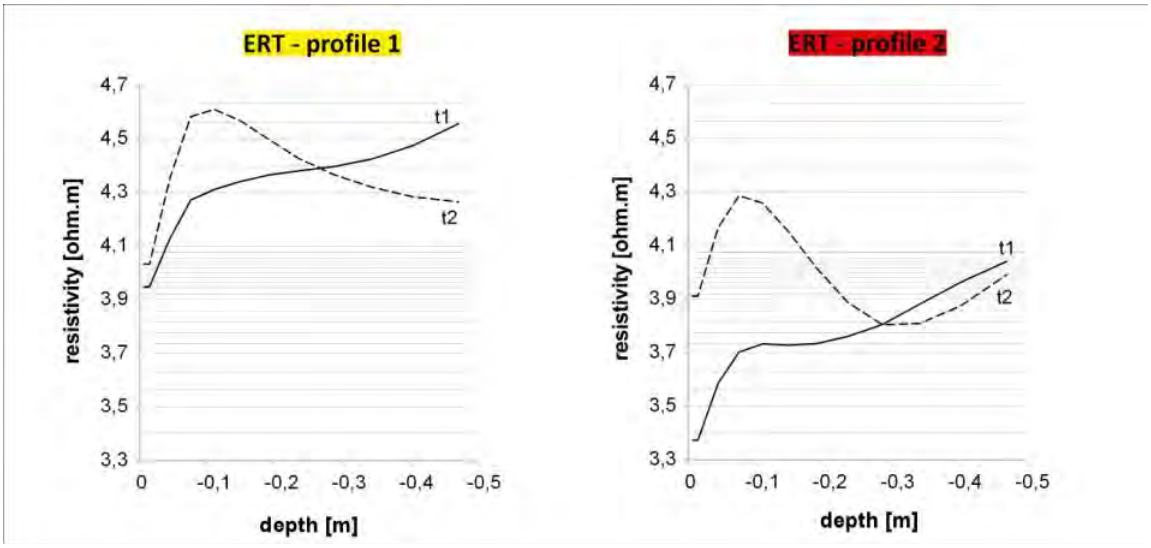

Fig. 6: Change of mean resistivity values at different depths for t1 and t2 at the profiles 1 and 2.

Discussion

The results point to a high importance of hydrostatic pressures during freezing and the generated pore water movement for the process of freeze-thaw weathering in rock walls (Sass 2004). This principally confirms the ideas on frost weathering as conceptualised by McGreevy and Whalley, with ice formations causing hydrostatic pressure in the unfrozen rock being the main agent of frost weathering. However, the idea of slow moisture movement towards the freezing front during long spells of subzero temperatures cannot be confirmed or disconfirmed, as longer measurements are necessary.

The reliability of the results has to be carefully assessed in the future. The surprising resistivity drop under the freezing front might be in parts attributed to an over-compensation artefact of the inversion routine, caused by extremely high resistivity in the frozen area. Therefore additional ERT-measurements, with a reduced current flow to enable reliable measurements under high electrical resistances, are carried out. An accurate analysis of future results in matters of arisen artefacts due to inversion calculations will be done.

To get information on the factual moisture content of the rock, it is necessary to convert the resistivity values to moisture graphs through laboratory calibration work. At this stage, only first hypotheses based on the resistivity values could be made to describe the moisture content of the rock. In the near future, fixed moisture, heat-capacity and temperature sensors at different depths will be installed. To assess mechanical changes in the rockwall due to generated hydrostatic pressures, additional piezoelectric sensors will be used.

Acknowledgements

This is a pre-study for the project 'ROCKING ALPS – Rockfall and Weathering in the Eastern Alps' financed by the Austrian Science Fund (FWF) through project no. FWF P24244. Mag. Matthias Rode was funded by a stipend provided by the URBI faculty of the University of Graz, which is gratefully acknowledged.

References

COUTARD, J. and FRANCOU, B., 1989: Rock temperature measurements in two alpine environments: implications for frost shattering. – Arctic and Alpine Research, **21**, 399-416.

FAHEY, B.D. and LEFEBURE, T.H., 1988: The freeze-thaw weathering regime at a section of the Niagara Escarpment on Bruce Peninsula, Canada. – Earth Surface Processes, **13**, 293-304.

HILBICH, C., MARESCOT, L., HAUCK, C., LOKE, M.H. and MÄUSBACHER, R., 2009: Applicability of Electrical Resistivity Tomography Monitoring to Coarse Blocky and Ice-rich Permafrost Landforms. – Permafrost and Periglacial Processes, **20**(3), 269-284

HUDEC, P.P., 1980: Durability of carbonate rocks as function of their thermal expansion, water sorption and mineralogy. – American Society for Testing and Materials, Special Technical Publication, **691**, 497-508.

ISHIKAWA, M., KURASHIGE, Y. and HIRAKAWA, K., 2004: Analysis of crack movements observed in an Alpine bedrock cliff. – Earth Surface Processes and Landforms, **29**, 883-891.

KRAUTBLATTER, M., HAUCK, C. and WOLF, S., 2007: Geophysical 2D and 3D-monitoring of permafrost in rock walls. – Geophysical Research Abstracts, **9**, 09884.

KRAUTBLATTER, M., VERLEYSDONK, S., FORES-OROZCO, A. and KEMNA, A., 2010: Temperature-calibrated imaging of seasonal changes in permafrost rock walls by quantitative electrical resistivity tomography (Zugspitze, German/Austrian Alps). – Journal of Geophysical Resaerch - Earth Surface, **115**, F02003 (doi: 10.1029/2008JF001209).

MATSUKURA, Y. and TAKAHASHI, K., 2000: A new technique for rapid and non-destructive measurement of rock-surface moisture content; preliminary application to weathering studies of sandstone blocks. – Engineering Geology, **55**, 113-120.

MCGREEVY, J.P. and WHALLEY, W.B. 1985: Rock moisture content and frost weathering under natural and experimental conditions: A comparative discussion. – Arctic and alpine research, **17**, 337-346.

REGMI, D. and WATANABE, T., 2009: Rockfall activitiy in the Kangchenjunga Area, Nepal Himalaya. – Permafrost and Periglacial Processes, **20**, 390-398.

SASS, O., 2003: Moisture distribution in rockwalls derived from 2D-resistivity measurements. In: Geophysical applications in geomorphology. – Zeitschrift für Geomorphologie, Supplementband **132**, 51- 69.

SASS, O., 2004: Rock moisture fluctuations during freeze-thaw cycles - preliminary results derived from electrical resistivity measurements. – Polar Geography, **28**(1), 13-31.

SASS, O. and VILES, H.A., 2006: How wet are these walls? Testing a novel technique for measuring moisture in ruined walls. – Journal of Cultural Heritage, **7**, 257-263.

SASS, O. and VILES, H.A., 2010: Wetting and drying of masonry walls: 2D-resistivity monitoring of driving rain experiments on historic stonework in Oxford, UK. – Journal of Applied Geophysics, **70**, 72-83.

WALDER, J.S. and HALLET, B., 1986: The physical basis of frost weathering: Toward a more fundamental and unified perspective. – Arctic and Alpine Research, **18**, 27-32.

Applications in Hydrology

Salttracer infiltration test, Brixenbachtalm 2011; picture by A. Römer

Resistivity imaging and image analysis for estimating water and solute transport across the capillary fringe in laboratory experiments

TORLEIF DAHLIN[1], BENEDICT RUMPF[1], PONTUS POJMARK[2], KRISTOFER HELLMAN[1], MAGNUS PERSSON[2] and THOMAS GÜNTHER[3]

[1] Engineering Geology, Lund University, Box 118, 211 00 Lund, Sweden.
[2] Water Resources Engineering, Lund University, Box 118, 211 00 Lund, Sweden.
[3] Leibniz Institute for Applied Geophysics, Stilleweg 2, 30655 Hannover, Germany.

Torleif.Dahlin@tg.lth.se

Introduction

The rapid population growth combined with industrialisation and urbanisation results in an increasing demand for water and threatens the livelihoods of many people. Therefore, the maintenance and protection of groundwater, the largest freshwater resource in many areas, becomes one of the biggest challenges of our times. To assure a secure water supply for drinking, industry and agriculture it is essential to avoid groundwater contaminations and therefore to understand the subsurface water movement.

The hydrological cycle and its steps between precipitation and groundwater runoff are well known and were described e.g. by FETTER (2001), or PRESS and SIEVER (2003). The saturated as well as the unsaturated zone have been subject of many water movement surveys over the last decades (see e.g. WELLINGS and BELL, 1982; MCMAHON et al., 2001; MALI et al., 2006; MIKULEC and ORFANUS, 2005). However, the influence and complexity of the region of transition between these zones, the capillary fringe, has been more or less neglected in water movement investigations. Although a lateral movement of water within the capillary fringe was recognized already by LUTHIN and DAY (1955), the role of the capillary fringe in lateral transport of water and pollutants has not completely been explained in groundwater literature. Recent studies showed that this role might be more significant than expected.

The aim of this study was to analyse the lateral movement of water and solutes in the capillary fringe, regarding the impacts of the unsaturated infiltration rate and the hydraulic gradient of the groundwater table, by using a combination of image analysis and geoelectrical monitoring.

Method Description

The model used in this study involved a 150 cm long, 49 cm high and 48 cm deep glass aquarium. It consisted of 3 basins which were separated by perforated walls covered with a permeable geotextile. The main basin had a width of 122 cm and was situated between two smaller basins, each with a width of 10 cm. The main basin was filled up to a height of 32 cm with homogeneous sand. The sand had a grain size of 0.3-0.7 mm and allowed a capillary fringe of 13 cm above the saturated zone. The thickness of the saturated zone could be regulated by changing the water levels in the two smaller basins on both sides of the aquarium. A pump system was installed to circulate water through the aquarium and regulate the gradient across the basin. The maximum

water level varied between 9 and 12 cm. Therefore it was possible to establish a three-layer regime within the aquarium, including the saturated zone, the capillary fringe and an unsaturated zone of approximately 8-10 cm on top.

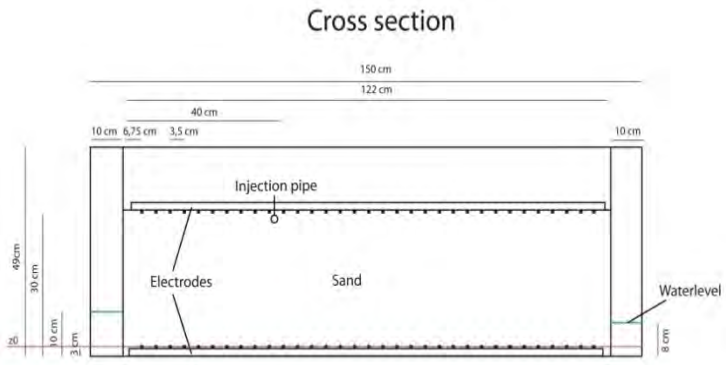

Fig. 1: Cross section of the aquarium layout.

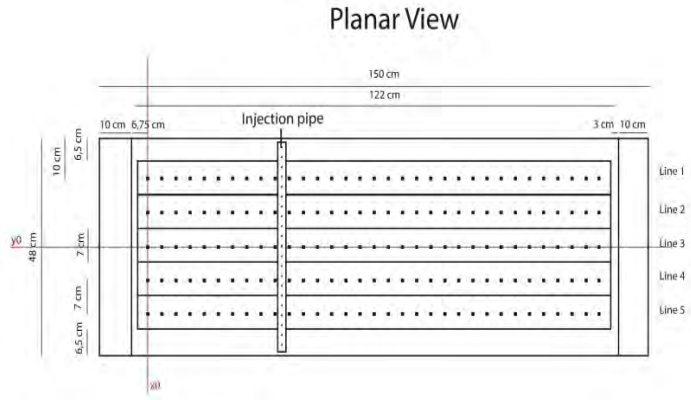

Fig. 2: Planar view of the aquarium layout.

Infiltration of the dye tracer Brilliant Blue FCF was regulated by a pump and injected through a pipe system on the sand surface. To keep the same water levels, even after the injection of the dye tracer, another pump was connected to a level gauge in the right basin, which extracted the same amount of water that was injected in form of the tracer. The cross sections of the aquarium can be seen in Figure 1 and 2, and a photograph of the laboratory setup is shown in Figure 3.

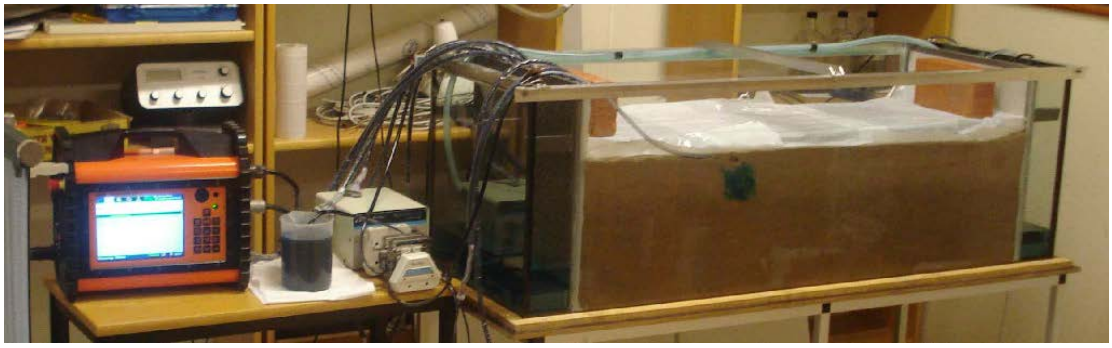

Fig. 3: Laboratory setup of the aquarium during tracer injection.

Photographs taken at a regular time interval of 3 minutes were used for the image analysis to visualize the flow paths through the front side of the aquarium. Every tenth picture, which corresponds to a time interval of 30 minutes, was modified with Adobe Photoshop CS ™ and Adobe Illustrator CS ™ to create a black and white template image. These modified template images were then combined to present the tracer distribution throughout the experiments in relation to the soil water regime within the aquarium.

An ABEM Terrameter LS was connected to a customised electrode system to measure the resistivity data during the experiments. Ten lines of electrodes were used; five in the bottom and five on top of the sand, containing a total of 320 electrodes (see Figure 1 and Figure 2). The electrode spacing was 3.5 cm. A combination of multiple-gradient array and cross-hole-dipole-dipole array was used for taking measurements along and between the electrodes on top of and in the bottom of the sand.

The Boundless Electrical Resistivity Tomography (BERT) software, which is described in GÜNTHER et al. (2006), was used to obtain a three dimensional model of the resistivity distribution within the aquarium. The dimensions and boundary conditions of the aquarium were incorporated in the model and different inversion parameters were adjusted to improve the model quality. A MATLAB ® script created a ratio between the resistivity values taken during the experiments and a background measurement which was taken before each experiment. ParaView was used to visualise the gained model with a 'blue to white' colour scheme. Blue colour represents ratio values smaller than 1, which corresponds to a decrease of resistivity. Areas with no change in resistivity (ratio = 1) were presented white.

The results of the geoelectrical monitoring were evaluated in respect to the correlation of the results of the image analysis by comparing the side views of the 3D ratio plots with the corresponding shape of the dye distribution from the image analysis.

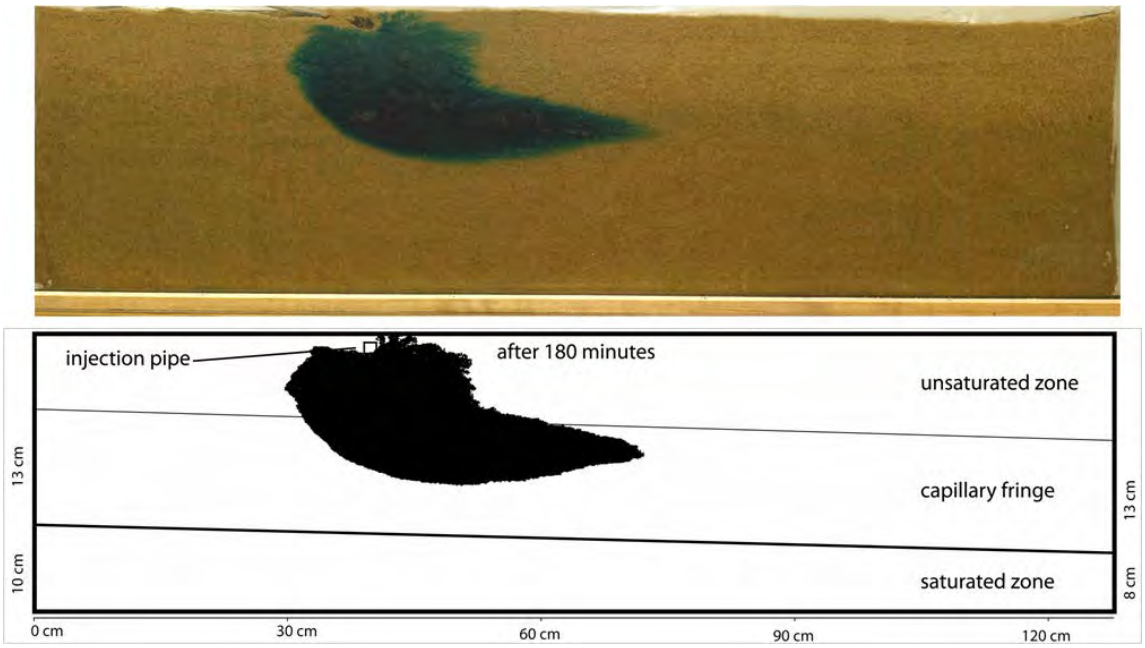

Fig. 4: Image analysis result from experiment 1 after 180 minutes, shown as photograph (upper) and outline of tracer plume from image analysis (lower).

Results and Discussion

Five experiments were conducted to investigate the lateral movement of the dye tracer within the capillary fringe of sand. All experiments revealed a strong horizontal movement across the capillary fringe, but only experiment 1 is presented here. The results of the image analysis (Fig. 4) show that the infiltrated dye tracer percolated vertically through the unsaturated zone, but moved horizontally as soon as it reached the capillary fringe, without intersecting the saturated zone.

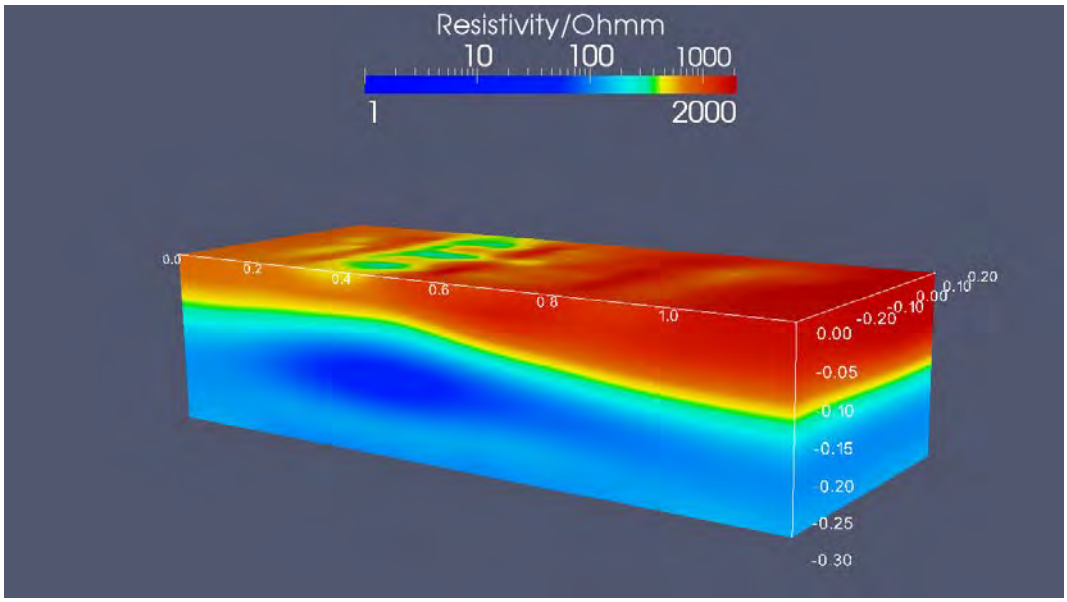

Fig. 5: 3D resistivity model from experiment 1 after 180 minutes.

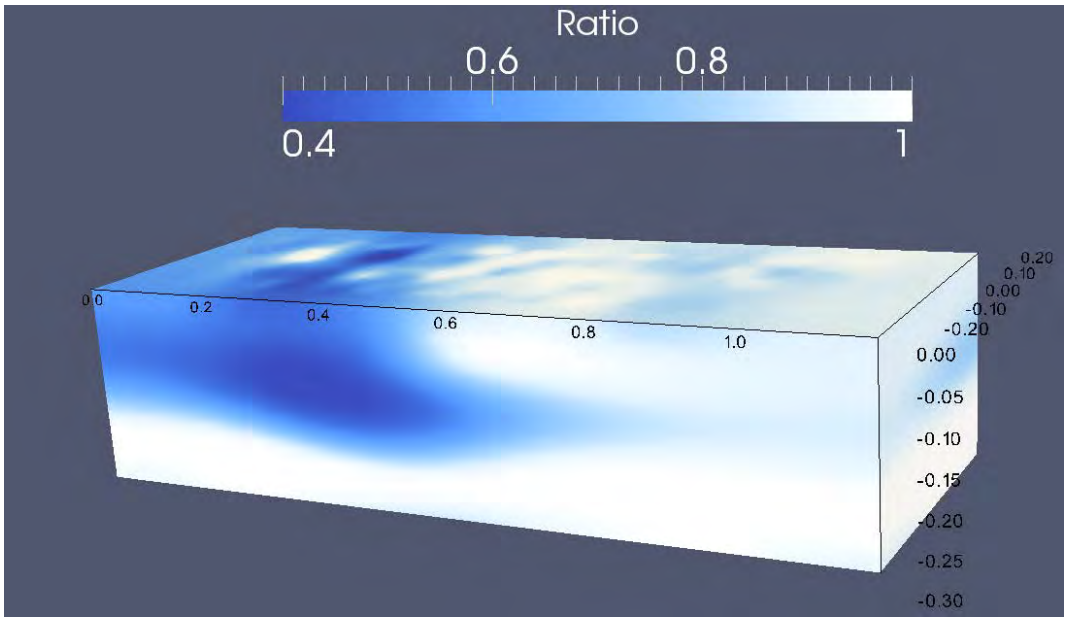

Fig. 6: 3D model of change in resistivity relative to before injection started from experiment 1 after 180 minutes.

The corresponding resistivity model resulting from inversion with BERT is shown in Fig. 5. Although the position and centre of the low resistive anomaly is easy to see, the result is clearer and easier to interpret by presenting a model of the change in resistivity since before tracer

injection started as shown in Fig. 6. An overall similarity of the shapes of the dye distributions can be seen in all experiments. In general, the plumes of the resistivity difference models are bigger than the plumes of the image analyses and seem to have smoother borders. However it must be considered that the borders of the image analysis only seem to be that sharp because of the schematic presentation method. The original photographs show a decreasing concentration of dye in the outer parts of the plume. The difference in the sizes of the plumes can be explained with the different minimal detection limits of the methods. While the resistivity analysis can measure even smallest changes caused by minimal variations in the concentration of dye, the lowest with human eyes detectable concentration of dye in sand is about 0.1 g/l.

It is interesting to note that in all experiments even if the plume of the modelled dye tracer distribution is bigger than the one seen in the image analysis, the dye never reaches the saturated zone.

Conclusions

The goal of this study was to analyse the water and solute transport across the capillary fringe using a combination of image and resistivity analysis. The comparison between the image analysis and the side views of the 3D models showed a clear correlation and therefore indicate a high reliability for the inversion. The models gave a clear impression of the dye distribution in the whole aquarium and proved that resistivity monitoring is a very useful tool for tracing subsurface processes involving change in water saturation or chemical composition.

The comparison of the experiments with different hydraulic gradients and infiltration rates revealed a high horizontal movement across the capillary fringe. In all experiments, the dye tracer moved vertically through the unsaturated zone, but moved laterally within the capillary fringe without intersecting the saturated zone.

The flow characteristics of the capillary fringe turned out to be more similar to the characteristics of the saturated zone, than to the characteristics of the unsaturated zone. If the result of this laboratory study can be verified under field conditions, it clearly shows that taking measurements and samples only in the saturated zone at contaminated sites can significantly underestimate the actual extent of the contamination plume.

Acknowledgements

The work presented here was funded by a research grant from Swedish Geological Survey.

References

FETTER, C.W., 2001: Applied Hydrogeology. – Fourth Edition, 598 S., Prentice-Hall Inc.

GÜNTHER, T., RÜCKER, C. and SPITZER, K., 2006: 3-D modelling and inversion of dc resistivity data incorporating topography – part II: Inversion. – Geophysical Journal International, **166**(2), 506-517.

LUTHIN, J.N. and DAY, P.R., 1955: Lateral flow above a sloping water table. – Proceedings of the Soil Science Society of America, **19**, 406 - 410.

MALI, N., URBANC, J. and LEIS, A., 2006: Tracing of water movement through the unsaturated zone of a coarse gravel aquifer by means of dye and deuterated water. – Environmental Geology, **51**(8), 1401-1412.

MCMAHON, P.B., DENNEHY, K.F., MICHEL, R.L., SOPHOCLEOUS, M.A., ELLET, K.M. and HURLBUT, D.B., 2001: Water Movement Through Thick Unsaturated Zones Overlying the Central High Plains Aquifer, Southwestern Kansas, 2000-2001. – USGS, Water Resources Investigations Report 03-4171, 32.

MIKULEC, V. and ORFANUS, T., 2005: Numerical Simulation of Soil Water Movement in Variably Saturated Zone of Heterogeneous Soil Profile during Growing Period of Corn. – Geophysical Research Abstracts, **7**, European Geoscience Union.

PRESS, F. and SIEVER, R., 2003: Allgemeine Geologie, Einführung in das System Erde, 3. Auflage, Spektrum.

WELLINGS, S.R. and BELL, J.P., 1982: Physical controls of water movement in the unsaturated zone. – Quarterly Journal of Engineering Geology and Hydrogeology, **15**, 235-241.

Sensitivity and resolution of ERT for soil moisture monitoring in contour hedgerow intercropping systems: a methodological analysis

SARAH GARRÉ[1, 4], THOMAS GÜNTHER[2], JAN DIELS[1] and JAN VANDERBORGHT[3]

[1] KU Leuven, Earth and Environmental Sciences, Soil and Water Management, Celestijnenlaan 200E, 3001 Leuven, Belgium
[2] Leibniz Institute for Applied Geophysics, Stilleweg 2, 30655 Hannover, Germany
[3] Forschungszentrum Juelich GmbH, Agrosphere (IBG-3), 52425 Juelich, Germany
[4] presently at Université de Liège, Gembloux Agro-Bio Tech, Passage des Déportés 2, BE-5030 Gembloux, Belgium

sarah.garre@ees.kuleuven.be

Introduction

Contour hedgerow intercropping is a simultaneous agroforestry system which involves planting hedgerows along the contour lines of a slope at a distance of 4–6 m (TANG, 2000) and is extremely effective in controlling erosion on steep slopes (LAL, 1989; CRASWELL et al., 1997; MORGAN, 2004). However, sometimes a negative impact on crop response in the alley has been observed (AGUS et al., 1997; TURKELBOOM et al., 1997; DERCON et al., 2006) due to competition. To get a more detailed understanding of the competition for water, 2- or 3-D monitoring of the water fluxes in the soil-plant-atmosphere system is necessary. Electrical resistivity tomography (ERT) may be an appropriate tool for this. The measured apparent electrical resistivity depends amongst others on soil moisture content and soil water salinity (ARCHIE, 1942; WAXMAN et al., 1968; REVIL and GLOVER, 1998; LINDE et al., 2006; LALOY et al., 2011), temperature, and in some cases on root biomass (AMATO et al., 2008; ZENONE et al., 2008; AMATO et al., 2009; AL HAGREY and PETERSEN, 2011). Changes of these variables with time, such as soil moisture changes, can thus be followed performing resistivity measurements at several times provided a good calibration relationship between electrical resistivity and the variable under consideration. In this work, we present a methodology to design an experimental ERT survey for soil moisture monitoring in the field, looking at the specific characteristics of the system under consideration and the research questions posed. The objectives are to (i) generate realistic soil moisture distributions and resulting resistivity as can be expected under a monocropping and intercropping systems, (ii) analyze the performance of different measurement arrays using measures looking at spatial variability and classical geophysical measures like e.g. recovery, coverage and resolution radius; and (iii) identify an optimal survey design to capture the generated patterns with ERT during a growing season.

Material and methods

General approach

The following approach was adopted to identify the optimal ERT survey design for studying water fluxes under two different agricultural systems. Firstly, a hydrological model is created approaching the soil, relief and climate conditions at a field site near Suan Phung, Ratchaburi

Province, Thailand. Two cases are simulated: a field plot with only maize and one with contour hedgerow intercropping with *Leucaena leucocephala L*. After a spin-up period of 30 days, the model was run for 130 days starting from maize sowing. Secondly, a pedo-physical relationship was used to convert the water content distribution of a few characteristic timeframes to a resistivity distribution. Thirdly, virtual ERT measurements were conducted by forward modeling using different measurement configurations and the simulated 2-D distribution of resistivities.
The data were inverted and the resolution and sensitivity matrix were analysed. Finally, we compared the original resistivity distributions with the inverted ones in order to obtain the model recovery. Measures for spatial variability as well as the resolution matrix, sensitivity matrix and model recovery were then used to judge the performance of the measurement arrays.

Hydrological model

The hydrological model was set up using a modified version of Hydrus2D/3D (ŠIMŮNEK et al., 1996), which allows modeling of root water uptake by two different crops simultaneously. The simulations were run on a soil cross section of 13 m length and 3 m depth with an inclination of 15%. Two cases were simulated: maize monocropping and contour hedgerow intercropping with rows of *Leucaena leucocephala*, maize and bare soil strips accounting for a few chili plants with low soil coverage. Figure 1 gives an overview of the model for the intercropping case. The soil consists of three horizons: Ap (loam), B (sandy-clay-loam) and C (clay loam) (CARSEL and PARRISH, 1988). We used the Van Genuchten model (VAN GENUCHTEN, 1980) for the hydraulic behavior of the soil and the Feddes model (FEDDES et al., 1978) for the root water uptake. Rainfall and potential reference evapotranspiration were taken from an on-site weather station for the growing season of 2009. The reference evapotranspiration for a grass reference surface was calculated for hourly time intervals using the Penman-Monteith equation (ALLEN et al., 1998) and then used to calculate the crop evapotranspiration rates. We selected three distinct timeframes of the growing season (0, 60 and 108 days after sowing) for the further analysis.

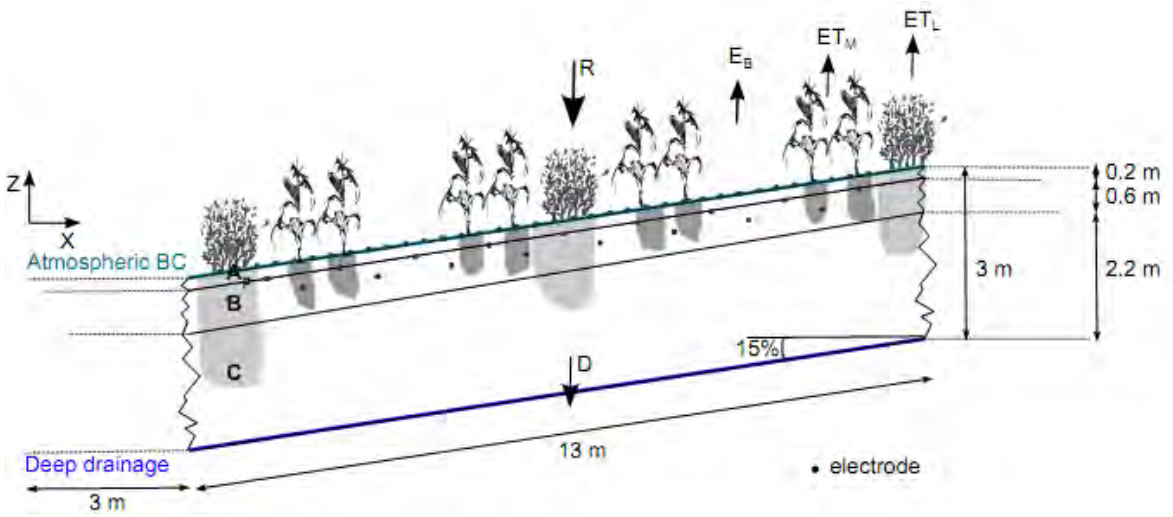

Fig. 1: Hydrological model set-up with top and bottom boundary conditions (BC) for a field plot with contour hedgerow intercropping with Leucaena, maize and bare soil strips. Three soil horizons are indicated on the scheme: Ap (0-0.2m), B (0.2-0.8m),C (0.8-3m). Symbols: ETM: evapotranspiration of maize rows, ETL: evapotranspiration of leucena strips, EB: evaporation from bare soil strip, R: rainfall, D: drainage.

Pedo-physical model

The water content of the selected timeframes was converted to a conductivity (EC) distribution using one single pedo-physical relationship for all horizons. We used the parameters of the pedo-physical model of the Bv1 horizon of GARRÉ et al. (2011) for a silty soil located in Merzenhausen, Germany. The pedophysical model is given by:

$EC = a.WC^n + b$,

with *EC* the bulk electrical conductivity (*ρ=1/EC*), *WC* the volumetric water content and *a,b,n* fitting parameters. The parameters used for our pedo-physical model are *a* = 1.20495 S.m^{-1}, *b* = 0.0001 S.m^{-1}, *n* = 3.4314.

Experimental design

The main water fluxes in the soil on a steep slope with crop rows following the contour lines are expected to be vertical, due to evapotranspiration, and along the slope, due to subsurface flow. A plane of surface and subsurface electrodes along the slope, generating a 2-D image of the subsurface along the slope, should be sufficient to capture these fluxes. On the subsurface, 36 electrodes are placed 0.33 m apart. At 0.25 and 0.50 m depth, nine electrodes were placed at each depth level with a horizontal separation of 1.32 m. Four classical measurement configurations were selected based on their distinct sensitivity distributions (Loke et al., 1996): the Wenner-array, the dipole-dipole array, the pole-dipole array and a combination of the dipole-dipole and the Wenner array. For each array, we considered data sets using only surface electrodes and datasets including also subsurface electrodes in order to assess the increase in data information due to deeper electrodes.

We conducted a smoothness-constrained inversion as in GÜNTHER et al. (2006) independently for each of the three timesteps. Several measures can be used to assess the quality of the information obtained by inversion of the measurements produced by a certain electrode array. We calculated the cumulative sensitivity (e.g. FURMAN et al., 2003; GÜNTHER, 2004), the resolution radius (FRIEDEL, 2003) and the model recovery (results not shown here). In hydrological studies, the main interest is often to capture the spatial patterns which are present in the soil moisture distribution. In order to test the performance of the different arrays to capture this spatial variability, we defined two criteria: an adjusted coefficient of determination (THEIL, 1971; p. 164, p. 175-178) and the spatial correlation using a semivariogram for each of the tested arrays.

Results

1-D water content

Figure 2 shows the 1-D water content (WC) profiles for the mono- and intercropping case at t = 0, 60 and 108 days for a profile of 2m width and 3 m depth in the middle of the simulated domain. In general, ERT predicts the 1-D profiles well. However, in the areas of sudden resistivity contrasts, the inverted profiles look smoothened and do not follow the jumps. ERT is also capable of measuring the differences between the mono- and the intercropping case. The different arrays give way to similar 1-D profiles, whereas in most cases, the combination of dipole-dipole and Wenner and the pure dipole-dipole measurements are closest to the model curve. As for the 1D profiles, there is no systematic difference between the arrays with deeper electrodes (All) and those with only surface electrodes (OS), although below -2m, many of the OS arrays end up further from the model profile than the All arrays.

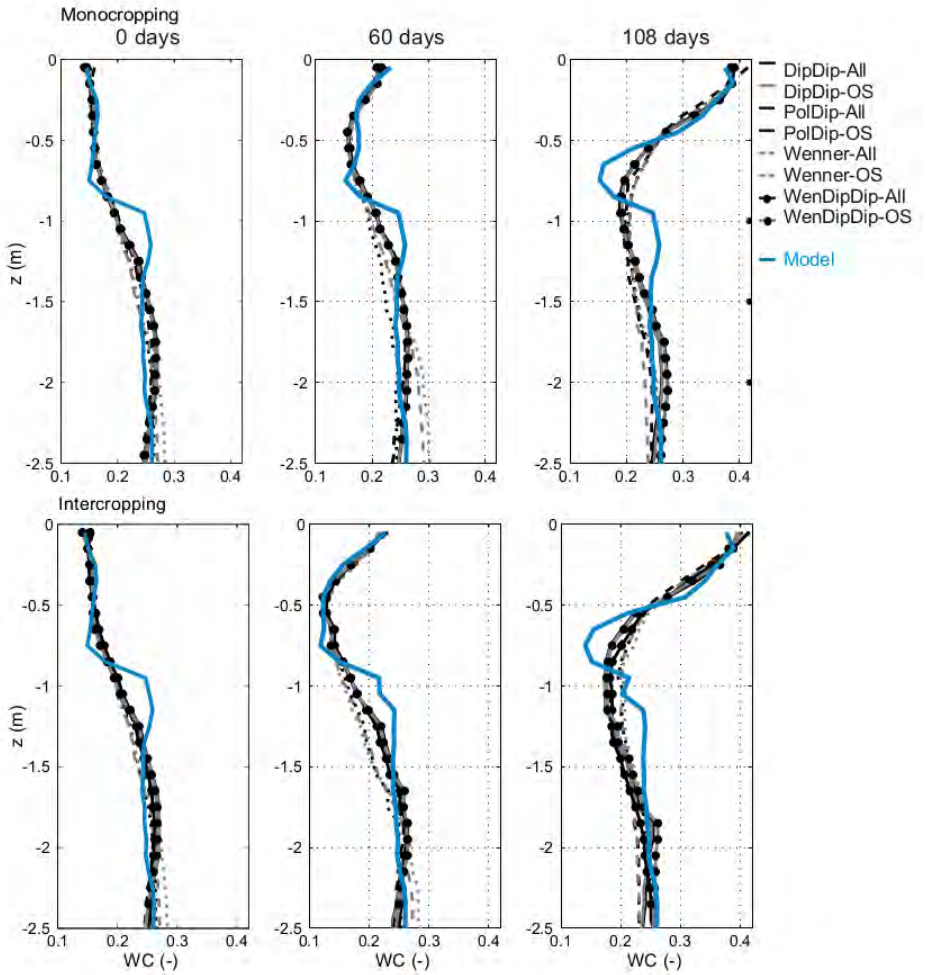

Fig. 2: 1-D water content profiles for the mono- and intercropping case at t= 0, 60 and 108 days for a profile of 2m width and 3 m depth in the middle of the simulated domain. The simulated values are represented by the thick, blue line. DipDip = dipole-dipole, PolDip = pole-dipole, WenDipDip = combination of Wenner & Dipole-dipole. Electrode arrays using only surface electrodes are marked by OS.

Spatial variability

Generally, the spatial variability of the inversion results is lower than the one of the synthetic model. All arrays capture a high variability between 0 and -1m and a decreased variability beneath 2m. For z < -1.75 m, the standard deviation was underestimated by almost all arrays. Using the WenDipDip array, the variability in 0-0.10 m was higher for the inverted WC than for the original model.

To calculate the adjusted coefficient of determination (R^2) for each electrode array under consideration, for each of the three times and for the mono- and the intercropping case, we excluded all mesh cells with a normalized coverage (log10) smaller than 0.8 from the computation. The dipole-dipole array and the combination of Wenner and dipole-dipole measurements give the best result in almost all cases and times. The pure Wenner array is inferior to the others except for the last timestep. The additional use of deep electrodes improves the result most of the time (data not shown).

Another way to look at spatial variability is the semivariogram. As we know from the previous measures that the highest spatial variability is present between 0 and -1 m depth, we used only this part of the soil region to compute the semivariogram. Figure 3 shows the semivariograms for both the mono- and the intercropping case at t = 60 days using 70 lag distances of 0.1 m. In the

monocropping case a clear periodicity can be seen in the model semivariogram, caused by the presence of maize plant roots at regular intervals of about 0.75 m. A similar, but more complex pattern represents the intercropping case. As the simulation contains not only maize, but also a Leucaena root zone and pieces of bare soil, the effects of different structures are visible. E.g. the distance between two Leucaena hedges is visible in the semivariogram (6 m). All electrode arrays produce a similar, but smoothened or flattened semivariogram. The sill of the inverted semivariograms, which is the limit of the semivariogram tending to infinity lag distances, is lower than the modeled one. The combination of Wenner and dipole-dipole arrays gives the best result. The Wenner array has the most difficulties to reproduce the spatial structure of both cases, which emerges from the very small amplitude of the periodicity in the semivariogram.

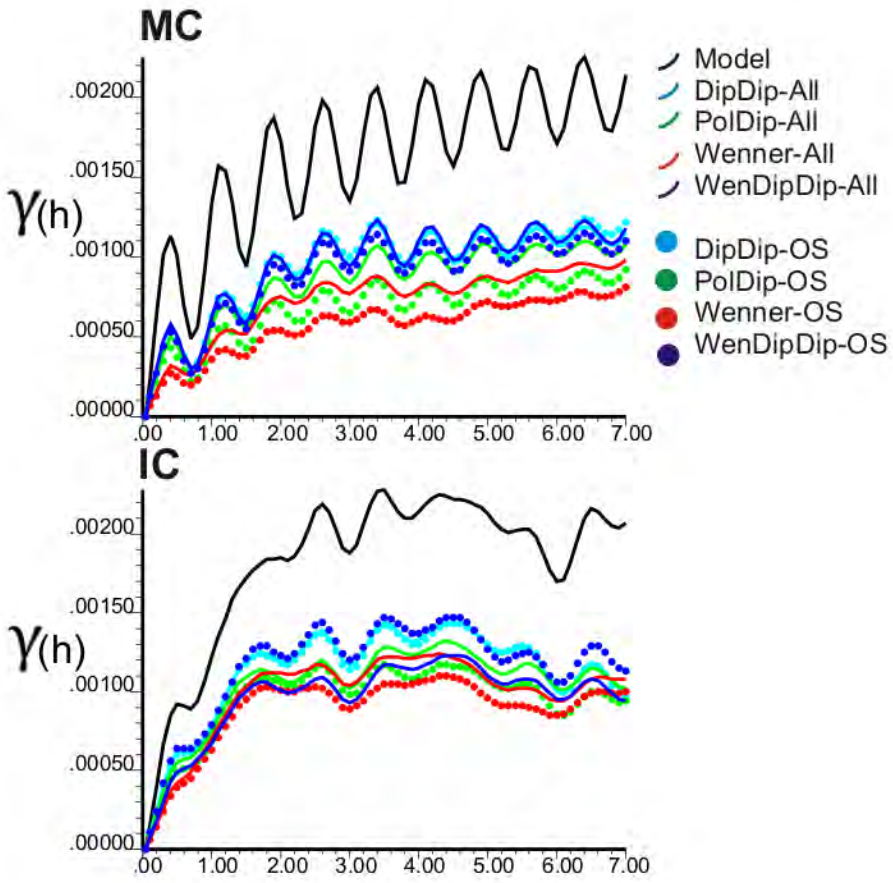

Fig. 3: Semivariograms of the water content (WC) of the synthetic and the inverted WC for the monocropping (MC) and intercropping (IC) case.

Conclusions

The general course of the 1-D WC profiles was well reproduced by the different ERT measurements. The largest deviations occurred where sharp jumps in water content occurred (boundary between two soil horizons, infiltration fronts, etc.). The resulting contrasts pose an extra difficulty for smoothness-constrained inversion of the resistivity data. All electrode arrays produce similar results in terms of 1-D profiles. The extent of the spatial variability is generally a little bit underestimated and smoothened by the ERT inversion, but the spatial structures remain present. The spatial variability is best reproduced by an array combining Wenner and dipole-

dipole quadrupoles, probably since it combines the resolving power for horizontal structures of the Wenner array with the resolving power for vertical structures of the dipole-dipole array. The standard deviations and consequently the sill of the semivariogram were underestimated more strongly by the Wenner and the pole-dipole array than by the others. We can conclude that ERT can be used to observe effects of cropping systems on soil moisture distribution. A major disadvantage of the classical smoothness-constrained inversion is the fact that sharp resistivity transitions are not well reproduced. The virtual measurements showed that it is possible to retrieve differences between 2 cropping systems on the same soil and under the same climatic conditions. Under wetter conditions, it might be difficult to distinguish single root water uptake regions below the rows by observing the spatial distribution of the data. Here, the use of a semivariogram might be the line to take, since it will reveal spatial structures which are not always clearly visible by the bare eye.

References

AGUS, F., CASSEL, D.K. and GARRITY, D.P., 1997: Soil-water and soil physical properties under contour hedgerow systems on sloping oxisols. – Soil and Tillage Research, **40**, 185-199.

AL HAGREY, S.A. and PETERSEN, T., 2011: Numerical and experimental mapping of small root zones using optimized surface and borehole resistivity tomography. – Geophysics, **76**, G25-G35.

ALLEN, R.G., PEREIRA, L.S., RAES, D. and SMITH, M., 1998: Crop evapotranspiration – Guidelines for computing crop water requirements. – In: N.R.M.a. Environment (ed.) FAO, Rome.

AMATO, M., BASSO, B., CELANO, G., BITELLA, G., MORELLI, G. and ROSSI, R., 2008: In situ detection of tree root distribution and biomass by multi-electrode resistivity imaging. – Tree Physiology, **28**, 1441-1448.

AMATO, M., BITELLA, G., ROSSI, R., GÓMEZ, J.A., LOVELLI, S. and GOMES, J.J.F., 2009: Multi-electrode 3D resistivity imaging of alfalfa root zone. – European Journal of Agronomy, **31**, 213-222.

ARCHIE, G.E., 1942: The electrical resistivity log as an aid in determining some reservoir characteristics. – Transactions of the American Institute of Mining, Metallurgical, and Petroleum Engineers, **146**, 54-67.

CARSEL, R.F. and PARRISH, R.S., 1988: Developing joint probability distributions of soil water retention characteristics. – Water Resources Research, **24**, 755-769.

CRASWELL, E.T., SAJJAPONGSE, A., HOWLETT, D.J.B, and DOWLING, A.J., 1997: Agroforestry in the management of sloping lands in Asia and the Pacific. – Agroforestry Systems, **38**, 121.

DERCON, G., DECKERS, J., POESEN, J., GOVERS, G., SÁNCHEZ, H., RAMÍREZ, M., VANEGAS, R., TACURI, E. and LOAIZA, G., 2006: Spatial variability in crop response under contour hedgerow systems in the Andes region of Ecuador. – Soil and Tillage Research, **86**, 15-26.

FEDDES, R.A., KOWALIK, P., and ZARADNY, H., 1978: Simulation of field water use and crop yield. – Simulation Monographs. 189 pp., PUDOC, Wageningen.

FRIEDEL, S., 2003: Resolution, stability and efficiency of resistivity tomography estimated from a generalized inverse approach. – Geophysical Journal International, **153**, 305-316.

FURMAN, A., FERRE, T.P.A. and WARRICK, A.W., 2003: A Sensitivity Analysis of Electrical Resistivity Tomography Array Types Using Analytical Element Modeling. – Vadose Zone Journal, **2**, 416-423.

GARRÉ, S., JAVAUX, M., VANDERBORGHT, J., PAGES, L. and VEREECKEN, H., 2011: Three-Dimensional Electrical Resistivity Tomography to Monitor Root Zone Water Dynamics. – Vadose Zone Journal, **10**, 412-424.

GÜNTHER, T., 2004: Inversion Methods and Resolution Analysis for the 2D/3D Reconstruction of Resistivity Structures from DC Measurements. – PhD Thesis University of Mining and Technology, Freiberg (Germany).

GÜNTHER, T., RUECKER, C. and SPITZER, K., 2006: Three-dimensional modelling and inversion of DC resistivity data incorporating topography - II. Inversion. – Geophysical Journal International, **166**, 506-517.

LAL, R., 1989: Agroforestry systems and soil surface management of a tropical alfisol. – Agroforestry Systems, **8**, 97-111.

LALOY, E., JAVAUX, M., VANCLOOSTER, M., ROISIN, C., and BIELDERS, C.L., 2011: Electrical Resistivity in a Loamy Soil: Identification of the Appropriate Pedo-Electrical Model. – Vadose Zone Journal, **10**(3), 1023-1033

LINDE, N., BINLEY, A., TRYGGVASON, A., PEDERSEN, L.B. and REVIL, A., 2006: Improved hydrogeophysical characterization using joint inversion of cross-hole electrical resistance and ground-penetrating radar traveltime data. – Water Resourources Research, 42, W12404, doi:10.1029/2006WR005131.

LOKE, M.H. and BARKER, R.D., 1996: Practical techniques for 3D resistivity surveys and data inversion. – Geophysical Prospecting, **44**, 499-523.

MORGAN, R.P.C., 2004: Soil Erosion and Conservation. – 3rd Edition, 320 S., Wiley-Blackwell.

REVIL, A. and GLOVER, P.W.J., 1998: Nature of surface electrical conductivity in natural sands, sandstones, and clays. – Geophysical Research Letters, **25**, 691-694.

ŠIMŮNEK, J., ŠEJNA, M. and VAN GENUCHTEN, M.T., 1996: The Hydrus-2D software package for simulating water flow and solute transport in two-dimensional variably saturated media. Version 1.0. IGWMC-TPS – 53. International Ground Water Modeling Center, Colorado School of Mines, Golden, Colorado.

TANG, Y., 2000: Manual on contour hedgerow intercropping technology. – International Centre for Integrated Mountain Development (ed.), Katmandu, Nepal p. 31.

THEIL, H., 1971: Principles of Econometrics. – 736 p., New York.

TURKELBOOM, F., POESEN, J., OHLER, I., VAN KEER, K., ONGPRASERT, S. and VLASSAK, K., 1997: Assessment of tillage erosion rates on steep slopes in northern Thailand. – Catena, **29**, 29-44.

VAN GENUCHTEN, M.T., 1980: A closed form equation for predicting the hydraulic conductivity of unsaturated soils. – Soil Science Society of America Journal, **44**, 892-898.

WAXMAN, M.H., and SMITS, L.J.M., 1968: Electrical Conductivities in Oil-Bearing Shaly Sands. – Society of Petroleum Engineers Journal, **8(2)**, 107-122.

ZENONE, T., MORELLI, G., TEOBALDELLI, M., FISCHANGER, F., MATTEUCCI, M., SORDINI, M., ARMANI, A., FERRE, C., CHITI, T. and SEUFERT, G., 2008: Preliminary use of ground-penetrating radar and electrical resistivity tomography to study tree roots in pine forests and poplar plantations. – Commonwealth Scientific and Industrial Research Organization, Collingwood, Australia.

SP Monitoring at a Sea Dyke

HYE-JIN KANG[1], IN-KY CHO[1], JUNG-HO KIM[2], HWAN-HO YONG[3], SANG-SUN YI[3], YOUNG-GYU PARK[3] and YOUNG-DUK KWEON[3]

[1] Department of Geophysics, Kangwon National University, Chuncheon, Korea
[2] Korea Institute of Geology, Mining and Materials, Daejeon, Korea
[3] Korea Rural Community Corporation, Eiwang, Geynggido, Korea

choik@kangwon.ac.kr

Introduction

SP has been widely used for the investigation of anomalous seepage in dams, sea dykes and waste disposal sites (BOGOSLOVSKY and OGILVY, 1971; OGILVY and BOGOSLOVSKY, 1969; SONG et al., 2005; TITOV et al, 2000). In this case, major origin of SP is the streaming potential generated by the flow of seepage water. Generally, it is known that SP voltage increases as seepage increases. In the sea dyke, leakage flow is very strong because of the great difference between rise and fall of the tide, which leads to great SP anomaly. However, it is really hard to define anomalous seepage zones from the SP profile measured at a particular time, since it fluctuates severely. Moreover, SP time sequences also demonstrate severe fluctuations at most of stations. To overcome this problem, we propose a simple but effective interpretation method of SP monitoring data.

SP monitoring

SP voltage in sea dykes is mainly generated by the flow of seepage water. Thus, SP voltage caused by subsurface current is directly related to the amount of seeping water. SP changes in time mean changes in current flow in the subsurface if changes in resistivity structure are negligible. The resistivity of the subsurface medium is highly variable, depending on the porosity, water content, temperature, etc. In the strict sense, the resistivity of subsurface changes when there are some changes in the flow of seepage water. In such a case, the interpretation of SP monitoring data becomes pretty hard because it requires the distribution of resistivity. This means that resistivity survey is additionally conducted to quantitatively interpret the SP monitoring data. If we assume that changes in resistivity structure with time are negligible, the problem becomes surprisingly simple.

From ohm's law, the potential is given as the product of current *I* and resistance *R*.

$$V = I \cdot R \tag{1}$$

If there is no change in resistance, potential change, ΔV, between time t_1 and t_2 is just the product of current change with time and resistance. Then, current change in time is directly proportional to potential change.

$$\Delta V = V_{t_2} - V_{t_1} \approx I_{t_2} \cdot R - I_{t_1} \cdot R = \Delta I \cdot R \tag{2}$$

From equation (2), SP voltage changes in time directly indicate the change in subsurface current caused by the changes in the flow of seepage water. Therefore, changes in SP voltage with time give helpful information to identify the leakage zones in sea dykes.

Data acquisition

SP voltages were monitored at a sea dyke that is located at the southern part of Korean peninsula. The dyke is 1528 m long and 6.6 m high and was constructed in 1997. First, we installed permanent electrodes at the flat step in the land side of the sea dyke. Instead of non-polarizing electrode, we used a stainless steel stake as an electrode because of the problem in maintenance. The station spacing was set to 20 m and the total length of the survey line was 1300 m. SP data were measured every six hours and transferred to office data base through CDMA communication.

Data processing

SP monitoring data were acquired from Feb. 8., 2011, 00:00, to Feb. 13., 2011, 12:00, measured every six hours at 62 stations and they are shown in Fig. 1. There are severe fluctuations with time at most of stations. Also, every profile at a particular time shows rapid changes. Thus it is impossible to identify anomalous seepage zone from both the profiles and time sequences.

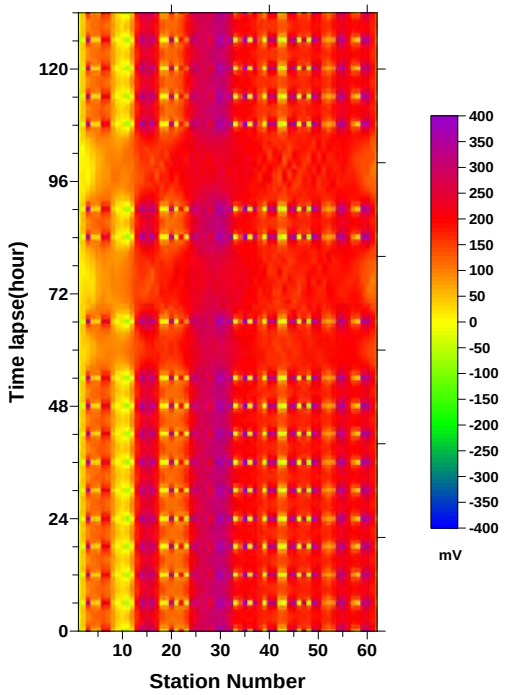

Fig. 1: SP monitoring data were acquired from Feb. 8., 2011, 00:00 to Feb.13., 2011, 12.00 measured every six hours at 62 stations.

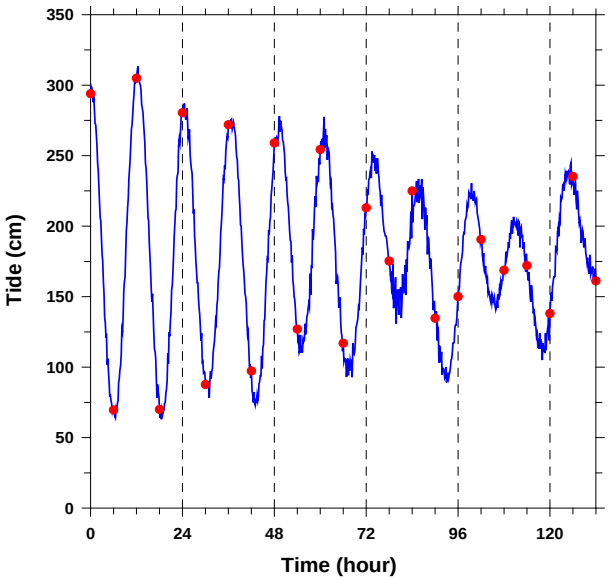

Fig. 2: Variation of tide levels with time at the sea measured every six houdyke. Red circles indicate SP measuring times.

Fig. 2 represents the tide level with time at the sea dyke. There is great difference between rise and fall of the tide: it reaches maximum 250 cm. The direction of seepage flow and the seepage rate are different at rise and fall of the tide. The amount of seepage water is closely related to the tide level: The higher tide level, the more seepage water. Thus, it is efficient to measure SP voltage when the tide level reaches maximum or minimum. In this case, the period of tide is smaller than 12 hours and SP was measured every six hours. Thus measurement time does not

exactly match rise or fall time of the tide. At some times, there is no difference of tide levels between two adjacent measurements with time. In such a case, SP changes with time will be negligible and we may fail to find out the leakage zones.

Fig. 3 shows SP changes with time. For comparison, we added the tide level at the left panel. Most of the stations show negligible SP changes with time. However, station no. 23 shows greater SP change with time, having the positive and negative values repeatedly. The station is considered to be possibly a leakage zone. Station no. 38 seems to be another possible leakage zone although SP changes are weaker than those at station no. 23. As was mentioned, SP voltage should become great when the tide level reaches maximum or minimum. Correspondingly, SP changes in time also have to be great at the rise or fall of tide. However, there is no clear correlation between SP change and tide. This somewhat strange phenomenon will be studied in future.

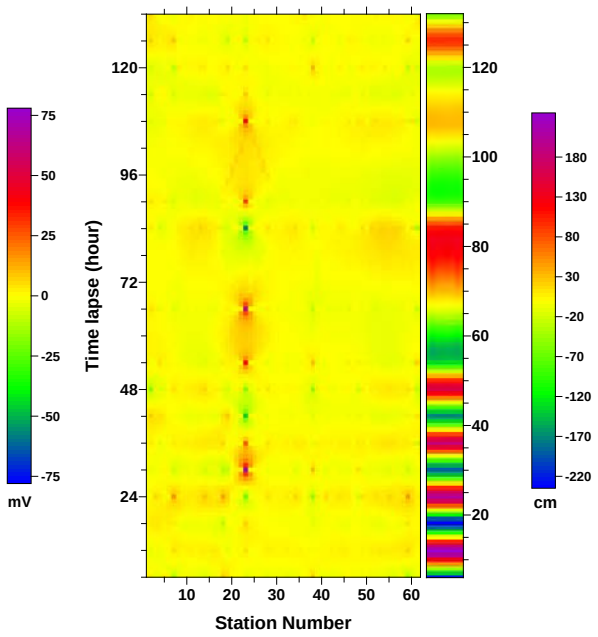

Fig. 3: SP changes with time. Tide level is added at the left panel for comparison

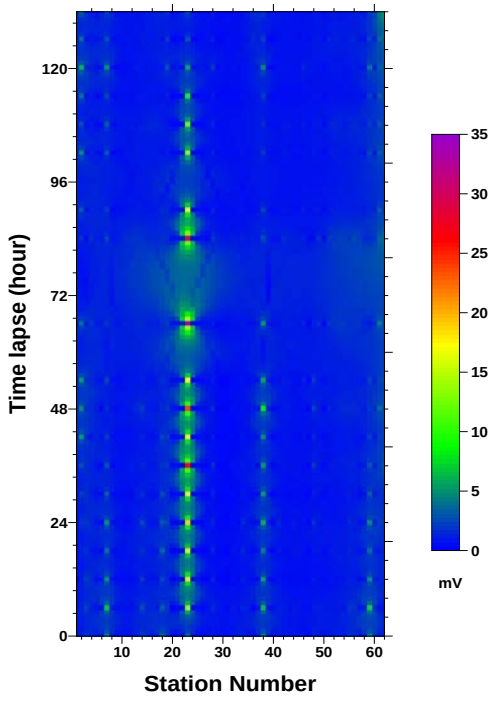

Fig. 4: RMS SP changes with time.

Calculation of SP changes from just two adjacent readings with time is very risky, especially when there are outliers. To suppress the outlier or noise, it looks to be more reliable to use SP changes calculated from RMS value of a moving time window. RMS SP changes from the SP data contained in the time window can be calculated from the following formula:

$$\Delta V_i = \frac{1}{2n-1}\sqrt{\sum_{j=-n}^{n}(V_{i+j}-V_i)^2}, \qquad (i=1,2,\cdots,N), \qquad (3)$$

where ΔV_i is the SP change at the *i*th time. *n* and *N* indicate the size of time window and the total number of measurements with time, respectively. Fig. 4 represents RMS SP changes with time. We can find much more clear SP anomalies at the station no. 23 and 38. But the sign of RMS SP change is always positive.

We carried out visual inspection at the sea dyke and found some symptoms of leakages near the station no. 23 and 38, such as the loss and loosening of riprap at the sea side and formation of large openings caused by the loss of riprap.

Conclusions

Simple but effective interpretation method of SP monitoring data is proposed. SP changes with time are directly related to changes in seepage flow in sea dykes if changes in resistivity structure are negligible with time. Thus, leakage zones in a sea dyke can be effectively identified from the strong SP changes with time. Applying this method, two suspicious leakage zones were detected at a sea dyke and symptoms of leakage were found from afterward visual inspection. However, SP monitoring data does not show some correlation with tide. This should be studied in the future work.

Acknowledgements

This research was supported by Basic Science Research Program through the National Research Foundation of Korea (NRF) funded by the Ministry of Education, Science and Technology (2010-0002440).

References

BOGOSLOVSKY, V.A. and OGILVY, A.A., 1971: Application of geophysical methods for studying the technical status of earth dam. – Geophysical Prospecting, **20**, 109-117.

OGILVY, A.A. and BOGOSLOVSKY, V.A., 1969: Geophysical studies of water leakages from reservoirs. – Geophysical Prospecting, **17**, 36-63.

SONG, S.H., SONG, Y.H. and KWON, B.D., 2005: Application of hydrogeological and geophysical methods to delineate leakage pathways in an earth fill dam. – Exploration Geophysics, **36**, 92-96.

TITOV, K., LOUKHMANOV, V. and POTAPOV, A., 2000: Monitoring of water seepage from a reservoir using resistivity and self polarization methods: case history of the Petergoph fountain water supply system. – First Break, **18**, 431-435.

3D crosshole ERT for aquifer characterization and monitoring of infiltrating river water

ILARIA COSCIA[1], STEWART GREENHALGH[1], LASSE RABENSTEIN[1], NIKLAS LINDE[2], ALAN GREEN[1], THOMAS GÜNTHER[3] and TOBIAS VOGT[4]

[1] Institute of Geophysics, ETH Zurich, Switzerland.
[2] Institute of Geophysics, University Lausanne, Switzerland.
[3] Leibniz Institute for Applied Geophysics, Hannover, Germany.
[4] Swiss Federal Institute for Aquatic Science and Technology, Dübendorf, Switzerland.

rabenstein@aug.ig.erdw.ethz.ch

We have investigated the hydrogeological properties and hydrological responses of a productive aquifer in northeastern Switzerland. For this purpose we used 3D crosshole electrical resistivity tomography (ERT) to define the main lithological structures within the aquifer (through static inversion) and to monitor the water infiltration from an adjacent river. During precipitation events and subsequent river flooding, the river water resistivity increases. As a consequence, the electrical characteristics of the infiltrating water can be used as a natural tracer to delineate preferential flow paths and flow velocities. The monitoring system comprises 18 boreholes each equipped with 10 electrodes straddling the entire thickness of the gravel aquifer. A multichannel resistivity system programmed to cycle through various four-point electrode configurations of the 180 electrodes in a rolling sequence allows the measurement of ~15,500 apparent resistivity values every seven hours on a continuous basis. The 3D static ERT inversion of data acquired under stable hydrological conditions provides a base model for time-lapse inversion studies and the means to investigate the resolving capability of our acquisition scheme.

The analysis of the ERT time series highlight the presence of several time-varying phenomena which simultaneously affect, and with comparable intensity, the measured apparent resistivity. In particular these are river water electrical resistivity variations and groundwater table fluctuations. In addition to these primary effects, the seasonal water temperature trend creates a non-negligible drift in the data. The need to correct for temperature and water height variations on the apparent resistivity (leaving only the groundwater resistivity component of the signal) led us to develop a deconvolution filtering method to separate the effects.

Our time-lapse resistivity models indicate rather complex flow patterns as a result of spatially heterogeneous bank filtration and aquifer heterogeneity. Time series of the reconstructed resistivity models match groundwater electrical resistivity data recorded on borehole loggers in the upper and middle parts of the aquifer, whereas the resistivity models display smaller variations and delayed responses with respect to the logging data in the lower part. This study demonstrates that crosshole ERT monitoring of natural electrical resistivity variations of river infiltrate can be used to image and quantify 3D bank filtration and aquifer dynamics at a high spatial resolution.

A salt tracer test monitored with surface ERT to detect preferential flow and transport paths in fractured/karstified limestones

TANGUY ROBERT[1], DAVID CATERINA[1], J. DECEUSTER[2], OLIVER KAUFMANN[2] and FRÉDÉRIC NGUYEN[1]

[1] University of Liege, Bât. B52/3, Chemin des Chevreuils 1, B-4000 Liège, Belgium.
[2] University of Mons, Belgium.

tanguy.robert@ulg.ac.be

Abstract

In hardrock aquifers, fractured zones constitute adequate drinking water exploitation areas but also potential contamination paths. One critical issue in hydrogeological research is to identify, characterize and monitor such fractured zones at a representative scale. A tracer test monitored with surface electrical resistivity tomography (ERT) could help delineating such preferential flow paths and estimating dynamic properties of the aquifer. However, multiple challenges such as the lower resolution of surface ERT compared to cross-hole ERT, the finite time that is needed to complete an entire data acquisition or the strong dilution effects exist. We conducted a natural gradient salt tracer test in fractured limestones. To account the high transport velocity, we injected the salt tracer continuously during four hours at a depth of 18 m. We monitored its propagation with two parallel ERT profiles perpendicular to the groundwater flow direction. Concerning the data acquisition, we always focused on the data quality over temporal resolution. We performed the experiment twice to prove its reproducibility by increasing the salt concentration in the injected solution (from 38 to 154 g/l). This paper focuses on how we faced every challenge to delineate a preferential flow and solute transport path in a typical calcareous valley of South Belgium and on the estimation of the transport velocity (more than 240 m/day). In this complex environment, we imaged a clear tracer arrival in both ERT profiles and for both tests. Applying filters (with a cut-off on the relative sensitivity matrix and on the background resistivity changes) was helpful to isolate the preferential flow path from artifacts. Regarding our findings, our approach could be improved to perform a more quantitative experiment. Indeed, with a higher temporal resolution, the estimated value of the transport velocity could be narrowed allowing the estimation of the percentage of tracer recovery.

Monitoring of short term geoelectric tracer experiments to investigate the shallow interflow in small alpine micro-catchments

ALEXANDER RÖMER[1], GERHARD BIEBER[1], BIRGIT JOCHUM[1],GERHARD MARKART[2] and KLAUS KLEBINDER[2]

[1] Geological Survey of Austria, Neulinggasse 38, 1030 Wien.
[2] BFW, Institut für Naturgefahren, Hofburg 1, 6020 Innsbruck.

alexander.römer@geologie.ac.at

Preferential subsurface runoff processes in soil and the geological substrate are still poorly understood at different scales. Dominant runoff processes in alpine catchments due to extreme precipitation can be analyzed either by field experiments or model simulations. But only a combination of both approaches will bring a sufficient insight in the characteristic of interflow processes. At the moment only few models are available, enabling considerations of soil and substrate characteristics in a near process manner. But for routine applications in flood estimation in practice, easy to use precipitation runoff models, describing runoff processes close to reality, are urgently needed. Therefore a step to a solution for bridging the knowledge deficits between plot scale and catchment scale as well as the requests of the practitioners in precipitation/runoff modeling is necessary.

Within the still ongoing project "Assessment of bandwidths of shallow interflow in alpine catchments (SHALLOW INTERFLOW)" financed by the Austrian Academy of Science (ÖAW), Commission of Hydrology, investigations on the interdependency of precipitation and storage capacity / near surface runoff potential of different groups of substrates in the Eastern Alps by use of a combination of different investigation methods in the field have been carried out so far in three catchment areas of the eastern Alps. For rain simulation, a transportable spray irrigation installation for large plots (50 m² up to 1200 m²) for simulating long term rain events was used to generate long term rain events on representative geological substrates of the Eastern Alps at four different test sites.

The locations of the test sites are depicted in Figure 1. During the field experiments interflow velocities are measured with

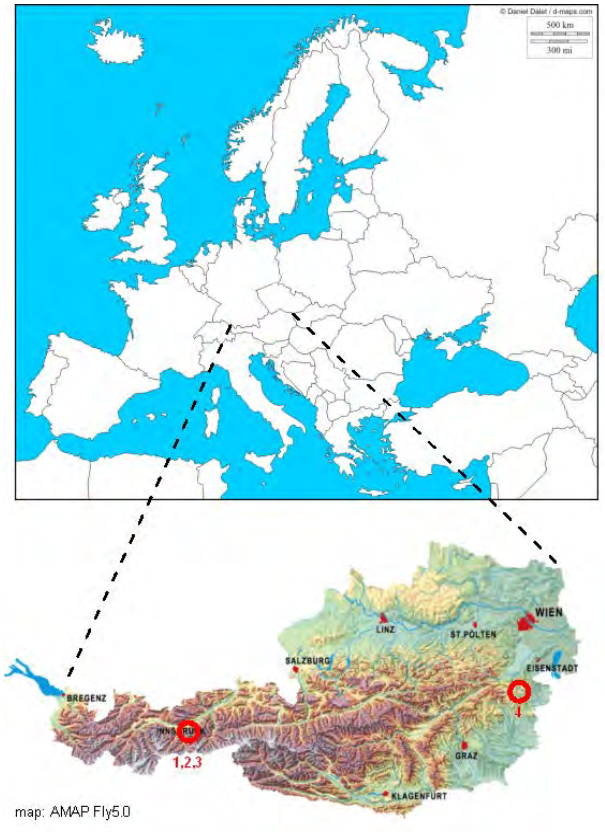

Fig. 1: Location of test sites in Austria.

different measuring devices (TDR-waveguides, FD-probes, geoelectrics, changes of conductivity in antecedent water courses, and others) for the assessment of bandwidths of lateral and vertical conductivity during and after long-lasting rainfall. In this study the bandwidth of near surface interflow and subsurface water flow has been investigated on different hillslope complexes at the military training centre Lizum/Walchen in Tyrol (test sites 1,2,3) and in a region in Lower Austria (test site 4). The experimental layout is exemplified in Figure 2 (test site 1, 2, 3).

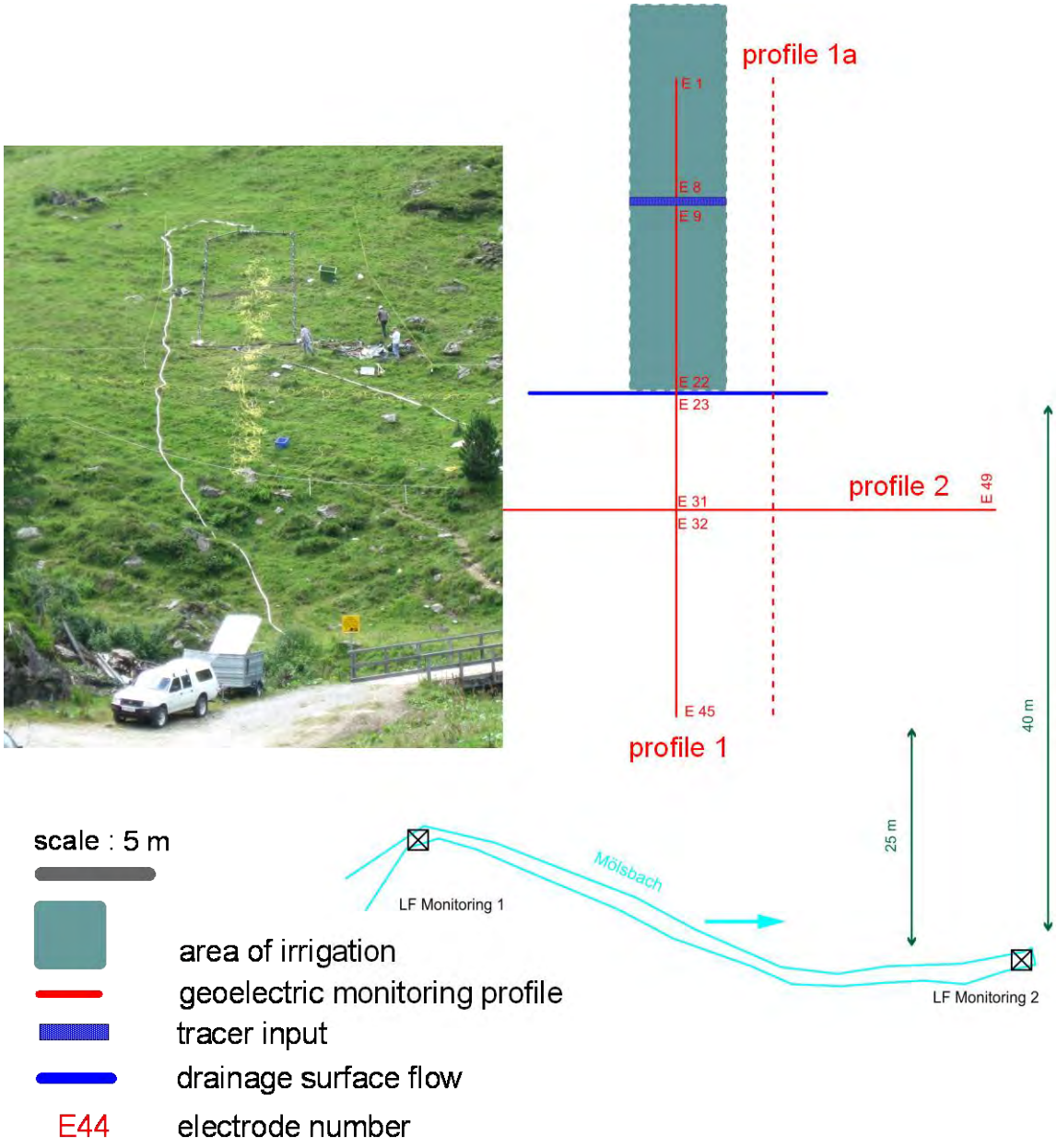

Fig. 2: Exemplified experimental layout (here: test site 1) for the assessment of shallow interflow velocities.

High amounts of precipitation (about 250 mm) – partially in combination with salt tracer - have been applied within a few days with the transportable spray irrigation. Surface runoff was registered and changes in soil moisture were measured with buried TDR-waveguides – arranged in four profiles from 15 cm to 115 cm soil depth in maximum. Expansion of the wetting front has been documented by different geoelectric profiles, which were measured periodically before,

during and after the rain simulation experiments. Figure 3 illustrates the results of geoelectric monitoring (difference plots to base measurement) of electrical conductivity for test site 1. The first profile at 09:53 shows no difference to the first measurement at 14.07. 08:54, before precipitation and salt tracer. After salt tracer input and irrigation for few hours the effect of the salt tracer movement is obvious. Also the short-term triggering of the interflow water course after restarting the precipitation is clearly visible. After 6:43 hours after the last irrigation, the effect of the salt tracer almost disappeared and is, aside from the lower part of the slope, only observable at the position of the trench and the drainage of the surface flow.

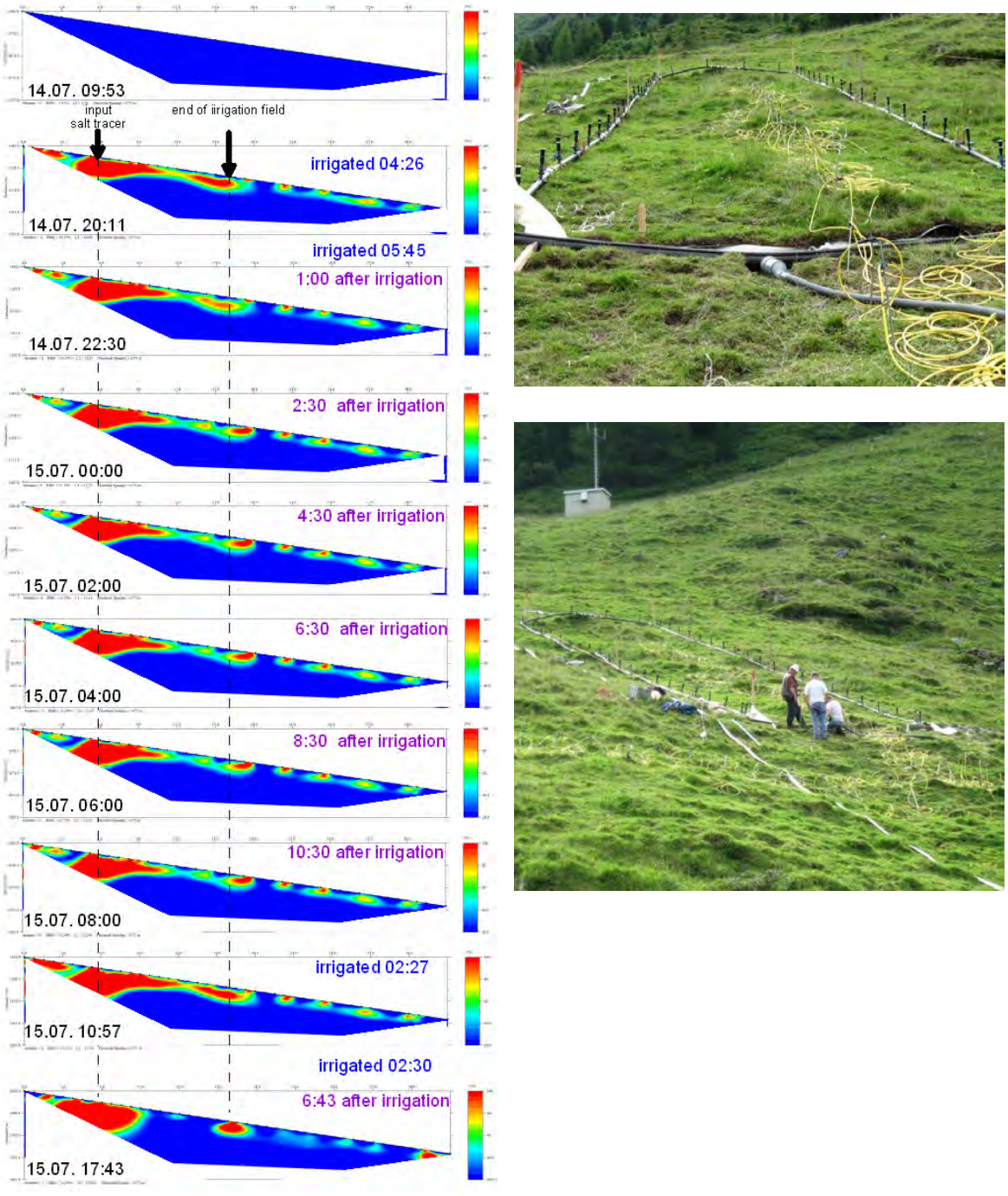

Fig. 3: Results of geoelectric monitoring of test site 1, profile 1 (difference plots of electr. conductivity to base measurement).

A similar experiment was carried out in the eastern part of Austria. The experimental layout for test site 4 is exemplified in Figure 4.

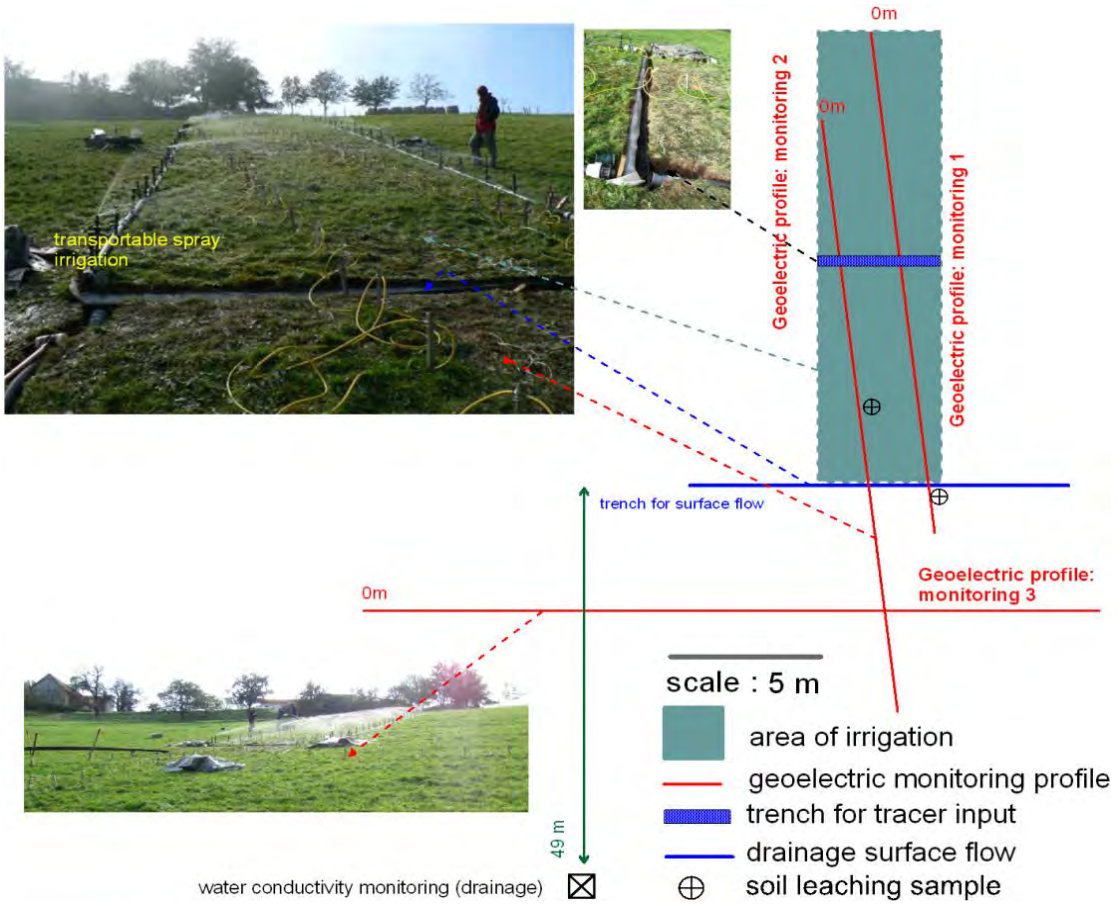

Fig. 4: Test arrangement for test site 4.

Figure 5 depicts the results of geoelectric monitoring (difference plots to base measurement) of electrical conductivity (and TDR measurements) for test site 4. The interpretation of the time lapse results show that already after 1 hour of precipitation, 20.10 14:30 – before the salt tracer input – the effect of the interflow is evident. With the input of the salt tracer, the differences enlarge. Also the dynamic of the interflow behavior can be derived from the time lapse results. After the irrigation stops, interflow decreases rapidly and vice versa. Also a 2D profile of the preferential flow path was interpreted. This geoelectric time lapse interpretation could be confirmed by the TDR profile and a soil sample leaching.

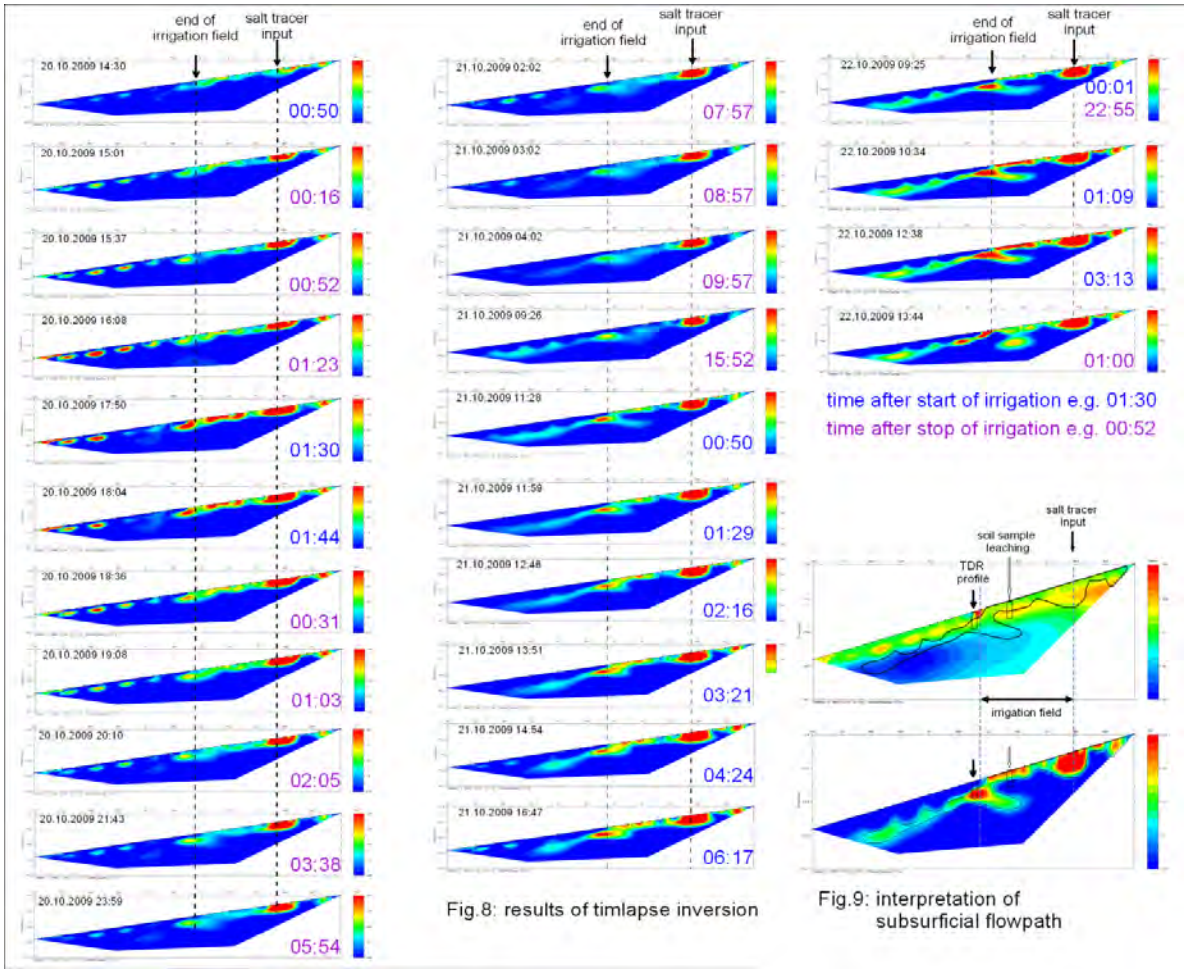

Fig. 5: Results of geoelectric monitoring of test site 4, profile 1 (difference plots of electr. conductivity to base measurement).

Table 1 shows the results of the estimation of shallow interflow velocities (SIV) from different field experiments for different substrata.

Location	Substratum	Method	SIV (m/h)
Wattener Lizum	carbonate talus	conductivity probe	25
	moraine	geoelectric, TDR	1 – 2
	alluvial fan,silty	geoelectric	0,4
Bromberg	weathered mica slate	geoelectric	0,3 – 0,75

Tab. 1: Results of the derived interflow velocities for different substrates.

On very high permeable substrates (group 1), results from tracer measurement of changes in conductivity at the receiving water course forms an easy and appropriate means for receiving reliable values of interflow velocities. E.g. at the test site P2 mean velocities about 25 m h^{-1} were measured. For permeable to very low permeable substrates (group 2) an integrated test arrangement (rain simulation, geoelectrics, soil moisture measurements, measurement of

conductivity at the receiving water course) allows detailed quantification of interflow velocities and detection of potential preferential flow paths.
Within the ongoing project the following further research work is aspired:

- Characterization of further substrates.
- Areal extension of parameters with geoelectrics & aerogeophysics.
- Test of P/R- Models - Recalculation of runoff events under long term rain conditions.

The investigations jointly offered by the Geological Survey of Austria (GBA) and the Federal Research and Training Centre for Forests, Natural Hazards and Landscape (BFW) can make a significant contribution for optimization of input parameters for well-established precipitation/runoff models in practical use. Based on data derived from the here described investigations, shallow interflow velocities for a selection of the most important groups of geological substrates are presented. This information will allow a better understanding of the dominant runoff processes in the prevailing groups of substrates and will lead to a better assessment of runoff contributions from different sub-catchments.

By use of these improved parameters results of well established precipitation/runoff-models (e.g. Time/Area-Concept, ZEMOKOST, HEC-HMS) in practice shall be optimized. The project shall also form the beginning of the development of a catalogue / handbook for assessment of interflow velocities which will be permanently under enhancement.

The report finishes with an overview on the state of research on the theme “Contributions of quick interflow to catchment runoff in persistent rain“ and suggestions for future development of field research on determination of input parameters of practical relevance for precipitation / runoff models.

Quantitative assessment of infiltration processes using ERT: more questions than answers

URSULA NOELL[1], THOMAS GUENTHER[2], CHRISTINA GANZ[3] and AXEL LAMPARTER[1]

[1] Federal Institute for Geosciences and Natural Resources, Stilleweg 2, D-30655 Hannover, Germany.
[2] Leibniz Institute for Applied Geophysics, Stilleweg 2, D-30655 Hannover, Germany.
[3] Institute of Soil Science, Leibniz University, Herrenhäuser Str. 2, 30419 Hannover, Germany.

ursula.noell@bgr.de

Summary

3D ERT measurements of infiltration processes observe a transient process. Water content of the subsurface and, most probably, resistivity of the pore fluid vary concurrently. The relationship between water content and resistivity changes with time and this relationship with its changing characteristics is to be known in order to establish the quantitative interpretation.

Three experiments were carried out in sandy soil and the infiltration processes were observed using 3D ERT. Subsequently the test sites were excavated and TDR measurements were conducted. Samples were taken and the relationship between water content and resistivity was established in the laboratory. In order to achieve the quantitative interpretation the ERT data were inverted, time lapse inversions were applied, and the relationship between resistivity and water content from field and lab-measurements was used to quantify the process. The quantitative interpretation of the first experiment seems convincing. During the second experiments a tracer with higher conductivity was applied and for this experiment the quantitative assessment remains doubtful. The changing relationship between resistivity and water content can be calculated if the mixing between original pore water and tracer is continuous, but measurements seem to indicate that this is not the case.

Introduction

During recent years monitoring of infiltration processes by ERT has become popular. The advantage of the method is striking: minimal invasive, information on 1 – 100 m scale, well developed instruments and inversion schemes, a growing community for scientific discussion and, last but not least, wide applicability with regard to hydrology, hydrogeology, agriculture, soil science and geological hazards i.e. landslides. For many applications the information about the "location" of the water flow paths is already "enough", however, many themes require also a quantitative interpretation. Groundwater recharge is a prominent example; we would like to know how much water reaches the groundwater, how fast does it infiltrate, and dependent on which parameters. And, of course, once we have achieved a qualitative/quantitative interpretation of the infiltration process, we long for evidence. In the predominantly sandy soil of Fuhrberg, a township close to Hannover, Germany, during recent years different ERT monitoring experiments were carried out and some results are summarized below.

The experiments

In order to evaluate the applicability of ERT to observe the infiltration of water through the soil three sprinkling experiments were carried out and monitored using 3D ERT. In this text we will concentrate on two sprinkling experiments with low and high concentration of a conductive colour tracer (brilliant blue).

The soil in the Fuhrberg region where the experiments were conducted is podzol with fine to medium fluviatile sand. The area is partly under agricultural use and partly covered with pine trees. This area is well known for its productive aquifer and the Fuhrberg water works supply drinking water to the city of Hannover. Contamination of this aquifer from agricultural sources is a matter of concern and, therefore, the soil water system has been studied intensively since more than 30 years.

The sprinkling experiment with low brilliant blue concentration

During this experiment 110 l of water is sprinkled on an area of 1.6 x 0.4 m using a semi porous pipe, the infiltration rate is 37 mm/h. The infiltration process is observed using a 3D ERT array comprising 200 electrodes with distances of 20 cm, the lay out was 4.8 m long and 1.4 m wide (Figure 1). The ERT measurements are done before, during, and after the experiment. These measurements used dipole-dipole-configuration and each array measurement comprised 2047 single quadrupole measurements. Only 1.3% of these were obviously outliers and therefore later removed. The error of a quadrupole measurement is calculated by the measuring device as RMS of repeated measurements. No error exceeded 1%, even the error of the outliers did not. For inversion the data errors for all measurements were set to 3% and the 3D inversion is done using the code DC3DInvRes by GÜNTHER (2004). In advance several forward models were calculated in order to estimate the presumably optimal parameter setting for the inversion of these process data. From these calculations it was decided to use minimal length constraint and a small lambda of 5, the model cells were 10 cm in x and y direction, 10 layers were used with increasing layer thickness with a maximum depth of 1.7 m. During this experiment the groundwater table was at about 1.3 m as measured in a nearby borehole.

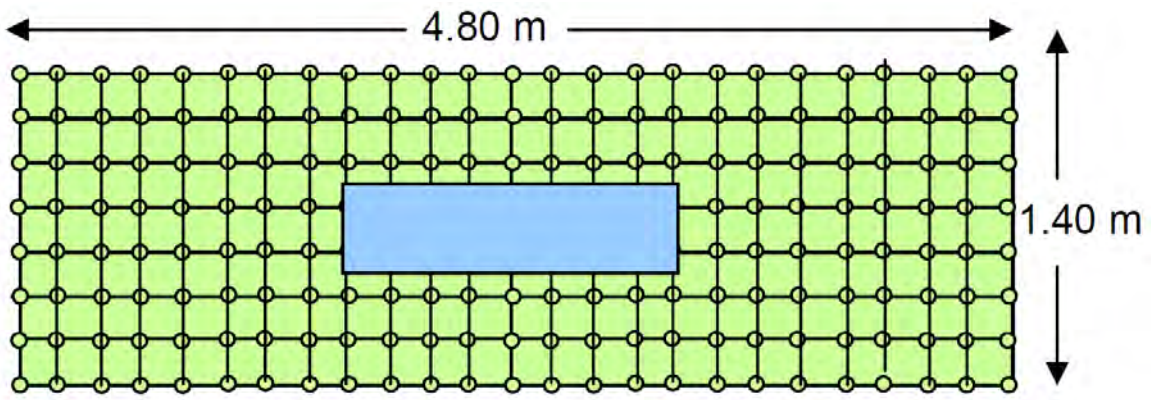

Fig. 1: Sketch of the experimental setup for the infiltration experiment. The infiltration area is located at the centre of the observation area.

The inversion result revealed a bath-tube like infiltration plume with only very minor hints for preferential flow during the early times of the experiment. Two days after the experiment the

central part of the area was excavated and along three vertical sections the water content was measured using TDR devices. These measurements revealed a relative strong heterogeneity with regard to water content and, surprisingly, no hint for the blue colour, and no indication that the infiltrated water still remained in this zone except, presumably, in the upper 10 cm which were not included in the TDR measurements. The only explanation seemed to be that the water had already flown through the soil and reached the groundwater.

From later analysis it became clear that the brilliant blue concentration was much to low to actually colour the soil and the conductivity of the infiltrated water was 586 µS/cm (ρ_w.= 17 Ωm) However, this relatively low conductivity had the advantage that the change in pore water conductivity during the experiment was negligible.

In order to calculate the infiltration process quantitatively using ERT the relationship between water content and resistivity is established. This is done using a combination of laboratory measurements and the results of the TDR measurements from the excavation. Firstly the ERT inversion result from the edge of the area where surely no water penetrated into is compared to the TDR results of the excavated section at exactly the same position. The result is a cross plot resistivity vs. water content as shown in Figure 2.

From the scatter in the cross plot (Figure 2) it is evident that for the field data no clear parameter fit for any Archie function can be done with certainty. Therefore, samples of the soil were taken in the field and the Archie function was measured in the laboratory. For these measurements the soil was stepwise saturated with artificial rain water and the resistivity was measured for every single saturation step. From these data the Archie parameter were calculated.

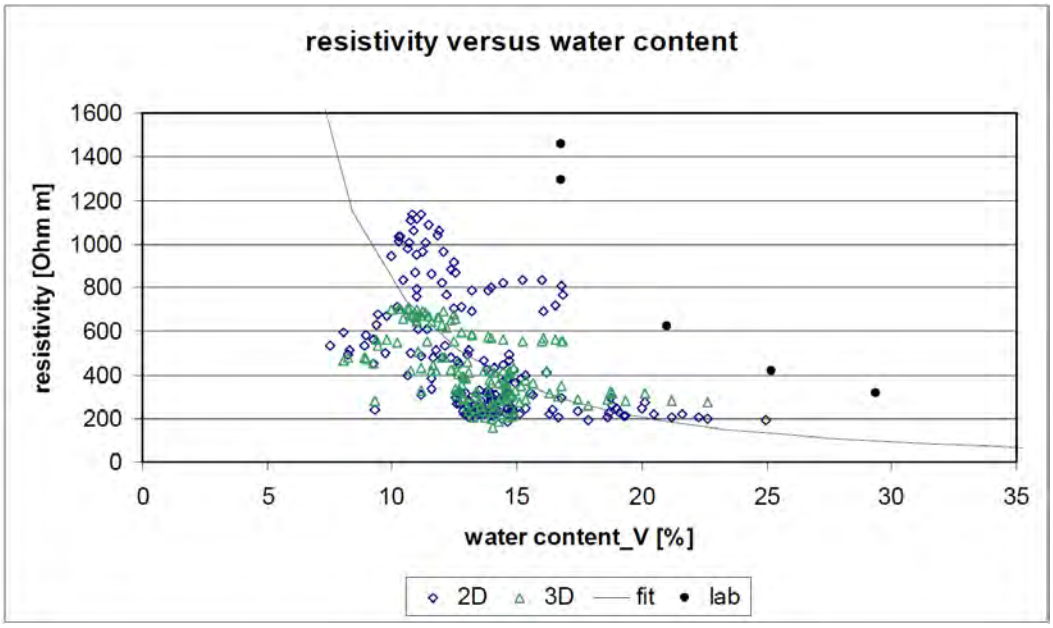

Fig. 2: Resistivity versus volumetric water content; lab-measurements, inversion results and fitting line (n=2, m=1.3, ρ_w = 15 Ωm).

The scatter plot (Figure 2) raises several questions: Why are the results of the 2D inversion and the 3D inversion that different and what are the reasons for the deviation between the laboratory and the “field” measurements? The latter is caused by the different pore water conductivities of the laboratory measurements and the field situation, respectively. The different inversion results

are not only due to the ill posed inversion problem leading to ambiguous results but as well to the heterogeneity of the soil and different inversion parameters.

Using the Archie function presented in Figure 2

$$\rho_f = \rho_w * S^{-n} * \Phi^{-m} \quad (1)$$

n = 2 = Saturation (S) exponent

m= 1.3 = cementation factor

ρ_f, ρ_w = bulk resistivity, pore water resistivity (15 Ωm)

Φ = porosity

the infiltration process is quantified. Firstly the original saturation at the site is calculated

$$S_0 = \left(\left({\rho_w}/{\rho_{f(t0)}}\right) * \Phi^{-m}\right)^{\frac{1}{n}} \quad (2)$$

from the inversion result of the array measurement before infiltration (t0).

Then, by using time lapse inversion strategies, the saturation change is calculated by

$$\Delta S_{tx} = S_0 * \left(\left(\frac{\rho_{f(tx)}}{\rho_{f(t0)}}\right)^{-\frac{1}{n}} - 1\right) \quad (3)$$

For this equation no change in pore water conductivity during the infiltration process is assumed. In this particular case this assumption seems to be justified since the resistivity of the infiltrated water (17 Ωm) is similar to the assumed pore water resistivity of 15 Ωm.

The results of the quantitative calculation are surprisingly close to the infiltrated amount of water (Figure 3).

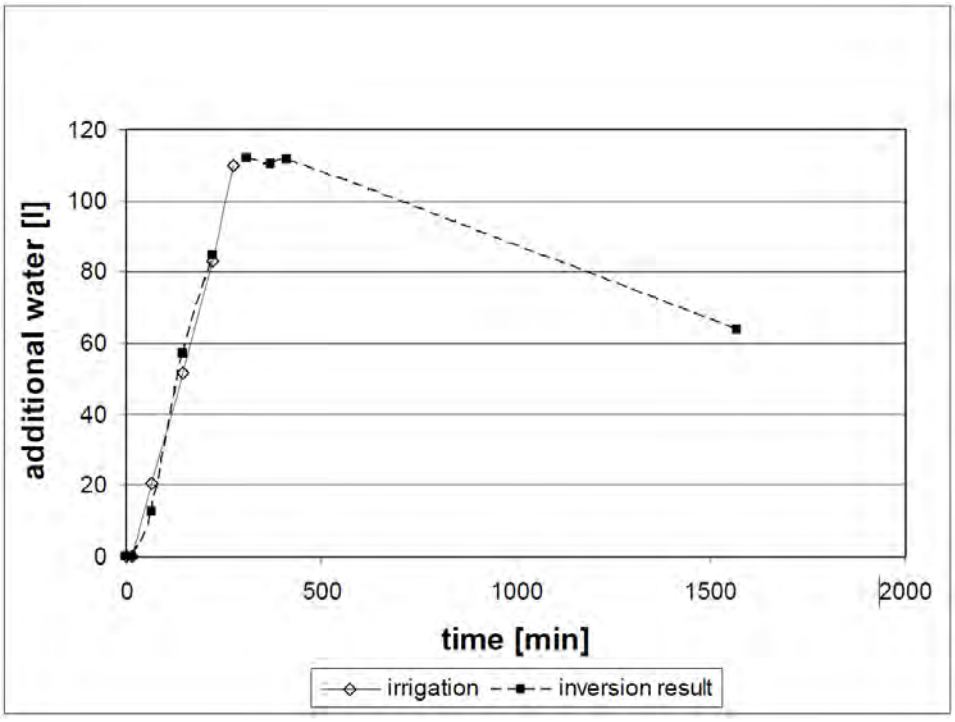

Fig. 3: Result of quantification as calculated from the timelapse inversion using the Archie function (1).

These results indicate that one day after infiltration already about 45% of the infiltrated water reached the groundwater. This coincides with the results of the TDR measurements showing two days after infiltration no increased water content in the central section of the experiment, where the water was irrigated onto.

By applying the error propagation law on formula 3 the error of the quantitative assessment can roughly be calculated. For this experiment it is in the range of 25 to 40 l. Most critical is the original pore water resistivity and it has to be taken into account that this might differ throughout the area depending on original saturation, soil type, and content of soluble matter.

The experiment with high brilliant blue concentration

For this experiment 80 l of water with a conductivity of 1213 µS/cm (ρ_{winf} = 8.2 Ωm) was sprinkled on an area of 0.4 x 1.0 m within 8 hours slightly off centre. In the excavated sections the deep blue colour marked the flow pathways which resembled a bath-tube rather than small preferential flow pathways (Figure 4). The soil at this site was similar to the first site although the TDR measurements showed lesser heterogeneity in terms of original water content.

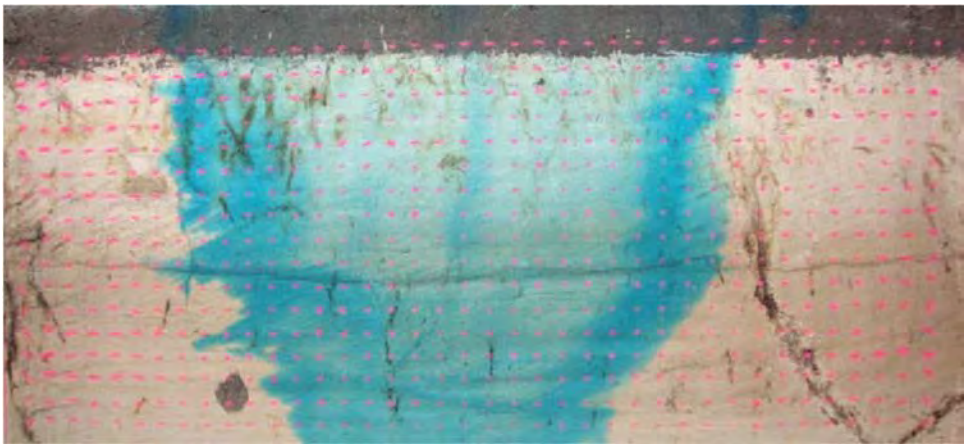

Fig. 4: Picture of the central section with blue infiltration plume

On account of the high pore water conductivity contrast between the original and the irrigated water the resistivity decreased enormously during infiltration. This called for the use of the FE-inversion code BERT (GÜNTHER et al. 2006) for inversion of the time lapse data. The FD code used for inversion of the data of the first experiment achieved no adequate data fit.
For the quantitative interpretation the same Archie parameters m, n and $\rho_{w(t0)}$ are used as for the first experiment. At this time the calculation of the saturation change has to take the change of pore water conductivity (ρ_w) during the infiltration process into account.

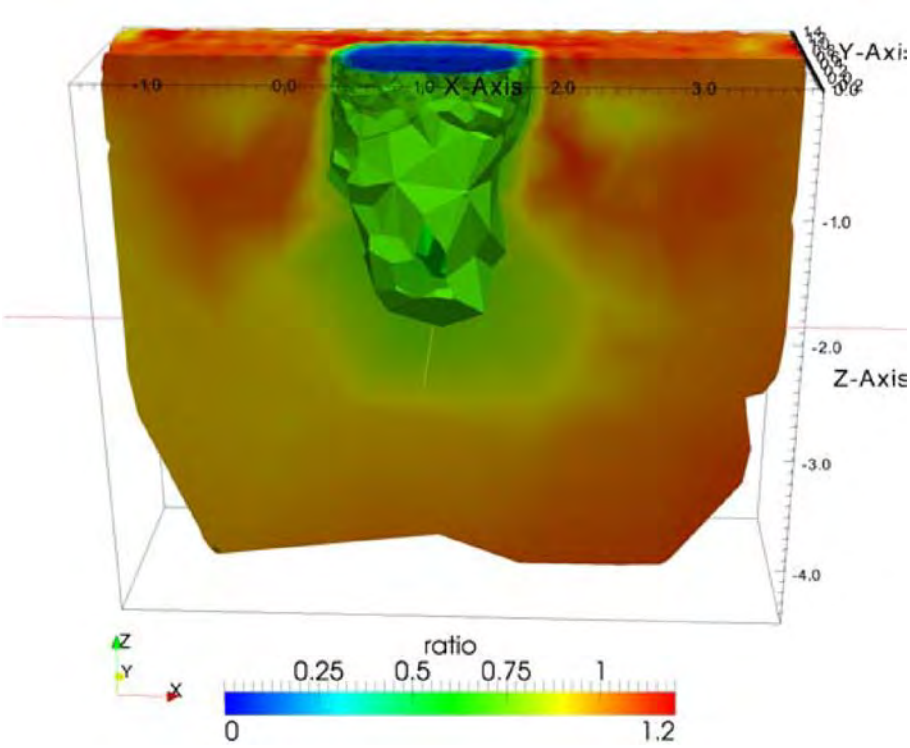

Fig. 5: Time lapse inversion result 21 h after start of infiltration.
Contour line marks the ratio = $\rho_{f(tx)}/\rho_{f(t0)}$ = 0.7.

$$\Delta S_{tx} = S_0 * \left(\left(\frac{\rho_{f(tx)}}{\rho_{f(t0)}} * \frac{\rho_{w(t0)}}{\rho_{w(tx)}} \right)^{-\frac{1}{n}} - 1 \right) \quad (5)$$

The calculation of $\rho_{w(tx)}$ for every time tx during a transient process needs either direct measurements of $\rho_{w(tx)}$ or a valid assumption. It is possible, however, to calculate a higher und lower limit of ΔS. The **higher limit** is given by the assumption that during infiltration no change in pore water conductivity takes place, consequently, the decrease in resistivity is caused by increased water content only. The **lower limit** can be calculated by the assumption that the pore water conductivity at time tx ($\rho S \Delta_{w(tx)}$) equals the value of the infiltrated water ρ_{winf}.

Conclusions and outlook

The infiltration experiments in sandy soil showed convincingly that the infiltration process can be observed by 3D ERT and that time lapse inversion permits not only a qualitative but as well a quantitative interpretation of the process if the change in pore water conductivity during the process is negligible. If a conducting tracer fluid is used the consecutive change in pore water conductivity during the infiltration process hampers the quantitative interpretation.

To achieve a reliable quantitative assessment of the infiltration process the measurement of the actual pore water resistivity seems indispensable although it will give only local information. Measurements of the pore water conductivity during the experiments are needed in order to formulate and test mixing laws to be applied for the quantification. The heterogeneity of the soil could complicate the situation and different mixing laws might be necessary.

References

GÜNTHER, T., 2004: Inversion methods and resolution analysis for the 2D/3D Reconstruction of Resistivity Structures from DC Measurements. – PhD Thesis, Freiberg University of Mining and Technology.

GÜNTHER, T., RÜCKER, C. and SPITZER, K., 2006: Three-dimensional modelling and inversion of DC resistivity data incorporating topography: II. Inversion. – Geophysical Journal International **166**, 506–517.

Four-year repeated geoelectrical surveys for the monitoring of temperature and water content in the unsaturated zone

SHINICHI TAKAKURA[1] and YUJI NISHI[1]

[1] National Institute of Advanced Industrial Science and Technology (AIST), Tsukuba West, 16-1 Onogawa, Tsukuba, Ibaraki 305-8569, Japan.

takakura-s@aist.go.jp

Introduction

Resistivity monitoring was used to understand the change of subsurface hydrological environment by many researchers (KEAN et al., 1988; WHITE, 1988; FLOHLICH and PARKE, 1990; DAILY et al., 1992; OSIENSKY and DONALDSON, 1995; SLATER and SANDBERG, 2000). The changes of subsurface water, moisture and temperature can be certainly detected by an observation well. However, making the well is expensive and disturbs the subsurface hydrological environment. Moreover the well provides information on a localized change of hydrological environment, which does not necessarily represent the whole change. In contrast, geoelectrical methods like DC resistivity and EM methods are relatively low-cost and noninvasive techniques. In addition, 2-D or 3-D geoelectrical methods including resistivity tomography can provide 2-D or 3-D images of subsurface structure.

This paper describes a result of repeated geoelectrical surveys that were carried out for about four years together with the measurements of near-surface soil temperature and soil water content. The purpose of this study is to detect the change of hydrogeological environment in the unsaturated zone and to evaluate the effectiveness of resistivity monitoring for the subsurface temperature and water content changes.

Observation site

Long-term repeated geoelectrical (DC resistivity) surveys were carried out in the KR-1 groundwater observation site, North-Kanto, central Japan (Fig.1). In this site, the measurements of near-surface soil temperature and soil water content were conducted with the meteorological observation. Continuous GPS and SP observations and repeated gravity measurements were also carried out. Twenty-five electrodes were placed at 1 m intervals along a 24-m long line that crossed immediately near the soil moisture and temperature meters. The volumetric water contents were measured every 10 minutes at five depths from 0.6 to 3 m. The soil temperatures were measured at depths of 1, 3 and 10 m. Using dipole-dipole and Wenner electrode arrays, resistivity data had been collected nearly every month since 15 August 2006. From September 2006 to March 2007, two groundwater observation wells, KR-1 and KR-2, were made to depths of 350 m and 90 m, respectively and some experiments like a production test were done. Various noises accompanying these works affected the resistivity data. Therefore, this paper discusses the resistivity data acquired after 11 May 2007. The depth to water level in this site is about 60 m,

indicating the repeated geoelectrical surveys monitored the resistivity changes in only the unsaturated zone.

Changes of resistivity structure

(1) Basic resistivity structure

In this study, a 2-D resistivity section was obtained for each measurement time using the 2-D inversion method described in UCHIDA (1993). This method is an iterative least-squares inversion with smoothness constraint, which uses the finite element method for a forward calculation. Fig. 2 shows the analysed resistivity section up to a depth of 10 m on 11 May 2007. The resistivity model is basically interpreted as homogeneous structure expect for near the surface. The low resistivity zone under near the electrode No. 10 is due to the steal casing of KR-2 well.

(2) Resistivity changes

Fig. 3 shows the analyzed resistivity sections on 24 August 2007, 22 November 2007, 19 February 2008, 23 May 2008, 31 May 2009, and 31 May 2010. A large change of resistivity is not seen in the figure. In order to detect the resistivity change in detail, we calculated the rate of resistivity of each measurement time by the following equation.

$R = \frac{\rho_2 - \rho_1}{\rho_1} \times 100$, where ρ_1 and ρ_2 are layer resistivities of two different time.

Fig. 4 shows 2-D images of the resistivity change at 24 August 2007, 22 November 2007, 19 February 2008, 23 May 2008, 31 May 2009, and 31 May 2010 relative to May 11 2007. The resistivity near the surface decreased over 20 % in wet summer season and increased over 60 % in winter season. The difference of the resistivities between May 2007 and May 2008 is relatively small. This means that the resistivity change near the surface is a cycle of one year, which is a seasonal change. In the past three years, the resistivity of shallower than 5m increased, while the resistivity of deeper than 5 m decreased gradually.

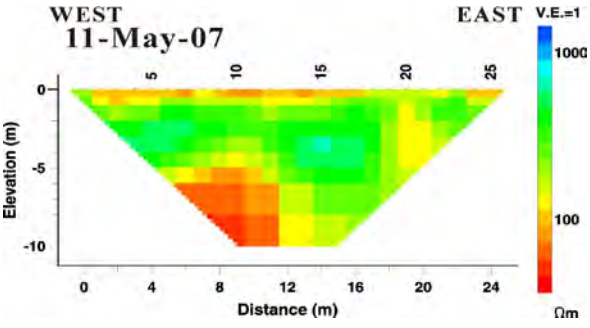

Fig.2: Analyzed 2-D resistivity section along the 24-m long survey line at 11 May 2007.

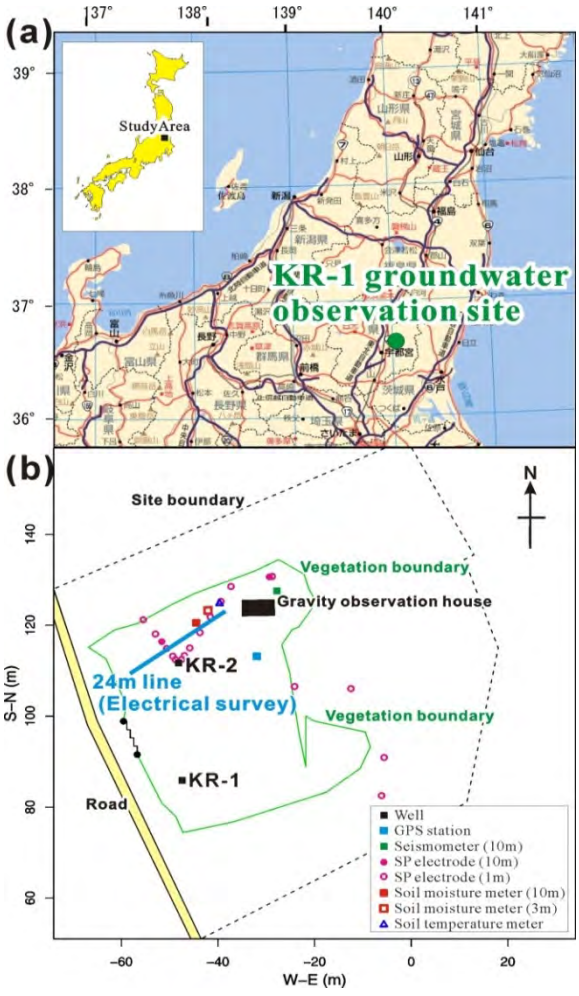

Fig. 1: Location map of the KR-1 groundwater observation site showing a repeated electrical survey line, observation wells and other observation points.

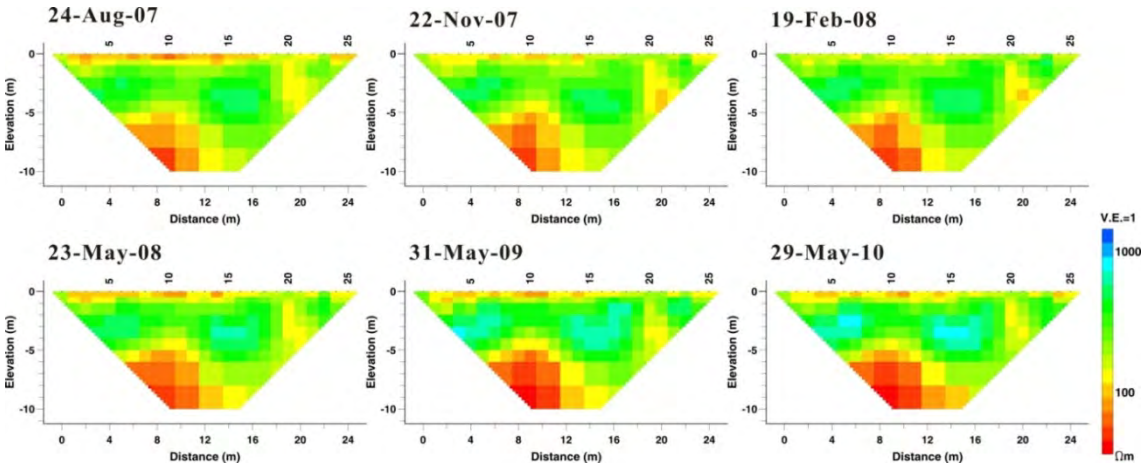

Fig.3: Analyzed 2-D resistivity sections along the survey line on 24 August 2007, 22 November 2007, 19 February 2008, 23 May 2008, 31 May 2009, and 31 May 2010.

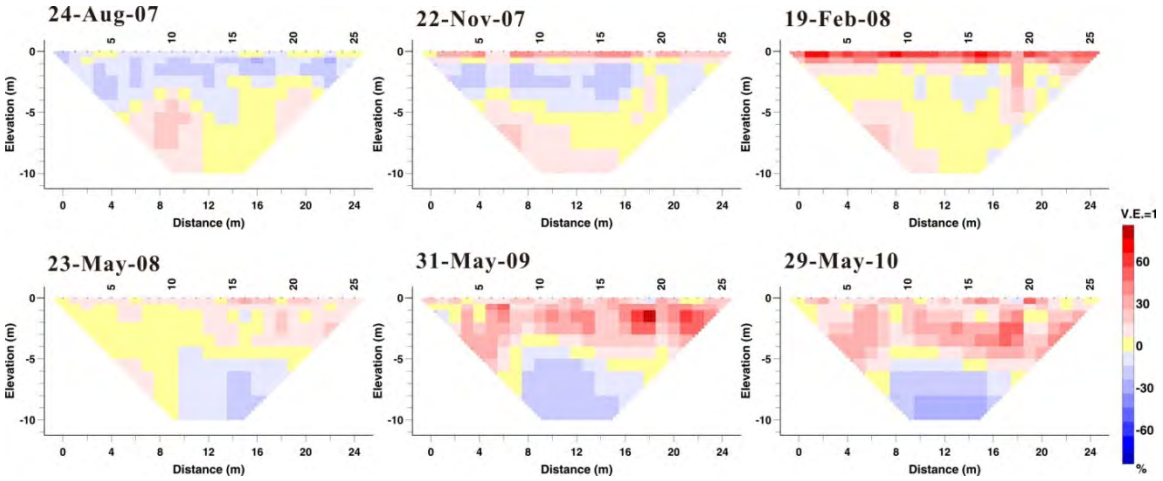

Fig. 4: 2-D images of the resistivity change at 24 August 2007, 22 November 2007, 19 February 2008, 23 May 2008, 31 May 2009, and 31 May 2010 relative to 11 May 2007.

(3) Comparison of resistivity with soil temperature

Fig. 5 shows the changes of soil temperature at depths of 1, 3 and 10 m with daily mean air temperature and the changes of resistivity analyzed from the repeated geoelectrical data at some depths near the soil temperature meter from 1 May 2007 to 19 February 2011. The soil temperature changes at depths of 1 and 3 m lag about 1 and 3.5 months behind the air temperature change, respectively. The change at a depth of 10 m is not observed. The analyzed resistivity change is the largest at the surface and decreases with depth. The resistivity and temperature are inversely related at the depths of 1 m and 3 m, indicating that the seasonal change of resistivity near the surface is mainly due to the change of temperature. Except for the depth of 8 - 10 m, the resistivities have trends which increased gradually.

(4) Comparison of resistivity with water content

Because the resistivity change is greatly influenced by the temperature change, we compensated for temperature variations using the equation suggested by HAYLEY et al. (2007).

$$\rho_{STD} = \left[\frac{m(T-25)+1}{m(T_{STD}-25)+1} \right] \cdot \rho ,$$

where T_{STD} is a standard reference temperature and ρ_{STD} is the temperature-corrected resistivity. T and ρ are the in situ temperature and resistivity, respectively, and m is a temperature correction coefficient and is generally around 0.02 (HAYLEY et al., 2007). Fig.6 shows the changes of volumetric water content at depths of 0.6m and 2.4 m and the changes of temperature-corrected resistivity at depths of 0-1 m and 2-3 m. In this case, the value of m was chosen to be 0.02 and T_{STD} was 15.5 °C that was average soil temperature. It became clear that the changes of temperature-corrected resistivity are inversely proportional to the changes of the volumetric water content. This means that the resistivity monitoring method may be effective for detecting the change of water content in the unsaturated zone if temperature compensating is made.

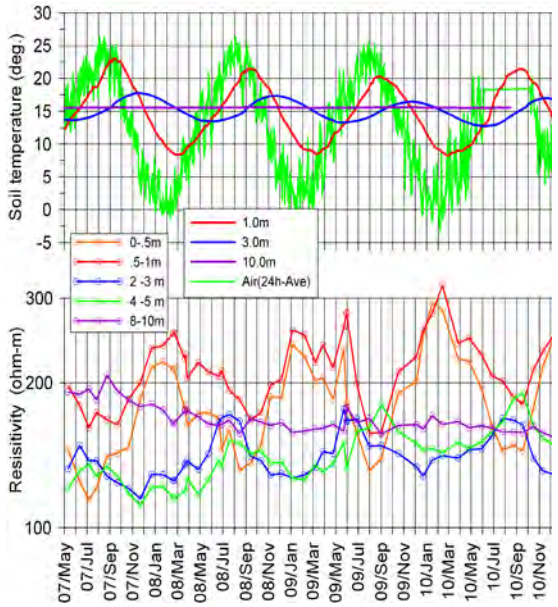

Fig.5: Changes of soil temperature at depths of 1, 3, 10 m with daily mean air temperature (upper graph), and changes of analyzed resistivity at five depths up to 10 m near the soil temperature meter (lower graph) since 1 May 2007.

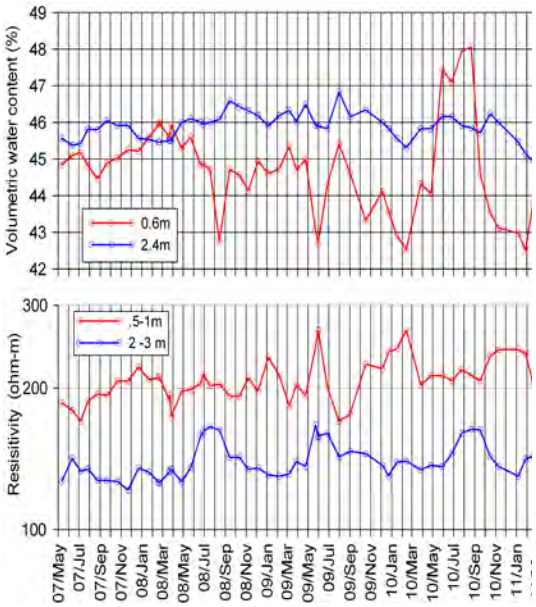

Fig.6: Changes of volumetric water content at depths of 0.6m and 2.4 m (upper graph), and changes of temperature-corrected resistivities at depths of 0.5-1 m and 2-3 m (lower graph) since 1 May 2007.

Conclusions

Repeated geoelectrical surveys were carried out in the KR-1 groundwater observation site for four years. Analyzed 2-D resistivity sections show the seasonal resistivity change is recognized near the surface. The resistivity change is the largest at the surface and decreases with depth. It seems that the long cycle change of resistivity was most influenced by the change of soil temperature. The changes of temperature-corrected resistivity are inversely proportional to the changes of the volumetric water content. These facts indicate that the geoelectrical method can be used for subsurface temperature monitoring, and may be effective for detecting the change of water content in the unsaturated zone if temperature compensating is made.

Acknowledgements

A part of the observations at the KR-1 site was conducted under the research contract with the Nuclear and Industrial Safety Agency (NISA) till March 2007. Then, we did original observations at the site in the AIST research project. We would like to thank T. Ishido and M. Sugihara of AIST for their help during the observations.

References

DAILY, W., RAMIREZ, A., LABRECQE, D. and NITAO, J., 1992: Electrical resistivity tomography of vadose water movement. – Water Resources Research, **28**, 1429-1442.

FLOHLICH, R.K. and PARKE, C.D., 1990: The electrical resistivity of the vadose zone – field survey. – Ground Water, **27**, 524-530.

HAYLEY, K., BENTLEY, L.R., GHARIBI M. and NIGHTINGALE, M., 2007: Low temperature dependence of electrical resistivity: Implications for near surface geophysical monitoring. – Geophysical research letters, **34**, L.18402.

KEAN, W.F., WALLER, M.J. and LAYSON, H.R., 1988: Monitoring moisture migration in the vadose zone with resistivity. – Ground Water, **25**, 562-571.

OSIENSKY, J.R. and DONALDSON, P.R., 1995: Electrical flow through an aquifer for contaminant source leak detection and delineation of plume evolution. – Journal of Hydrology, **169**, 243-263.

SLATER, L.D. and SANDBERG S.K., 2000: Resistivity and induced polarization monitoring of salt transport under natural hydraulic gradients. – Geophysics, **65**, 408-420.

UCHIDA, T., 1993: Smoothness-constrained 2D inversion for DC resistivity data by ABIC minimization method (in Japanese with English abstract). – Butsuri-Tansa, **46**, 105-110.

WHITE, P.H., 1988: Measurement of ground-water parameters using salt-water injection and surface resistivity. – Ground Water, **26**, 179-186.

Applications in Contamination Monitoring

Installation of Geoelectrical Monitoring System 2001, picture by R. Supper

Monitoring the freshwater/saltwater transition zone on the North Sea Island Borkum using vertical electrode systems

MICHAEL GRINAT[1], WOLFGANG SÜDEKUM[1], DIETER EPPING[1], ROBERT MEYER[1] and THOMAS GÜNTHER[1]

[1] Leibniz Institute for Applied Geophysics, Stilleweg 2, 30655 Hannover, Germany.

michael.grinat@liag-hannover.de

Resistivity is a key parameter in water sciences. In order to investigate the dynamics of the freshwater/saltwater boundary in the scope of climate change monitoring measurements are necessary. Besides repeated surface measurements using electromagnetic or electric methods in-situ measurements are required. Especially the long-lasting installation of electrodes in the target depth can provide continuous information.

In September 2009 the Leibniz Institute for Applied Geophysics (LIAG) Hannover installed two newly developed automated electrical resistivity tomography systems in the water catchment areas Waterdelle and Ostland at the North Sea island Borkum. The objective is the observation of changes in the thickness of the freshwater lens that can be caused by pumping of freshwater and upconing of saltwater. This work is part of the Interreg project CLIWAT (http://www.cliwat.eu).

The vertical electrodes were installed in the two boreholes CLIWAT 1 (Waterdelle) and CLIWAT II (Ostland) between 45 m and 65 m depth below the surface. In both boreholes this depth interval comprises the transition zone between the freshwater lens and the underlying saltwater. While in CLIWAT I sand was encountered at these depths, sand layers as well as silty / clayey layers were found in CLIWAT II.

Main part of the system is a vertical electrode chain of about 20 m length with 78 stainless steel ring electrodes mounted on a rigid PVC pipe. The distance between adjacent electrodes is 0.25 m. The measurements are carried out using a modified 4point light 10W (LGM Lippmann). The power is supplied by solar panels and the data are transmitted to an FTP server in Hannover. The time interval between subsequent measurements is 5 hours. Each data set comprises 975 single measurements using a Wenner-Alpha array with electrode distances between 0.25 m and 6.25 m. The correct geometry of the ring electrode is accounted for using the complete electrode model. The pseudosections can be inverted into real resistivities using a 1D-layered model.

Within the first months after installing the system the resistivity changes observed mainly in saltwater-dominated depths were caused by the readjustment of the disturbed conditions at the drilling locations to the normal situation. Afterwards the ongoing measurements in most depths show only small resistivity changes of less than five percent. This suggests a stable freshwater lens. But a more thorough analysis of the data shows that in some small depth intervals the change in resistivity may reach 20 %. Moreover, a different time-dependent behavior of resistivity is observed in different depths: In the freshwater and the saltwater layer the resistivity can be almost constant during a year, while resistivities change according to a sine wave in the transition zone. In the sandy and silty/clayey layers in CLIWAT II time behavior is different.

The ongoing in-situ measurements could be used to calculate TDS values. Moreover, they are necessary input parameters for the calibration of modeling studies that calculate future changes in this groundwater system caused by climate change.

Development of an integrated monitoring concept to detect possible brine migration

MARCUS MÖLLER[1], CORNELIA SCHMIDT-HATTENBERGER[1], FLORIAN WAGNER[1] and STEPHAN SCHRÖDER[1]

[1] Helmholtz Centre Potsdam, GFZ German Research Centre for Geosciences, Telegrafenberg, 14473 Potsdam, Germany.

marcus.moeller@gfz-potsdam.de

Introduction

Carbon dioxide is considered to be one cause of climate changing. Therefore, the preferential objective is to reduce the greenhouse gas, produced by industrial production. The long term storage in underground reservoirs represents one possible way to this aim. The most important research focus of the multidisciplinary integrated project BRINE is to ensure the safe storage operation (KEMPKA et al., 2010). That means an adequate monitoring of possible brine migration into freshwater aquifers from lower saline aquifers by gas displacement. For both the qualitative and quantitative investigation, a combination of several geophysical methods is needed. The electrical resistivity tomography (ERT) is a measurement method with a comparatively high spatial resolution on small scales. Therefore, it will be generally used for borehole and near subsurface investigations.

Geological setting

This research work refers to an area in eastern Brandenburg (Germany). However, the analysis can be applied to regions with comparable geological characteristics. The area is part of the North German Basin. The relevant reservoir horizon is located within a classic anticlinal structure, generated by salt tectonic processes. The Rupelian clay formation with an average thickness of 100 m is a natural liner between the deep brine aquifers and the freshwater zone. The layer is located at depths of 100 up to 300 m below the surface. Glaciogenically formed channels have partially deleted the formation structure implicating a potential upward migration of the underlying saltwater. Finally, the anticlinal structure is easterly flanked by a large fault-zone (STACKEBRANDT and MANHENKE, 2004).

Monitoring concept

Geological characteristics and technical limitations make high demands on an integrated monitoring system. The concentration of total dissolved solids (TDS) in the region of investigation is comparatively high, even at shallow depths. It ranges from 1 to 10 g/l above and 10 to 50 g/l below the Rupelian clay and from 50 to 350 g/l below the tertiary base (GRUBE et al., 2002). Therefore, only a small change in resistivity is expected due to a brine migration. The volume of investigation strongly depends on the electrode distance, which should be practicable in field surveys. Otherwise a depth of the storage horizon of about 1000 m makes it difficult to deploy ERT. Typically, the number of installed borehole electrodes is limited. In order to achieve an adequate resolution in critical depths and at the same time get an overview over the entire length of the borehole, a division of the profile should be performed. The adapted electrode array should

consist of segments of short electrode distances near the reservoir and near the aquifer zone as well as long distances in between.

The presented monitoring concept focusses on three potential pathways. One cause of the upward brine migration could be a pressure build-up within the reservoir horizon. The injected CO_2 neither dissolves immediately, nor completely in the pore fluid. Hence, if the pressure is not regulated in time, the saline fluid could spread along zones of weakness. The most probable pathways are permeable fault-zones, wellbores with leakages along their annuli and formation defects within impermeable layers. The concept of a comprehensive monitoring system must take into account these critical points (Figure 1).

The fault-zones can extend over several kilometres. In addition to other monitoring methods, ERT provides a locally limited but high resolution. Using parallel profiles, the infiltration zone can be narrowed down by geoelectrical measurements. The most important application of ERT, however, is the monitoring of the near region of injection and observation wells. In addition, it offers the only possibility to detect small changes already at the storage horizon. A combination of shallow boreholes and surface measurements is particularly suitable for the monitoring of the Rupelian defects. They are circular to channel-like shaped with an extension of 100 m up to several hundred metres.

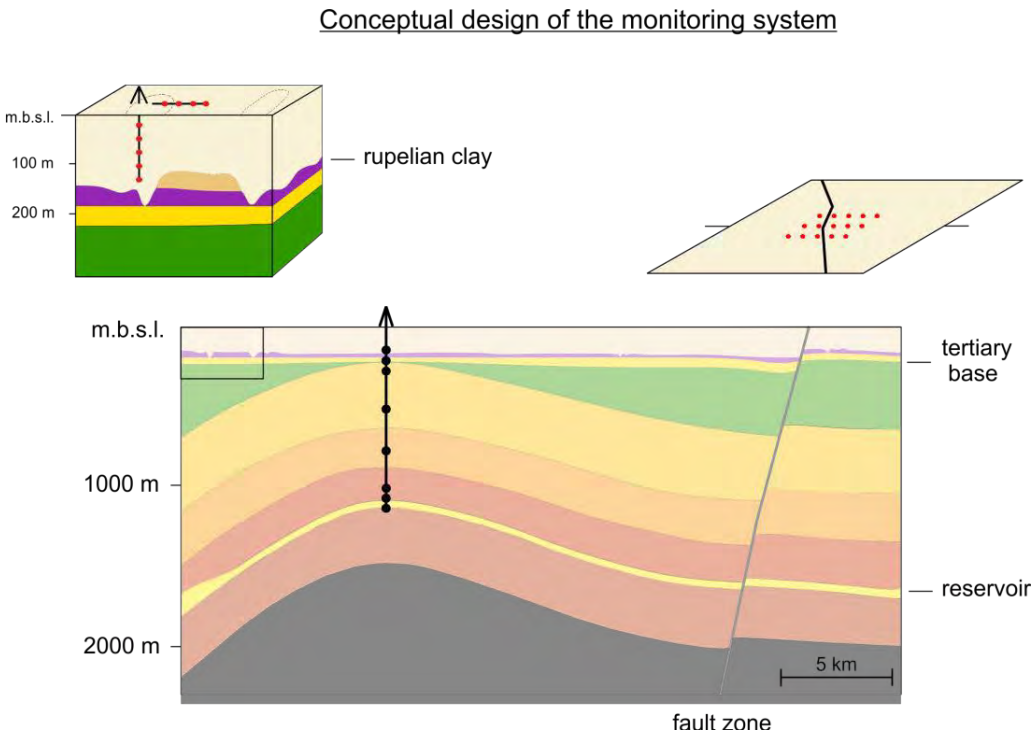

Fig. 1: Concept of a monitoring system including combined surface-downhole measurements near the formation defects, an adapted electrode array in the wellbore and parallel profiles along the fault zone (f.l.t.r.).

Model and experiment

The main objective is to find an optimal combination of several electrode arrays to detect time-lapse effects of the subsurface resistivity distribution. The presented study is divided into two work packages. In the first part, real-scale resistivity models of the described critical areas are created. For this purpose a simplified geological model of three layers (reservoir, consolidated sediments and unconsolidated deposits) is used. The increasing salinity is realised by decreasing

electrical resistivity values. For different electrode geometries (e.g. inhole, crosshole, surface-downhole, etc.) and various electrode configurations (e.g. pole-pole, pole-dipole and dipole-dipole), a forward modelling study is performed. Subsequently, we invert the synthetic electrical resistances with an additional noise of 5 %. A well-established method to detect even small changes in resistivity is the ratio inversion technique (e.g. HAYLEY et al., 2011). For this analysis, however, a common difference method is used, which shows more distinct results. An example, calculated for the injection well, is demonstrated in Figure 2.

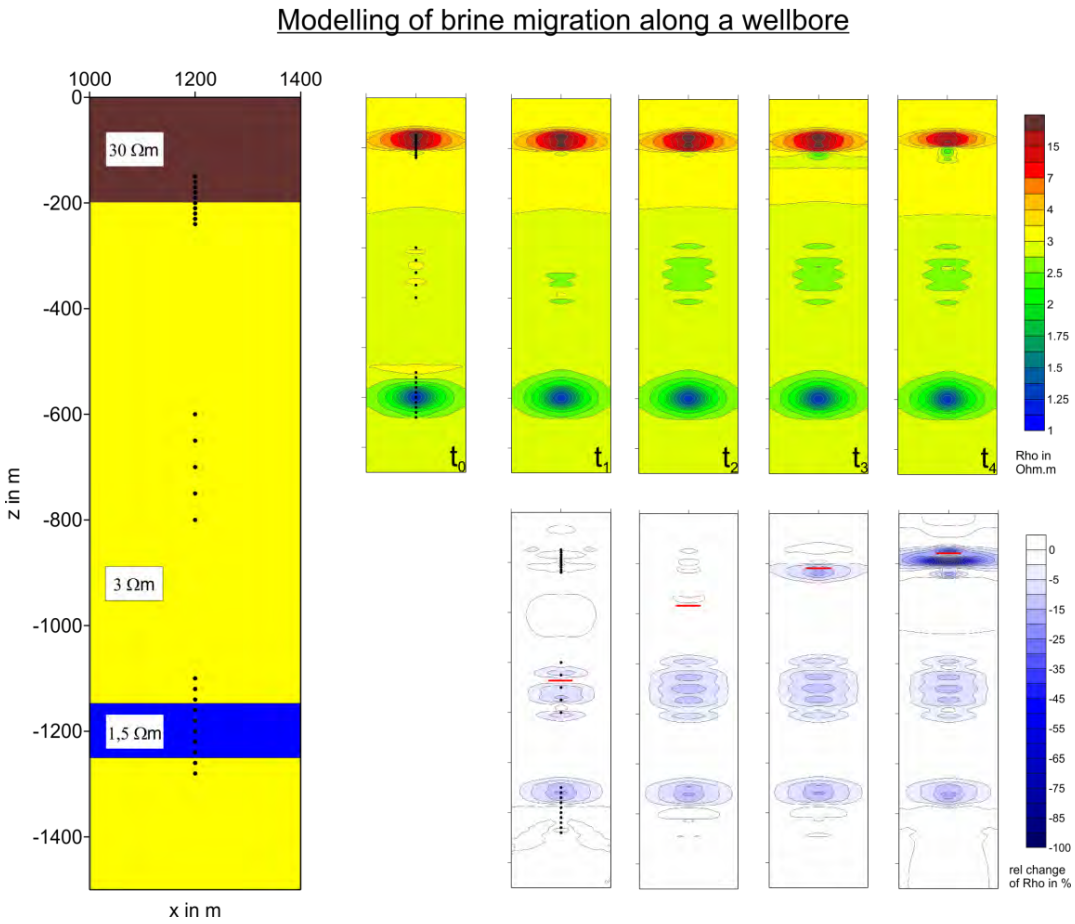

Fig. 2: Modelling of a brine upward migration in four steps. For modelling and inversion a bipole-bipole (cp-cp) configuration with an adapted geometry was used. The upper line shows the inversion results with t0 for the undisturbed model, the bottom line shows the differences (tn-t0) of inverted results. The red line marks width and height of the saltwater column.

In the second part of this study, the results are validated under controlled and well-defined laboratory conditions. In a cylindrical sandbox with a diameter and a height of 0.6 m, various combinations of borehole and surface electrodes can be installed in order to test certain configurations. For the filling, materials with different hydraulic characteristics can be used.

In a first experiment, homogeneous *Fontainebleau* sand with a porosity of 45 per cent and a permeability of 23 Darcy was used. The material was fully saturated with tap water at the beginning of the experiment. Synthetic brine with a concentration of 200g/l NaCl was injected at the bottom of the tank over a period of 6 days. With a combination of 50 surface- and 25 borehole electrodes the standard configurations (Wenner, Schlumberger and dipole-dipole) were measured.

Conclusions

First results of the modelling study compared with laboratory measurements demonstrate the potential of ERT for leakage detection, especially in the near subsurface and the surrounding of the wellbores. Obviously the adapted arrangement of electrodes both gives an adequate overview and limits the number of electrodes and subsequently the costs of a monitoring system. Next we will focus on the formation defects and fault-zones with more complex models. Other points of interest are the limit of spatial resolution and the limit of brine detection.

References

GRUBE, A., HERMSDORF, A., LANG, M., RECHLIN, B. and STEFFENS, A., 2002: Numeric and hydrochemical modelling of saltwater intrusion into a pleistocene aquifer – case study Großbeuthen (Brandenburg). – 17th Salt Water Intrusion Meeting, Delft, 6.–10. May 2002.

HAYLEY, K., PIDLISECKY, A. and BENTLEY, L.R., 2011: Simultaneous time-lapse electrical resistivity inversion. – Journal of Applied Geophysics, **75**(2), p. 401-411.

KEMPKA, T., HERD, R., HUENGES, E., JAHNKE, C., KÜHN, M., MOECK, I., MUNOZ, G., RITTER, O., SCHMIDT-HATTENBERGER, C., VOIGT, H.J. and ZIMMERMANN, G., 2010: Brine – CO_2 Storage in eastern Brandenburg: Implications for geo-thermal heat provision and conception of a salinisation early warning system. – In: HOPPE, A., RÖHLING, H.-G. and SCHÜTH, C. (Eds.): Geowissenschaften sichern Zukunft, GeoDarmstadt 10.–13. Oktober 2010, Schriftenreihe der Deutschen Gesellschaft für Geowissen-schaften, **68**, p. 301.

STACKEBRANDT, W. and MANHENKE, V. (Ed.), 2004: Atlas zur Geologie von Brandenburg. – Landesamt für Geowissenschaften und Rohstoffe Brandenburg, Kleinmachnow.

Geoelectrical Monitoring for Mapping of Gas and Water Migration in Landfills

TORLEIF DAHLIN[1], HÅKAN ROSQVIST[2], SARA JOHANSSON[3], CARL-HENRIK MÅNSSON[3], MATS SVENSSON[3], MAGNUS LINDSJÖ[3] and MENG HENG LOKE[4]

[1] Engineering Geology, Lund University, S-211 00 Lund, Sweden.
[2] Rosqvist Resurs, Gamla Malmövägen 25, S-230 41 Klågerup, Sweden.
[3] Tyréns AB, Kungsgatan 6, S-252 21 Helsingborg, Sweden.
[4] Geotomo Software, 5 Cangkat Minden Lorong 6, 11700 Gelugor, Penang, Malaysia.

Introduction

Buried waste in old landfills is an increasing problem as cities expand and grow into areas with former waste deposits. In order to be able to manage and as far as possible reclaim land in such areas, better tools are needed for mapping and characterisation of buried waste and contaminated land. Combined resistivity-IP surveying has shown great potential for this (e.g. DAHLIN et al., 2010). Another problem associated with landfills is methane emissions. Methane is a powerful greenhouse gas and a growing concern regarding global climate changes. Landfill gas is regarded as one of the major sources for methane migration to the atmosphere. The migration of methane and carbon dioxide from a specific landfill depends on several aspects, such as the nature of the soil cover system, the gas collection system, and daily management.

A short term 3D resistivity and time-domain induced polarisation (IP) monitoring field experiment was carried out over part of a Municipal Solid Waste (MSW) landfill, the Filborna landfill site, Helsingborg, Sweden. Short term monitoring experiments have been conducted at the Filborna landfill site on several occasions during 2008, 2009 and 2011 (e.g. ROSQVIST et al., 2011). The objective was to detect variations in gas and fluid content due gas migration in the landfill. In this paper we present results from a short term monitoring performed in 2011.

Method

An area measuring 40 by 22 meter was monitored during a couple of weeks in June-July 2011. A grid with 21 x 12 electrodes was monitored, with an electrode spacing of 2 m in both directions (Fig. 1). A remote controlled data acquisition system based on ABEM Terrameter LS with 12 measuring channels complemented by 3 external relay switches, lightning protection, internet modem, etc was employed. In addition to the resistivity-IP monitoring the weather was recorded locally. The data acquisition was done measuring induced polarisation (IP) as well as resistivity using a duty cycle with 1 second current-on and current-off, where the timing is a compromise between acquisition speed and ability to capture the IP characteristics. In this way eight 3D resistivity-IP data sets were recorded daily, but only the resistivity data results are presented here. It can be noted that even if only resistivity data were measured, shorter measurement cycle times lead to underestimation of the measured resistivity due to the large IP-effects associated with waste. Res3dinv was used for time-lapse inversion of the resistivity data.

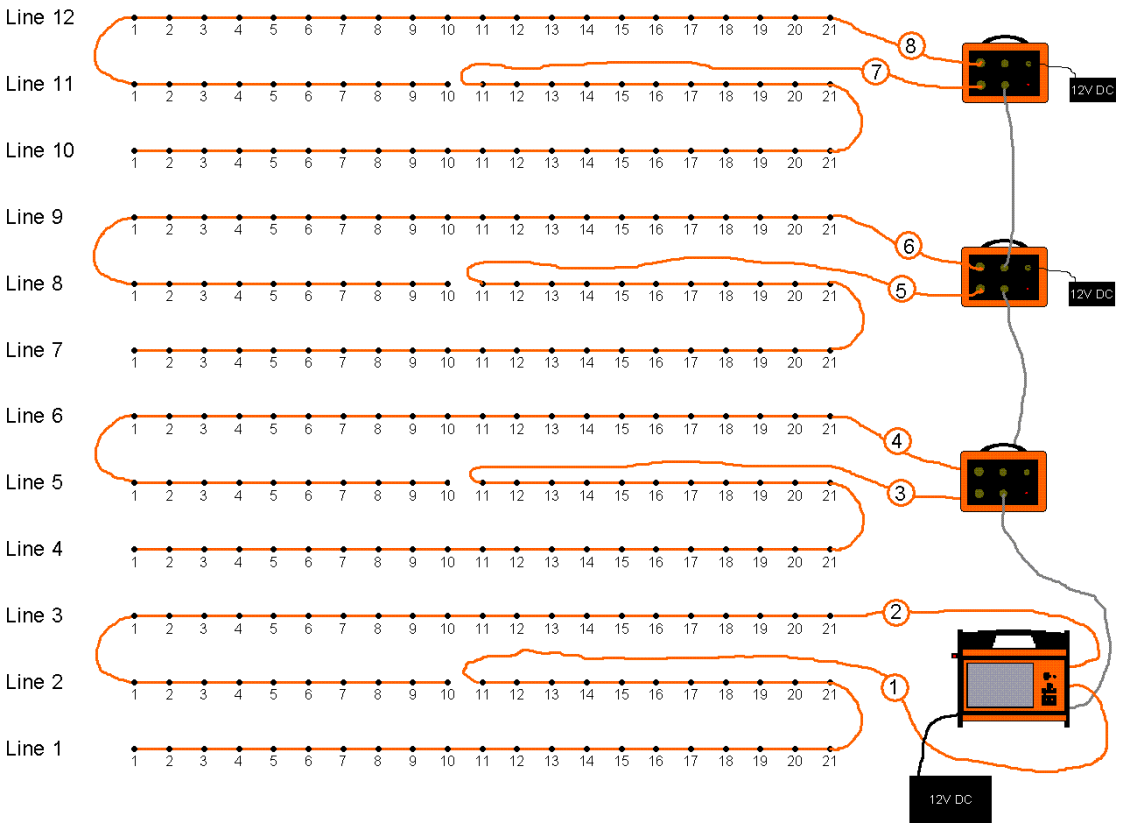

Fig. 1: Sketch of short term monitoring setup with 12 x 21 electrodes.

Results

The predominant material in the investigated volume in the short term monitoring is mixed waste, with a layer of cover material on top. According to the waste company the cover material consists of 0.4 m compost, 0.8 m excavation masses, 0.3 m gravel and 0.3 m clay, plus possibly 0.1 to 0.2 m compost, under which there is waste. The groundwater level is expected at some metres depth according to observations in the surrounding areas. The waste is underlain by sedimentary rock dominated by sandstone at depths beyond the depth penetration of the investigation presented here.

The inversion model used cells of 1 metre width so that large near surface resistivity variations could be more accurately modelled. Higher damping factors were also used for the first two layers as well as a diagonal roughness filters to reduce banding effects in the inversion (LOKE and DAHLIN, 2010). The resistivity model from one time step is shown in Fig. 2, where a strong decrease in resistivity is seen at around 4 metres depth which is interpreted as due to the groundwater surface. The IP results (see example in Fig. 3) show a strong increase in chargeability a couple of metres below the decrease in resistivity. This is interpreted as a change in type of material, and that there is mixed waste below this level which gives rise the high chargeability.

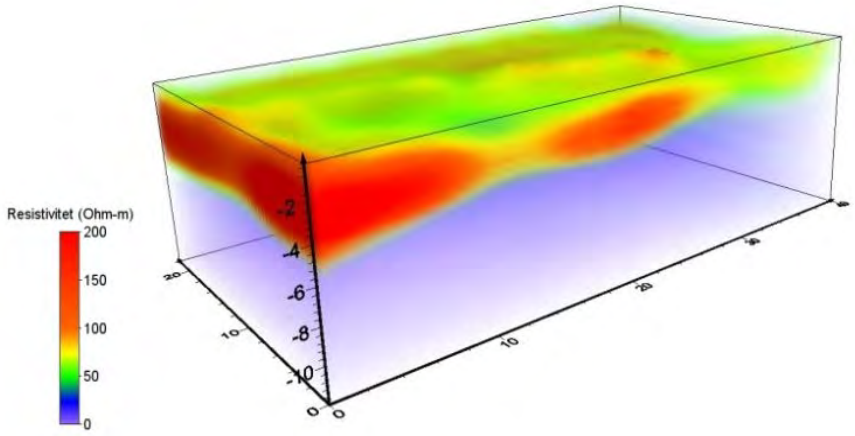

Fig. 2: Example resistivity model from short term monitoring (distances are in metres).

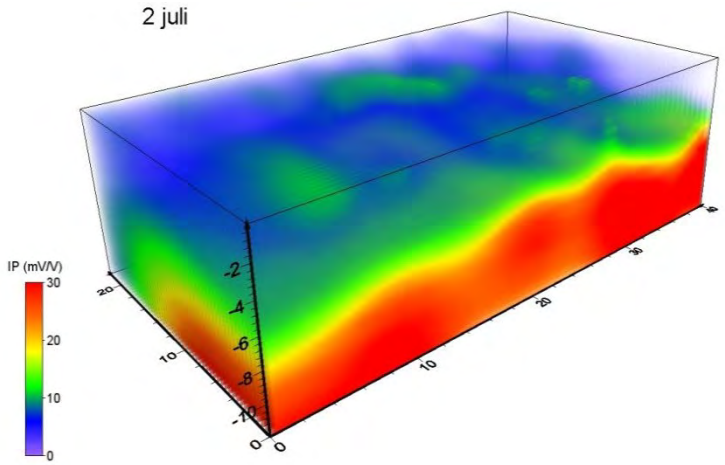

Fig. 3: Example chargeability (IP) model from short term monitoring (distances are in metres).

There were some rainfall events during the monitoring period, and the resulting change in resistivity is shown in Fig. 4. As can be seen much of the decrease in resistivity is very shallow, but there is a zone in the central part of the volume where it penetrates to some metres depth.

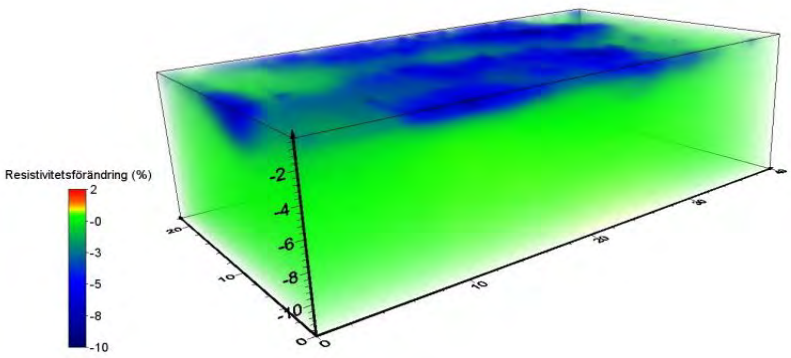

Fig. 4: Change in resistivity during the monitoring period (distances are in metres).

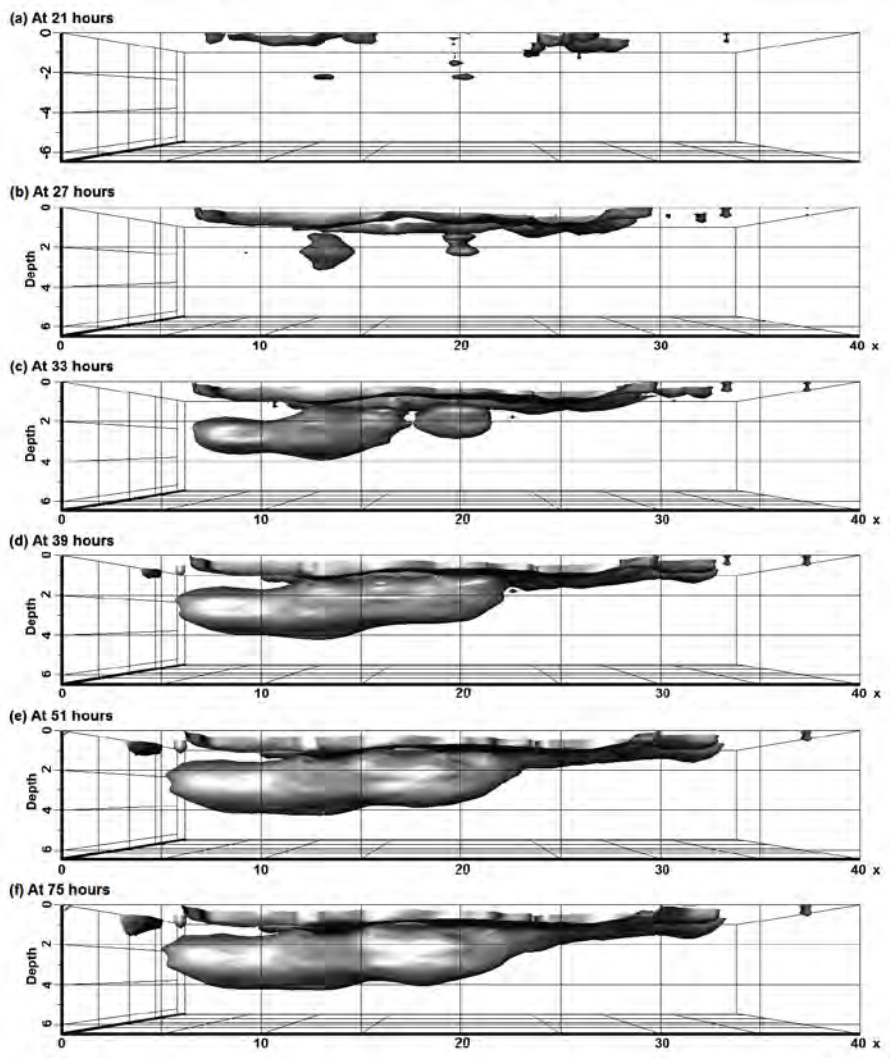

Fig. 5: 3-D iso-surface plots showing the positions of the -6% resistivity change boundary with time.

Fig. 5 shows iso-surface plots of the -6% resistivity change boundary with time, which provides a set of 3-D views of the movement of the rainwater. At 21 hours (Fig 5a), or about 10 hours after the start of the downpour, most of the water is still confined to near the surface. At 27 hours (Fig 5b) more of water has migrated downwards which then forms a significant plume reaching to 4 metres depth at 33 hours (Fig. 5c). At 39 hours (Fig. 5d) the bottom boundary of the plume has moved slightly below 4 metres accompanied by a greater lateral migration. There is a slight increase in the volume of plume at 51 hours (Fig. 5e), after which there were no significant changes up to the 75 hours mark (Fig. 5f).

The particularly heavy rainfall event that occurred 2nd July and that event tends to dominate the change during the period. However if the change in resistivity relative to the preceding day is plotted more subtle changes can be seen, as shown in Fig. 6 where the increase in resistivity can be interpreted as due to increase in gas contents below the water saturated horizons above.

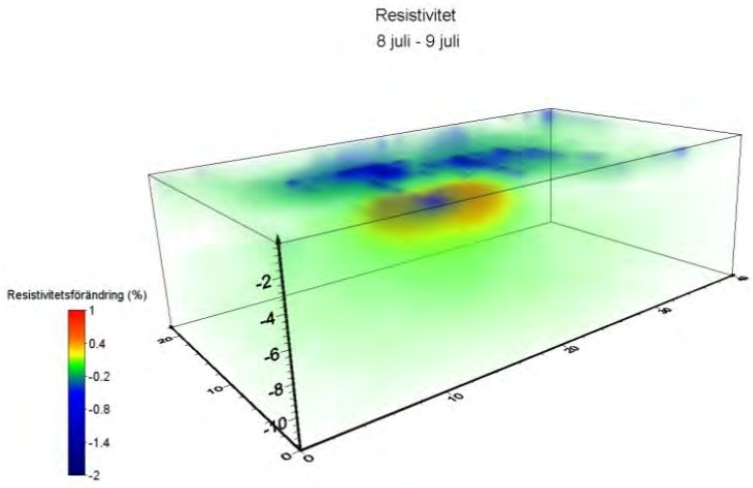

Fig. 6: Change in resistivity 8.–9. July (distances are in metres).

Conclusions

Internal landfill structure was successfully mapped using a combination of resistivity and time-domain IP. Variations in resistivity and chargeability are interpreted to be related to different types of materials. Continued evaluation against historical documentation of the landfilling is underway, and it is planned to do sampling by test pits or drilling as follow up.

Variations in resistivity that we interpret being linked to variation in fluid and gas content were captured by short term monitoring. A rainfall event that occurred during the monitoring period acts as an infiltration test and the changes in resistivity outlines the water migration pattern. After this event there are signs of gas increasing contents below the saturated zone, which is expected as the water will tend to act as a lit above the gas that is generated inside the landfill. The results show the potential of resistivity monitoring for tracing fluid migration in the ground, and also shows patterns that may be due to increasing gas contents in line with previous results.

Acknowledgements

The work at Filborna was carried out within the MaLaGa project (**Ma**pping of **La**ndfill structures and **Ga**s migration based on geophysical measurements) in co-operation between Lund University, NSR AB and Tyréns AB, with funding from Swedish Waste Management (Avfall Sverige), Swedish Gas Centre (Svenskt Gastekniskt Center AB), Sven Tyréns Stiftelse and NSR AB.

References

DAHLIN, T., ROSQVIST, H., LEROUX, V., 2010: Resistivity-IP for landfill applications. – First Break, **28**(8), 101-105.

LOKE, M.H. and DAHLIN, T, 2010: Methods to reduce banding effects in 3-D resistivity inversion. – Proceedings 16th European Meeting of Environmental and Engineering Geophysics, 6.–8. September 2010, Zurich, Switzerland, A16.

ROSQVIST, H., LEROUX, V., DAHLIN, T., SVENSSON, M., LINDSJÖ, M., MÅNSSON, C-H. and JOHANSSON, S., 2011: Mapping landfill gas migration using resistivity monitoring. – Waste and Resource Management, **164**(1), 3-15.

Historical Aspects of Geoelectric Monitoring

Geoelectrical monitoring of salt infiltration experiments at Leibnitzer Feld, 1991; picture by W. H. Kollmann

Geoelectrical Monitoring behind the "Iron Curtain"

KAREL MÜLLER[1], PAVEL BLÁHA[2], SHAVKAT ABDULLAEV[3] and ROMAN DURAS[2]

[1] UGN AV CR, 709 00 Ostrava, Studentska 1768, Czech Republic.
[2] GEOtest Brno, a.s., 708 00 Ostrava, 28. rijna 287, Czech Republic.
[3] Institut Gydroingeo, Branch Manager Tashkent, 100041, N. Khodzhibaeva 64, Uzbekistan.

blaha@geotest.cz

Introduction

In the countries of the Eastern Bloc, geoelectrical monitoring began in the 1970s in the form of repeated check or regime measurements. These were particularly measurements of the hydrodynamic regime using the method of an embedded probe (the mise-a-la-masse method), resistivity measurements made in workings and exploratory tunnels, check resistivity measurements (e.g. for detecting the homogeneity of compaction of large-area embankments) and repeated geoelectrical measurements made on slope failures.

At the end of the 1980s, further development took place also in the use of geoelectrical monitoring on slope failures. This work was carried out on landslides in the Crimea, in the Caucasus, in Uzbekistan and in Czechoslovakia. Resistivity measurements made from the surface were very often supplemented by geoelectrical measurement made in boreholes. In addition to the geoelectrical methods mentioned above, measurement of "pulsation electromagnetic emissions" is sometimes used, applied also as simple monitoring on slope failures, both in the areal surface version, and more often in the borehole option. The interpretation of results obtained by this method is, however, very deceptive.

Geoelectrical monitoring became more widely applied in the use of geoelectrical measurement with a multi-electrode array in the 1990s. This is a measurement carried out on landfills of waste material. Modern landfills are constructed mostly with a system of fixed electrodes underneath impermeable sheets, thus repeated geoelectrical measurements enable the identification of damaged places in the sheet and places of possible leaks of contaminated water from landfills.

In all of the states of the Eastern Bloc, the application of geoelectrical monitoring declined at the beginning of the 1990s, perhaps with the only exception which is the check of landfills. In this case, geoelectrical monitoring applies as the check of the tightness of impermeable sheets in the basement of landfills on the one hand, and also as the check of the flow of groundwater and its quality around landfills on the other.

Applications in Construction Industry

Geoelectrical methods began to be used in construction engineering immediately at the beginning of the use of geophysical methods in construction industry. First, these mostly concerned applications in the survey of dam sites; other types of construction work were also investigated geophysically in the course of time. In the 1970s, resistivity methods were chiefly used, namely in the form of vertical electrical sounding and symmetrical resistivity profiling. Other geoelectrical methods were also used, but rarely. The first example shows the use of the mise-a-la-masse method (Fig. 1). The results of measurement presented in this figure are from 1971.

One of the hydrogeological problems encountered during the preliminary stage of a survey for dams is the need to know the direction and velocity of flow of groundwater at the dam site and at

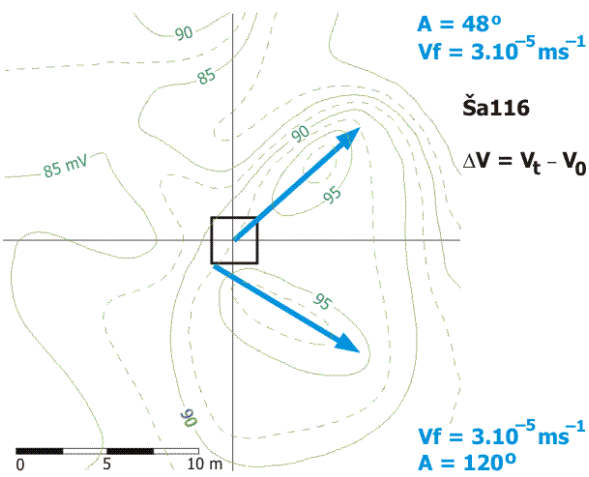

Fig. 1. Plan showing the flow pattern of groundwater determined by geoelectrical measurements in the vicinity of a test pit at the Josefův Důl dam site

sites where other buildings will be constructed, as well as in the backwater area. At this stage of the site investigation, the results of deep drilling are not yet available, so it is necessary to use all pre-existing information in combination with surface geophysics. A survey by the mise-a-la-masse method using a fixed electrode is an effective electrical procedure. An example of the application of this method in the investigation of the Josefův Důl dam site is illustrated in Figure 1. The direction and velocity of groundwater flow were interpreted using the measured difference in the direct-current potential field following salination of the water in a pit (V_0) and after an appropriate period of time had elapsed (V_t). Using these measurements, two different directions of flow were distinguished. By coincidence both of them showed the same velocity of groundwater flow. The pattern of the potential contours was used to determine the flow in the direction 120°. This method was preferred to that in which the direction of flow is given by connecting the centre of the elliptical field to the centre of the pit. In this case, the possibility that the fracture system controlling the flow of groundwater was most developed in the south-western corner of the pit could not be ruled out.

We also used repeated geoelectrical measurements to check compaction of embankments. The measurement below was carried out in 1975. If we are able to perform repeated surface measurements, it is also possible to estimate the changes in absolute values of apparent resistivity. This fact was also used during the monitoring of pouring homogeneity on a large-scale waste rock and fly ash used as a foundation material for the construction of a chemical plant on the bottom-land of the Odra River in Ostrava (MÜLLER, et al., 1994, BLÁHA and MÜLLER, 2008). Every bottom surface was measured with micro-resistivity profiling with double maximum depth. Experimental works proved that the mound is homogeneously solidified when the apparent resistivity values vary from 25 to 75 Ωm. In cases when places of higher apparent resistivity were noticed, these were interpreted as places of higher porosity and were recommended for reconstruction. Fig. 2 shows the outcomes of repeated measurements before adjustments; the places recommended for adjustments were marked with section lines. After the reconstruction it is clear that apparent resistivity values have been lowered to the requested figures.

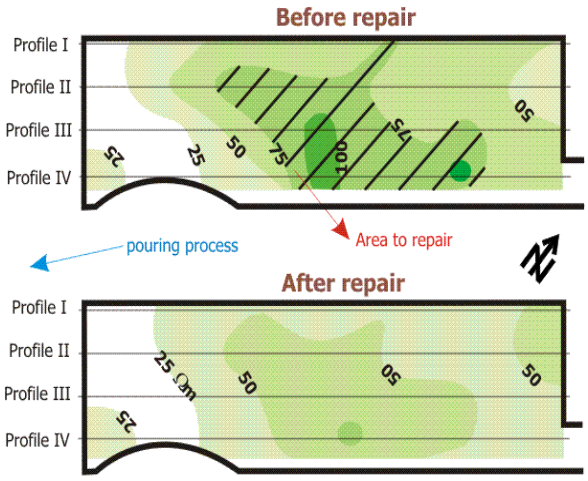

Fig. 2 Ostrava - repeated geoelectrical measurements

Applications in Mining

Monitoring of changes in the rock mass after a mine working has been excavated is one of the most important tasks of geotechnics. Some of the applications of high-frequency seismology are the most suitable geophysical methods for this monitoring. In the next figure we want to show that the application of geoelectrical measurements also yields very interesting information. Fig. 3 shows the outcomes of repeated geoelectrical resistivity measurements in the limestone massif in Viola 1 gallery in the Hrhov locality (Slovak Republic), which was considered to be the site for the construction of a pumped-storage hydroelectric plant. The measurement was carried out in 1973. Four quasi-homogeneous blocks were determined using geophysical and geological logs:

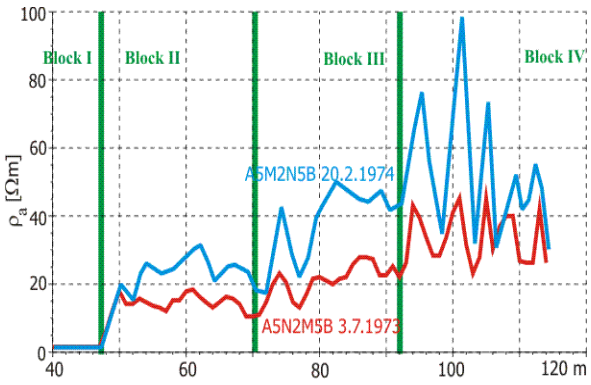

Fig. 3 Hrhov - repeated geoelectrical measurements

- Block I consisting of slope debris.
- Block II with wide cracks and fissures.
- Block III faulted with steep tension karstified fissures.
- Block IV faulted with narrow tension non-karstified fissures (MÜLLER et al., 1976).

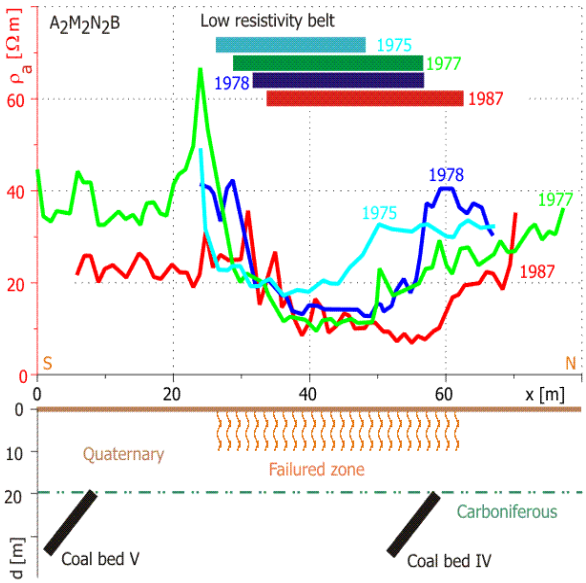

Fig. 4 Changes in apparent resistivity above the mining area (after Hofrichterová L. et al. 1999)

The use of repeated geophysical measurements to identify impacts of mining on the surface dates from relatively older times. In 1975 – 1987, manifestations of the so-called Hladnov Fracture were monitored in the mining area of the Petr Bezruc Mine in Slezska Ostrava (Fig. 4). Its delineation was required particularly in relation to the construction of a new road and the stadium Bazaly. This fracture had an effect on buildings extending from the embankment by the River Ostravice through Hladnov up to the urban park Stromovka. Conventional resistivity profiling and, experimentally, also thermal and emanation profiling were used to locate this fracture. The fracture was indicated by low apparent resistivity values and the centre of the fracture shifted by about ten metres in the course of twelve years (HOFRICHTEROVÁ et al., 1999, Fig. 4). In 2007, several profiles across the Hladnov Fracture were measured using multi-electrode resistivity tomography; the results showed the same indications of resistivity as in the previous years (VAŠÍČKOVÁ, 2007).

Applications to Slope Failures

In the 1970s and 1980s, the staff of the research institutes VSEGINGEO in Moscow and UZBEKGIDROGEOLOGIE in Tashkent (ABDULLAEV, 1983) carried out the most extensive study of manifestations of time changes in individual mechanical and physical properties on slope failures.

In these institutes, within the basic research, time changes in individual physical properties on slope failures were fully systematically studied, including changes in resistivity. They monitored these changes not only on natural landslides in the Crimea, in the Caucasus and in the foothill regions of Uzbekistan, but they also made model measurements that preceded field measurements. The results of these works were summarised by N. GORYAINOV and his team in a book on the study of landslides using geophysical methods, which was published by the Publishing House NEDRA in Moscow in 1987. It is natural that not only this team of authors gave attention to time changes in physical properties on slope failures, but these problems were also investigated in the Czech Republic.

The first repeated measurements were carried out in 1977 and 1987 and are given in Figure 5 showing the slope failure Trinec (BLÁHA, 1993, 1997, 2009). Measurements in both years were carried out in the same season under roughly the same climatic conditions. In the case of this particular landslide we can see that during 10 years no dramatic changes occurred in the distribution of tension and that the landslide was not developing progressively in this period. It is natural that a substantially larger amount of data can be obtained if a larger amount of measurements is available. We also tried to use perpendicular profiling. This work had an experimental character because perpendicular profiling is extremely demanding in fieldwork in terms of operation, particularly on forested terrain where the whole spacing of electrodes must again be installed for each point of measurement. An example of such work is given in Figure 5.

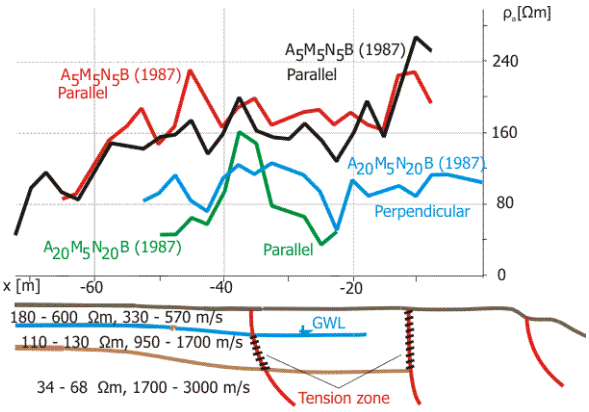

Fig. 5 Resistivity profiling on the landslide Trinec

The pattern of curves shows that parallel profiling yields substantially more jagged curves of ρ_a. The only advantage of transverse profiling is the possibility that in the case of a steep scarp we obtain results of profiling right to that scarp.

Another row of examples is from monitoring geoelectrical measurement on slope failures in Uzbekistan, particularly on the landslide Chashli. The site of Chashli lies close to the Town of Almalik about 60 km SSE of Tashkent. A huge body of loess lying on the limestone mass was affected by slope movement. The loess liquefied during a strong increase in moisture following the spring thaw and subsequently flew downslope. The slope failure of the type of flow passed then into slow sliding. A series of experiments was carried out on such a consolidated slope failure, during which the landslide was again set into movement using artificial watering. The landslide was watered so that water was pumped into open cracks. The volume of water that was introduced into the landslide at the individual stages of watering is given in Figure 6. In addition to the conventional methods of monitoring of movement of slope failures, a series of geophysical measurements was made on this landslide. During this series of experiments, symmetrical resistivity profiling and vertical electrical sounding were measured using stationary and portable electrodes.

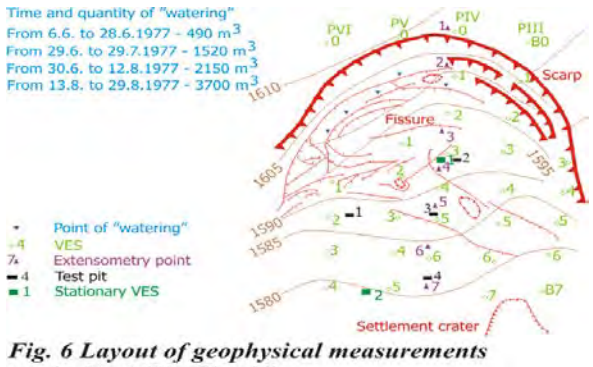

Fig. 6 Layout of geophysical measurements on the landslide Chashli

Figure 7 shows the changes that occurred before and after the renewal of slope movement. At the beginning of movement, the apparent resistivity for spacings of AB/2 being 1.5 to 6 metres records a marked decline, or the decline begins several days before the shear itself. It is possible to prove in the curve for AB/2 = 1.5 metres that tension cracks, manifested by increasing ρ_a at shallow depths, form before the shear itself. After the shear, the values of ρ_a do not change strongly anymore. Only in the spacing 1.5 metres, a slight increase of ρ_a was recorded at the turn of July and August 1977. It is possible that changes in the landslide take place in narrow spacing during its movement, i.e. that documented are the periods during which tension applied to an increased extent. This tension is accompanied by the formation of new cracks in the landslide, which are not filled by water, but by air. The increase of ρ_a for the spacing AB/2 = 11 metres is interesting. This increase, albeit negligible, agrees with the shear of the landslide in terms of time. This can prove that the shear of the shallow landslide is manifested by the change in the states of tension also in the basement of this landslide.

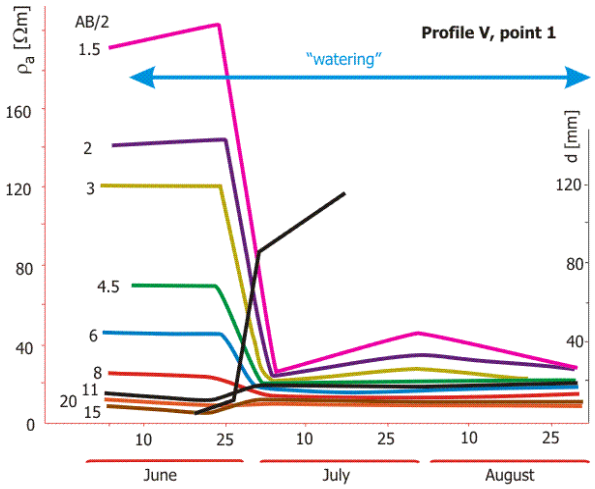

Fig. 7 Changes in apparent resistivity with moistening

Figure 8 also shows that the changes in ρ_a with moistening have mostly a similar character, i.e. that the apparent resistivity decreases. The right part of the figure shows the measured curves of ρ_a and the left part the derived parameter R, i.e. the ratio between ρ_a of moistened loess and ρ_a of loess with natural moisture content. In this manner it is possible to monitor not only changes in moisture content according to changes in apparent resistivity, but also to determine the depth of the shear plane. It is likely that the water introduced into the landslide is drained on the shear plane, and hence it is possible to determine the shear plane in the places in which the R values are approaching 1. However, we know cases from other sites that the parameter R can also assume values larger than 1. Such changes occur in the places in which newly forming pores cannot be fully filled by groundwater. It has been detected that in some cases the parameter R increases with time. This is caused by a gradual increase in porosity. However, to find a direct conversion relationship between the parameter R and porosity has not been successful, even for a given lithological type.

Another parameter in which it is possible to monitor time changes in sliding is the coefficient of anisotropy. Figure 9 shows an example taken from a paper in which the ratio of the major semi-axis of the ellipse of anisotropy to its minor semi-axis is plotted, namely for the beginning of sliding and for the developed stage of slope movement. This example is taken from the landslide Krasnogorsk, which lies in the same region as the landslide Chashli and has a similar geological

structure as well. In the areas lying outside the slope failure (KV1 and KV9), we can see that the changes outside the landslide are minimal. At these sites, only extreme curves are plotted for a better arrangement of the figure (all curves were measured). The central part of the figure shows curves from the landslide (KV4 and KV5). At first sight it is obvious that in these curves far greater changes in the size of the apparent resistivity of loess occur with time. The values of the coefficient of anisotropy in sliding are up to double the ones before sliding. This is also one of the possible methods how to monitor the development of a slope failure or how to determine the depth of a shear plane. In this way it is possible to determine the depth of the shear plane on point KV4 at about 18 metres and on point KV5 at 10 metres.

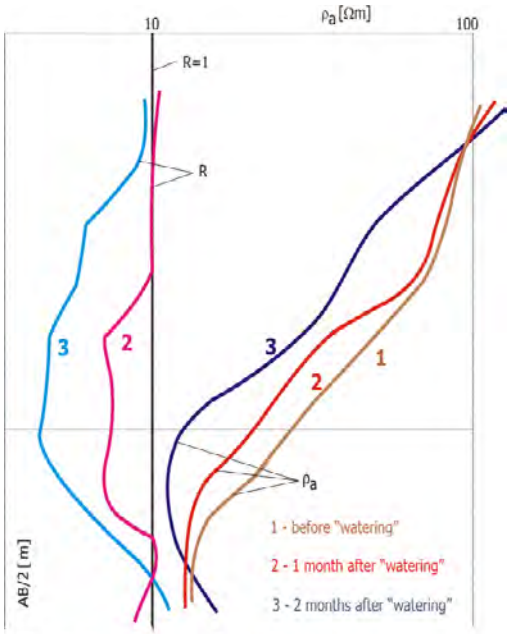

Fig. 8 Changes in ρ_a in VES curves

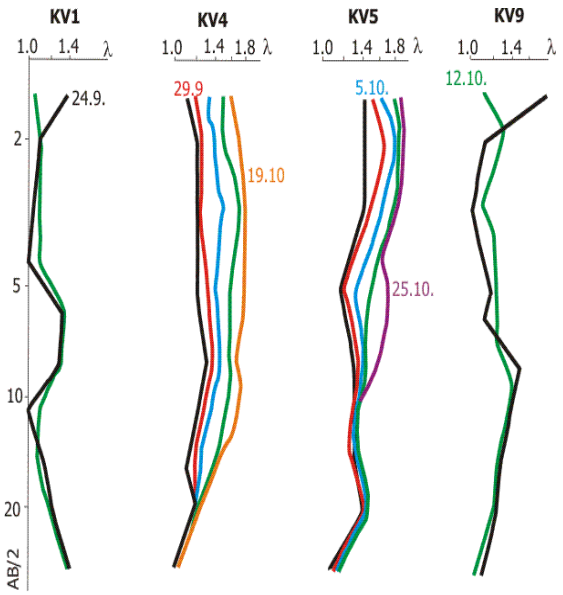

Fig. 9 Time changes in the coefficient of anisotropy

Conclusion

In this paper we show the readers which paths the development of applications of geoelectrical methods took in monitoring the time development of changes in the rock mass in the countries of the former Eastern Bloc before 1989. We paid attention not only to the changes governed by natural processes, but we made efforts to show the specialists from other branches the possibilities of using geoelectrical methods also in monitoring the changes caused by human activity. During the presentation at the December workshop, we tried to show our experience gained from the entire branch of geoelectrical monitoring. In this paper we focused only on applications in construction industry and mining and on monitoring slope failures.

References

ABDULLAEV, S., 1983: Izucheniye rejima rozvitiya opozney v lesovikh porodakh geofizicheskimi metodami (Research of the regime of the development of landslides in loess rocks using geophysical methods). Kandidátská dizertační práce (candidate dissertation thesis), Gidroingeo, Tashkent, MS.

BLÁHA, P., 1993: Geofyzikální metody při výzkumu svahových deformací (Geophysical methods in research of slope failures), Geotest Brno, NIS ČR (National Information Centre of the CR), Department of Geofond, Brno, Prague, pp. 1-71 and 1-64.

BLÁHA, P., 1997: Inženýrská geofyzika svahových deformací v hornické a stavební geotechnice (Engineering geophysics of slope failures in mining and building geotechnics)., doktorská disertační práce (doctoral dissertation thesis), VŠB (School of Mines), Ostrava, MS.

BLÁHA, P., 2009: Landslide and its complex investigation. Acta Montanistica Slovaca, **14**(3), pp. 221-231, ISSN 1335-1788.

BLÁHA, P. and MÜLLER, K., 2008: Geophysical monitoring as an information source of rock massif behaviour., Acta Montanistica Slovaca, **13**(2), pp. 223-228.

GORYAINOV, N.N., BOGOLYUBOV, A.N., VARLAMOV, N.M., MATVEYEEV, V.S., NIKITIN, V.N. and SKVORCOV, A.G., 1987: Izucheniye opolzney geofizicheskimi metodami (Research of landslides using geophysical methods)., Nedra, Moscow, 1-156.

HOFRICHTEROVÁ, L., MÜLLEROVÁ, J., POLÁČEK, A. and MÜLLER, K., 1999: Contribution of geophysics to the study of mining subsidence basins. – Publication of the Institute of Geophysics of Polish Academy of Science M-**22**., pp. 323-329.

MÜLLER, K., BLÁHA, P. and NEŠVARA, J., 1976: Časové změny zdánlivého měrného odporu v horninovém masívu (Time changes in apparent resistivity in the rock mass). – Sb. II. konf. Aplikace geofyziky v IG a HG (Proceedings of the 2nd conference "Applications of Geophysics in IG /Engineering Geology/ and HG /Hydrogeology/"), Vol. I. **1**, pp. 193-203, Brno.

MÜLLER, K., HOFRICHTEROVÁ, L. and MÜLLEROVÁ, J., 1994: Engineering geophysical investigations of rock fill bodies made out coal mine waste materials. – Proceedings of the international Conference on Environment, Energy, and Society, Carbondale, USA, 94-98.

VAŠÍČKOVÁ, Š., 2007: Hladnovská porucha karbonského masívu v Ostravě a její vliv na zástavbu (Hladnov's failure of Carboniferous massif in Ostrava and its influence to the build-up area). Bakalářská práce (bachelor thesis). PřF OU Ostrava, MS.

Appendix

List of Participants

Surname, Name	Institute	Country
Ahl, Andreas	Geological Survey of Austria, Department of Geophysics	Austria
Ahn, Hee-Yoon	Heesong Geotek Co., LTD.	Korea
Antretter, Norbert	GEO-data GmbH	Austria
Baron, Ivo	Geological Survey of Austria, Department of Geophysics	Austria
Bell, Rainer	Institut fuer Geographie und Regionalforschung Universitaet Wien	Austria
Bernard, Jean	IRIS Instruments	France
Bieber, Gerhard	Geological Survey of Austria, Department of Geophysics	Austria
Binder, Daniel	ZAMG, Section Climate Change Impacts	Austria
Blahut, Jan	Institute of Rock Structure and Mechanics, Academy of Sciences of the Czech Republic	Czech Republic
Burda, Jan	Charles University in Prague; Brown Coal Research Institute, j.s.c.	Czech Republic
Caterina, David	University of Liège	Belgium
Chambers, Jonathan	British Geological Survey	United Kingdom
Cho, Gye-Chun	Geosystems Engineering Laboratory, Dept. of Civil & Environmental Eng., KAIST	Korea
Cho, In-Ky	Dept. of Geophysics, Kangwon National Univ.	Korea
Dahlin, Torleif	Engineering Geology, Lund University of Technology	Sweden
Di Maio, Rosa	University of Naples "Federico II" – Department of Earth Sciences	Italy
Drahor, Mahmut G.	Center for Near Surface Geophysics and Archaeological Prospection (CNSGAP)	Turkey
Džuppa, Peter	Szemere H. spol. s r.o.	Slovakia
Fischer, Tomas	Inst. of Hydrogeology, Engineering Geol. and Applied Geophysics, Charles University in Prague	Czech Republic
Flechsig, Christina	Universität Leipzig Institut für Geophysik und Geologie	Germany
Fusco, Francesco	Department of Earth Sciences, University of Naples Federico II, Naples,	Italy
Fuss, Christian	AlpS, University of Salzburg	Austria
Gance, Julien	School and Observatory of Earth Sciences, Institute of Earth Physics, University of Strasbourg	France
Garré, Sarah	KULeuven	Belgium
Gozzi, Andrea	C.S.G.	Italy
Günther, Thomas	Leibniz Institute for Applied Geophysics Hannover	Germany
Hartmeyer, Ingo	AlpS, University of Salzburg	Austria
Hartvich, Filip	Department of Physical Geography and Geoecology, Faculty of Science, Charles University in Prague	Czech Republic
Holzner, Stefan		Austria
Janik, Markus	geoFact	Germany
Jeong, Ji-Min	Heesong Geotek Co., LTD.	Korea
Jinguuji, Motoharu	Exploration Geophysics Research Group, AIST	Japan
Jochum, Birgit	Geological Survey of Austria, Department of Geophysics	Austria

Just, Anita	University of Leipzig, Institute of Geophysics and Geologie	Germany
Karousova, Magda	Charles University in Prague, Institute of Hydrogeology, Engineering Geology and Applied Geophysics	Czech Republic
Kauer, Stefanie	Geological Survey of Austria, Department of Geophysics	Austria
Keuschnig, Markus	AlpS, University of Salzburg , Research Group Geomorphology and Environmental Systems	Austria
Kim, Jung-Ho	Korea Institute of Geoscience and Mineral Resources (KIGAM)	Korea
Kim, Ki-Seog	Heesong Geotek Co.,LTD.	Korea
Klimeš, Jan	Institute of Rock Structure and Mechanics	Czech Republic
Kneisel, Christof	Universität Würzburg, Institut für Geographie und Geologie, Physische Geographie	Germany
Kociu, Arben	Geological Survey of Austria	Austria
Kreuzer, Gerhard	LIFTOFF	Austria
Krummel, Heinrich	geoFact	Germany
Lagmanson, Mats	Advanced Geosciences, Inc.	USA
Lamert, Hendrik	Helmholtz Centre for Environmental Research - UFZ Department Monitoring and Exploration Technologies	Germany
Lebourg, Thomas	Geoazur Lab CNRS UNS	France
Lippmann, Erich	LGM	Germany
Martini, Edoardo	Helmholtz Centre for Environmental Research - UFZ Department Monitoring and Exploration Technologies	Germany
Matthes, Katrin	University of Leipzig, Institute of Geophysics and Geology	Germany
Merritt, Andrew	University of Leeds	United Kingdom
Möller, Marcus	Helmholtz Centre Potsdam, GFZ German Research Centre for Geosciences	Germany
Noell, Ursula	Federal Institute for Geosciences and Natural Resources	Germany
Otto, Jan-Christoph	Uni Salzburg, Geographie und Geologie	Austria
Ottowitz, David	Geological Survey of Austria, Department of Geophysics	Austria
Papadopoulos, Nikos	Foundation for Research and Technology	Greece
Perrone, Angela	CNR - IMAA	Italy
Pfeiler, Stefan	Geological Survey of Austria, Department of Geophysics	Austria
Popp-Hofmann, Steffen	Helmholtz Centre for Environmental Research – UFZ	Germany
Rabenstein, Lasse	ETH Zurich, Institute of Geophysics	Switzerland
Robert, Tanguy	Département ArGEnCo Geo³-Géophysique Appliquée Université de Liège	Belgium
Rode, Matthias	Institut für Geographie und Raumforschung, Karl-Franzens-Universität Graz	Austria
Römer, Axl	Geological Survey of Austria, Department of Geophysics	Austria
Rudolph, Sebastian	Institute of Bio- and Geosciences, IBG-3: Agrosphere Institute, Forschungszentrum Jülich GmbH	Germany
Ryu, Heehwan	Geosystems Engineering Laboratory, Dept. of Civil & Environmental Eng., KAIST	Korea

Sailhac, Pascal	School and Observatory of Earth Sciences, Institute of Earth Physics, University of Strasbourg	France
Sass, Oliver	Institut für Geographie und Raumforschung, Karl-Franzens-Universität Graz	Austria
Sauer, Uta	Helmholtz Centre for Environmental Research – UFZ	Germany
Schmidt-Hattenberger, Cornelia	Helmholtz Centre Potsdam, GFZ German Research Centre for Geosciences	Germany
Schütze, Claudia	UFZ Helmholtz Centre for Environmental Research	Germany
Scognamiglio, Solange	Department of Earth Sciences, University of Naples Federico II, Naples	Italy
Seiberl, Wolfgang	Geological Survey of Austria	Austria
Seidel, Knut	GGL Geophysik und Geotechnik Leipzig GmbH	Germany
Seifert, Peter	Geological Survey of Austria	Austria
Sporrer, Peter	KTS	Austria
Steirer, Fritz	Dep. of Environmental Geosciences University of Vienna	Austria
Supper, Robert	Geological Survey of Austria, Department of Geophysics	Austria
Szalai, Sándor	GGRI HAS	Hungary
Szokoli, Kitti	GGRI HAS	Hungary
Tábořík, Petr	Institute of Hydrogeology, Engineering Geology and Applied Geophysics, Charles University in Prague	Czech Republic
Takakura, Shinichi	National Institute of Advanced Industrial Science and Technology (AIST)	Japan
Tilch, Nils	Geological Survey of Austria	Austria
Treichel, Andrea	IBG-3 Forschungszentrum Jülich	Germany
Tsourlos, Panagiotis	Department of Geophysics, Aristotle University of Thessaloniki	Greece
Vecchiotti, Filippo	Geological Survey of Austria, Department of Geophysics	Austria
Woitzuck, Rafael	University of Vienna	Austria
Zhao, Yulong	ZEL Forschungszentrum Jülich	Germany